

The application of reusable hollow core slab connections in steel frames

Investigating the behaviour of a newly proposed reusable connection with increased tolerances

M.W. Wintermans



The application of reusable hollow core slab connections in steel frames

Investigating the behaviour of a newly proposed reusable connection with increased tolerances

M.W. Wintermans

Student number

[5411068]

An electronic version of this thesis is available at <http://repository.tudelft.nl/>.

Thesis committee: Prof. Dr. M. Veljkovic - TU Delft, Steel and composite structures (chair)
Dr. F. Kavoura - TU Delft, Steel and composite structures (daily supervisor)
Prof. Dr. H.M. Jonkers - TU Delft, Materials and environment
M. Poliotti PhD - TU Delft, Concrete structures
Ing. R. Stark - IMd Raadgevende Ingenieurs (company supervisor)

Project Duration: 18 April, 2023 - 22 February, 2024

Faculty: Civil Engineering and Geosciences, Delft

Company: IMd Raadgevende Ingenieurs Rotterdam

Cover credits: Tijdelijke Rechtbank Amsterdam, cepezed (L. van Woerkom)


TU Delft

IMd

Raadgevende
Ingenieurs

Preface

This thesis is the final chapter of my student career and the last hurdle in obtaining the Master of Science degree in Civil Engineering from Delft University of Technology. The aim of this research is to investigate the behaviour and environmental impact of reusable connections between hollow core slabs and steel frames. The purpose of this research is particularly interesting, as it applies structural engineering competencies to create additional economic value and reduce the environmental impact of the building industry. The results of the research are directly applicable in the industry and improve the environmental impact of the building industry from tomorrow onwards.

I would like to express my appreciation to my assessment committee, consisting of Prof. Dr. Milan Veljkovic, Dr. Florentia Kavoura, Prof. Dr. Henk Jonkers, Mauro Poliotti PhD, and ing. Rob Stark. I am grateful for the valuable insights, feedback, and questions you provided during our meetings. Your critical attitude helped me improve my academic competencies and guided me in the right direction. In addition, I want to thank Giorgos Stamoulis for his help with performing experiments on short notice.

Special thanks to IMd Raadgevende Ingenieurs and, in particular, Rob for giving me the opportunity to work on this interesting topic and connecting the academic world with the engineering-world application. During my time, I had the freedom to create my own path; however, the help and knowledge of IMd were there when needed. I am thankful for the opportunity to go on the company excursion to Copenhagen.

Although, no commercial interest was served with this thesis, many market parties helped me during the process. I thank Cugla B.V. for providing me with advice and the mortar used in the experiments. Special thanks to Vic Obdam and, in particular, Pieter Klijn for helping me during the design process by sharing valuable insight from the steel construction industry and providing me with the steel components to perform the experiments. From the first meeting we had you were always willing to contribute in whatever way possible.

Last, I am thankful for all the support of my friends, family and girlfriend. During the process, they were always there and helped me in different aspects. From offering me a sympathetic ear, providing feedback, reviewing my report, and supporting me throughout the process. Thank you, this means a lot to me!

*M.W. Wintermans
Delft, February 2024*

Abstract

To align with the objective of the European Green Deal [46] policy of achieving net-zero greenhouse gas emissions by 2050, the construction sector must transition to a circular built environment. Most of the waste in the Netherlands is related to construction and demolition waste, with the industry accounting for approximately 35% of CO₂ emissions [89]. The goal of the circular built environment is to minimise waste by reducing, reusing, recycling, and recovering materials throughout the life cycle of a product [66]. Therefore, making an impact in the construction industry can lead to a significant reduction in CO₂ emissions and contribute to the achievement of the European Green Deal [46].

This research contributes to the "reuse" component of the aforementioned circular built environment goals. Specifically, the focus is on developing a reusable connection between hollow core slabs and steel frames by implementing increased execution tolerances. Increased tolerances are necessary to allow reuse, as alignment-related problems often occur. The research consists of several parts: the design process, structural verification, experimental research on demountability, and environmental impact assessment. The design process comprises a tolerance analysis supported by a Monte Carlo simulation¹, variant studies, and a comprehensive qualitative trade-off analysis. After the best scoring alternative is determined, the verification part assesses the structural behaviour of the connection in terms of strength and stiffness. This is done using a combination of analytical and numerical calculations. The purpose of the experimental research is to investigate the demountability potential of the reusable connection. The final part of the research investigates the impact of the reusable connection compared to conventional connections for different lifecycle scenarios.

The research demonstrated that incorporating additional tolerances in the connection between the hollow core slab and steel frame is crucial to achieve a reusable construction. Three connection alternatives were generated that can incorporate these tolerances based on a literature review and meetings with experts in the field of building construction. The alternatives were weighted on tolerance inclusion, ease of installation, demountability potential, and costs. The best option was identified as a connection consisting of a square hollow section and a bolted shear stud encased in mortar. This alternative outperformed competitors in terms of tolerances, installation, and costs. However, the demountability potential was identified as a critical part of the connection and, therefore, was further investigated experimentally. The experiments showed an increased demountability potential in situations that include pre-treatment². Vaseline-treated specimens showed no signs of chemical bonding and better lubrication compared to oil-treated specimens, resulting in the lowest resistance and, therefore, the best demountability. The last step of the research investigated the environmental impact of the reusable connection and compared it with the conventional construction technique. Results showed that a marginal addition of 1.3% to the initial environmental impact of the superstructure results in a significant reduction over the full lifespan of the structural elements. This was attributed to the reusability of the connection and the ability to reuse structural elements in another building in a second life cycle.

From the results, it is concluded that a reusable and structurally feasible connection between hollow core slabs and integrated steel beams can be created with a small additional investment upfront, resulting in a substantially reduced environmental impact. The purpose of this study is to provide guidance and persuade decision makers, such as project developers, building owners, and government organisations, to consider implementing reusable construction methods in their real estate projects. By doing so, they can contribute to the objective of the European Green Deal [46] policies and the goal of achieving net-zero greenhouse gas emissions by 2050.

¹A mathematical technique that estimates probable outcomes through repeated random sampling.

²Treatment applied before final installation to prevent bonding between the steel section and mortar.

Contents

Preface	i
Abstract	ii
Nomenclature	xii
I Introduction and Literature review	1
1 Introduction	2
1.1 Relevance	2
1.2 Problem statement	4
1.3 Scope	4
1.4 Research objective and question	5
1.5 Research methodology	6
1.6 Outline	8
2 Literature review	10
2.1 Hollow core slabs	10
2.1.1 Manufacturing process	11
2.1.2 Loading conditions	11
2.2 State of the art: demountable connections	13
2.2.1 Agro NRG building	13
2.2.2 Temporary courthouse Amsterdam	14
2.3 Tolerances	15
2.4 Tolerance inclusive fasteners	16
2.4.1 Injection bolts	16
2.4.2 Friction grip bolts	20
II Connection design	23
3 Tolerance study	24
3.1 Tolerance origin and measures	24
3.2 Tolerances according to standards and literature	25
3.2.1 Tolerances in the structural grid	26
3.2.2 Tolerances in hollow core slab	28
3.2.3 Out-of-straightness of the beam	29
3.2.4 Geometric deviation of the bolt hole location	31
3.2.5 Geometric deviation of the shear connector location	31
3.2.6 Total deviation	32
3.3 Monte Carlo Simulation	33
3.3.1 Method	33
3.4 Case study	33
3.4.1 Results	34
4 Design alternatives	37
4.1 Connection requirements	37
4.2 Connection loads	40
4.2.1 Floor loads	40
4.2.2 Roof loads	40
4.2.3 Wind loads	41

4.2.4	Column imperfection	42
4.2.5	Load combinations	43
4.3	Alternatives	46
4.3.1	Injected connection	46
4.3.2	Demountable bolted shear connector connection	50
4.3.3	Pretensioned connection	53
5	Qualitative trade-off analysis	56
5.1	Tolerances	56
5.2	Installation	57
5.3	Demountability	58
5.4	Costs	59
5.5	Results	62
5.5.1	Tolerances	62
5.5.2	Installation	62
5.5.3	Demountability	62
5.5.4	Costs	62
5.5.5	Matrix	63
III	Connection verification	65
6	Strength verification	66
6.1	Hollow core slab sleeve	69
6.1.1	Sleeve concrete	69
6.1.2	Reinforcement	70
6.1.3	Unity check	70
6.2	Connection	71
6.2.1	Bolted shear connector	71
6.2.2	Square Hollow Section	71
6.2.3	Adjustment bolt	72
6.2.4	Mortar	73
6.2.5	Unity check	73
6.3	Beam	74
6.3.1	Transverse bending resistance of the bottom flange and plate	75
6.3.2	Longitudinal bending resistance of the beam	76
6.3.3	Bearing resistance	76
6.3.4	Unity check	76
7	Stiffness analysis	77
7.1	Torsional stiffness of the integrated beam	77
7.1.1	Beam rotation	78
7.1.2	Hollow core slab bending	81
7.1.3	Beam flange bending	81
7.1.4	Result	81
7.2	Connection stiffness	81
7.2.1	Bolted shear connector	82
7.2.2	Top plate	83
7.2.3	Combined stiffness	85
8	Experimental research on the demountability	87
8.1	Method	87
8.1.1	Expected resistance (hypothesis)	88
8.1.2	Experimental setup	88
8.1.3	Testing procedure	90
8.2	Data collection	93
8.2.1	Load cell	93
8.2.2	Manual demolition	98

8.3	Data analysis	99
9	Environmental impact assessment	101
9.1	Method	101
9.2	Goal and scope	102
9.2.1	Goal	102
9.2.2	Scope	102
9.3	Impact assessment	104
9.3.1	Demountable shear connector connection	104
9.3.2	Conventional connection	105
9.3.3	Structure	106
9.3.4	MPG	109
9.4	Interpretation	111
IV	Research outcome	112
10	Discussion	113
10.1	Interpretation	113
10.2	Implications	114
10.3	Limitations	115
10.3.1	Tolerance study	115
10.3.2	Case study	117
10.3.3	Trade-off analysis	117
10.3.4	Experiments	117
10.3.5	Environmental impact assessment	118
11	Conclusion and recommendations	119
11.1	Conclusion	119
11.2	Recommendations	121
	Bibliography	122
A	Hollow core slab manufacturing tolerances	127
B	Case study building	128
B.1	Geometry	128
B.1.1	Dimensions	128
B.2	Isometric 3D building overview	130
B.3	Ground floor plan	132
B.4	First floor plan	134
B.5	Cross-sectional views	136
C	Monte Carlo Simulation	138
C.1	Simulation results	139
C.2	Python script	141
D	Stiffness comparison	144
D.1	Output IDEA StaTiCa	145
D.2	Output Maple hollow core slab	157
D.3	Output Maple beam flange	162
E	Installation and demountability costs	167
E.1	Sensitivity analysis	170
F	Load verifications	171
F.1	Bolt verification	171
F.2	Beam verification	171
G	Experimental set-up	174
G.1	Materials	174
G.2	Equipment	174

H Environmental impact categories and monetisation factors	177
---	------------

List of Figures

1.1	National Circular Economy Programme [66]	2
1.2	Longevity per building layer [13], adopted from [87]	3
1.3	Steel beam types for prefabricated concrete floor systems in mid and end beam configuration	5
1.4	Research methodology	7
2.1	Hollow core slab overview [63]	10
2.2	Imposed loads for residential (A), office (B), congregate (C), and shopping areas (D) [19]	12
2.3	Diaphragm working with load distribution method [7]	12
2.4	hollow core slab connection Agro NRG VBI [16]	14
2.5	Hollow core slab connection temporary courthouse Amsterdam [39]	15
2.6	Material properties of Rengel@SW404 with Ren@HY 5159 in confined and unconfined conditions for resin injected and steel-reinforced resin-injected material [76]	17
2.7	Creep displacement of epoxy resin (verschuiving {nl} = displacement {en}) [12]	18
2.8	Injection bolt in a double lap joint [27]	18
2.9	Nominal stress-strain performance for unconfined resin and steel-reinforced resin specimens [76]	20
2.10	Contact asperity of steel surfaces [51]	22
3.1	Column location tolerances according to B.20-1 of NEN-EN 1090-2 [27]	26
3.2	Erection tolerances for beam centre line and column spacing according to B.16-1 and B.20-3 of NEN-EN 1090-2 [27] respectively (L = left beam, R = right beam, C ₁ – C ₄ = column numbering).	27
3.3	Out-of-straightness amplitude for an allowable tolerance of L/1000 ([27], Class 1)	30
3.4	Deviation of the actual position (red) of the bolt hole and shear connector from the nominal (grey) position	32
3.5	Connection detail between hollow core slabs, SFB and columns	34
3.6	Deviation of the mean value of r (mm) along the beam axis for $\pm L/500$	35
3.7	Monte Carlo simulation with $N = 10^4$ simulations based on literature and manufacturer data (simulation 3) for a prefabricated situation	35
4.1	Design requirements	38
4.2	Wind loading on a building with windward (D) and leeward (E) side [22]	41
4.3	Critical loading situations	43
4.4	Load transfer principle for all of the alternatives, green arrows indicate the actions and orange arrows the reactions	46
4.5	Connection detail with resin injection (exploded view)	47
4.6	Connection detail with resin injection in installed position	48
4.7	Flow of forces for the resin injected connection	49
4.8	Connection detail with bolted demountable shear connector (exploded view)	50
4.9	Connection detail with demountable shear connector in installed position	51
4.10	Flow of forces for the demountable bolted shear connector connection	52
4.11	Connection detail with pretensioned connector in exploded view position	53
4.12	Connection detail with pretensioned connector in installed position	54
4.13	Flow of forces for the pretensioned injected connection	55
5.1	Connection costs vs. number of reuse cycles, initial investment costs are presented at reuse cycle 0 and for every reuse cycle the reinstallation costs are added cumulative	63

6.1	Slab eccentricity for the most inward and outward position on the beam flange, all dimensions in millimetres	67
6.2	Mechanical scheme for shear and bending of the SHS section; orange line is at the location of the compressive bolt, green line is located in the heart of the reinforcement bar, and the blue line at the heart of the beams bottom flange	68
6.3	Components of the hollow core slab sleeve; reinforcement is shown in orange and the sleeve concrete in pink	69
6.4	Load spreading of the compressive force, vertically (left) and horizontally (right)	70
6.5	Components of the connection; shear stud is shown in blue, SHS section in orange, adjustment bolt in pink, and the mortar in yellow	71
6.6	Bottom plate principle	75
7.1	Rotations in the connection	78
7.2	Shear force and bending moment distribution along the hollow core slab length	79
7.3	Isometric view of connection modelled in IDEA StaTiCa	80
7.4	Rotation of an unhindered integrated edge beam with contact stresses shown	80
7.5	Bolted shear connectors in various configurations [75]	82
7.6	Results of the push-out test performed by Pavlovic et al. [75]	83
7.7	Compressive top plate in cross sectional and isometric view	84
7.8	Forget me knots for connection stiffness	84
7.9	Cropped top view of the integrated beam with mobilised area for flange bending (A), all dimensions in millimetres	85
7.10	Connection behaviour due to slip of the bolted shear connector (s), and deformation of the compressive plate (w)	85
7.11	Isometric view of the integrated beam with the top plate and stiffener plate	86
8.1	Schematization of the experimental setup	89
8.2	Application of different treatments to the specimens	90
8.3	Mixing and pouring procedures of phase II	91
8.4	Specimens during preparation and testing	92
8.5	Specimens during manual demolition	93
8.6	Plot of displacement vs. force for untreated specimens (U), lines are adjusted to start at same point (1 kN of compression)	94
8.7	Plot of displacement vs. force for oil-treated (O) specimens, lines are adjusted to start at same point (1 kN of compression)	95
8.8	Plot of displacement vs. force for Vaseline-treated (V) specimens, lines are adjusted to start at same point (1 kN of compression)	96
8.9	Plot of displacement vs. force for untreated (U), oil-treated (O), and Vaseline-treated (V) specimens. Lines are adjusted to start at same point (1 kN of compression)	97
8.10	Plot of the initial part of displacement vs. force for untreated (U), oil-treated (O), and Vaseline-treated (V) specimens. Lines are adjusted to start at same point (1 kN of compression)	97
8.11	Bonded piece of mortar (U4)	98
8.12	Mortar specimens after hand demolition	99
9.1	Environmental impact assessment, step by step	101
9.2	LCA stages [64]	103
9.3	Environmental Cost Indicator for three lifespan scenarios, 20, 50, and 100 years for reusable and conventional design with LCA stages A1-A3 + (D)	108
9.4	Close up of the Environmental Cost Indicator for three lifespan scenarios, 20, 50, and 100 years for reusable and conventional design with LCA stages A1-A3 + (D)	108
9.5	MPG calculation for the superstructure for a life span of 30 to 70 years	110
9.6	MPG calculation for the superstructure for a life span of 30 to 300 years	110
10.1	Monte Carlo simulation with $N = 10^4$ simulations based on literature and manufacturer data (simulation 3) for a prefabricated situation with different confidence intervals (CI) of 90%, 95%, and 99% for the input variables	116

10.2	Monte Carlo simulation based on literature and manufacturer data (simulation 3) for a prefabricated situation with different number of simulations	116
10.3	Plot of the displacement vs. force for untreated (U), oil-treated (O), and Vaseline-treated (V) specimens. Lines are adjusted to start at same point (1 kN of compression)	118
A.1	Measured tolerances of the hollow core slab length, data obtained from VBI for unit 3 and 4 in 2022	127
C.1	Monte Carlo simulation with $N = 10^4$ simulations for NEN-EN class 1 and class 2 for a on site installed situation at $y = 0 = L$	139
C.2	Monte Carlo simulation with $N = 10^4$ simulations for NEN-EN class 1, class 2, and literature data for a prefabricated situation at $y = 0 = L$	140
E.1	Sensitivity analysis on the installation costs	170
F.1	HEB260 + 570x12 cross section and area division	172

List of Tables

2.1	Values for hole clearance factor k_s [20]	21
2.2	Nominal hole clearances for bolts and pins (mm) [27]	21
3.1	Tolerances of hollow core slabs for construction purposes according to NEN-EN 1168 [25] and the MNL-116 [77].	28
3.2	Maximum out-of-straightness amplitude for integrated and under-mount floor beams	29
3.3	Out-of-straightness tolerances Δ_{oos} according to [47]	30
3.4	Horizontal deviations for anchor bolts in concrete [2]	31
3.5	Overview of the Monte Carlo simulations for on site and prefabricated construction (^a only the length value is adopted from VBI, ^b no European Standard data available).	32
3.6	Variables with a normal distribution	33
3.7	Variables with a uniform distribution	33
3.8	MCS tolerance results for case study geometry and the Temporary Courthouse connection, all dimensions in millimetres	36
4.1	Floor loads	40
4.2	Roof loads	41
4.3	External pressure coefficients for zone A, B, C, D, and E according to National Annex of NEN-EN 1991-1-4 [36]	42
4.4	Combination factors ψ [30]	43
5.1	Cost overview for the resin injected design in euros per slab element	60
5.2	Cost overview for the demountable bolted shear connector design in euros per slab element	61
5.3	Cost overview for the prestressed connection design in euros per slab element	61
5.4	Trade-off matrix for the design alternatives, scoring scale from 1-5, where 1 represents the lowest possible score and 5 the highest	64
6.1	Connector loads	68
6.2	Unity check for the hollow core slab sleeve components	70
6.3	Unity checks for the connection components	74
6.4	Unity check for the beam components	76
7.1	Connection loads IDEA StaTiCa	80
7.2	Rotation results and displacements	81
7.3	Bolted connector stiffness comparison	83
8.1	Method of hand demolition	98
9.1	Materials and quantities for the main load bearing structure of the case study building as presented in Appendix B, the substructure was excluded	104
9.2	Materials and quantities for a reusable hollow core slab to beam connection, values per connector	105
9.3	Environmental Cost Indicator calculation for the demountable shear connector connection per individual connector	105
9.4	Materials and quantities for a conventional hollow core slab to beam connection, values per connector	106
9.5	Environmental Cost Indicator calculation for conventional connection per individual connector	106
9.6	ECI calculation for stage A1 to A3 for the main load bearing structure including connections and excluding substructure	106

9.7	ECI calculation for stage A1 to A3 + stage D for the main load bearing structure including connections and excluding substructure	107
9.8	Share of the beam to hollow core slab connection ECI in the total superstructure ECI .	107
E.1	Cost overview for the installation of the resin injection in euros per plate (4 connectors)	167
E.2	Cost overview for the installation of the demountable shear connector in euros per plate (4 connectors)	168
E.3	Cost overview for the installation of the pretensioned connector in euros per plate (4 connectors)	168
E.4	Cost overview for the demounting process of the resin injection in euros per plate (4 connectors)	168
E.5	Cost overview for the demounting process of the demountable shear connector in euros per plate (4 connectors)	169
E.6	Cost overview for the demounting process of the pretensioned connector in euros per plate (4 connectors)	169
F.1	Classification demands for integrated Slim Floor Beams [50]	171
H.1	Environmental Impact Categories, units, and monetisation factors	177

Nomenclature

Abbreviations

Abbreviation	Definition
ABAQUS	Finite element analysis software
ACI	American Concrete Institute
ASTM	American Society for Testing and Materials
BIM	Building Information Modelling
CEN	Comité Européen de Normalisation
CC2	Consequence Class 2
CNC	Computer Numerical Control
CI	Confidence Interval
DEMU	Cast in anchors with connecting possibilities
DIN	Deutsches Institut für Normung
ECCS	European Convention for Constructional Steelwork
EC	Eurocode
ECI	Environmental Cost Indicator
EN	European Norm
EPD	Environmental Product Declaration
FEA	Finite Element Analysis
HVAC	Heating Ventilation Air Conditioning
IDEA StaTiCa	Finite element analysis software for connection analysis
ISO	International Organization for Standardization
LCA	Life Cycle Assessment
LVDT	Linear Variable Differential Transformer
MCS	Monte Carlo Simulation
MPG	MilieuPrestatie Gebouwen
NEN	Netherlands Standardization Institute
PPU	Price Per Unit
SHS	Square Hollow Section
SFB	Slim Floor Beam
SRR	Steel-Reinforced Resin
THQ	Top Hat Q beam
UTM	Universal Testing Machine
VAT	Value Added Tax

Latin symbols

Symbol	Definition	Unit
A	Area	$[\text{mm}^2], [\text{m}^2]$
A_s	Bolt shear area	$[\text{mm}^2]$
A_{rf}	Roof area of the case study building	$[\text{m}^2]$
A_{fl}	Floor area of the case study building	$[\text{m}^2]$
b	Shear stud eccentricity measured from beam heart	$[\text{mm}]$
b_u	Width between bearing points of the bottom flange	$[\text{mm}]$
c	Concrete cover	$[\text{mm}]$
c_b	Dimension of the bolt head measured over the angles	$[\text{mm}]$

Symbol	Definition	Unit
$c_{pe,10}$	External wind pressure coefficient (global analysis)	[-]
$c_{pe,1}$	External wind pressure coefficient (local analysis)	[-]
D	Length of case study building	[m]
d	Bolt diameter	[mm]
d_0	Bolt hole diameter	[mm]
e	Connection eccentricity	[mm]
e_1	Width of the bottom flange	[mm]
e_2	Width of the bottom plate	[mm]
$F_{b,Rd}$	Design bearing resistance of the bolt	[kN]
F_h	Horizontal load in the connection	[kN/m ¹]
$F_{h,Ed}$	Design horizontal load on the connection	[kN]
$F_{h,d,s}$	Horizontal load for the bolted shear connector	[kN]
$F_{h,d,u}$	Horizontal load for the upper compressive bolt	[kN]
f_{cd}	Design value of the compressive resistance of the mortar	[MPa]
f_{ck}	Concrete characteristic strength	[MPa]
f_{ub}	Ultimate tensile strength of the bolt material	[MPa]
f_u	Ultimate strength of construction steel	[MPa]
f_y	Yield strength of construction steel	[MPa]
f_{yb}	Yield strength of bolt steel	[MPa]
G_k, g_k	Permanent loads	[kN/m ¹], [kN/m ²]
H_i	Storey height of case study building, index $i = 1 - 3$	[m]
h	Height	[mm]
h_{plate}	Compressive plate height	[mm]
h_{sc}	Height of shear stud	[mm]
I_y	Area moment of inertia in the y-axis	[mm ⁴]
k_1	Bearing resistance parameter	[-]
k_2	Bolt reduction factor for tensile resistance	[-]
k_b	Factor accounting for edge distance and spacing	[-]
k_1	Factor for bearing resistance	[-]
l_{bd}	Reinforcement anchorage length	[mm]
L_i	Slab span of case study building, index $i = 1 - 3$	[m]
$M_{c,Rd}$	Design bending moment resistance	[kNm]
$M_{pl,y,Rd}$	Design plastic longitudinal bending moment resistance	[kNm]
N	Newton (unit of force)	[1 kg*m/s ²]
$N_{b,Rd}$	Design buckling resistance of the adjustment bolt	[kN]
$N_{c,Rd}$	Design compressive resistance of the mortar	[kN]
P	Load cell load	[kN]
P_b	Bearing load on the bolt	[N]
P_{rk}	Characteristic resistance shear resistance of a bolt	[kN]
P_t	Tensile load in the bolt	[N]
P_u	Ultimate load applied to the bolt	[N]
P_u	Ultimate shear capacity of a dowel	[kN]
q	Total factored beam load	[kN/m ¹]
Q_k, q_k	Variable loads	[kN/m ²]
r	Tolerance radius	[mm]
r_μ	Mean value of tolerance radius	[mm]
r_σ	Standard deviation value of tolerance radius	[mm]
S	Sample standard deviation	[-]
t_f	Thickness of the flange	[mm]
t_u	Thickness of the bottom flange	[-]
W	Width of case study building	[m]
W_{pl}	Plastic section modulus	[mm ³]

Symbol	Definition	Unit
$W_{pl,y}$	Plastic section modulus for longitudinal bending resistance	[mm ³]
z_1	Internal lever arm	[mm]
\bar{X}	Sample mean	[-]
q_p	Peak velocity wind pressure	[kN/m ²]

Greek symbols

Symbol	Definition	Unit
α	Statistical division parameter, range 0 - 1	[-]
α_b	Bearing resistance parameter	[-]
β	Statistical division parameter, range 0 - 2	[-]
β_{rel}	Beam classification parameter	[-]
δ_1	Displacement of the beam's upper side due to torsion	[mm]
δ_2	Displacement of the hollow core slab's upper side due to global bending	[mm]
δ_3	Displacement of the hollow core slab's upper side due to bottom flange bending	[mm]
γ_G	Partial safety factor for permanent loads	[-]
γ_{M0}	Partial safety factor	[-]
γ_{M1}	Partial safety factor	[-]
γ_{M2}	Partial safety factor	[-]
γ_Q	Partial safety factor for variable loads	[-]
μ	Mean value	[-]
ν	Poisson factor	[-]
σ	Standard deviation	[-]
σ_{sd}	Stress on reinforcement bar	[MPa]
$\sigma_{c,Ed}$	Design concrete compressive stress	[MPa]
σ_{sd}	Stress on reinforcement bar	[MPa]
ϕ_1	Rotation of the beam due to torsion	[rad]
ϕ_2	Rotation of the hollow core slab due to global bending	[rad]
ϕ_3	Rotation of the bottom flange due to local bending	[rad]
χ	Buckling reduction factor	[-]
χ_{rel}	Beam classification parameter	[-]
ψ	Longitudinal bending resistance reduction factor	[-]
ψ_0	Load factor	[-]
ψ_1	Load factor	[-]
ψ_2	Load factor	[-]
ρ	Volumetric mass density	[kg/m ³]
σ	Standard deviation	[-]
ζ	Out-of-balance parameter	[-]
Δ_{bs}	Tolerance requirement for beam spacing	[mm]
Δ_{cloc}	Tolerance requirement for column placement	[mm]
Δ_{ci}	Tolerance requirement for column inclination	[mm]
Δ_{cs}	Tolerance requirement for column spacing	[mm]
$\Delta_{hcs,l}$	Tolerance requirement for hollow core slab length	[mm]
$\Delta_{hcs,w}$	Tolerance requirement for hollow core slab width	[mm]
Δ_{oos}	Tolerance requirement for the beam out-of-straightness	[mm]
δ_u	Bolt slip	[mm]
Ω	Uniform distributed variable of the angle of the shear connector location	[rad]

Symbol	Definition	Unit
Θ	Uniform distributed variable of the angle of the bolt hole location	[rad]

Part I

Introduction and Literature review

1

Introduction

In the first chapter of the first part, the research topic of this master thesis is presented. The first chapter aims to familiarise the reader with the background and relevance of the topic. Subsequently, the problem is addressed, and the research objective, scope, and question(s) are described. The chapter ends with the research methodology and an outline of the report to guide the reader.

1.1. Relevance

As the world moves towards a circular economy, the building construction industry must take its responsibility. Most of the waste in the Netherlands is related to construction and demolition waste, with the industry accounting for approximately 35% of CO₂ emissions [89]. Therefore, making an impact within the construction sector can lead to significant reductions and help the European objective of achieving net-zero greenhouse gas emissions by 2050 [46].

To take this responsibility and achieve a reduction in material use, the Dutch government has set a goal of being completely circular by 2050. To do so, they presented the National Circular Economy Programme 2023-2030 [66]. The ambitions and targets are written down in an extensive document which focusses on two main goals; these goals are "From vision to policy" and "From policy to implementation". A graphical representation of the structure is presented in Figure 1.1.

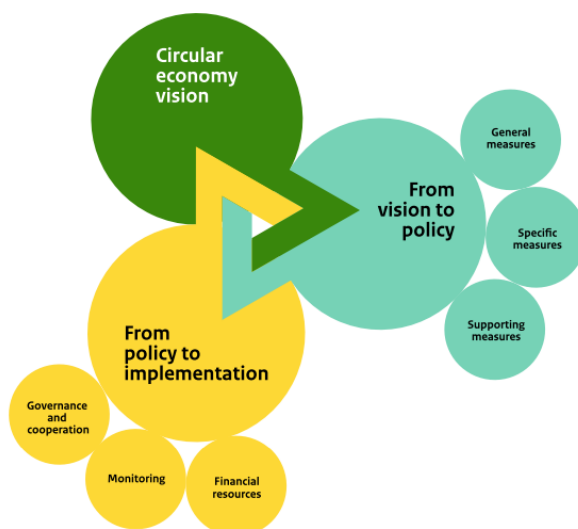


Figure 1.1: National Circular Economy Programme [66]

Within this thesis, the most important goals are specified in the general measures of the from vision to policy part. According to [66], there are four main options to become completely circular by 2050:

1. **Reducing raw material usage**, using fewer (primary) raw materials by abstaining from the production or purchase of products, sharing products or making them more efficient ('narrow the loop').
2. **Substituting raw materials**, replacing primary with secondary raw materials and sustainable bio-based materials.
3. **Expanding product lifetime**, making longer and more intensive use of products and components through reuse and repair will slow demand for new raw materials ('slow the loop').
4. **High-grade processing**. closing the loop by recycling materials and raw materials. This will not only reduce the amount of waste being incinerated or dumped, but ensure a higher quality supply of secondary raw materials ('close the loop').

What is observed from the general measures listed above is that there are various possibilities to reach the target. Within this thesis, the main focus is put on the third and fourth option; expanding product lifetime and high-grade processing. An extended lifespan can severely reduce the impact of buildings. Buildings are often demolished due to repurposing of the area or becoming unnecessary after a certain time while structural elements are still in good condition, also known as obsolescence [15]. A building can lose its function due to location obsolescence [14]. This is compared to movable goods being one of the main drivers for the demolition of buildings. The main problem is found in the fact that the design, functional, economic, and technical lifespan do not match. To deal with these types of problems, a reusable structure could be implemented, resulting in a longer life expectancy of the structure or structural elements. This enables the full potential of the structural elements which equals the technical life span. Reusable or circular constructions are made with the help of connections between structural components that are disconnected without demolition. In an ideal world, structural components are disassembled and assembled infinitely or until their technical lifespan is reached. After their final technical lifespan is reached, the components can be easily recycled due to their design, which is focused on demountability.

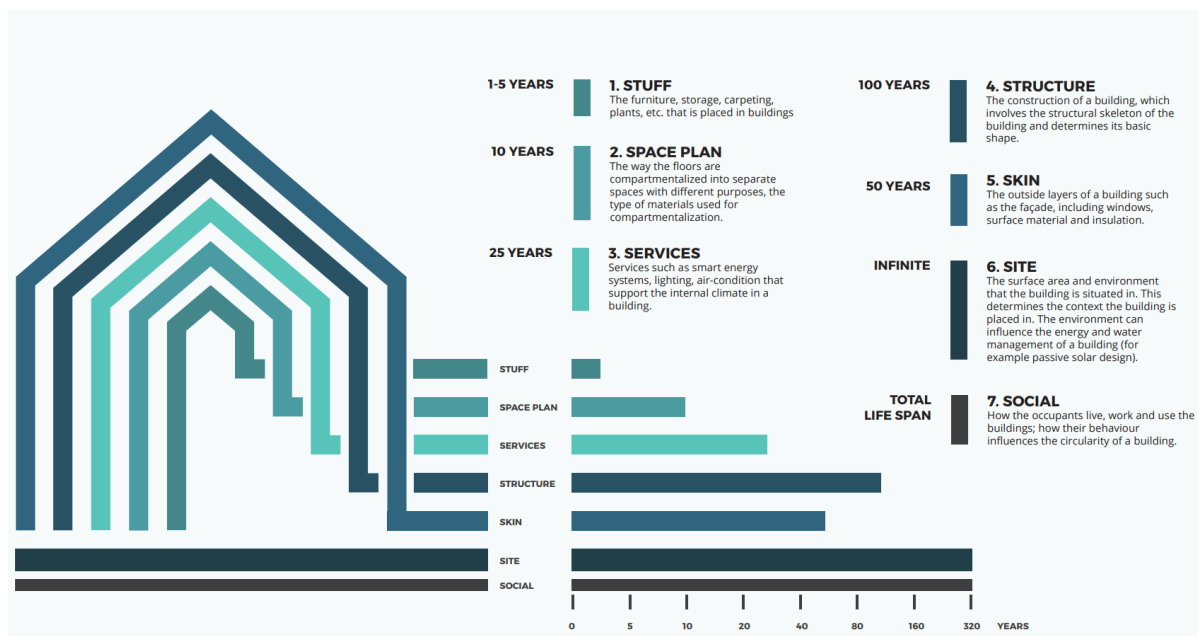


Figure 1.2: Longevity per building layer [13], adopted from [87]

To underpin the importance of the reusability of structural elements, the longevity of the various building layers according to Brand is presented in Figure 1.2. This drawing shows that according to Brand [13] the site has the longest lifespan. In theory, this is indeed true, but due to developments in the area or changes in the land use plan, the site changes more often in practice. Therefore, it could be seen

that the structure has the longest lifespan and outlives other parts such as the skin, space, services, and possibly the site. A reusable structure could solve this discrepancy between the longevities of the components.

1.2. Problem statement

As previously stated, the implementation of reusable constructions is a crucial solution to reduce the environmental impact of the building industry. For a reusable construction, materials and the construction procedure are key components to consider. On the other hand, the financial aspect plays an important role. Real estate developers are driven mainly by costs, and this often conflicts with the implementation of reusable constructions. Solving this contradictory of interest results in an increasing number of reusable structures. A possible solution is found by modifying conventional economical construction techniques to make them reusable. The first idea to implement this methodology was formed in 2016 for the temporary courthouse in Amsterdam. The design idea was to create a building that could serve as a courthouse for 5 years, after which it could be repurposed elsewhere as an office or educational building [88].

The problem with the current "reusable" connection is the absence of additional tolerances in the design. The Temporary Courthouse connection is made on-site and does not consider additional tolerances for easy installation during the reuse phase. The idea behind this connection is explained in more detail in [chapter 2](#). After a disassembling-assembling cycle, the steel structure faces tolerances due to the margins in the structural elements and the grid. This results in the fact that the floor slabs do not fit in their original positions, and additional measures should be taken. To overcome these problems, a design with significantly increased tolerances should be implemented. This would result in the fact that the structure can be reused on component level.

1.3. Scope

The type and technique of construction are key considerations when determining the scope. Construction materials and techniques depend on the type of building. Within this thesis, the non-residential buildings and residential complex buildings are considered. These buildings are generally designed with larger floor spans compared to residential buildings. For a non-residential building or residential complex building the floor system is often made out of concrete [79]. Concrete floors are often chosen due to their good acoustic behaviour and low cost. The materials most widely used for the load bearing structure are steel and concrete. A major advantage of steel construction is that steel frames can be easily adjusted to become reusable by creating bolted connections between the beams and columns. The substructure is disregarded from the research since these components are location-specific and cannot be reused. Furthermore, components such as stuff, space, services, and skin mentioned by Brand [13] and shown in [Figure 1.2](#) are excluded because the predicted longevity is significantly lower. Leaving the scope of the research to the load bearing superstructure. The main focus is put on the connections between the concrete floor slabs and the steel frames or more specific the steel beams.

Steel beams

The main choice for a steel frame structure is the advantage of easy allowance for disassembly and subsequent reuse of steel members [73]. Regarding the beam selection, two options exist; an integrated steel beam or a steel beam that is mounted below the floor slabs. The integrated floor can be made as a torsional stiff variant and a non-torsional stiff variant. Both variants have different pros and cons, and good consideration should be taken when choosing one. In [Figure 1.3](#) the different variants are shown. The main reason to use integrated steel beams instead of under-mount steel beams is the reduced storey height and the increased flexibility to place and reroute ducts, vents, and cables due to the flat bottom surface of the floor. In [Figure 1.2](#) the longevity of the services is given as approximately 25 years. This would imply that it should be replaced approximately four times before the longevity of the structure (100 years) is reached [13]. This flexibility is even more important if a structure is repurposed due to different needs and demands. The main advantage of under-mount steel beams is the centric loading of the beam; this results in fewer torsion and, subsequently, simple connections.

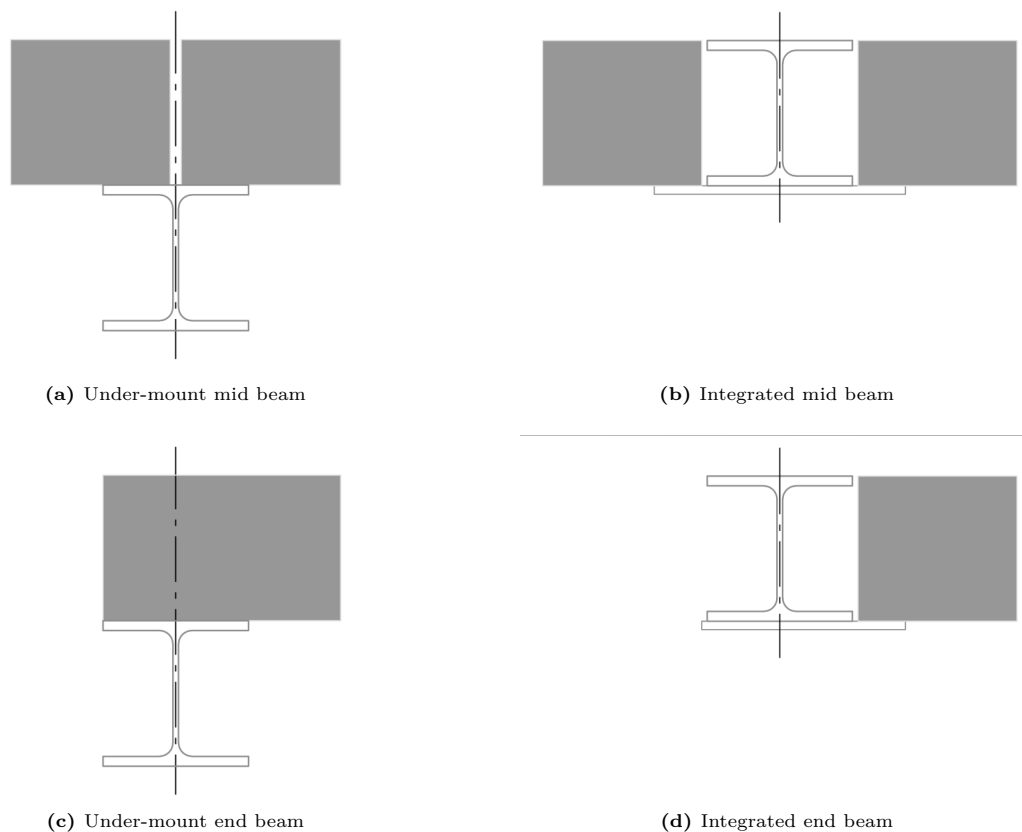


Figure 1.3: Steel beam types for prefabricated concrete floor systems in mid and end beam configuration

Concrete floors

One of the main problems in the reusability of structural components is the floor system. More specifically, the connection between the floor slabs and the beams. The most widely used concrete flooring systems are monolithic, composite, ribbed, bubble deck, and hollow core slabs. The latter of these systems is a well-known option in the design of demountable structures. Please note that a demountable structure is not necessarily reusable. The demountability potential of hollow core slabs comes from the fact that, from the slabs listed above, these are the only slabs that can be completely prefabricated and consist of smaller individual elements. Another advantage of hollow core slabs is their versatility. The hollow core slab is one of the most widely used concrete flooring systems in the Netherlands due to its easy prefabrication, good acoustic behaviour, fast assembly, large spans with relatively low self-weight and material usage compared to other floor systems [79]. Due to these properties, the hollow core slab is the preferred slab for the reusable connection development.

1.4. Research objective and question

The objective of the research is to develop a connection between a hollow core slab and a steel frame. The design should be such that the connection is easily reusable and complies with the structural requirements. An intermediate step in achieving this goal is to perform a statistical Monte Carlo simulation to determine the required level of tolerances for reusable connections. A secondary objective is to analyse the environmental impact of the reusable structure compared to conventional non-reusable structures. This is achieved by conducting an environmental impact assessment.

The main research question is formulated to answer the main research objective.

”Does the structural behaviour of a newly proposed reusable connection between a hollow core slab and a steel frame comply with structural requirements while increasing execution tolerances beyond the allowed values according to the standard?”

To answer the main research question, several subquestions must be answered. Using this method, more structured research is conducted. The research questions answered are related to three of the main parts of the thesis: the literature review, the connection design, and the connection verification.

- SQ1. What are the tolerances required to create a reusable connection between a hollow core slab and a steel frame?
- SQ2. To develop a reusable connection between a hollow core slab and a steel frame, what changes can be made in the manufacturing process?
- SQ3. What are the requirements for reusable connections with adequate tolerances?
- SQ4. What is the environmental impact of a reusable connection compared to a conventional connection?

1.5. Research methodology

This section aims to present the methodology of the research. The structure of the research is organised into several parts. The thesis consists of four parts, namely:

- Part I - Introduction and Literature review,
- Part II - Connection design,
- Part III - Connection verification,
- Part IV - Research outcome.

The structure and relations of the research are shown in [Figure 1.4](#), and detailed descriptions of each chapter are provided in the outline ([section 1.6](#)). In the figure, the different colours represent a chapter, and the complementary colours outline which chapters are within a certain part. What is observed from the figure is that the first and fourth parts are missing. The first part focusses on the introduction and review of the literature. The literature review provides input on several parts of the thesis and is linked to any part or chapter. For the fourth part, the research outcome, a similar reasoning is adopted. The research outcome analyses all chapters of the research presented.

What is observed from the diagram is that the design block has a relationship with almost every chapter. This is a characteristic of the design process, where different iterations are performed to produce the most optimal design. Feedback during, for example, the verification of stiffness and strength could result in an improvement in the design. Subsequently, this improved design is verified.

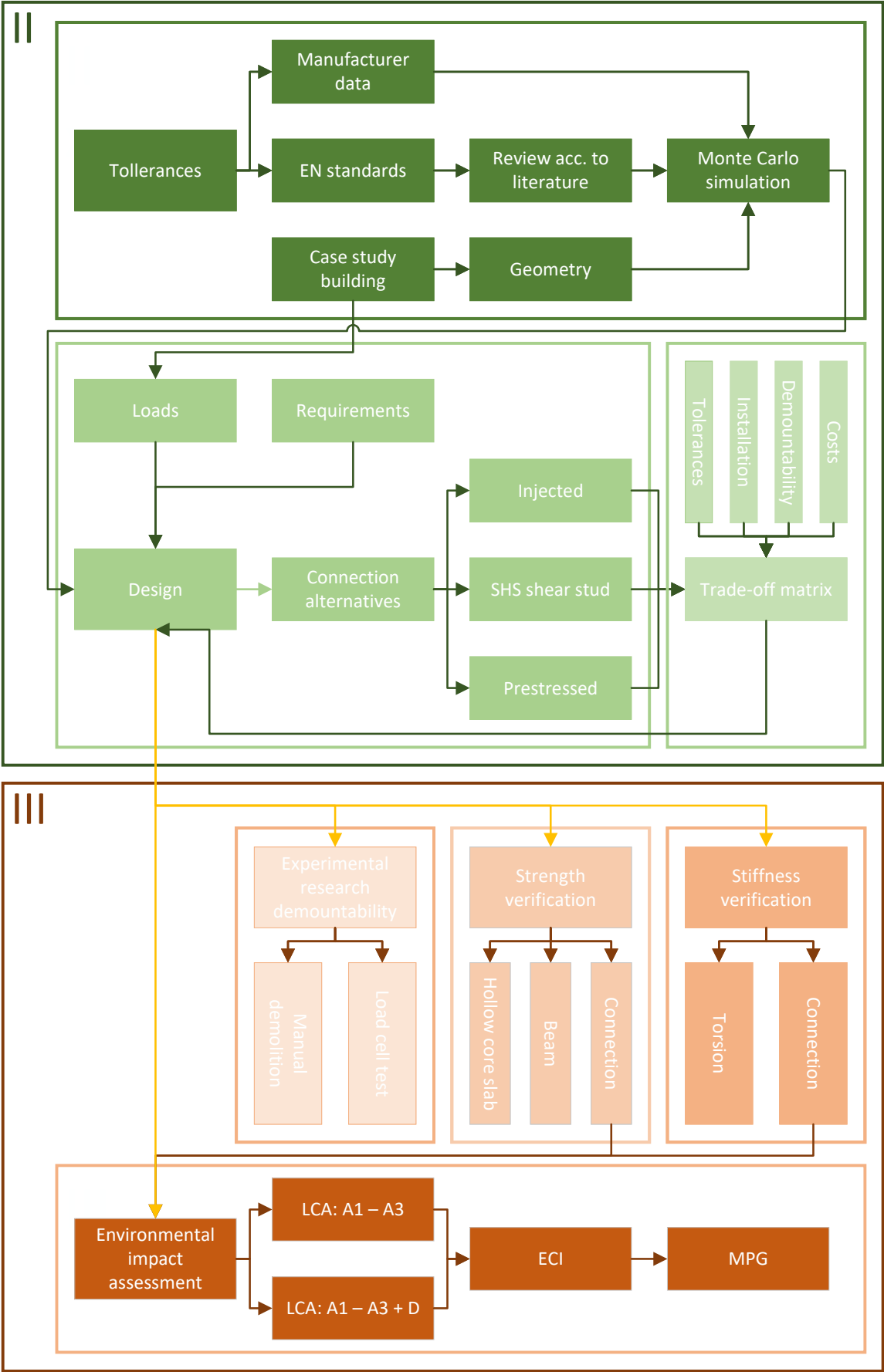


Figure 1.4: Research methodology

1.6. Outline

The structure of the research was introduced in [section 1.5](#). In this section the 11 chapters are outlined and information on the contents of the different chapters is provided.

Part I - Introduction and Literature review

chapter 1 - Introduction

The introduction shows the relevance of the research and gives a clear description of the problem. In addition to this, the goals are presented in terms of a research objective. To achieve this objective, the main and sub-questions for the research are presented. The scope is defined to narrow down the focus of the study, while the research methodology outlines the approach used to gather information.

chapter 2 - Literature review

The literature review has various purposes. First, an overview of the fabrication process and loading conditions of precast hollow core slabs is given. In addition to this, a state of the art review of the existing connections between steel frames and hollow core slabs is made. Lastly, various options are investigated to improve the design of the connection with the help of different tolerance-inclusive fasteners.

Part II - Connection design

chapter 3 - Tolerance study

The tolerance study provides an overview of the different tolerances used in the European Standards. Besides the data from the European Standards, the data from the literature and experts are investigated to narrow down the required level of tolerances for the various components. With the help of a Monte Carlo simulation, a minimum required tolerance is calculated. Various simulations are performed to account for different tolerance classes and scenarios.

chapter 4 - Design alternatives

The chapter on design alternatives comprises three main parts critical for the design of the connection. In order to develop a functional design, the initial step is to establish the requirements. Subsequently, the loads are calculated based on the geometry of the case study building but with taking in account the connector geometry as a variable. Based on the two previous steps, the calculated tolerances and the literature study three different alternatives for the connector are generated.

chapter 5 - Qualitative trade-off analysis

The alternatives in the previous chapter are weighted in the qualitative trade-off analysis. In order to make a substantiated decision on the best alternative, the design requirements of [chapter 4](#) are evaluated. This is done by means of qualitative and quantitative assessment. The outcome of the chapter is a trade-off matrix in which one of the alternatives outperforms the other two.

Part III - Connection verification

chapter 6 - Strength verification

The most favourable design of [chapter 5](#) is verified in terms of strength. The conceptual design created in [Part II](#) is optimised and the structural behaviour is verified according to the current standards.

chapter 7 - Stiffness analysis

The stiffness analysis verifies the assumed mechanical behaviour of the design and checks the stiffness of the connection. The first part of the stiffness analysis focusses on the torsional stiffness of the integrated beam compared to the stiffness of the concrete hollow core slab. The second part verifies the elements in the connection design that determine the stiffness of the connection and verifies if the resulting deformations of the floor slab are within the set boundaries.

chapter 8 - Experimental research on the demountability

In the experimental research chapter, the demountability of one of the alternatives was experimentally assessed. In the design chapter and trade-off analysis concerns were raised about the demountability of one of the alternatives. Experiments are performed to investigate the actual demountability performance of this alternative. The findings of the experiment determine whether the alternative is feasible or not.

chapter 9 - Environmental impact assessment

The chapter on environmental impact assessment evaluates the effect of the reusable design perspective compared to the traditional design. To do so, the information from Life Cycle Assessment (LCA) provided by manufacturers is collected and assessed. This LCA data are combined into an Environmental Product Declaration (EPD) and weighted against certain monetisation factors to obtain an Environmental Cost Indicator (ECI). The ECI shows the environmental costs of the connection and the entire load bearing superstructure of the building.

Part IV - Research outcome

chapter 10 - Discussion The discussion section evaluates the results obtained in terms of the interpretation, implications, and limitations of the research. All the steps of the research are thoroughly reviewed.

chapter 11 - Conclusion

The conclusions and recommendations are the final chapter of the report. In this chapter, the results obtained from the research are summarised and an overall conclusion is drawn. This is done by answering the main and sub questions. Subsequently, recommendations and optimisations are presented for further research.

resisting elements [67]. The concrete top layer made in-situ has a negative effect on the demountability performance of the structure. When the building is dismantled, the top layer has to be demolished and often the supporting frame and slab are damaged. To overcome this problem, the cast-in-situ concrete layer is removed and the system could be considered demountable. The structural performance that was dedicated to the in-situ layer; like the diaphragm working and taking compressive forces induced by bending moments, is transferred via various measures. These measures include additional reinforcement bars in the sleeves of the hollow core slab, the enclosure of the slabs by the floor beams, and an increased thickness of the hollow core top flange.

2.1.1. Manufacturing process

Understanding the production process of hollow core slabs is crucial for the design of a new reusable connection. Research of the production process results in an increased understanding of possible modifications to the hollow core slab. For existing processes, it is necessary to understand that the amount of time it takes to produce is the most crucial factor. Faster production of the hollow core elements increases the production plants' capacity, which goes hand in hand with the turnover. This results in the usage of early-strength concrete.

For the fabrication of hollow core slabs, there are several methods. Traditionally, slabs were made using a dry casting technique. This technique uses a steel mould of a specific length and the cores are made using steel moulding pipes inside the slab. Due to several limitations in terms of labour intensity, operating speed, and flexibility, this method is barely applied nowadays. Instead, the most widely used fabrication methods are slip forming and extrusion [54]. Both methods use steel pallets or beds that are up to 200 metres in length. Before concrete is poured, a release agent is sprayed on the steel formwork and the prestressing strands are stretched. The location, amount, and type of prestressing strands are determined by the length of the slab and the intended load. After the strands are prestressed with the use of hydraulic cylinders, the hollow core slab is casted with an extruder or slipformer. To conclude, the prefabrication process of hollow core slabs is completely standardised and automated; this results in the fact that changes in the process are highly undesirable. Implementing components for a demountable connection would therefore be difficult, costly, and time consuming. Nevertheless, modifications to the slabs are possible afterward. This includes opening sleeves, drilling holes, and creating openings. These points should be taken into account when creating a new connection design. In a future scenario where the connection becomes an industry standard, the production process might be altered. This can be seen in the fact that the hollow core slabs from VBI can nowadays be ordered with Hilti HUS3 cast-in anchors. Implementing this on the production line was initially undesirable, but the high demand forced the manufacturer to change the production process and invest in additional machinery.

2.1.2. Loading conditions

Vertical loads

The main function of the slab is to transfer vertical surface loads to adjacent beams. Surface loads in residential, social, commercial, and administration buildings consist of dead loads (self-weight and permanent) and imposed loads. The self-weight is dependent on the thickness of the slab and the number of reinforcement strands. The self-weight varies from 268 kg/m² up to 490 kg/m² for a slab thickness of 150 mm to 400 mm respectively [90]. Permanent loads are nonstructural elements that are permanently present. The imposed loads are related to the type of building, in [Figure 2.2](#) an overview of the surface loads for the global effects and nodal loads for the local effects are shown.

Table 6.2 - Imposed loads on floors, balconies and stairs in buildings

Categories of loaded areas	q_k [kN/m ²]	Q_k [kN]
Category A		
- Floors	1,5 to <u>2,0</u>	<u>2,0</u> to 3,0
- Stairs	<u>2,0</u> to 4,0	<u>2,0</u> to 4,0
- Balconies	<u>2,5</u> to 4,0	<u>2,0</u> to 3,0
Category B	2,0 to <u>3,0</u>	1,5 to <u>4,5</u>
Category C		
- C1	2,0 to <u>3,0</u>	3,0 to <u>4,0</u>
- C2	3,0 to <u>4,0</u>	2,5 to 7,0 (<u>4,0</u>)
- C3	3,0 to <u>5,0</u>	<u>4,0</u> to 7,0
- C4	4,5 to <u>5,0</u>	3,5 to <u>7,0</u>
- C5	<u>5,0</u> to 7,5	3,5 to <u>4,5</u>
category D		
- D1	<u>4,0</u> to 5,0	3,5 to 7,0 (<u>4,0</u>)
- D2	4,0 to <u>5,0</u>	3,5 to <u>7,0</u>

Figure 2.2: Imposed loads for residential (A), office (B), congregate (C), and shopping areas (D) [19]

The vertical imposed loads should be placed so that the most unfavourable loading condition is generated. Different checks require different loading conditions; for example, the deflection and bending moment capacity of the beams are checked when all floor fields are fully loaded. For the torsional resistance of the beam, the situation when one side of the beam is fully loaded and the other completely unloaded is the most critical.

Horizontal loads

Besides the vertical imposed loads, the slabs also have to transfer horizontal loads generated by the wind load and the column inclination imperfection. This is done by the so-called "diaphragm working". The hollow core slabs work together as one slab and transfer the shear forces to the vertical resisting elements by shear stresses along the longitudinal joints in between the individual plates. In Figure 2.3 the load distribution under wind loading conditions is shown. In this figure, the vertical resisting elements are shear walls, but within the scope of the thesis, these are replaced by columns in combination with in-plane bracing elements.

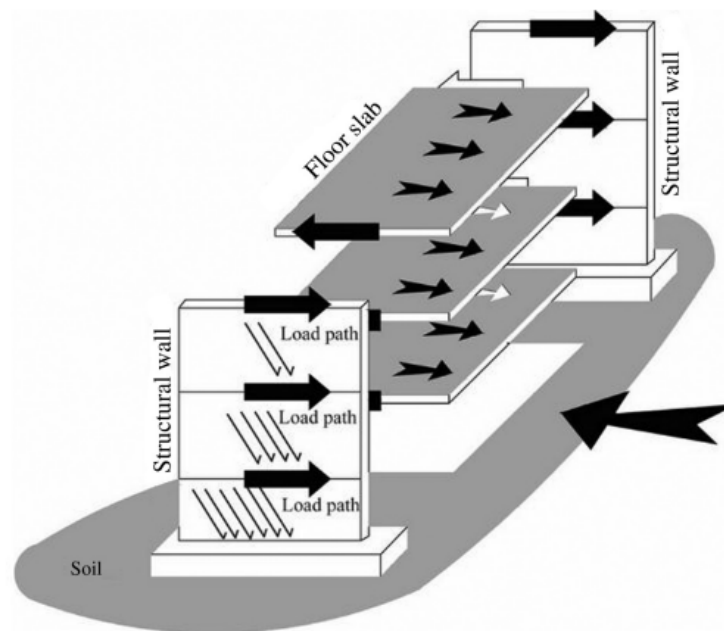


Figure 2.3: Diaphragm working with load distribution method [7]

2.2. State of the art: demountable connections

To make the floor system demountable and minimise floor height, the in-situ compressive layer can be integrated into the hollow core slab in combination with an integrated beam. Possible integrated beam options are a Top Hat Q beam (THQ), a Slim Floor Beam (SFB), or an Integrated floor beam (IFB). For the situation without a compressive layer, lateral loads are transferred in the form of shear forces along the longitudinal joints of the slabs. These joints are usually filled with grouting mortar to ensure that the diaphragm functions properly. A disadvantage of integrated beams is that they are loaded eccentrically, and the torsional moments introduced by this eccentricity must be transferred by the steel elements or by the concrete slab. In the situation where the torsional load is taken by the steel elements, the beam should be designed so that it can withstand torsion. Besides the torsional capacity of the beam, the beam-to-column connections need to be sufficiently rigid. If both design checks are satisfied, the bottom flange of the integrated beam acts as a pure hinge and solely the loads from diaphragm working should be transferred. The other option is to introduce these torsional moments back into the slab. The prestressed concrete slab acts as a rigid plate and can easily handle the magnitude of the loads. However, a specialised connection between the components is needed. Traditionally seen, for non-reusable design the second option is chosen. The connection is ensured by opening up 2 of the hollow cores and adding reinforcement bars and concrete. This ensures the transfer of the torsional moments and the so-needed diaphragm working of the slab.

At the moment, two demountable or in theory even reusable structures with hollow core slabs and steel beams have been engineered. The constructions are listed below:

- Agro NRG building by VBI;
- Temporary courthouse Amsterdam by IMd Raadgevende Ingenieurs.

Both beam-to-floor connections for these two buildings have a different design perspective and accompanying pros and cons. In the following paragraphs, more in-depth details and design visions are explained.

2.2.1. Agro NRG building

For the connection designed by hollow core slab producer VBI, the reinforcement that is normally located in the cores is placed in the longitudinal mortar joint. The detail is shown in [Figure 2.4](#).

The feasibility of the [Figure 2.4a](#) connection is under discussion due to the fact that its eccentricity should be transferred by a single reinforcement bar (labelled with number 2 in [Figure 2.4a](#)) per slab with a minimal lever arm. The traditional connection consists of two reinforcement bars and an increased lever arm. Due to the geometry of the longitudinal joint in combination with the concrete cover, the lever arm is limited for the design of [Figure 2.4a](#). Moreover, it is necessary to weld the reinforcement bars to the THQ beam, which typically has slender webs. Resulting in additional measures to redistribute the stresses. An option to solve this is to increase the thickness of the web and add steel plates inside the beam. Another disadvantage of this solution is that it would still use grout pouring and the demolition of the connection afterwards.

The other scenario shown in [Figure 2.4b](#) is when the beam is below the floor slab. In this case, the longitudinal reinforcement bars need to be continuous. This detail is executed for the Agro NRG building in Ootmarsum. Due to the almost centric loading of the beam the torsional moments are substantially smaller. With the smaller loads, this simple connection is feasible.

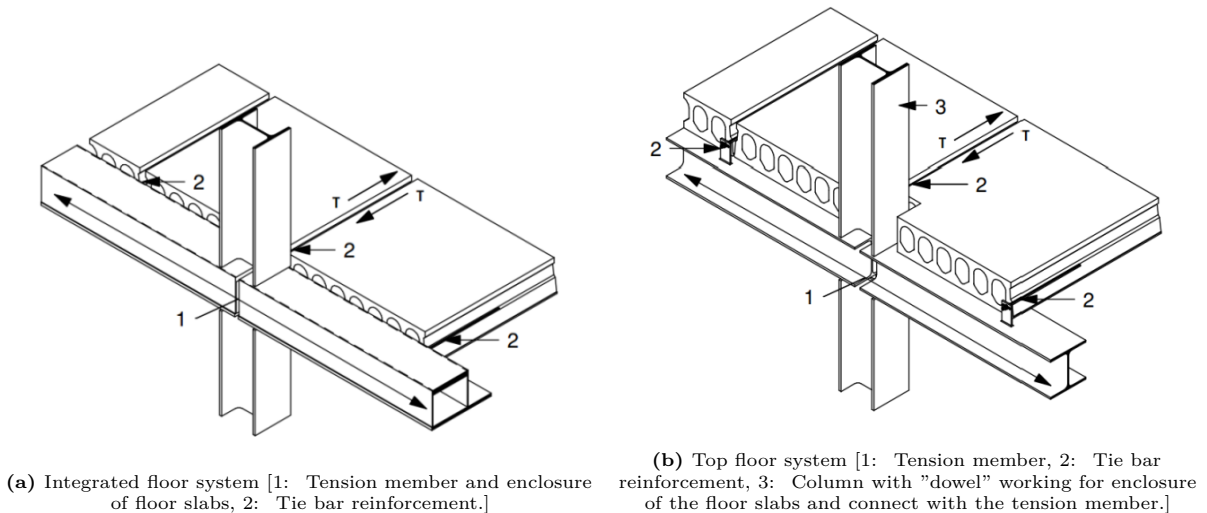


Figure 2.4: hollow core slab connection Agro NRG VBI [16]

To conclude, only the option shown in [Figure 2.4b](#) is feasible and a connection still exists of a wet mortar joint that must be demolished before dismantling the structure. Therefore, the bonding of the mortar should be limited, and close attention should be paid when making these joints. Classifying this connection as reusable is debatable due to the number of steps that would be involved in carrying out this procedure. In addition, the Dutch building industry is highly dependent on the certification of construction elements. Demolition requires recertification of the structural elements. This is a time-consuming and costly procedure. Therefore, a connection without demolition requires fewer checks and simpler recertification.

2.2.2. Temporary courthouse Amsterdam

The solution in the temporary courthouse in Amsterdam is shown in [Figure 2.5](#). It is more complex than the VBI connection, and this also means that it is more expensive. The connection works by bolting the hollow core slab to the widened bottom flange of a THQ, SFB or IFB. To do so, a DEMU anchor is cast in two of the cores, and the bolt is connected through the bottom flange into the threaded part of the DEMU. In addition to this, an end plate is added and some nuts with adjustable bolts are welded to the beam. This creates a tight fit and allows the connection to take moments due to eccentricity, uneven loading (torsion), and wind loads. In this design, the beams do not have to take the torsional moments.

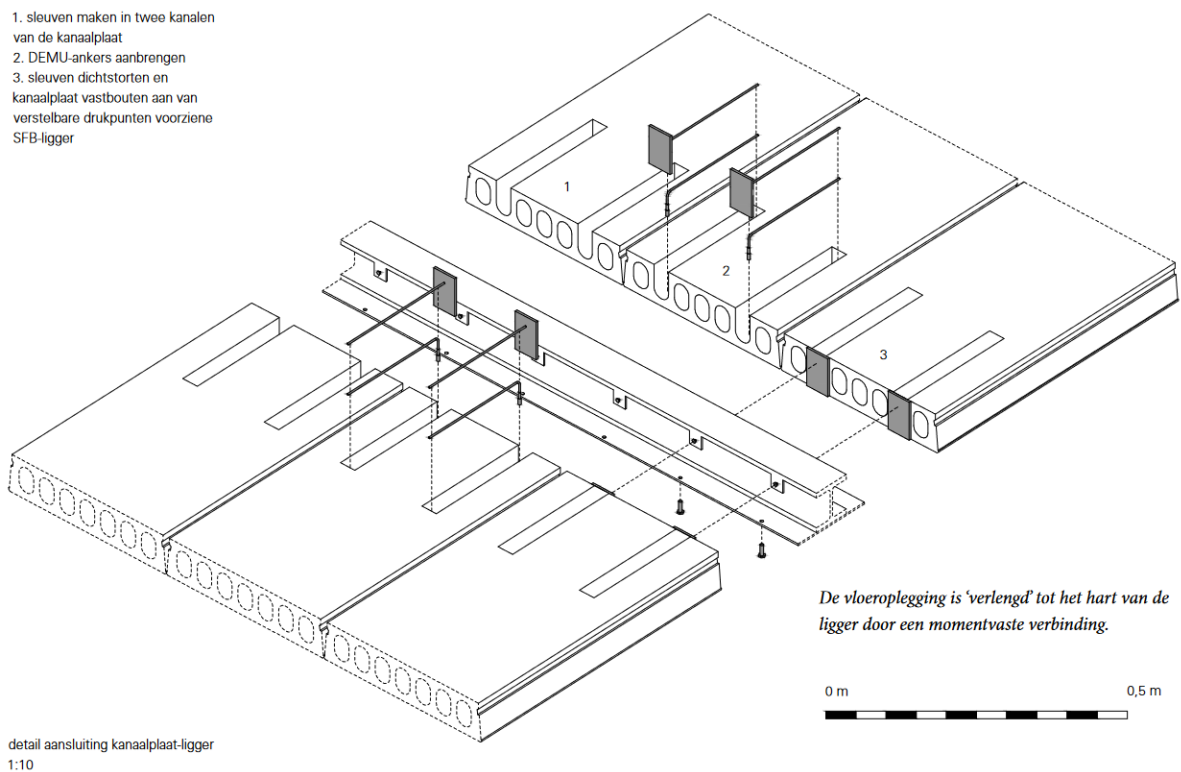


Figure 2.5: Hollow core slab connection temporary courthouse Amsterdam [39]

The fact that the anchors were cast in after the bolt was connected to the flange made it possible to use standard bolt hole clearances. To improve this design, an idea is to use oversized holes in combination with an injection of epoxy resin. At the current stage, no feasibility study has been conducted.

2.3. Tolerances

The complexity of the connection design is mainly determined by having sufficient tolerances included in the design. Having sufficient tolerances can improve the speed of erection due to the absence of additional bracing structures. To design an improved connection, a tolerance study is necessary. The magnitude of the tolerances is determined by the geometric and dimensional tolerances. Dimensional deviations concern the variation of a given dimension at a fixed point in space, whereas geometrical deviations are related to the variation of positions [70].

Tolerances for steel structures are stated in Annex B of the EN 1090-2 [27] and for the hollow core slabs the demands are stated in EN 1168 [25]. For the analysis, the following tolerances are taken into account:

- Tolerances in the structural grid;
- Tolerances in the hollow core slab;
- Out-of-straightness of the structural member;
- Bolt hole location in the beam;
- Connector location in the hollow core slab;
- Slip due to elastic deformations (self-weight).

The connection shown in subsection 2.2.2 does not consider additional tolerances on top of the standard tolerance included in the bolt hole. The prefabricated steel structure was erected and subsequently the hollow core slabs were placed. The connections were made and then fresh mortar was poured into the sleeves on the construction site. This connection deals with product tolerances, but execution and reassembly tolerances are neglected. Reassembly of the structure may result in alignment-related problems.

In the literature studies, tolerances are investigated. This study is carried out on the basis of EN and ISO standards and input from the building partners involved. The following partners are involved in the building process:

- Hollow core slab manufacturer;
- Steel structure manufacturer;
- Main contractor.

As a result, a statistical analysis can be performed to determine the desired tolerances. This could be done with a Monte Carlo simulation, which is a simulation to model the probability of different outcomes that cannot be predicted due to the intervention of random variables [59]. The simulation assigns variables to random values and multiple analyses are performed. As a result, a large scatter of the results is averaged. Based on this average an estimate of the required tolerances is made.

Eventually, two possibilities exist to deal with the required tolerances. First, the design could accommodate the required level of tolerances that come from the Monte Carlo simulation. Another possibility is to provide more strict building regulations; this would limit the level of tolerances needed in the connection. In the end, the design could be made by accommodating the necessary tolerances, limiting the necessary tolerances, or a combination of both options.

2.4. Tolerance inclusive fasteners

To deal with the various tolerances presented in the previous section, tolerance inclusive fasteners can be applied. The state of the art in tolerance inclusive fasteners prescribes two main types: injected and friction grip bolted connections. For both connections, tolerances are included by creating an oversize in the bolt hole. The critical part is the transfer of shear forces; for the alternatives, the method of force transfer differs. Injected bolted connections are based on the principle that the void between the oversized bolt hole and the bolt is filled with a resin. As a result, a bearing load transfer mechanism is created. Friction grip bolts are a pretensioned connection in which the resistance originates from the friction resistance generated by the clamping package. In the following subsections, the characteristics, main advantages, and disadvantages are presented.

2.4.1. Injection bolts

Oversized bolt holes in combination with an injection can play an important role in designing a reusable connection. The concept of using injection bolts was first developed in the 1970s to replace riveted connections in existing (railway) bridges [49]. Nowadays the application of injection bolts can be seen mostly in large infrastructural objects. Since the technique has proven itself over the past several decades, it can be considered a safe technology. Within the building sector, injection bolts are not commonplace, but within this research, the application of oversized holes in combination with an epoxy injection can accommodate the necessary additional tolerances without compromising structural behaviour. As mentioned above, the application of injection bolts is wider and, therefore, extensive research has been performed on the application of injection bolts. The master thesis of Nijgh [69] focusses on the type of injection material. For this, the strength, stiffness, creep, and demountability of the material are reviewed. Furthermore, the application of shot-reinforced resin-injected connections was investigated and showed positive results with high load capacity and low connection slip.

Material behaviour

For the injection of bolt holes, the most widely used material is a 2-component epoxy. The most widely used resin is RenGel®SW404, which can be used with 2 different hardeners, Ren®HY 2404 or Ren®HY 5159. The 2-component injection material is the only one approved by the Dutch Ministry of Infrastructure and Water Management [76]. The advantage of the latter hardener is a longer pot life and a higher maximum temperature for deflection. Both components have been on the market for a longer period of time, but were previously sold as Araldit. The material behaviour of the injection material is important; a bolt that is placed in a fitted bolt hole has the possibility of having a maximum instantaneous slip between 1 and 3 mm depending on the diameter of the bolt and initial positioning. After this, the bolt shaft is in direct contact with the steel element and the slip is very limited due to the low compressibility of the steel parts. The compressibility of a material can be expressed by the

bulk modulus; this modulus is the pressure-to-strain ratio as shown in Equation 2.1. In this equation, ρ represents the mass density, V_0 the initial volume, and V_n the volume after compression.

$$\text{Bulk modulus} = K = \frac{\rho}{(V_0 - V_n)/V_0} \quad (2.1)$$

The bulk modulus is directly related to the modulus of elasticity and the Poisson coefficient. The resin has an elasticity modulus of about $E = 9.9.5$ GPa and a Poisson of $\nu \approx 0.3$, resulting in a bulk modulus of $K \approx 7.5$ GPa [69]. However, these values are related to an unconfined loading condition; in practice, the resin is enclosed and a confined condition is ensured. In the paper of Pedrosa [76] tests were performed for resin-injected and steel-reinforced resin (SRR) injected material under confined and unconfined conditions. The results of these tests are shown in Figure 2.6.

Property		Resin		Steel-reinforced resin	
Components		RenGel® SW 404 + Ren® HY 5159		[RenGel® SW 404 + Ren® HY 5159] + Steel shots	
Density [g/cm ³]		1.86		5.26	
Poisson's ratio [-]		0.315		0.220	
Stiffness [GPa]	Unconfined	7.8		21.9	
	Confined	11.6		29.8	
Drucker-Prager model	φ [°]	25		65	
	c [MPa]	39.8		21.7	
	β [°]	35.42		54.28	
	K [-]	0.778		0.778	
	ψ [°]	35.42		54.28	
Hardening law		<u>True stress [MPa]</u>	<u>True plastic strain [-]</u>	<u>True stress [MPa]</u>	<u>True plastic strain [-]</u>
		125.0	0.0000	135.0	0.0000
		120.0	0.0115	136.2	0.0039
		115.0	0.0395	130.0	0.0074
		110.0	0.0895	100.0	0.0154
		106.0	0.1895	20.0	0.0354

Figure 2.6: Material properties of Rengel®SW404 with Ren®HY 5159 in confined and unconfined conditions for resin injected and steel-reinforced resin-injected material [76]

What can be observed from this research is that the confined modulus of elasticity of the tests is approximately 20% higher than the value used by Nijgh [69] and originates from the manufacturer's data. Another interesting observation is that the Poisson coefficient of the SRR is lower ($\nu_{\text{SRR}} = 0.220$) than the two constituents ($\nu_r = 0.315$, $\nu_s = 0.3$). Despite the higher modulus of elasticity, epoxy resin still has a significantly lower bulk modulus compared to construction steel ($K = 175$ GPa). This implies a higher compressibility of the material and a larger connection slip.

Besides instantaneous behaviour such as compressibility, time-dependent behaviour, such as creep affects relative displacement. For a standard Category A connection, specified in NEN-EN 1993-1-8 [20] that transfers through bearing, slip movement is allowed. Adding an injection bolt limits slip and is therefore beneficial in terms of structural performance. However, the injected-bolted connection suffers from time-dependent effects such as creep. The creep of resins is generally large and therefore should be investigated thoroughly. In Figure 2.7 a graphical representation of the movement of an injection bolt is shown in a fitted hole. For use in a reusable structure, the diameter of the bolt hole is significantly larger than that of a fitted hole, and the creep effects can be more severe.

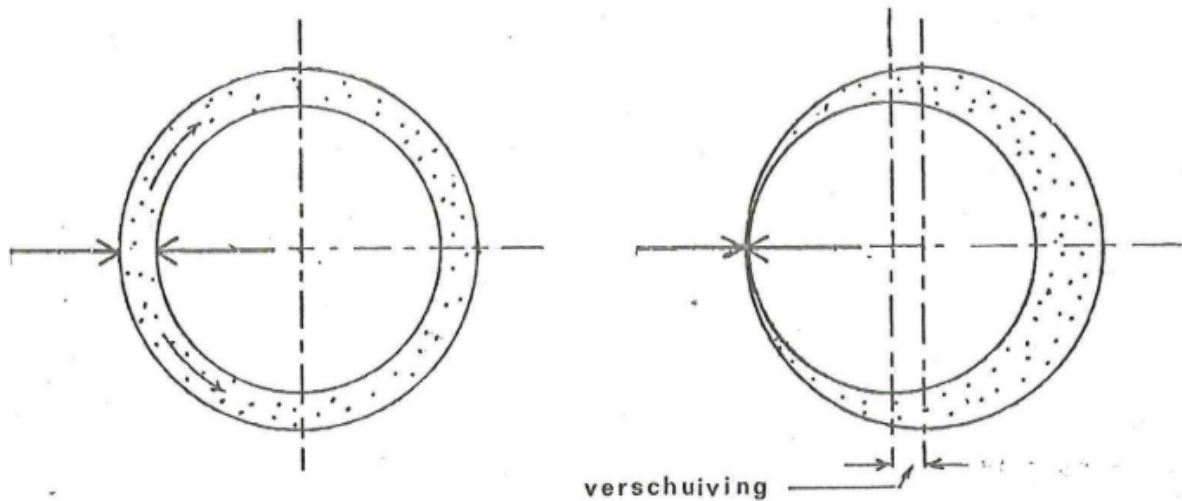
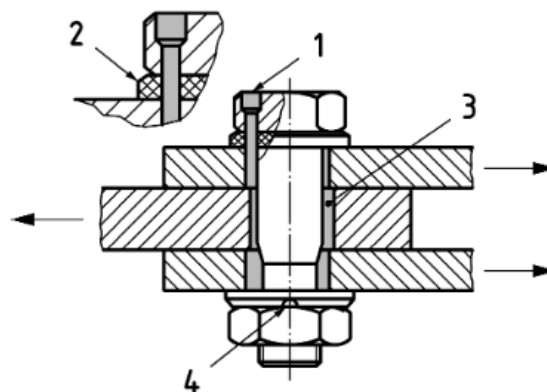


Figure 2.7: Creep displacement of epoxy resin (verschuiving {nl} = displacement {en}) [12]

Installation

The installation of resin-injected bolts is described in Annex J of NEN-EN 1090-2 [27]. The information in the code is based on a nominal hole clearance of 3 mm, for the application of larger hole sizes, no recommendations are provided. In Figure 2.8 an overview of a double-lap injected connection is shown.



Key

- 1 injection hole
- 2 chamfered washer
- 3 resin
- 4 air escape groove in the washer

Figure 2.8: Injection bolt in a double lap joint [27]

The bolt that is used can be any of class 8.8 or 10.9. During installation it is always necessary to first tighten the bolt; this is a similar procedure to what would be done within an uninjected connection. For pre-tensioned injected connections, the same sequence applies. Since full injection of the cavity is desirable, a special washer is applied. This washer has an air escape channel and ensures proper injection. In case another type of connection is used, close attention should be paid to this detail.

Design resistance

The design resistance of an injected bolt loaded in bearing is specified in EN 1993-1-8 [20]. In Equation 2.2 the formula is given. Where k_t is a factor that takes into account the loading duration, k_s the

bolt hole clearance, d the diameter of the bolt, $t_{b,resin}$ the bearing thickness of the resin, β takes into account the thickness ratio of the connected plates, $f_{b,resin}$ the bearing strength of the resin, and γ_{M4} a partial safety factor.

$$F_{b,Rd,resin} = \frac{k_t \cdot k_s \cdot d \cdot t_{b,resin} \cdot \beta \cdot f_{b,resin}}{\gamma_{M4}} \quad (2.2)$$

The bearing strength of the resin, $f_{b,resin}$, is one of the most important factors in determining the bearing strength of an injection bolt $F_{b,Rd,resin}$. To determine the bearing strength of the resin, Annex G of NEN-EN 1090-2 [27] should be used. The first to determine the bearing strength of the resin was [12], he found that the bearing strength of the resin was dependent on the thickness ratio between the main plate and the cover plates. As the bottom limit, a value of $f_{b,resin}$ of 150 MPa was advised. Another important factor is the factor k_s , this factor takes into account the hole clearance. For a fitted hole, k_s is equal to 1.0. However, for oversized holes, the k_s factor is reduced with $1 - 0.1 \cdot m$, where m expresses the hole oversize in mm. As a result, the design bearing resistance would be equal to zero if the hole oversizing is greater than 10 mm.

Demountability

The purpose of applying resin-injected bolts to the connection is to provide demountability of the structural elements. Oversized bolt holes can account for geometric and dimensional deviations. The application of resin-injected bolts in a demountable structure was first investigated by [71] for steel-concrete composite floor systems. In the test of Nijgh [71] all structural parts were fully demounted and completely removed. The bolts can be easily unscrewed and the epoxy material is easily removed. Previous research by Smits [82] shows that the use of a releasing agent strongly improves demountability performance. Two different agents were tested, both showing that easy demountability could be accomplished; in addition to this, the research also focused on potential influences of the releasing agent. In conclusion, no significant influence was found.

Steel Reinforced Resin (SRR)

The difference between "normal" resin-injected bolt holes and shot-reinforced resin-injected is that a part of the resin volume fraction is replaced by steel shot grit. The steel shot reinforces the resin, since it is made from a material that is stiffer than the resin. In addition to the superior mechanical behaviour, the application of steel shot also has a positive influence on costs and environmental impact. Steel shot is a by-product of the steel industry; it is used to remove paints and surface contaminants. The study into demountable shear connectors performed by Kavoura [58] showed that SRR outperformed normal resin-injected bolt holes in terms of instantaneous stiffness and time-dependent deformations. In terms of shear resistance, conventional injected bolt holes scored similar to the SRR with only a marginal difference.

On the downside, the SRR show a more brittle failure mechanism which is undesirable, see [Figure 2.9](#). Furthermore, the scatter of the test results in the paper of Pedrosa [76] was large due to the heterogeneity of the material. Larger-scale research could be performed to minimise the scatter and find more adequate results.

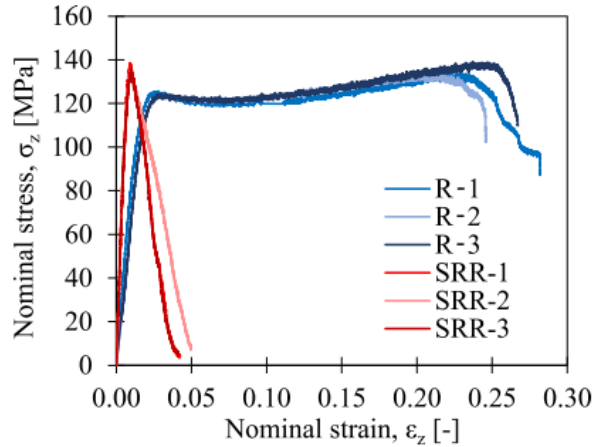


Figure 2.9: Nominal stress-strain performance for unconfined resin and steel-reinforced resin specimens [76]

Additional costs

Injected connections have additional costs compared to the bolts in fitted holes. The build-up of the additional costs can be split up into three different parts:

1. Labour costs;
2. Material costs;
3. Adaptation costs.

The labour costs are based on the additional time for the injection of the bolt. The injection time per bolt according to [43] is approximately 1 to 2 minutes, more recent research from [70] shows it is possible in approximately 30 seconds. With an estimated hourly labour rate in the Netherlands of € 80 this results in an additional cost of € 0.67 - 2.67.

Material costs for epoxy materials are fairly high; however, the amount of injected material is limited. The price of epoxy resin for Rengel@SW404 with Ren@HY 5159 is estimated to be roughly € 100 / L. This implies the following costs for an M20 bolt with 20 mm oversized hole in a 15 mm thick flange:

$$\frac{1}{4} \cdot \pi \cdot (20 + 20)^2 \cdot \frac{1}{4} \cdot \pi \cdot (20)^2 \cdot 15 = 0.014 \text{ L} \quad (2.3)$$

This results in additional material costs of € 1.40 per injected bolt. Using SRR can even lower these costs due to their volume fraction of around 60%.

For the injection connection, the bolts and washers need to be prepared. The bolts can be ordered with an injection channel, or this channel can be drilled afterwards. Special attention should be paid to ensure a perfect fit with the injection nozzle. The exact costs cannot be found but are probably not excessive. From the above cost breakdown, the conclusion can be drawn that the installation of injection bolts brings additional costs. However, if the application of injection bolts improves the percentage of reusability of the construction, these costs are negligible.

2.4.2. Friction grip bolts

Friction grip connections transfer loads, as the name suggests, through friction. Standard or injected bolted connections transfer their loads via bearing. To achieve this friction connection, high-strength (8.8 or 10.9) preloaded bolts are used to create pressure on the contact surfaces. The external shear loads are resisted by the induced friction force and there is no mechanical slip [56]. The amount of friction force that can be transferred depends on the area, the number of friction surfaces, the slip factor, and the preload force of the bolt. The slip factor, μ , differs depending on the surface treatment, where rolled surfaces have the lowest slip factor (0.20) and shot or grit blasted surfaces have the highest (0.50) [27]. The design slip resistance for a shear-loaded connection can be calculated according to Equation 2.4. Where k_s represents the hole clearance factor, n the number of friction surfaces, μ the slip factor, γ_{M3} a partial safety factor, and $F_{p,C}$ the preload force.

$$F_{s,Rd} = \frac{k_s n \mu}{\gamma_{M3}} F_{p,C} \quad (2.4)$$

The hole clearance factor, k_s , distinguishes the type of hole and the level of oversize. In [Table 2.1](#) an overview of the different values is given. For the application in a demountable structure the oversize is significant. The largest specified oversize is the long slotted hole, with a value of $1.5d$ as shown in [Table 2.2](#). When holes are more oversized than specified in [Table 2.2](#) no guidelines are provided. In other engineering industries, such as mechanical engineering, no design formulas for oversized or slotted bolt holes are used; the designs use some sort of experimental validation of the analytical results. The hole clearance factor of EN 1993-1-8 can also be seen as rather conservative and can lead to uneconomical overdimensioning [\[40\]](#). Recent research from Barelts [\[8\]](#) investigated the viability of implementing significant oversized holes in high-strength friction grip (HSFG) bolted connections, this research used an experimental setup and a 3D ABAQUS model.

Description	k_s
Bolts in normal holes.	1.0
Bolts in either oversized holes or short slotted holes with the axis of the slot perpendicular to the direction of load transfer.	0.85
Bolts in long slotted holes with the axis of the slot perpendicular to the direction of load transfer.	0.7
Bolts in short slotted holes with the axis of the slot parallel to the direction of load transfer.	0.76
Bolts in long slotted holes with the axis of the slot parallel to the direction of load transfer.	0.63

Table 2.1: Values for hole clearance factor k_s [\[20\]](#)

Nominal bolt or pin diameter ^d (mm)	12 ^a	14	16	18	20	22	24	27 to 36 ^b
Normal round holes ^c	1 ^{d e}		2				3	
Oversize round holes	3		4			6	8	
Short slotted holes (on the overall length) ^f	4		6			8	10	
Long slotted holes (on the overall length) ^f	1.5 d							

Table 2.2: Nominal hole clearances for bolts and pins (mm) [\[27\]](#)

Oversized bolt holes

Oversized bolt holes negatively influence slip resistance. To overcome this, thick cover plates or heavier washers can be used. Dorre [\[40\]](#) advises the use of heavier washers according to DIN 7349 or DIN 6340, the result of these washers in combination with long slotted bolt holes showed results for k_s near or even greater than 1.0. The DIN 7349 washers have a low relative hardness that can result in creep effects; therefore, the washers specified in DIN 6340 are preferred. Barelts experimental research [\[8\]](#) tested the use of cover plates in combination with significantly oversized bolt holes (proposed). The experiment was also compared to a set-up with fitted holes (control) and one with washers instead of cover plates (regular). The main conclusion from the experiments is that the difference between the slip of the proposed and control specimens is negligible (0.081 and 0.078 mm). The regular specimen had only a slip of 0.052 mm and this difference can be considered significant. A possible explanation for this difference is the fact that the regular specimen has fewer contact interfaces. The conclusion can be drawn that the application of significantly oversized holes in combination with thick cover plates is viable and does not affect the slip behaviour of the connection as long as the same number of contact interfaces is present [\[8\]](#).

Bolt relaxation

Another important aspect to consider is the loss of preload. Loss of preload can be divided into short- and long-term relaxation. There are various causes for preload loss according to [1], such as:

- Embedment relaxation,
- Gasket creep (if present),
- Elastic interactions,
- Stress relaxation (creep).

Short-term relaxation, like embedment relaxation, has a large effect on the preload loss. To overcome this phenomenon of contact asperity, it is recommended to retighten the bolt after 12-24 hours. In Figure 2.10 the effect of contact asperity is shown that occurs mainly in the first hours after preloading and is dependent on the number of interfaces connected by the bolt. The cause of this effect is that the stress concentrations in the imperfections exceed the yield stress of the material, and this process stops when the contact area is large enough to have a stress lower than the yielding stress of the material. The type of coating can also play an important role in this process, hard coatings such as epoxy-zinc showed better performance than their soft alkyd-based counterparts [8].



Figure 2.10: Contact asperity of steel surfaces [51]

Stress relaxation, such as creep, is more substantial in high-temperature applications [68], the increase in temperatures is decreasing the bolt stiffness. Due to creep, the bolt elongates and resulting in a loss of preload. Since the application of the bolts is in a temperature-controlled environment (inside), the stress relaxation of the bolt can be considered as not governing.

Part II

Connection design

3

Tolerance study

The first chapter of the connection design part addresses tolerances. Considering sufficient tolerances is one of the main contributors to a proper design for the reusable connection between the hollow core slab and the steel frame. An important condition for any reusable structure is the fact that the (re)assembling of the structural elements should be done without any alignment-related issues. In a conventionally designed structure, the building tolerances to guarantee this successful assembly are specified in NEN-EN 1090-2 [27]. These rules and recommendations are made so that a structure can be assembled with accepted certainty and in a reasonable time frame. A distinction in two tolerance classes can be made according to the EC standards. NEN-EN 1090-2 Annex B clause 11.3.2 prescribes the following: "Tolerance shall apply unless the execution specification specifies otherwise" [27]. This implies that, for standard design situations, Class 1 should be applied. In the case where the structure requires stricter tolerances, the decision can be made to apply Class 2 tolerances.

NEN-EN 1090-2 provides information on execution tolerances for almost all structural components; however, certain elements are not covered. For these situations, data from the American Institute of Steel Construction [3, 4], the American Concrete Institute [2, 77], and the American Society for Testing and Materials [6] provide more information on tolerances. In addition to the standards, the literature is reviewed to provide tolerances in practice. Generally speaking, the conclusion can be drawn that increasing standard tolerances can result in higher installation success and, subsequently, faster execution times. Increasing the tolerances of the standards and the literature can result in an improved success rate.

3.1. Tolerance origin and measures

The demand for tolerances arises from imperfections in fabrication and in situ deviations. In an ideal situation, tolerances are not necessary. According to Melcher [65], there are three types of initial imperfections. These can be divided into the following groups:

1. Geometrical imperfections,
2. Internal structural imperfections,
3. Construction imperfections: deviations and imperfections in the fabrication of all elements that result in the behaviour deviation of the real structure in comparison with the ideal structure.

For a structural element, there are several geometrical imperfections. The type of geometric imperfection depends on the structural element. For example, a floor beam deals with bow, sweep, or twist. Internal structural imperfections can be caused by dispersion of mechanical properties or the initial stress state. In this tolerance study, they are not taken into account because they affect material properties and not dimensional properties. Construction imperfections are mainly related to the offset or misalignment of the elements compared to the intended location; these are also referred to as dimensional imperfections by Nijgh [72]. Geometric tolerances can be divided into functional and structurally essential criteria [27]. The purpose of structurally essential criteria is to ensure that the mechanical resistance and stability of the structure are not compromised. Functional tolerances are there to ensure that the elements fit

and that their appearance is within limits. The values specified in Annex B of NEN-EN 1090-2 [27] are normative values that meet both functional and structurally essential criteria. To deal with geometric and dimensional imperfections in a reusable connection, the design can be adjusted in three different ways:

1. Increasing the tolerances in the connection design,
2. Setting stricter tolerances for the designed elements,
3. Adding more supporting structures for alignment of the elements.

All of these adjustments help with the design of a reusable connection and have their own pros and cons. As a result, either one of them or a combination of adjustments can be made. The first option requires more engineering work and a more complex connection design. A more complex connection design also has higher execution costs. The second possibility increases the costs of fabrication; the stricter tolerances require additional measures during the fabrication process. These measures result in slower fabrication and therefore higher costs of the structural elements. The latter of the possibilities affects the execution phase. Adding supporting structures decreases the speed of erection or increases the amount of manpower needed, and this eventually also affects the cost of execution. Within this thesis, the ideology is to design a connection with sufficient tolerances, so that additional structures or stricter tolerances are not necessary.

3.2. Tolerances according to standards and literature

The level of tolerances required in the reusable structure depends on three variables: the dimensions of the structure, the type of connection and the execution method. In the tolerance simulation, the first variable can be easily adjusted. Multiple analyses can be performed with various spans (in x- and y-directions), heights of the storeys, and the number of storeys. Variations in connector type are more difficult to implement. To deal with this uncertainty, the geometry of the Temporary Courthouse connection (subsection 2.2.2) is used. The concept of this connection without additional tolerances has already been proven, and therefore this connection is a good and feasible reference. The method of execution is of great importance for the required level of additional tolerances. Execution of the connections can be done in two ways, on-site or prefabricated. For the situation that a structure is rebuilt with the exact same layout, the application of on-site fabrication for the connections can have advantages. For instance, the initial out-of-straightness of a beam will not cause any problems, since this imperfection is already accounted for when creating the connection on-site. However, this method of execution reduces the speed of erection due to additional steps and more complex propping of the structure. A more standardised approach can be beneficial for the situation of reusing structural elements, and not the complete structure. In this situation, the floor elements must be compatible with multiple steel structures and vice versa. This results in a higher tolerance demand since not only fabrication tolerances should be accounted for but also initial imperfections and geometric deviations. In this research, the difference between both options is investigated, and a motivated choice should be made to choose one or the other. As a result, all tolerances in the x- and y-directions are combined and the required nominal hole clearance is quantified.

For the connection of the Temporary Courthouse the following tolerances should be assessed and included in the calculation of the nominal hole clearance:

- 3.2.1 - Tolerances in the structural grid,
- 3.2.2 - Tolerances in the hollow core slab,
- 3.2.3 - Out-of-straightness of the beam,
- 3.2.4 - Geometric deviation of the bolt-hole location,
- 3.2.5 - Geometric deviation of the connector location.

To ensure that the connector can be installed, the size of the bolt hole, d_0 should be at least:

$$d_0 = d + 2 \cdot r, \quad (3.1)$$

where d is the dimension of the bolt and r is the magnitude of the distance between the centre mark of the bolt hole and the centre mark of the shear connector. Since deviations can occur in all directions

from the centre mark, r is doubled. To calculate the magnitude of r , the tolerances in x - and y -direction are combined with the help of the Pythagorean theorem. In Equation 3.2 the combined result is shown.

$$r = \sqrt{(X_{\text{beam}} - X_{\text{slab}})^2 + (Y_{\text{beam}} - Y_{\text{slab}})^2} \quad (3.2)$$

The alternative is to create slotted holes instead of oversized holes. This would imply that the tolerances in the x - and y -directions are considered separately. For this situation, r_x and r_y are calculated. Since there is no quadratic term, the absolute value is taken; otherwise, it is not possible to calculate the sample standard deviation.

$$r_x = |\Delta X_{\text{beam}} - \Delta X_{\text{slab}}| \quad (3.3)$$

$$r_y = |\Delta Y_{\text{beam}} - \Delta Y_{\text{slab}}| \quad (3.4)$$

3.2.1. Tolerances in the structural grid

When building the steel frame, tolerances can be initiated in the structural grid due to various deviations. For the connection between the frame and the hollow core slab, deviations in the beam centre lines or column spacing can be caused by the location of the column relative to its intended position or the inclination of the column. The tolerance in column location is regulated by Table B.20-1 of NEN-EN 1090-2 [27] and allows for a deviation of $\Delta_{\text{cloc}} = \pm 10$ mm and $\Delta_{\text{cloc}} = \pm 5$ mm in the x - and y -directions for Class 1 and Class 2 respectively. The column inclination of multi-storey buildings is limited to $\Delta_{\text{ci}} \pm h/300$ and $\Delta_{\text{ci}} \pm h/500$ for classes 1 and 2, respectively.

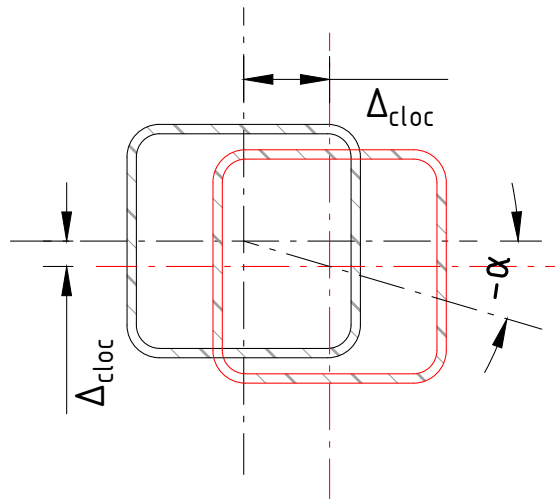


Figure 3.1: Column location tolerances according to B.20-1 of NEN-EN 1090-2 [27]

The sum of these tolerances should be within the limits of Table B.16-1 of NEN-EN 1090-2 [27] for the beam spacing and Table B.20-2 for the column spacing. In Figure 3.2 a schematic view of a structural grid with 4 columns, integrated beams and a hollow core slab is shown, which represents the actual situation. In this figure, the beam spacing is indicated by $S + \Delta_{\text{bs}}$ and the column spacing by $L + \Delta_{\text{cs}}$. For the beam spacing, Δ_{bs} is equal to ± 10 mm and ± 5 mm for Class 1 and Class 2 respectively. The spacing of the columns depends on the distance between adjacent columns at the base level; the Δ_{cs} value can be determined with Equation 3.5 and Equation 3.6.

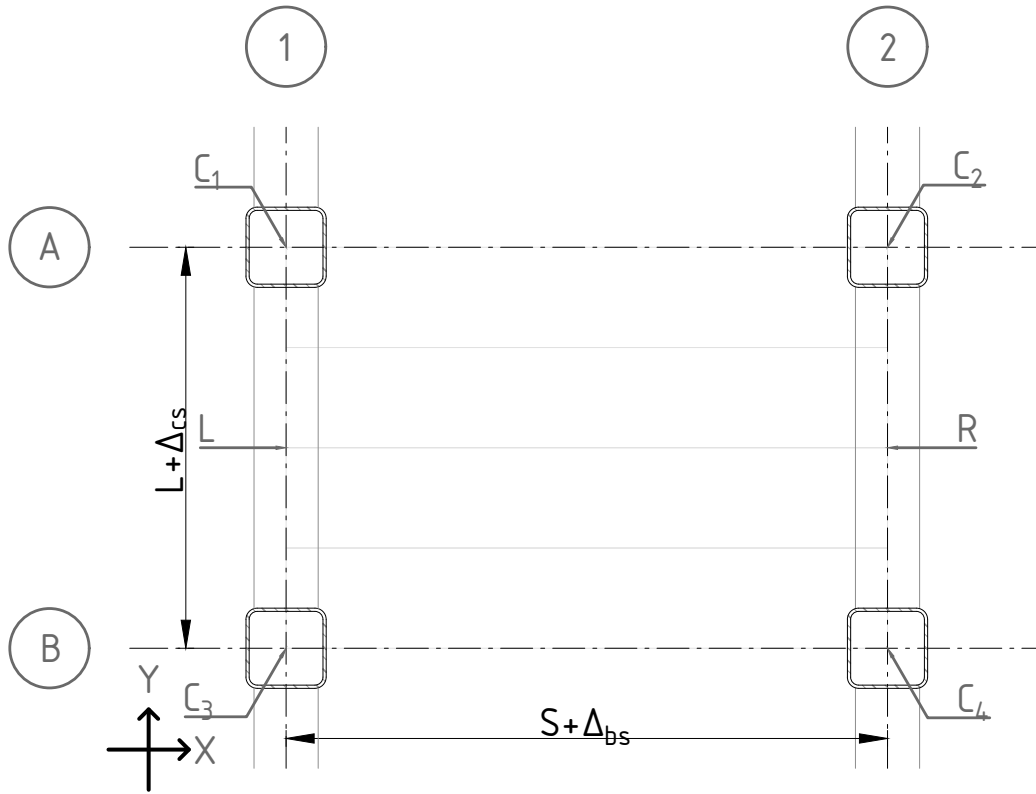


Figure 3.2: Erection tolerances for beam centre line and column spacing according to B.16-1 and B.20-3 of NEN-EN 1090-2 [27] respectively (L = left beam, R = right beam, $C_1 - C_4$ = column numbering).

$$L \leq 5 \text{ m}; \Delta_{cs, \text{class1}} = \pm 10 \text{ mm}, \Delta_{cs, \text{class2}} = \pm 7 \text{ mm} \quad (3.5)$$

$$L > 5 \text{ m}; \Delta_{cs, \text{class1}} = \pm 0.2(L + 45) \text{ mm}, \Delta_{cs, \text{class2}} = \pm 0.2(L + 30) \text{ mm} \quad (3.6)$$

For all columns, C_n ($n = 1 - 4$), the relative displacements are caused by Δ_{cloc} and Δ_{ci} but the global displacements are limited by Δ_{bs} and Δ_{cs} . This implies that, for example, C_1 can displace a certain amount of millimetres, but the column C_2 can be limited in its displacement by Δ_{bs} .

Since all individual columns can displace and incline randomly but, on the other hand, are limited by the spacing of the beam and the column, the tolerance study would become rather complex. To simplify the tolerance study, the columns are not considered individually. Instead, the columns are divided into groups; there are 2 column groups for the x-direction and two column groups for the y-direction. These groups, denoted by the subscripts $m = A, B, 1$ and 2 according to the axis system presented in Figure 3.2. In the x-direction, the amount of beam spacing is determined first for groups A and B. Subsequently, the tolerance distribution between the left and right columns is given by variables α and β in the interval $[0, 1]$. For the y-direction, the column deviation is determined by the column spacing and are equal for both columns; this is due to the axial stiffness of the beam. The Δ_{cs} and Δ_{bs} are variables with random character and normal distribution.

$$\Delta X_m = \Delta_{\text{bs}} \quad (3.7)$$

$$\Delta Y_m = \Delta_{\text{cs}} \quad (3.8)$$

As stated above, the positions of the columns are limited by the maximum beam and column spacing. As a result, Equation 3.9 prescribes the displacement of the columns in x-direction and Equation 3.10 does the same for the y-direction.

$$\Delta X_{C_1} = \alpha \cdot \Delta X_A \quad ; \quad \Delta X_{C_2} = (1 - \alpha) \cdot \Delta X_A \quad ; \quad \Delta X_{C_3} = \beta \cdot \Delta X_B \quad ; \quad \Delta X_{C_4} = (1 - \beta) \cdot \Delta X_B. \quad (3.9)$$

$$\Delta Y_{C_1} = \Delta Y_{C_3} = \Delta Y_1 \quad ; \quad \Delta Y_{C_2} = \Delta Y_{C_4} = \Delta Y_2. \quad (3.10)$$

For the x-direction, the deviation along the beam axis can be described with a linear function between the columns. The function to describe this displacement can be divided into 3 situations: $\Delta X_A > \Delta X_B$, $\Delta X_A < \Delta X_B$, and $\Delta X_A = \Delta X_B$. The latter situation most likely will not occur and is not taken into account. For the first situation where $\Delta X_A > \Delta X_B$, the left and right beams can be described as follows:

$$\Delta X_L = \Delta X_{C_1} + (\Delta X_{C_3} - \Delta X_{C_1}) \cdot \frac{y}{L}, \quad (3.11)$$

$$\Delta X_R = \Delta X_{C_2} - (\Delta X_{C_2} - \Delta X_{C_4}) \cdot \frac{y}{L}. \quad (3.12)$$

For the other situation where $\Delta X_A < \Delta X_B$ the following equations should be used:

$$\Delta X_L = \Delta X_{C_1} - (\Delta X_{C_1} - \Delta X_{C_3}) \cdot \frac{y}{L}, \quad (3.13)$$

$$\Delta X_R = \Delta X_{C_2} + (\Delta X_{C_4} - \Delta X_{C_2}) \cdot \frac{y}{L}. \quad (3.14)$$

For displacement in the y-direction the value is constant along the beam and for the left beam equal to ΔY_1 and for the right beam ΔY_2 .

3.2.2. Tolerances in hollow core slab

Tolerances in the hollow core slab are prescribed in NEN-EN 1168 [25]. The number of allowable deviations in length, width, and thickness influences the location of the connectors relative to the intended location. Depending on whether the installation is on-site or prefabricated, these deviations could be essential for the design. In a prefabricated situation, the connectors are placed in a fixed location measured from the edges of the slab. If the length of the slab is larger than intended, this would result in a different position of the connector relative to the beam. In Table 3.1 an overview of the maximum allowable deviations for the European and American standards is provided.

Table 3.1: Tolerances of hollow core slabs for construction purposes according to NEN-EN 1168 [25] and the MNL-116 [77].

	Δ_{hcs}	
	NEN-EN 1090-2 [mm]	MNL-116 [inch]
Slab length	± 25	$\pm 1/2$ (12.7 mm)
Slab width	± 5	$\pm 1/4$ (6.4 mm)

What can be observed is that the difference between the European and American standard is significant. The tolerance for the length of the slab has a deviation of almost 100%. The literature does not provide a definitive answer as no studies have been found on the precision of hollow core slabs. However, the manufacturing process, as briefly described in subsection 2.1.1 shows that the slabs are sawn to length after casting. Therefore, well-calibrated high-precision sawing machines could result in significantly smaller tolerances. After requesting data from VBI, this assumption was confirmed. Measurements for the actual slab length compared to the designed one of two of their slip-forming units (3 and 4) in Huissen (NL) were provided for the year 2022. In Appendix A the data is presented; unfortunately, no exact data size values were provided, but according to the VBI spokesperson, it was several thousands of slabs per year. From this graph it can be observed that with a 95% CI the maximum slab tolerance can be set to 10 mm and that the mean value is approximately equal to zero.

The tolerance margins in the hollow core slab for the x- and y-direction are given by:

$$(\Delta X_{\text{hcs}}; \Delta Y_{\text{hcs}}) = (\Delta_{\text{hcs,l}}; \Delta_{\text{hcs,w}}). \quad (3.15)$$

3.2.3. Out-of-straightness of the beam

All structural members face imperfections, and one of the results of these geometric imperfections is the out-of-straightness. The out-of-straightness of the member is a critical parameter when determining the required tolerances, and is therefore reviewed in this section. The out-of-straightness of the beam affects the location of the bolt holes in the bottom flange. For the geometry specified in Figure 3.2, the out-of-straightness directly influences the location of the bolt hole in the x-direction. This displacement in x-direction subsequently gives some displacement in the y-direction; the effect is marginally and neglected.

Out-of-straightness imperfections are related to the residual stresses that are induced by manufacturing processes such as heat treatment, welding or machining [78]. To account for this imperfection, NEN-EN 10034 [18] and NEN-EN 1090-2 [27] have imposed limits for hot-rolled sections and all other profiles, respectively. This results in the fact that the integrated floor beams such as THQ, SFB, and IFB face tolerances as stated in NEN-EN 1090-2 and the under-mount floor beams are required to follow the tolerances as given in NEN-EN 10034.

For NEN-EN 1090-2 the functional tolerances with respect to the straightness of the beam are specified in Table B.16-3, the erection of beams in buildings. The maximum amplitude for the deviation is given as $\Delta_{\text{oos}} = \pm L/500$ and $\pm L/1000$ for Class 1 and Class 2, respectively, where L represents the beam span. For the undermount I and H profiles the maximum out-of-straightness is related to the height of the cross-section and varies between $\pm L/333$ and $\pm L/1000$. An overview of the maximum out-of-straightness is given in Table 3.2.

Table 3.2: Maximum out-of-straightness amplitude for integrated and under-mount floor beams

Beam type	Type	Δ_{oos} [mm]
I- and H-sections, NEN-EN 10034 [18]	$80 < h \leq 180$	$\pm L/333$
	$180 < h \leq 360$	$\pm L/667$
	$h > 360$	$\pm L/1000$
THQ-, SFB- and IFB-sections, NEN-EN 1090-2 [27]	Class 1	$\pm L/500$
	Class 2	$\pm L/1000$

Along the beam length, the out-of-straightness of an unbraced beam can be visualised as a half-sine wave [10] with a maximum amplitude of Δ_{oos} . For braced and double-braced systems, the values for Δ_{oos} are reduced with a factor 1/2 and 1/3 respectively, due to the shorter system length. The unbraced, braced, and double-braced systems are denoted in this paragraph with a "u", "b" and "db" subscript respectively.

$$\begin{aligned} \Delta_{y,\text{oos,u}} &= \Delta_{\text{max,u}} \cdot \sin\left(\frac{\pi x}{L}\right) \\ \Delta_{y,\text{oos,b}} &= \Delta_{\text{max,b}} \cdot \sin\left(\frac{2 \cdot \pi x}{L}\right) \\ \Delta_{y,\text{oos,db}} &= \Delta_{\text{max,db}} \cdot \sin\left(\frac{3 \cdot \pi x}{L}\right) \end{aligned} \quad (3.16)$$

In Equation 3.16 the formulas for the calculation of the deviations are shown, and in Figure 3.3 a visual representation is given for a beam of 10 m with an allowable out-of-straightness of $L/1000$. This results in maximum deviations of 10.0, 5.0 and 3.3 mm for the unbraced, braced, and double-braced variants. This can also be verified by the fact that the system length of the beam stays constant and the representations of the out-of-straightness are prescribed by a half-sine, sine and one-and-a-half sine wave.

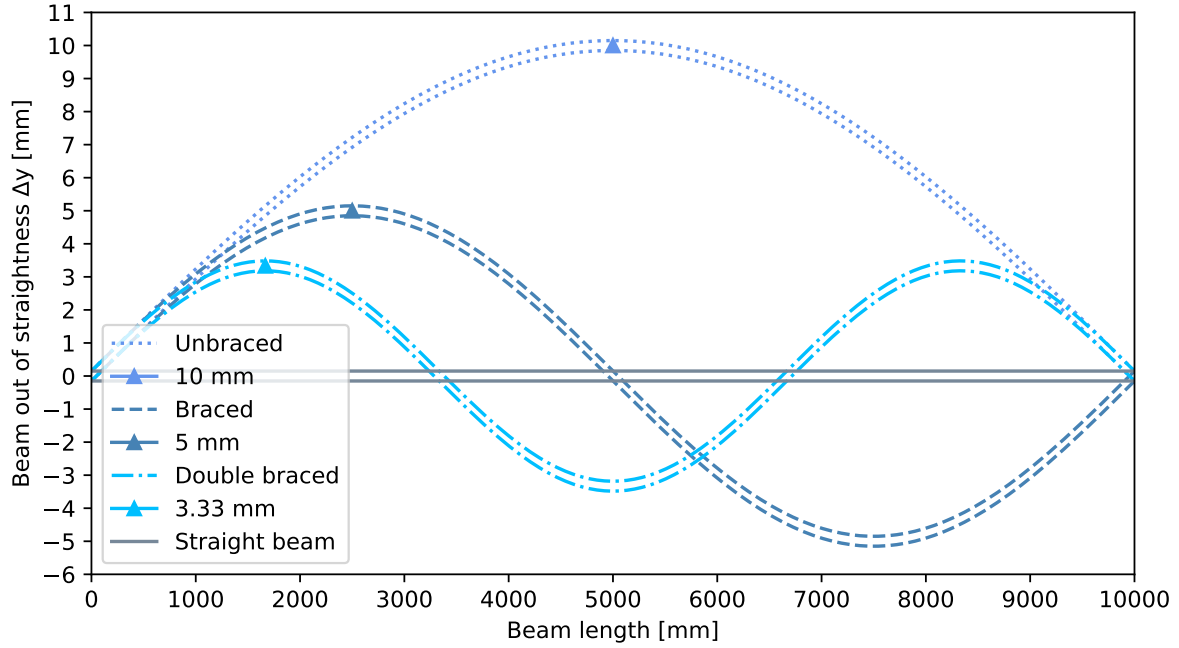


Figure 3.3: Out-of-straightness amplitude for an allowable tolerance of $L/1000$ ([27], Class 1)

The out-of-straightness values are the maximum values allowed by NEN-EN 1090-2 and NEN-EN 10034. A review of actual tolerances on fabricated beams could result in smaller imperfections; which is positive for the needed tolerances. Nijgh [70] reviewed the data from several investigations for his research on reusable steel-concrete composite floor systems. The data originates from 6 investigations by Beer [10], Strating [84], Tebedge [86], Dux [41], Aoki [5], and Essa [44]. The initiation of the research was the investigation into buckling curves of the NEN-EN 1993-1-1, for these curves, the initial imperfections are of great importance since the out-of-straightness imperfections lower the buckling resistance significantly. The result of the data analysis by Nijgh [70] is a mean of $L/2800$ with a standard deviation of $L/5700$.

Another large-scale study was performed by Fukumoto et al. [47]. They conducted a survey on column tests and an evaluation of information on steel column strength. One of the points surveyed was the initial crookedness. In total, data from 208 IPE160 columns and 437 other I-section columns were analysed. The data for the IPE160 columns came from the European Convention for Constructional Steelwork (ECCS) and the other I-sections came from the Numerical Data-Base for Steel Structures (NDSS). In Table 3.3 an overview of the results is shown.

Table 3.3: Out-of-straightness tolerances Δ_{oos} according to [47]

Beam type	n, Number of specimens	μ	σ
IPE160	208	$L/1300$	$L/3100$
I-section	437	$L/2000$	$L/2300$
Average		$L/1774$	$L/2558$

Fukumoto's results were more in line with the limitations set in NEN-EN 1090-2 and NEN-EN 10043 than the data review carried out by Nijgh [70]. As a result, the measured beam out-of-straightness is smaller than the regulations from the EC. Since the test data are already from a couple of decades ago, fabrication tolerances are improved over time, generally speaking. Within this tolerance study, the mean member out-of-straightness is denoted as follows:

$$(\Delta X_{\text{oos}}; \Delta Y_{\text{oos}}) = (\Delta_{\text{oos}}; 0). \quad (3.17)$$

3.2.4. Geometric deviation of the bolt hole location

The bolt hole on the bottom flange of the integrated beam can face manufacturing tolerances. The tolerance in the position of this hole is specified in Table B.8-1 of NEN-EN 1090-2 [27]. The deviation between the actual and nominal position is graphically presented in Figure 3.4a. The maximum allowable tolerance is set to ± 2 mm for Class 1 structures and ± 1 mm for Class 2 structures. Other data from AISC 360-16 [3] prescribe a tolerance of $1/16''$ (1.6 mm), this is an intermediate value between classes 1 and 2 of the NEN-EN. More interesting would be the actual tolerances in practice. Unfortunately, no data are found in the literature. However, discussions with Vic Obdam, a steel construction manufacturer in the Netherlands, learnt that a tolerance of $1/10$ of a millimetre is possible with modern day CNC-operated machinery.

The magnitude of the variation is denoted by the random variable R and the direction is determined by the angle Θ .

$$(\Delta X_{bh}; \Delta Y_{bh}) = (R \cos \Theta; R \sin \Theta) \quad (3.18)$$

3.2.5. Geometric deviation of the shear connector location

For the geometric deviation of the shear connector, the principle is similar to that for the geometric deviation of the location of the bolt hole. However, the precision of drilling used for the bolt hole location cannot be achieved with the shear connector. The shear connector consists of a DEMU casted (anchor bolt) in the sleeves of the hollow core slabs. In European standards, no value is available for these tolerances. However, according to the concrete construction specification ACI [2], the acceptable deviations for anchor bolts in concrete are as follows:

Table 3.4: Horizontal deviations for anchor bolts in concrete [2]

Bolt dimension [inch]	Horizontal deviation [inch]
3/4, 7/8	$\pm 1/4$
1, 1-1/4, 1-1/2	$\pm 3/8$
1-3/4, 2, 2-1/2	$\pm 1/2$

As a result, the allowable tolerances depend on the dimensions of the bolt. Since the European standards do not specify any values, the values of the American Concrete Institute is adopted. The variation for the location of the shear connector is indicated with the random variable D . The direction is random and the angle is denoted by Ω .

$$(\Delta X_{sc}; \Delta Y_{sc}) = (D \cos \Omega; D \sin \Omega) \quad (3.19)$$

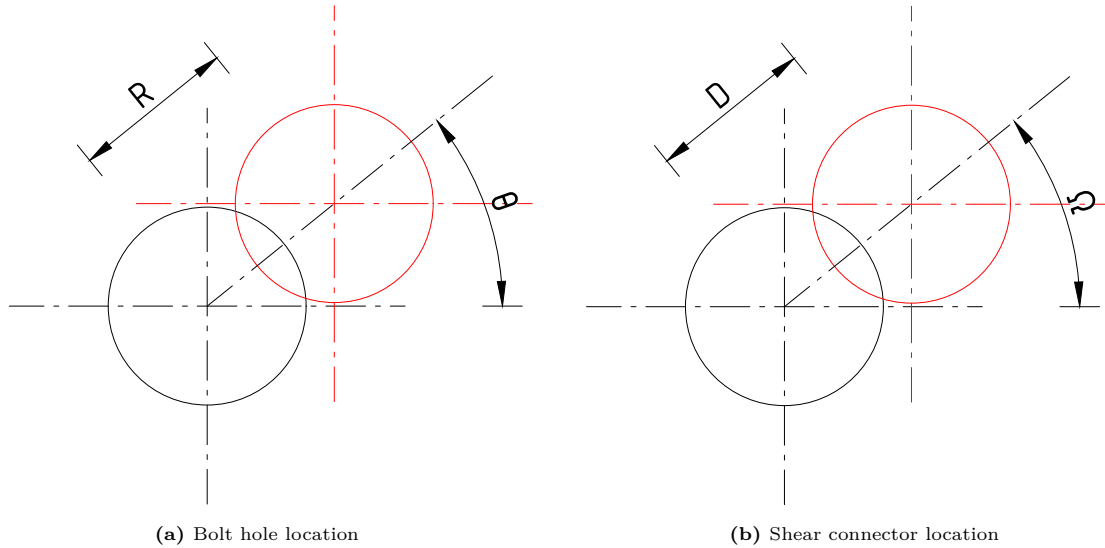


Figure 3.4: Deviation of the actual position (red) of the bolt hole and shear connector from the nominal (grey) position

3.2.6. Total deviation

To determine the total tolerances required, several options are simulated. There is a distinction between the prefabricated situation and the on-site installation. An overview of the simulations is shown below.

Table 3.5: Overview of the Monte Carlo simulations for on site and prefabricated construction (^a only the length value is adopted from VBI, ^b no European Standard data available).

		Simulation 1	Simulation 2	Simulation 3
On site	<i>Structural grid</i>	EN 1090-2 Class 1	EN 1090-2 Class 2	n/a
Prefabricated	<i>Structural grid</i>	EN 1090-2 Class 1	EN 1090-2 Class 2	EN 1090-2 Class 2
	<i>Hollow core slab</i>	EN 1168	EN 1168	VBI ^a
	<i>Out-of-straightness</i>	EN 1090-2 Class 1	EN 1090-2 Class 2	Fukumoto & Itoh
	<i>Bolt hole location</i>	EN 1090-2 Class 1	EN 1090-2 Class 2	Vic Obdam
	<i>Shear connector location</i>	ACI 117-10 ^b	ACI 117-10 ^b	ACI 117-10

Cumulative tolerances are given by Equation 3.2 for round oversized bolt holes and by Equation 3.3 and Equation 3.4 for slotted holes. For a prefabricated structure, the tolerances in x- and y-direction are given by Equation 3.20, Equation 3.21, Equation 3.22, and Equation 3.23. The tolerance that is initiated by the slab length can be taken by two beams and therefore this value is divided by two.

$$\Delta X_{\text{beam}} = \Delta X_L + R \cdot \cos(\Theta) + \Delta_{\text{oos}} \cdot \cos\left(\frac{\pi \cdot y}{L}\right) \quad (3.20)$$

$$\Delta X_{\text{slab}} = \frac{\Delta X_{\text{hcs}}}{2} + D \cdot \cos(\Omega) \quad (3.21)$$

$$\Delta Y_{\text{beam}} = \Delta Y_L + R \cdot \sin(\Theta) \quad (3.22)$$

$$\Delta Y_{\text{slab}} = \Delta Y_{\text{hcs}} + D \cdot \sin(\Omega) \quad (3.23)$$

For the fabrication of the connections on site, the only tolerances that should be implemented are the tolerances that occur from the structural grid. It is assumed that in case of reassembly all structural elements are labelled and the elements are placed at the exact same location. As a result, the tolerances originate solely from ΔX_L and ΔY_L .

3.3. Monte Carlo Simulation

The desired level of tolerances is reviewed in this section; this is done with the help of a multiple probability simulation. This multiple probability simulation, also known as a Monte Carlo simulation, uses uncertain variables to perform numerous simulations [59]. The results of these simulations can be used by averaging the results or by calculating a confidence interval (CI). Nijgh [70] performed a similar simulation for the application of reusable steel-concrete composite floor systems.

For the Monte Carlo simulation, the various tolerances are used to calculate the combined tolerances. In general, all imperfections are of random character [57]. Since NEN-EN 1090-2 does not specify the probability of success for any of the tolerance values, an assumption is made for their CI. The standard confidence intervals are 90%, 95%, and 99%, where the 95% CI is the most commonly used [74]. This 95% is also the CI used by Eurocode 7 [35] for geotechnical design. Kala [57] assumed a similar 95% confidence interval for the NEN-EN 1090-2 values used in his dissertation.

3.3.1. Method

To perform the Monte Carlo simulation, the mean and standard deviation of the variables determined in subsection 3.2.1 to subsection 3.2.5 are calculated. The variables have a normal, uniform or deterministic distributed character. The only variable with deterministic character is the diameter of the bolt.

In Table 3.6 an overview of the normal distributed variables is given. These normal distributions have a bell shape and is also known as a Gaussian distribution. As stated above, a 95% CI is assumed and this corresponds to a z-score of ± 1.96 . Therefore, the tolerance values found in the European design standards or other literature are divided by z.

Table 3.6: Variables with a normal distribution

Variable	Distribution	Mean	Standard deviation	Unit
ΔX_A	Normal	0.0	Δ_{bs} / z	[mm]
ΔX_B	Normal	0.0	Δ_{bs} / z	[mm]
ΔY_1	Normal	0.0	Δ_{cs} / z	[mm]
ΔY_2	Normal	0.0	Δ_{cs} / z	[mm]
ΔX_{hcs}	Normal	0.0	$\Delta_{hcs,l} / z$	[mm]
ΔY_{hcs}	Normal	0.0	$\Delta_{hcs,w} / z$	[mm]
ΔX_{oos}	Normal	0.0 ¹	Δ_{oos} / z^1	[mm]
ΔR	Normal	0.0	R / z	[mm]
ΔD	Normal	0.0	D / z	[mm]

In Table 3.7 an overview of the uniform distributed variables is given. For the uniform distribution, the generated values are equally distributed over their interval.

Table 3.7: Variables with a uniform distribution

Variable	Distribution	Interval	Unit
α	Uniform	[0,1]	[-]
β	Uniform	[0,1]	[-]
Θ	Uniform	[0,2 π]	[rad]
Ω	Uniform	[0,2 π]	[rad]

3.4. Case study

The nominal hole clearance was calculated for a case study example. This approach eliminates various variables in Monte Carlo simulation and gives values for a real-life situation. The building geometry parameters are provided in Appendix B.

¹For the literature reviewed values L/1774 and L/2558 are used for the mean and standard deviation respectively.

In [Figure 3.5](#) a detailed drawing of the connection between the hollow core slab and the SFB is shown. From this detail, the geometry of the connection is visualised. The result of the MCS determines the oversize of the bolt hole in the bottom flange. For the bolt dimension, the deterministic variable d is equal to 16 mm.

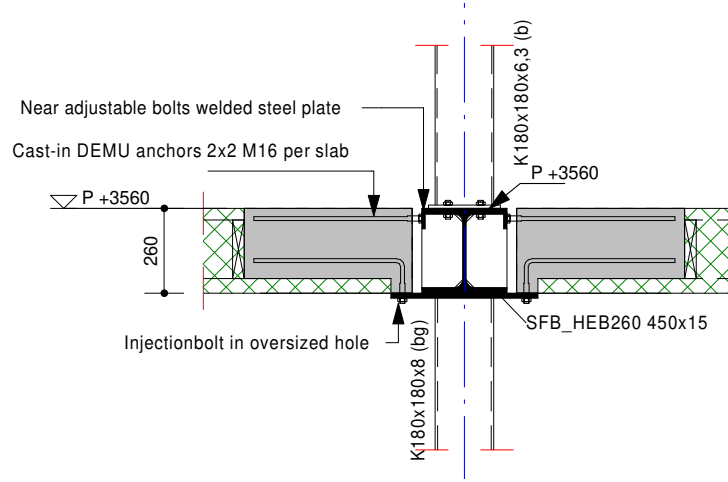


Figure 3.5: Connection detail between hollow core slabs, SFB and columns

3.4.1. Results

To obtain the results, several analyses are executed as presented in [subsection 3.2.6](#). In [Figure 3.7](#) the result of one simulation is shown, the other results can be found in [section C.1](#). The Python script for the Monte Carlo simulation is shown in [section C.2](#). The graph shows the distribution of r for $N = 10^4$ simulations. These simulations combine the random variables and calculate the total tolerance needed. From all of this data, the arithmetic mean value and standard deviation are calculated according to [Equation 3.24](#) and [Equation 3.25](#).

$$\mu = \frac{1}{N} \sum_{i=1}^N a_i = \frac{a_1 + a_2 + \dots + a_N}{N} \quad (3.24)$$

$$\sigma = \sqrt{\frac{1}{N} \cdot \sum_{i=1}^N (a_i - \mu)^2} \quad (3.25)$$

Since the tolerances are still span dependent, the most critical position along the beam axis should be determined. Since the deviation between the columns ΔX_A and ΔX_B is assumed to be linear, the tolerances due to the structural grid are largest at the location of the columns. However, the out-of-straightness is maximum at beam midspan, and therefore this value has a big influence. If the out-of-straightness or the beam length is significantly large, the most critical location can shift along the beam axis. To verify this, the highest value of Δ_{oos} , which is equal to $\pm L / 500$, and the length according to the case study are used. In [Figure 3.6](#) the results for the mean value of r are shown for $N = 10^4$ and an interval of $y = 100$ mm. From this it can be observed that the most critical positions are $y = 0$ and $y = L$.

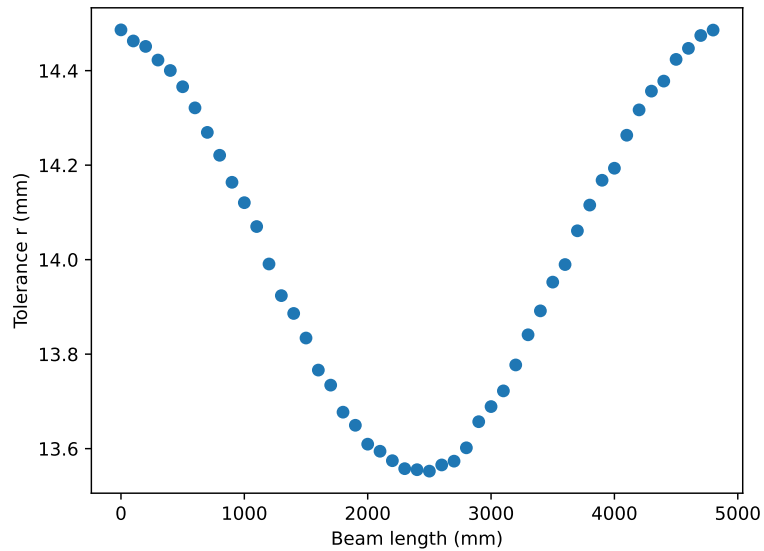


Figure 3.6: Deviation of the mean value of r (mm) along the beam axis for $\pm L/500$

In [Figure 3.7](#) the result obtained from one of the simulations is shown. The result shows a skewed (to the right) bell-shaped histogram that is limited by the bottom line value of $r = 0$ mm. In [Appendix C](#) the results of the other simulations are presented in a graphical way and in [Table 3.8](#) an overview of the results is given at $y = 0 = L$. In this table, the subscripts r_μ , r_σ , r_{95CI} represent the mean value, standard deviation value and confidence interval, respectively. [Equation 3.26](#) shows the calculation of the diameter of the bolt hole. This diameter represents the oversize of the bolt hole, but can also be used for other geometries as an indication for the required tolerances.

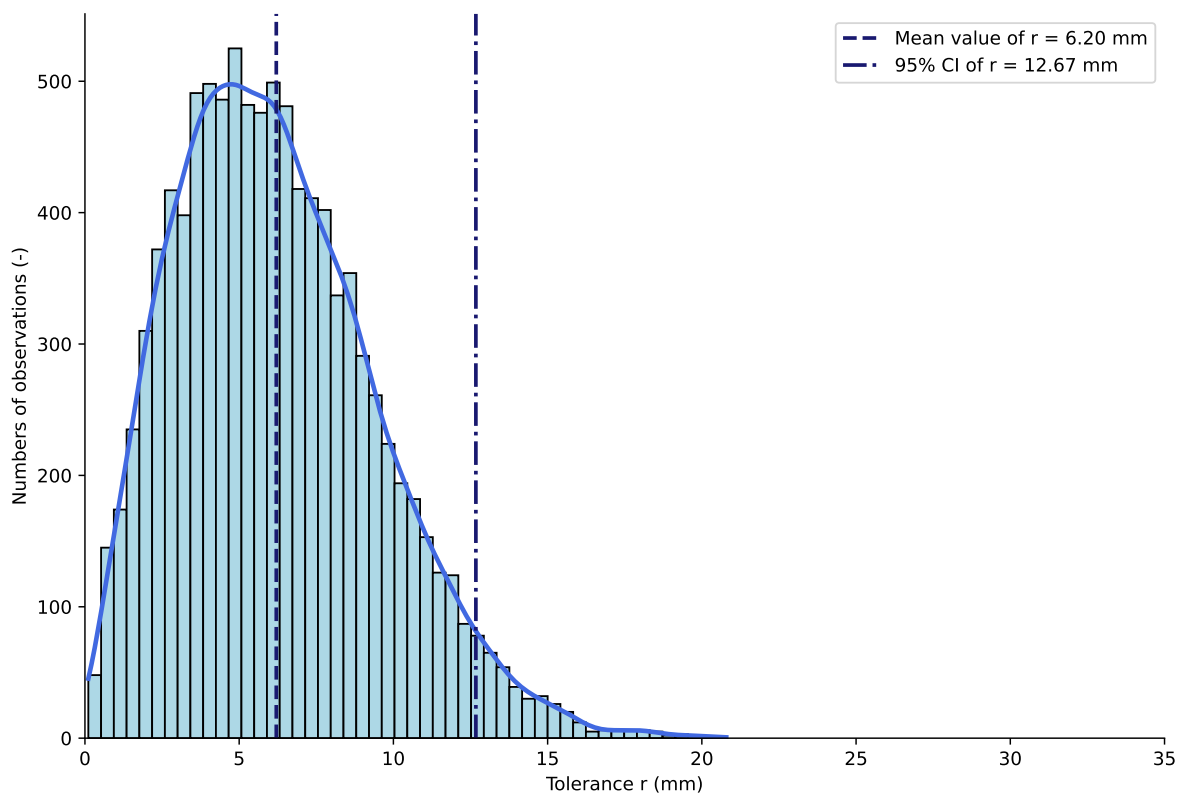


Figure 3.7: Monte Carlo simulation with $N = 10^4$ simulations based on literature and manufacturer data (simulation 3) for a prefabricated situation

$$d_0 = d + 2 \cdot r_{95CI} = d + (r_\mu + 2 \cdot r_\sigma) \quad (3.26)$$

Table 3.8: MCS tolerance results for case study geometry and the Temporary Courthouse connection, all dimensions in millimetres

		d	r_μ	r_σ	r_{95CI}	$2 \cdot r_{95CI}$	d_0
On-site	<i>Simulation 1</i>	16.0	3.95	2.42	8.79	17.6	33.6
	<i>Simulation 2</i>	16.0	3.26	2.08	7.43	14.9	30.9
Prefabricated	<i>Simulation 3</i>	16.0	8.85	5.08	19.01	38.0	54.0
	<i>Simulation 4</i>	16.0	7.78	4.30	16.38	32.8	48.8
	<i>Simulation 5</i>	16.0	6.20	3.24	12.67	25.3	41.3

The table presents the result for the on-site and prefabricated installation for the different simulations mentioned in [Table 3.5](#). The total required bolt hole dimension is based on the summation shown in [Equation 3.26](#), the two parts of the summation are shown in bold. Installation on-site results in a lower tolerance demand with 33.6 and 30.9 for Class 1 and Class 2 data, respectively. For the prefabricated installation values of 54.0 and 48.8 mm are found, this is an increase of 20.4 and 17.9 mm compared to their on-site installed counterparts. The third prefabricated simulation was based on literature data and showed the lowest tolerance demand. From this, the conclusion is drawn that the tolerances in practice are smaller than the values prescribed in the European design standards, even for the more strict Class 2 demand. For reusable structures, it is advised to use the stricter Class 2 data of the NEN-EN 1090-2. This results in a tolerance of $d + 14.9$ mm for on-site installed constructions, and $d + 32.8$ mm for prefabricated installations, shown in orange in [Table 3.8](#).

4

Design alternatives

In the chapter on design alternatives, three different designs are proposed. The basis of a feasible design starts with certain requirements. The connection requirements specify the boundaries in terms of functionality, manufacturability, installationability, demountability, and economic feasibility. Part of the connection functionality is the ability to transfer the loads that are exerted on the system. Therefore, in [section 4.2](#) the loading conditions for the connector are determined based on the geometry of the case study building. The final section comprises the proposal of the alternatives. For the three designs, the installation, demountability, and the force transfer mechanism of the system are explained. These designs serve as the foundation for the trade-off analysis presented in [chapter 5](#), which is the final chapter of [Part II](#).

4.1. Connection requirements

The principles of connection design are based on a predetermined set of requirements. This set of requirements specifies the important characteristics of the connection to ensure success. In order to create a successful design, it is necessary to consider a few topics and meet certain requirements. An overview of the requirements and sub-requirements is shown in [Figure 4.1](#). Functionality, manufacturability, ease of installation, demountability, and economic aspects are the five main categories with requirements that have been identified. Functional and production requirements are essential for the design, and these requirements must be met for all alternatives. However, the inclusion of installation, dismantling, and economical requirements can vary for the different alternatives. Consequently, the trade-off analysis is based on these requirements.

Functional requirements

Functional requirements are a set of specifications that define the fundamental capabilities and features of the system. The design alternatives proposed in [section 4.3](#) should be able to implement these requirements. For the reusable connection between the hollow core slab and the steel frame, the main function is to provide a connection between the beams and the slab. The purpose of this connection is to transfer the loads as specified in [section 4.2](#). The two main aspects of the design are regarding strength and stiffness.

The strength aspects are related to the loading conditions. The maximum load depends on the specific connection, but some general design principles can be formulated. First, the eccentricity; a smaller eccentricity results in smaller moments, and therefore the loads in the connection are reduced. Second, the moments mentioned above need to be transferred to the slab by means of a torque. This results in the fact that a larger lever arm results in lower loads and more beneficial loading conditions. The above-mentioned aspects should be taken into account for the design. The loading conditions from the wind and imperfections need to be transferred in the design, but the magnitude of these loads is not influenced by the geometry.

The stiffness of the connection is important to consider for the serviceability limit state. Stiffness directly affects the slippage of the connection. The slip should be limited to prevent excessive deformation of

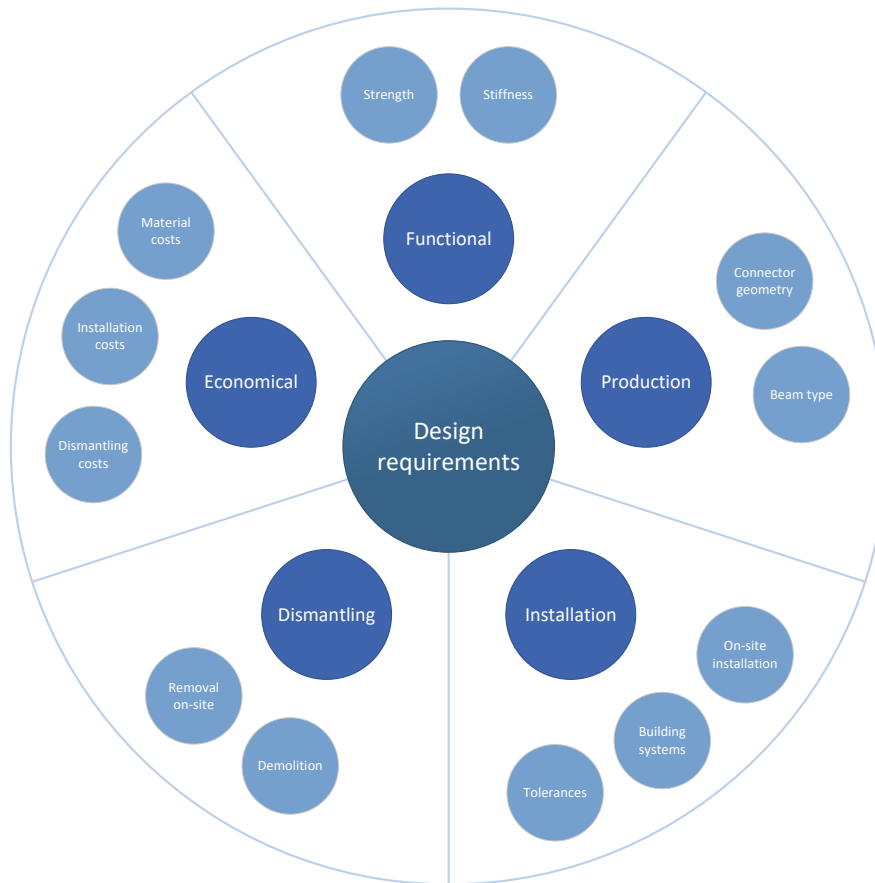


Figure 4.1: Design requirements

the floor slab. Hollow core slabs are generally designed with deflections near the serviceability limit state criterion of $L/250$. Insufficient connector stiffness could result in exceeding the deflection criteria.

Production requirements

Production requirements focus on the adjustments made to create the connection. Since the slab production process is an optimised and automated process, adjustments are made after slab fabrication. This implies that an additional step should be taken after slab production to implement the facilities for the reusable structure. For the design of the connection, the installation of these facilities should consider the makeability.

Besides the adjustments made to the slab, the beam should also be adjusted. As mentioned in the installation requirements, the use of integrated beams is preferred. This results in the selection of three possible beam options, namely Top Hat Q (THQ) beams, Integrated Floor Beams (IFB) or Slim Floor Beams (SFB). To limit the deflections and maximum sagging moments, the beams are often designed as the continuous type. Of the three options, SFB and IFB beams are the easiest to produce and adopt to certain needs. Connections can be easily made with end plates that have bolts in between the flanges of the hot rolled section and do not exceed the width of the section. For the enclosed THQ section, the end plate needs to be outside of the box perimeter since connecting from the inside is impossible. Therefore, the end plate should extend the height or width of the box section. Both are undesirable since the height is critical and the end plates wider than the box interfere with the bearing points of the slab.

Installation requirements

The installation requirements refer to two types of installations. First of all, the installation of the

beams and slabs should be addressed. Subsequently, the installation of buildings systems such as wiring, heating, ventilation, and air conditioning is of major importance for a reusable structure.

Installation of the beams and slabs should be as easy as possible. The standard procedure should be followed as much as possible; this means installing with lifting clamps from above. After the slabs are in the correct position, the connection should be made as easy as possible. Minimising steps on site and having access from above is the preferred installation technique.

After installation of the main structure, the installation of the building systems takes place. Since the bearing structure outlasts the installations with ease, 7-15 years versus 30-300 years [13], respectively, it is important to be able to reroute the building systems. During the lifetime of a reusable structure, it can serve various functions. To avoid openings in the floor beams, the structure can be designed with a flat ceiling. This accounts for the easy installation of new building systems during the life span of the building or after repurposing the building with a different function. Therefore, integrated beams are the preferred option over the alternative of beams mounted below the floor. This is a hard requirement for the design of all alternatives.

Within the installation requirements, the most important part is the inclusion of tolerances. In the previous chapter, [chapter 3](#), a detailed analysis on the minimum required level of tolerances is performed. This level of tolerances are needed to ensure successful installation in its reuse phase without having to take severe measures. This analysis was performed for a certain geometry; however, in the alternative designs, the chosen geometry could not be representative. The conclusion of the analysis is that the minimum required tolerances would be the diameter of the bolt + 20 mm. The inclusion of this tolerance in the design could be achieved by an oversize of the bolt hole, but this does not necessarily need to be the case. The tolerances could also be accommodated in the connector located in the slab element. In short, there are two options: accommodate tolerances in the beam or accommodate tolerances in the slab.

Dismantling requirements

For a reusable structure, the dismantling process is as important as the installation process. Having a procedure similar to the standard construction technique makes the design easier to implement and does not require additional training of the construction workers. When looking into the dismantling process, the number of steps and time the dismantling process costs are weighted between the alternatives. An easy dismantling process could result in reduced costs and could convince decision makers to take the building apart instead of scrapping the structure.

Economic requirements

The economic requirements are related to three parts. First, the additional costs for the reusable connection are reviewed. These costs can be calculated based on the manufacturer's data and consist only of material costs without installation. The additional costs should be compared to the traditional costs that are normally made when building with steel beams and hollow core slabs. This traditional construction consists of reinforcement in the hollow core sleeves that is welded to the beam. After this, the sleeves and the space between the beam is filled with concrete. Subsequently, the installation and demountability of the elements should be expressed in monetary value.

4.2. Connection loads

The following section reviews the loads on the connection for integrated beams. For all the calculations the specific connection geometry is set as a variable so the final load calculations can easily be adopted to the certain geometry of the best performing connection. The loading conditions are determined according to European standards as prescribed in Eurocode 0 [29] and Eurocode 1 [28]. Data from the Dutch national annexes [30] [31] are adopted since the case study building is built in the Netherlands and the first implementation of the connection detail is expected to take place in the Netherlands. All loads are based on the geometry and location of the case study as described in [Appendix B](#), however, for some situations deviations from the case study parameters are made. For these cases, a comprehensive reasoning is provided. Since only the effect caused by global loads on the structure is important for the connection design, local effects caused by nodal loads are excluded from the analysis. The sources of the loads can be classified into four categories: those from the floor, roof, wind, and those caused by column imperfections.

4.2.1. Floor loads

For floor loads, only the first floor is considered, as the hollow core slabs on the ground floor are placed directly on the concrete strip foundation. The strip foundation has concrete piles below and is assumed to be sufficiently stiff against rotations and, therefore, this part of the building does not require a demountable connection but consists of a contact bearing. The loads exerted on the first floor consist of a variable and a permanent part. The permanent part consists of the hollow core slab mass, the screed, the ceiling weight, and the installations suspended from the roof. The permanent part is assumed to be the same since the entire building is made up of hollow core slab elements of equal thickness. The variable load changes based on the use of the floor area. A small section of the first floor is used for technical installations and has a higher class E load than the class B office load. This small section is deliberately chosen to be in the shorter middle span, so it will not generate the most critical floor loading. The loads shown in [Table 4.1](#) are used for the verification of the elements.

Table 4.1: Floor loads

	g_k [kN/m ²]	q_k [kN/m ²]
Hollow core slab	3.85	
Screed	1.40	
Ceiling and installations	0.30	
Light partition walls		0.80
Office load cat. B [31]		2.50

4.2.2. Roof loads

The roof of the case study buildings consists, similarly to the floor, of hollow core slab elements. However, the loads applied to this slab are slightly different. The permanent one comprises the hollow core slab weight, insulation, ballast, ceiling weight, roof installations, and solar panels. The middle part of the roof is designated as a space for installations and is accessible to persons; therefore, this part of the roof is considered to be load class E, storage. The other sections of the roof are classified as class H, and for a flat roof structure this results in a load of 1.0 kN/m² [31]. In [Table 4.2](#) an overview of the roof loads is shown for the standard part and the part with installations.

Table 4.2: Roof loads

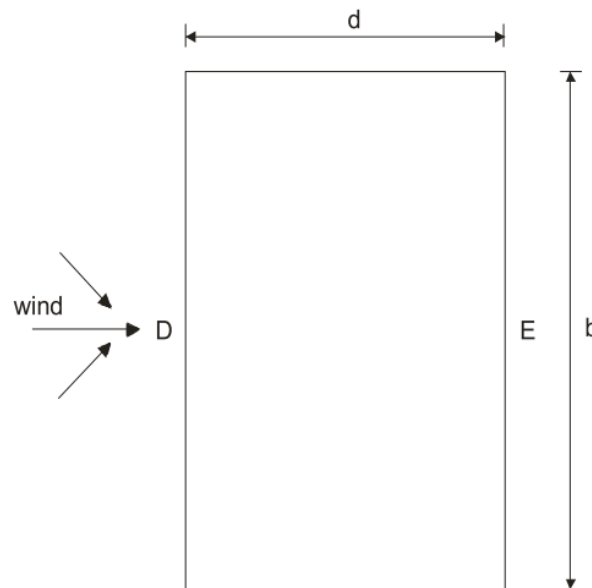
	g_k [kN/m ²]	q_k [kN/m ²]
Hollow core slab	3.85	
Finishings and insulation	0.35	
Ballast	1.00	
Ceiling and installations	0.30	
Solar panels	0.50	
Roof load cat. H, $\alpha = 0^\circ$ [31]		1.00
Storage load cat. E [31]		5.00

4.2.3. Wind loads

The wind load acts on the walls and roof of the building. The loads exerted on the walls create a horizontal load on the floor slabs that should be transferred to the bracing elements. This load is transferred by the so-called diaphragm working of the floor slab. In more traditional construction, the voids between the slab elements and the beam are filled with concrete; this ensures full contact between the slabs and beams so horizontal forces can be introduced in the slab. For reusable construction techniques, this concrete is undesirable, as it affects the demountability. To overcome this problem, horizontal loads introduced by the wind should be transferred via the beam to slab connections and are eventually taken by the bracing structure. All loads are calculated with respect to EN 1991-1-4 [22] and the Dutch National Annex [36].

The hollow core slabs in the case study span the transverse direction of the building. This suggests that the connection experiences the highest wind load when the wind is applied in the transverse direction of the building. Distinguishment is made between the horizontal load on the first floor slab and the roof slab. This is due to variation in the height of the storey, H_1 , H_2 , and H_3 as prescribed in Appendix B. The loading area on the first floor and on the roof is given in Equation 4.1. In this equation, the subscripts $_{fl}$ and $_{rf}$ refer to the floor and roof, respectively.

$$\begin{aligned} H_{fl} &= \frac{H_1 + H_2}{2} = \frac{3.65 + 3.65}{2} = 3.65 \text{ m/m}^1 \\ H_{rf} &= \frac{H_2 + H_3}{2} = \frac{3.65 + 2.49}{2} = 3.07 \text{ m/m}^1 \end{aligned} \quad (4.1)$$

**Figure 4.2:** Wind loading on a building with windward (D) and leeward (E) side [22]

The load transferred by the slabs comes from the external wind pressure exerted on wall D and the suction on wall E. To calculate the wind load, the peak velocity wind pressure at the maximum elevation of the building is used. Table NB.5 [36] gives a value of $q_p = 0.85 \text{ kN/m}^2$ for undeveloped land. This gives an upper bound, safe starting point, since built environments use a slightly lower peak velocity wind pressure. The peak velocity wind pressure is calculated by multiplying it by the external pressure coefficient for global analyses, $c_{pe,10}$. In Table 4.3 an overview of the external pressure coefficients according to the national annex is given [36]. Since the building is relatively low, the h-over-d ratio is less than 1.0, where h represents the total height of the building and d the length of the building facade parallel to the direction of the wind.

Table 4.3: External pressure coefficients for zone A, B, C, D, and E according to National Annex of NEN-EN 1991-1-4 [36]

Zone	A		B		C		D		E	
h/d	$c_{pe,10}$	$c_{pe,1}$	$c_{pe,10}$	$c_{pe,1}$	$c_{pe,10}$	$c_{pe,1}$	$c_{pe,10}$	$c_{pe,1}$	$c_{pe,10}$	$c_{pe,1}$
5	-1.2	-1.4	-0.8	-1.1	-0.5		+0.8	+1.0	-0.7	
≤ 1	-1.2	-1.4	-0.8	-1.1	-0.5		+0.8	+1.0	-0.5	

Due to the lack of correlation between the windward and leeward side, the wind pressure coefficients should be corrected by a factor of $c_{corr} = 0.85$. In Equation 4.2 the wind load is given on the first floor and in Equation 4.3 the roof load is presented. In these equations, the subscript w represents the wind loading, pre the wind pressure, suc the wind suction, and k the characteristic value.

$$\begin{aligned} Q_{w,pre,fl,k} &= H_{fl} \cdot q_p \cdot c_{pe,10,D} \cdot c_{corr} = 3.65 \cdot 0.85 \cdot 0.8 \cdot 0.85 = 2.11 \text{ kN/m}^1 \\ Q_{w,suc,fl,k} &= H_{fl} \cdot q_p \cdot c_{pe,10,E} \cdot c_{corr} = 3.65 \cdot 0.85 \cdot -0.5 \cdot 0.85 = -1.32 \text{ kN/m}^1 \end{aligned} \quad (4.2)$$

$$\begin{aligned} Q_{w,pre,rf,k} &= H_{rf} \cdot q_p \cdot c_{pe,10,D} \cdot c_{corr} = 3.07 \cdot 0.85 \cdot 0.8 \cdot 0.85 = 1.77 \text{ kN/m}^1 \\ Q_{w,suc,rf,k} &= H_{rf} \cdot q_p \cdot c_{pe,10,E} \cdot c_{corr} = 3.07 \cdot 0.85 \cdot -0.5 \cdot 0.85 = -1.11 \text{ kN/m}^1 \end{aligned} \quad (4.3)$$

4.2.4. Column imperfection

Theoretically pure axially loaded columns generate a horizontal component due to imperfections in the foundation and members. This horizontal component is transferred to the bracing elements by means of diaphragm working. According to NEN-EN 1090-2 [27] the maximum column inclination is set at $\Delta = \pm h/300$ with h as the height of the column. For analysis, the total permanent and variable load are placed on the building as a nodal load. For the roof, the total variable load is dependent on the location. For the area with technical installations, the variable load is significantly higher at 5 kN/m^2 compared to 1 kN/m^2 for the other roof areas. The self-weight is assumed constant for the roof with 6 kN/m^2 . For the floor, the self-weight is 5.55 kN/m^2 and the variable load is equal to 3.3 kN/m^2 . In Equation 4.4 the equivalent nodal load is calculated for the roof and in Equation 4.5 the same is done for the floor. Dimensions and symbols are shown in section B.2 and section B.5.

$$\begin{aligned} A_{rf} &= D \cdot W - d_1 \cdot w_1 = 62.4 \cdot 30.0 - 43.2 \cdot 8.0 = 1526.4 \text{ m}^2 \\ A_{rf,tech} &= d_1 \cdot w_1 = 43.2 \cdot 8.0 = 345.6 \text{ m}^2 \\ P_{cat,H} &= Q_{cat,H} \cdot A_{rf} = 1.0 \cdot 1526.4 = 1526.4 \text{ kN} \\ P_{cat,E} &= Q_{cat,E} \cdot A_{rf,tech} = 5.0 \cdot 345.6 = 1728.0 \text{ kN} \end{aligned} \quad (4.4)$$

$$\begin{aligned} A_{fl} &= D \cdot W = 62.4 \cdot 30.0 = 1872 \text{ m}^2 \\ P_{fl} &= Q_{fl} \cdot A_{fl} = 3.3 \cdot 1872 = 6177.6 \text{ kN} \end{aligned} \quad (4.5)$$

In the most critical situation, the eccentricities of the column generate only horizontal loads along the longitudinal side of the building. Horizontal loads are derived from vertical loads, calculated in

Equation 4.4 and Equation 4.5, by multiplying by a ratio of $1/300$. These horizontal loads are divided by the width of the building, D , to get a line load. In Equation 4.6 the characteristic values of the horizontal line loads caused by the eccentricities of the column are shown. The letter e denotes the eccentricity and k the fact that it is a characteristic value.

$$Q_{e,rf,k} = \frac{(P_{cat,H} + P_{cat,E}) \cdot \frac{1}{300}}{D} = 0.17 \text{ kN/m}^1$$

$$Q_{e,fl,k} = \frac{P_{fl} \cdot \frac{1}{300}}{D} = 0.33 \text{ kN/m}^1 \quad (4.6)$$

4.2.5. Load combinations

For the design of the connection, the most critical load combination should be determined according to 6.10a and 6.10b of EN 1991-1-1 [30]. As mentioned in Appendix B the building is a CC2 construction. This influences the load factors used in Equations 6.10a and 6.10b. In addition to load factors, reduction factors also play an important role in load combinations. The reduction factors are based on the type of loading, in Table 4.4 an overview of the reduction factors used in the design is presented.

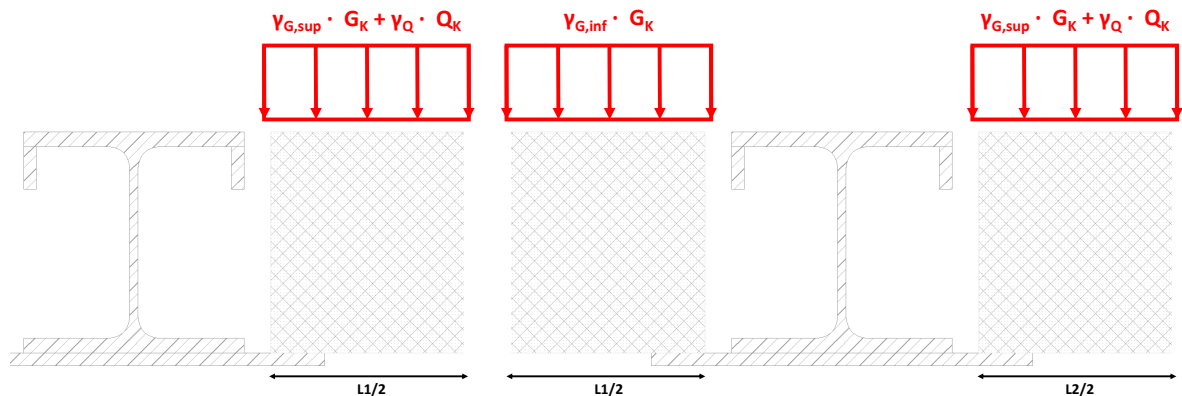
	ψ_0	ψ_1	ψ_2
Category B - office	0.5	0.5	0.3
Category E - storage	1.0	0.9	0.9
Category H - roof	0.0	0.0	0.0

Table 4.4: Combination factors ψ [30]

The connection should be able to withstand vertical and horizontal loads. Vertical loads directly affect the dimensions of the beam but also act as the primary forces on the connection. The eccentricity of the slab bearing point results in a bending moment that can be taken by a torque; one force in tension and one in compression with an internal lever arm. This couple acts in the horizontal plane and is the primary load for the connection; horizontal loads originating from the wind and the inclination of the column act as subordinate loads.

At the first floor, the most critical situation is the edge beam. The edge beam will not have the largest vertical load in magnitude, but due to the eccentric bearing and the absence of a floor slab on the opposite side of the beam, the moment has the largest magnitude. Therefore, only the following scenario is relevant:

- i. Edge beam fully loaded with category B - office load (Figure 4.3a).



(a) Loading situation i for roof and floor edge beam

(b) Loading situation ii for roof mid beam

Figure 4.3: Critical loading situations

In Equation 4.7 the vertical design load, denoted by subscript v , is determined for Equations 6.10a and 6.10b of the NEN-EN 1990 National Annex [30]. The partial safety factor for self-weight is equal to $\gamma_{G,sup} = 1.35$ and 1.20 for 6.10a and 6.10b respectively. The safety factor for the variable load is equal to $\gamma_Q = 1.50$. Due to the relatively large share of variable load, Equation 6.10b governs the design.

$$\begin{aligned} q_{v,fl,6.10a} &= \gamma_{G,sup} \cdot G_k + \psi_0 \cdot \gamma_Q \cdot Q_k = 1.35 \cdot 5.55 + 0.5 \cdot 1.50 \cdot 3.3 = 10.0 \text{ kN/m}^2 \\ q_{v,fl,6.10b} &= \gamma_{G,sup} \cdot G_k + \gamma_Q \cdot Q_k = 1.20 \cdot 5.55 + 1.50 \cdot 3.3 = 11.6 \text{ kN/m}^2 \end{aligned} \quad (4.7)$$

The roof structure has an area dedicated to technical installations in the middle of the roof; this creates additional critical loading situations due to the substantial difference in the magnitude of variable load. The following two scenarios are reviewed:

- i. Edge beam fully loaded with category H - roof load (Figure 4.3a),
- ii. Mid beam with uneven spans and loaded fully with category E - storage load (Figure 4.3b).

In Equation 4.8 and Equation 4.9 the vertical design load for the roof structure is provided, in these equations subscripts i and ii refer to the two scenarios, and l and r for the left and right beams as shown in Figure 4.3. For the mid beam with uneven loading, the self-weight of one side balances the load on the other side. Therefore, this load is multiplied by a factor $\gamma_{G,inf} = 0.90$.

$$\begin{aligned} q_{v,rf,i,6.10a} &= \gamma_{G,sup} \cdot G_k + \psi_0 \cdot \gamma_Q \cdot Q_k = 1.35 \cdot 6.0 + 0.0 \cdot 1.50 \cdot 1.0 = 8.1 \text{ kN/m}^2 \\ q_{v,rf,i,6.10b} &= \gamma_{G,sup} \cdot G_k + \gamma_Q \cdot Q_k = 1.20 \cdot 6 + 1.50 \cdot 1 = 8.7 \text{ kN/m}^2 \end{aligned} \quad (4.8)$$

$$\begin{aligned} q_{v,rf,l,6.10} &= \gamma_{G,inf} \cdot G_k = 0.9 \cdot 6.0 = 5.4 \text{ kN/m}^2 \\ q_{v,rf,ii,6.10a} &= \gamma_{G,sup} \cdot G_k + \psi_0 \cdot \gamma_Q \cdot Q_k = 1.35 \cdot 6.0 + 1.0 \cdot 1.50 \cdot 5.0 = 15.6 \text{ kN/m}^2 \\ q_{v,rf,ii,6.10b} &= \gamma_{G,sup} \cdot G_k + \gamma_Q \cdot Q_k = 1.20 \cdot 6.0 + 1.50 \cdot 5.0 = 14.7 \text{ kN/m}^2 \end{aligned} \quad (4.9)$$

What can be observed is that for the first scenario, i, Equation 6.10b governs, while for scenario ii 6.10a governs. Both situations still need to be reviewed in combination with wind and imperfections due to the different ψ -factors, as shown in Table 4.4. Design values for subordinate loading types are calculated in Equation 4.10 and Equation 4.11. The design value is generated by multiplying the loads by the loadfactor γ_Q .

$$\begin{aligned} Q_{w,fl,d} &= 1.5 \cdot (Q_{w,pre,fl,k} - Q_{w,suc,fl,k}) = 1.5 \cdot (2.11 - -1.32) = 5.14 \text{ kN/m}^1 \\ Q_{w,rf,d} &= 1.5 \cdot (Q_{w,pre,rf,k} - Q_{w,suc,rf,k}) = 1.5 \cdot (1.77 - -1.11) = 4.33 \text{ kN/m}^1 \end{aligned} \quad (4.10)$$

$$\begin{aligned} Q_{e,fl,d} &= 1.5 \cdot Q_{e,fl,k} = 1.5 \cdot 0.33 = 0.50 \text{ kN/m}^1 \\ Q_{e,rf,d} &= 1.5 \cdot Q_{e,rf,k} = 1.5 \cdot 0.17 = 0.26 \text{ kN/m}^1 \end{aligned} \quad (4.11)$$

The vertical load in combination with the eccentricity generates a bending moment, since the slab is assumed to be simply supported the force can be calculated with the formula shown in Equation 4.12. The bending moment divided by the internal lever arm z_1 gives the horizontal force that is part of the torque. The magnitude of this bending moment depends on the beam spans and the geometric properties of the connection. The beam spans $L1$ and $L2$ are adopted from the case study shown in section B.3, but geometric properties can vary for different types of connections and are therefore given in terms of variables e and z_1 . For the case study geometry the e and z_1 parameters are shown in section B.4.

$$M_e = \sum_{n=0}^e V(x) = \left[q \cdot \left(\frac{L1 - e}{2} \right) \right] \cdot e \quad (4.12)$$

In Equation 4.13 the horizontal load on the connection that originates from the eccentricity is calculated first. In addition to this, the wind load according to Equation 4.10 and the column inclination load according to Equation 4.11 are added. The total horizontal load per metre beam is shown in Equation 4.14.

$$\begin{aligned}
F_{h,fl,d} &= \max [q_{v,fl,6.10a}, q_{v,fl,6.10b}] \cdot \left(\frac{L1 - e}{2} \right) \cdot \frac{e}{z_1} = 11.6 \cdot \left(\frac{11 - e}{2} \right) \cdot \frac{e}{z_1} \text{ [kN/m}^1\text{]} \\
F_{h,rf,i,d} &= \max [q_{v,rf,i,6.10a}, q_{v,rf,i,6.10b}] \cdot \left(\frac{L1 - e}{2} \right) \cdot \frac{e}{z_1} = 8.7 \cdot \left(\frac{11 - e}{2} \right) \cdot \frac{e}{z_1} \text{ [kN/m}^1\text{]} \\
F_{h,rf,ii,d} &= \max [q_{v,rf,ii,r,6.10a}, q_{v,rf,ii,r,6.10b}] \cdot \left(\frac{L2 - e}{2} \right) \cdot \frac{e}{z_1} - q_{v,rf,l,6.10a} \cdot \left(\frac{L1 - e}{2} \right) \cdot \frac{e}{z_1} = \\
& 15.6 \cdot \left(\frac{8 - e}{2} \right) \cdot \frac{e}{z_1} - 5.4 \cdot \left(\frac{11 - e}{2} \right) \cdot \frac{e}{z_1} \text{ [kN/m}^1\text{]}
\end{aligned} \tag{4.13}$$

$$\begin{aligned}
F_{fl,d} &= F_{h,fl,d} + \psi_2 \cdot Q_{w,fl,d} + \psi_3 \cdot Q_{e,fl,d} \\
F_{rf,i,d} &= F_{h,rf,i,d} + \psi_2 \cdot Q_{w,rf,d} + \psi_3 \cdot Q_{e,rf,d} \\
F_{rf,ii,d} &= F_{h,rf,ii,d} + \psi_2 \cdot Q_{w,rf,d} + \psi_3 \cdot Q_{e,rf,d}
\end{aligned} \tag{4.14}$$

From the total horizontal load calculation in Equation 4.14 the most critical loading condition is determined. As a result, the fully loaded edge beam of the floor slab is most critical. In Equation 4.15 the design formula for the horizontal load is given, where $\psi_2 = 0.5$, $\psi_3 = 0.3$ and parameters e and z_1 are geometry dependent.

$$\begin{aligned}
F_{h,d} &= F_{h,fl,d} + \psi_2 \cdot Q_{w,fl,d} + \psi_3 \cdot Q_{e,fl,d} \text{ [kN/m}^1\text{]} \\
F_{h,fl,d} &= 11.6 \cdot \left(\frac{11 - e}{2} \right) \cdot \frac{e}{z_1} \text{ [kN/m}^1\text{]} \\
Q_{w,fl,d} &= 5.14 \text{ kN/m}^1 \\
Q_{e,fl,d} &= 0.50 \text{ kN/m}^1
\end{aligned} \tag{4.15}$$

The total horizontal load that should be transferred is denoted by $F_{h,d}$ and consists of three parts. $F_{h,fl,d}$ is the design value of the horizontal load resulting from the vertical floor load, $Q_{w,fl,d}$ is the wind line load that results in the diaphragm working of the slab, and $Q_{e,fl,d}$ is the horizontal load resulting from the eccentricity of the columns.

4.3. Alternatives

Based on the requirements and loads specified in the two previous sections, three different design alternatives are created. All the designs have the capability to fulfill the requirements stated in [section 4.1](#). The result consists of the following three connections:

- Injected connection,
- Demountable bolted shear connector connection,
- Pretensioned connection.

Load transfer principle

For the three different designs, the load transfer principle is similar. The connection consists of an integrated non-torsional stiff beam and a hollow core slab. The stiffness of the hollow core slabs in terms of bending is assumed to be larger than the torsional stiffness of the beam. This results in compression on the upper side of the connection and tension on the lower side. This tensile force is transferred for all alternatives via a shear force at the bearing point of the slab. The assumption of lower torsional stiffness for the beam compared to the stiffness of the slab is verified at a later stage in [section 7.1](#). In [Figure 4.4](#) the principle is shown, the green arrows indicate the actions on the beam, and the orange arrows the reactions on the slab. The zero bending moment point of the slab is located in the heart of the integrated beam.

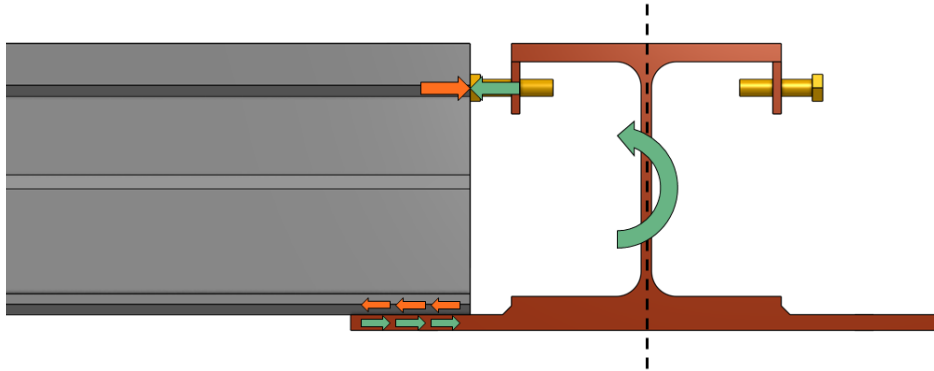


Figure 4.4: Load transfer principle for all of the alternatives, green arrows indicate the actions and orange arrows the reactions

What can be observed from the figure is that the upper compressive bolt is placed in a threaded hole. A nut on the inside of the beam would be difficult to reach due to the tight margins between the face of the hollow core slab and the beam. For the lower side, the load is transferred by a shear load in the bottom flange. The tensile force in the beam flange can be taken by the bottom plate of the integrated beam, for the hollow core slab the shear load needs to be introduced in the slab. All the above-mentioned alternatives have a different principle to transfer these loads and introduce them into the hollow core slab.

In the following sections, the three alternative designs are presented. Three-dimensional drawings with exploded views are shown for the alternatives. In addition to the connection drawings, the steps required for installation and disassembly are provided, as well as an explanation of the force flow for the specific alternative.

4.3.1. Injected connection

The first design alternative is based on the design that was used for the temporary courthouse, this idea was already presented in the literature review ([subsection 2.2.2](#)). The main change in the design is the implementation of additional tolerances, which is achieved by adding an oversized bolt hole to the bottom flange of the beam. The dimensions of these holes are determined on the basis of data from [chapter 3](#). In [Figure 4.5](#) an exploded view of the connection is shown. In this figure, the following parts can be distinguished: hollow core slab (grey), integrated beam (red), sleeve concrete (light grey),

end plate with stirrup (green), injection resin (dark blue), cover plate (orange), and bolts (yellow). In addition, a curved DEMU anchor is casted inside of the hollow core slab sleeve to create the shear connection at the bottom flange. A cross-sectional view at the heart of the hollow core slab sleeve is shown in [Figure 4.7](#) which shows the DEMU anchor in blue and the stirrup in green.

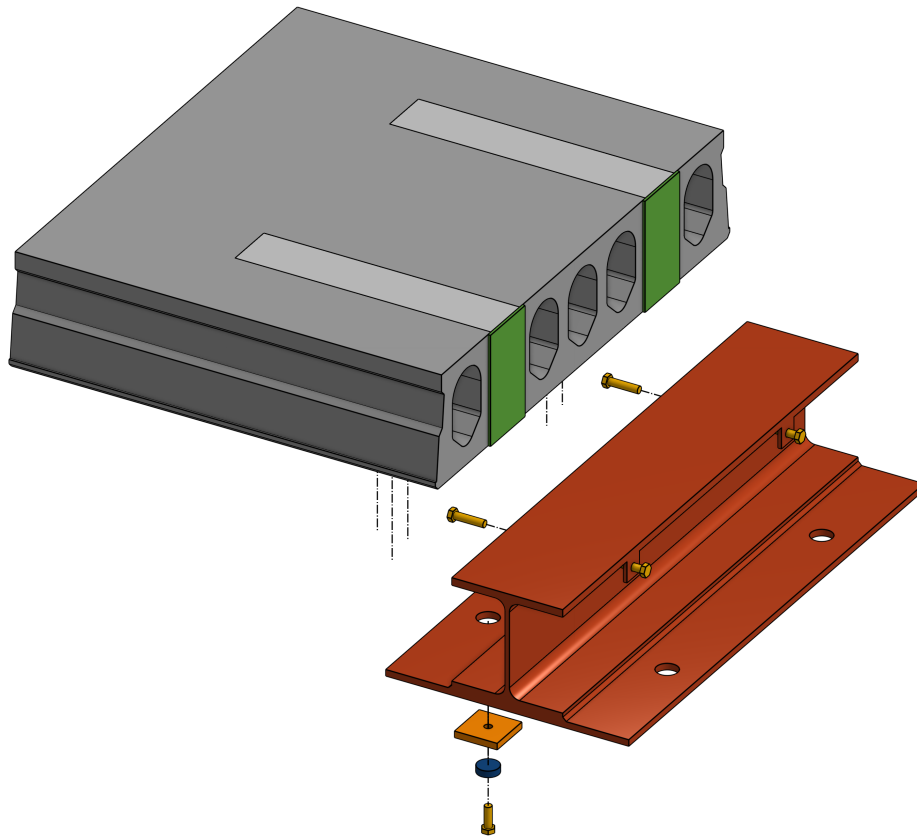


Figure 4.5: Connection detail with resin injection (exploded view)

Installation

The installation procedure for this connection is based on two steps. First, as an intermediate step after construction and before installation on site, the DEMU anchor and end plate are placed in two of the hollow core sleeves per side of the slab, this is denoted with phase (a). The opening of the hollow core sleeves is part of the standard procedure and is performed during production at the manufacturing site. The end plate functions as a formwork and closes the face of the hollow core slab sleeve. Special attention should be paid to the placement of the DEMUs to achieve the required tolerance level. To achieve this precision, a tailor-made formwork element can be used to ensure perfect alignment of the DEMUs and prevent concrete from pouring out at the bottom side of the hollow core slab.

Subsequently, the slab with the implemented reusable measures is transported to the building site. At the construction site, the steps indicated with phase (b) are performed. The slab is placed on the beam flange and the bolts are tightened from underneath. It is important that the beam is propped during the construction stage to prevent the beam from unwanted rotations. As a final step, the oversized bolt hole is injected with resin material and the compressive bolt at the upper side is adjusted to ensure full contact between the beam and the slab. After the resin material has been cured, the props are removed and the structure is ready to use. To summarise, the following 7 steps should be executed:

- (a) 1) Opening of the hollow core sleeves,
- 2) Positioning of the DEMUs, end plate, and formwork,
- 3) Filling of the sleeve with Spramex concrete and compacting,
- (b) 4) Placing the slab on the flange of the integrated beam,

- 5) Placing the cover plate and tightening of the injection bolt at the bottom flange,
- 6) Inject the bolt hole with resin material,
- 7) Adjust the compression bolt at the top side.

Once the steps mentioned above are completed, the structure is ready, in [Figure 4.6](#) the installed situation of the connection is shown.

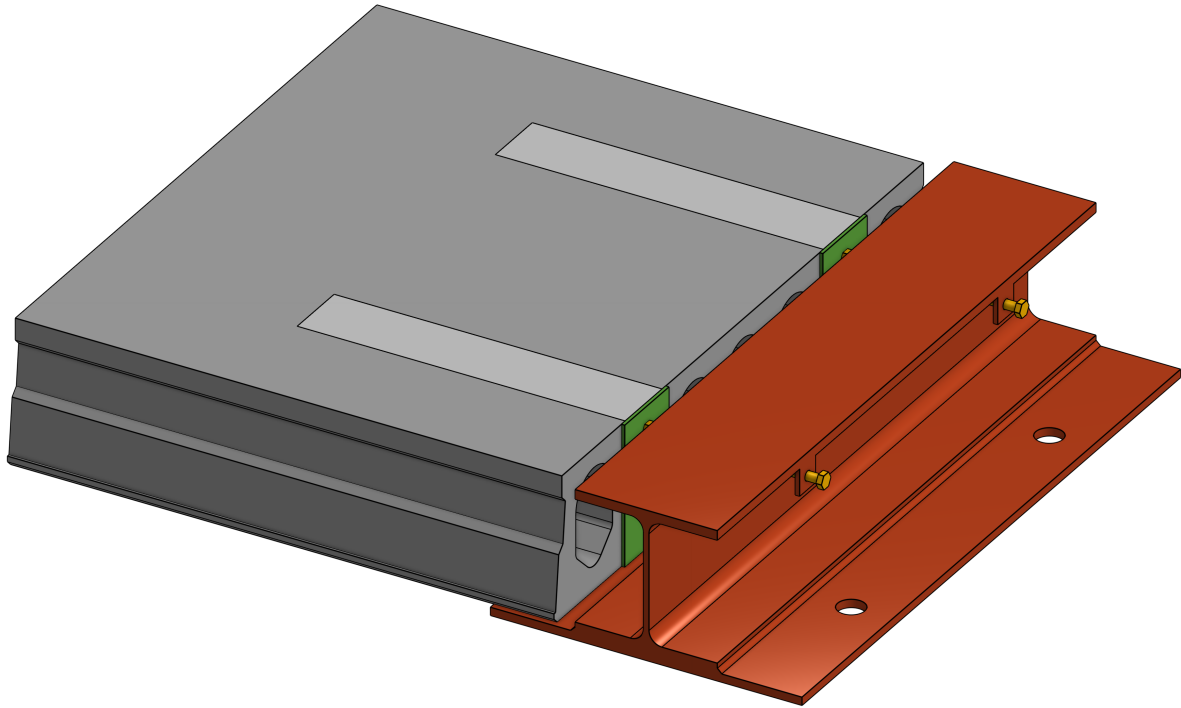


Figure 4.6: Connection detail with resin injection in installed position

Force transfer mechanism

The tensile force on the lower side of the slab is transferred by means of a shear force to the bolt on the bottom flange of the integrated beam. This is done using a curved DEMU anchor and an additional stirrup around the vertical part of the DEMU. This stirrup helps to create a larger lever arm, which reduces the magnitude of the forces. Close attention should be paid when determining the edge distances; concrete breakout failure should be avoided at all times. The force transfer on the upper side is ensured by the end plate and an adjustable bolt, the end plate will activate a larger concrete area to take the compressive forces. Unscrewing of the upper bolt ensures a compressive connection between the hollow core slab element and the integrated beam. The dimensions of this plate and the optional stiffeners should be determined accordingly. The bolt in the bottom flange, which is loaded in shear, transfers, as well as the force originating from the bending moment, the horizontal load from wind, and column inclination. In addition to the strength verifications, the stiffness of the connection should be checked. The stiffness for the injected connection is mainly based on the slip of the bolt and the deformation of the compressive plate at the upper side. Connection slip can be seen as critical since the bolt hole is oversized and the stiffness of the injection resin is significantly lower compared to the stiffness of steel.

In [Figure 4.7](#) the flow of forces in the connection is shown. The magnitude of the shear, tensile, and compressive forces depends on the lever arm z_1 and the eccentricity of the bearing point e . The lever arm z_1 is located from the upper compressive point until halfway between the stirrup and the DEMU anchor. The exact tensile zone is located between both tensile reinforcement bars.

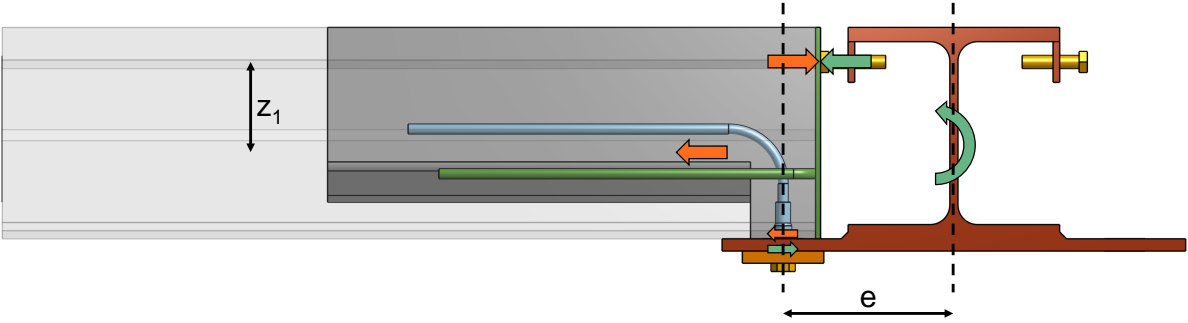


Figure 4.7: Flow of forces for the resin injected connection

Disassembly

The disassembly procedure comprises the steps described in phase (b) in reverse order. The upper bolt is loosened and the injected bolt in the bottom flange is removed. After this, the slabs can be removed with the help of special lifting clamps. For a reuse cycle, the steps of phase (b) are repeated.

4.3.2. Demountable bolted shear connector connection

The second design alternative is based on a demountable bolted shear connector. This demountable bolted shear connector, or also referred to as a bolted shear stud, is a bolted stud instead of the more widely used welded studs. The advantage of this bolted connector is that the structure can be easily demounted. The application of the demountable shear connector has already been thoroughly investigated; a state-of-the-art review was performed by Jakovljevic [55]. The application of these connections is usually in steel concrete composite floor systems. To ensure that the connection can be dismantled, the shear connector is placed in an enclosed environment in terms of a square hollow section (SHS). The gap between the demountable shear connector and the square hollow section is filled with mortar to ensure full load transfer. In Figure 4.8 an exploded view of the connection is presented. The parts can be distinguished from the figure: hollow core slab (grey), integrated beam (red), sleeve concrete (light grey), square hollow section (blue), bolted shear connector (green), mortar (dark grey), and compressive bolt (yellow).

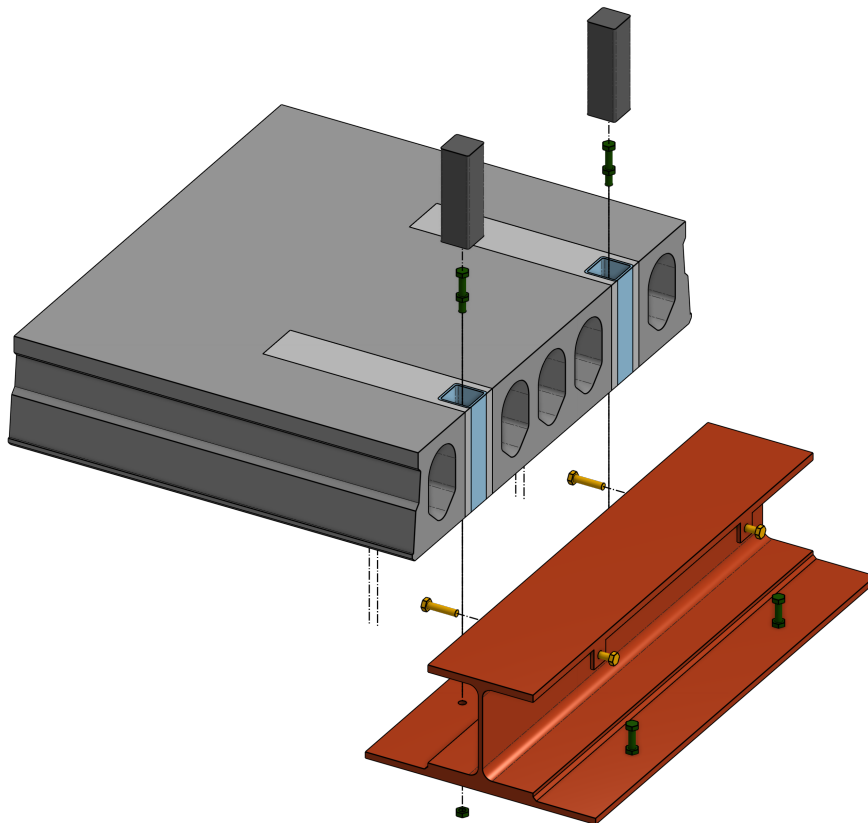


Figure 4.8: Connection detail with bolted demountable shear connector (exploded view)

Installation

Installation of the demountable shear-stud connection consists, similar to the injected connection, of two phases, (a) and (b). Phase (a) is similar to the injected connection and is performed after fabrication but before installation on site. For the first phase, there is one major advantage, the alignment of the SHS section is, compared to the injected alternative, more simple. This is due to the fact that there is only one element compared to the end plate with stirrup and DEMU anchor. The second part consists of steps 4 to 7 as presented in the list below. Installation of the elements is performed from above, which is a big advantage and is a procedure similar to that of the conventional installation.

- (a) 1) Opening of the hollow core sleeves,
- 2) Positioning of SHS section with anchor;
- 3) Filling of the sleeve with Sparamex concrete and compacting,
- (b) 4) Placing the demountable shear connectors in the beam flange;

- 5) Placing the slab on the flange of the integrated beam over the demountable shear connector;
- 6) Apply formwork release agent and add the concrete filling to the SHS section;
- 7) Adjust the compression bolt at the top side.

In [Figure 4.9](#) the installed situation is shown. From this figure, it can be observed that the SHS section is not completely filled with mortar but is casted slightly below the upper edge.

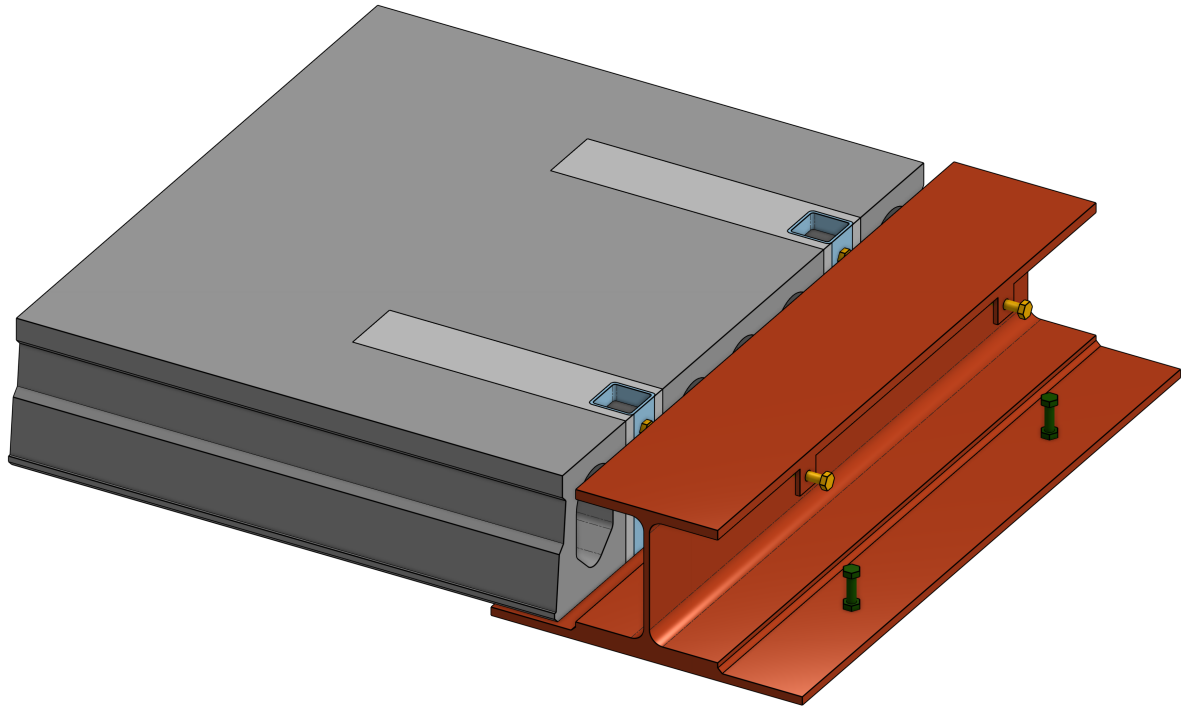


Figure 4.9: Connection detail with demountable shear connector in installed position

Force transfer mechanism

The origin of the forces in the connection is similar to the injected variant. Load magnitudes are slightly lower because of the optimised larger lever between the compressive zone and the reinforcement anchor. The bottom reinforcement bar is positioned at the bottom of the cores but with taking into account sufficient concrete cover to allow full bond between the reinforcement and the sleeve concrete. Compressive forces located at the upper side are taken by the SHS section, the mortar filling transfers the compressive stresses and prevents local buckling of the section web. The load on the bottom side is transferred via the bolt with an additional integrated nut. Research by Kwon [61] shows an increase in stiffness compared to a single bolt. In the ideal situation, a shear stud without a head and an embedded nut is used to create more tolerance inclusion. However, this would require a custom-made connection and is an expensive option.

In [Figure 4.10](#) the flow of forces in the connection is shown.

4.3.3. Pretensioned connection

The third design is an adapted version of the second design. The main difference is that the demountable shear connector with mortar is replaced by a prestressed connection. This is achieved by prestressing an anchor rod that puts the square hollow section under compression. The major advantage is that this connection can be classified as a "dry" connection; dry connections are marked by the absence of bonded products. In Figure 4.11 an exploded view of the connection is shown. In the figure the following elements are indicated: hollow core slab (grey), integrated beam (red), sleeve concrete (light grey), square hollow section (blue), compressive plate (orange), prestressed anchor rod (green) and compressive bolt (yellow).

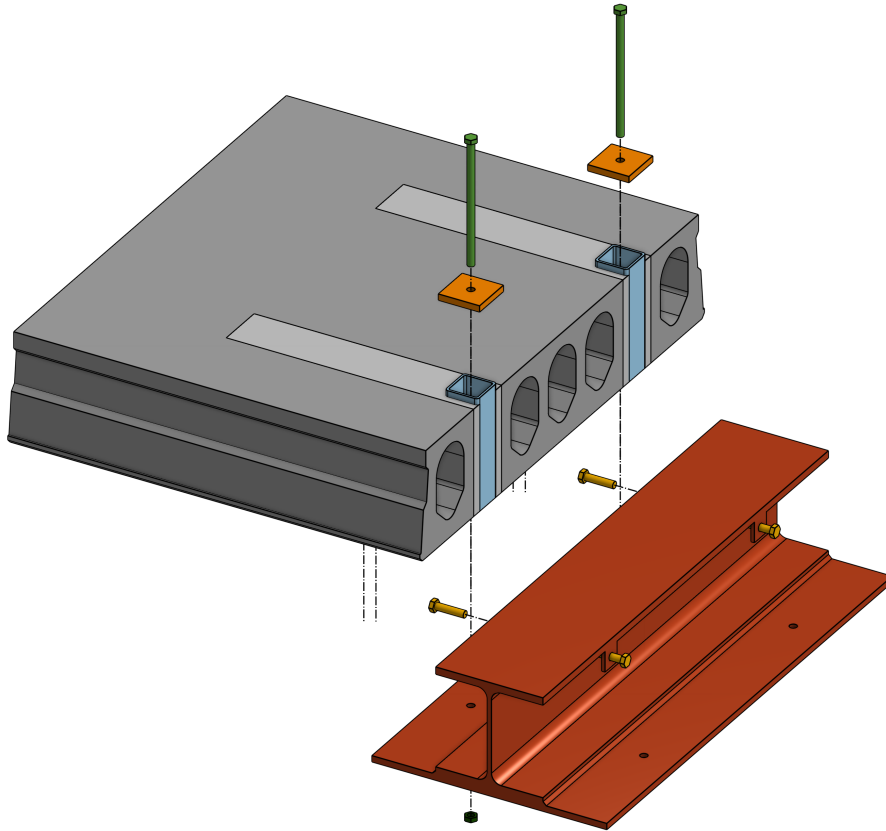


Figure 4.11: Connection detail with pretensioned connector in exploded view position

Installation

The installation procedure for the pretensioned connection covers the same initial steps of stage (a) as the demountable shear connector variant; the adjustments made to the hollow core slab are identical with the exception that the SHS section should be slightly longer to prevent prestressing of the concrete hollow core slab. However, the installation on site differs, the mortar and shear stud are replaced by an anchor rod and thick steel cover plate. The cover plate is designed to be large enough to account for alignment tolerances in the connection. The anchor rod with a nut on both sides is pretensioned with the help of specialised equipment. Due to initial pretensioning losses, the nut should be tightened twice as indicated by steps 7 and 9. The installation steps are shown in the list below.

- (a) 1) Opening of the hollow core sleeves,
- 2) Positioning of SHS section with anchor;
- 3) Filling of the sleeve with Spramex concrete and compacting,
- (b) 4) Placing the slab on the flange of the integrated beam;
- 5) Placing the thick cover plate and anchor rod;
- 6) Tightening of the nut at the bottom flange;
- 7) Pretension the nut at the top side;

- 8) Adjust the compression bolt at the top side;
- 9) Pretension the nut at the top side to compensate for initial prestress losses.

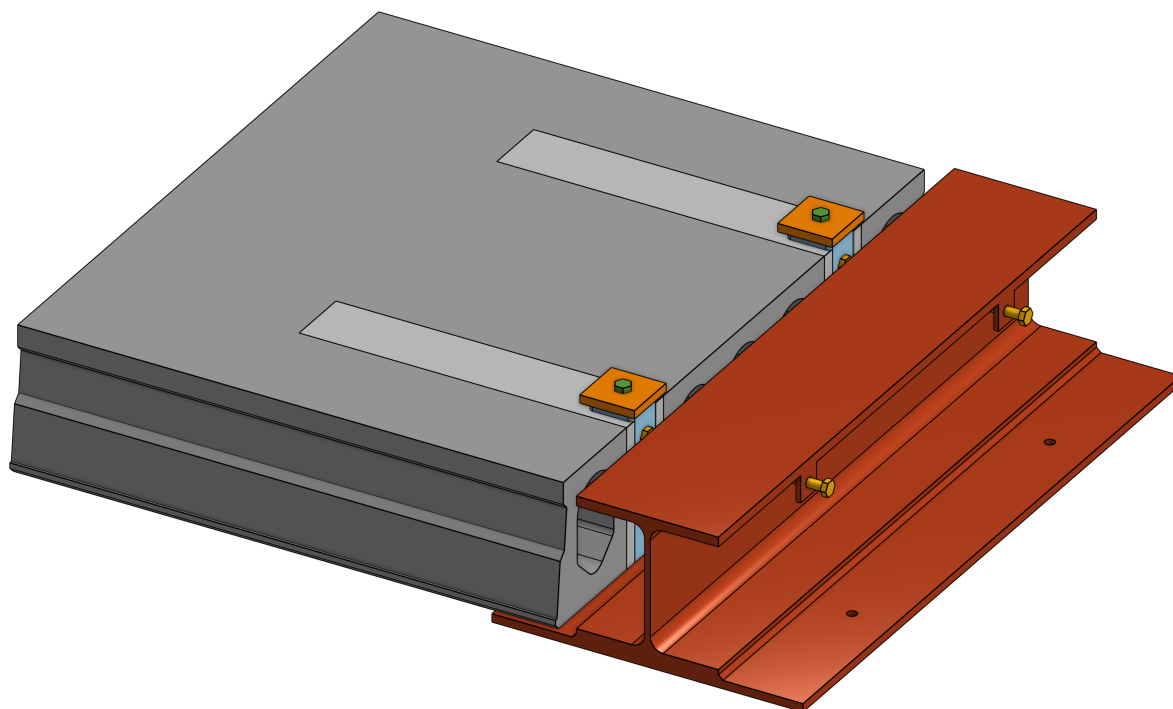


Figure 4.12: Connection detail with pretensioned connector in installed position

Force transfer mechanism

In the pretensioned variant, an additional force is introduced, namely the pretension force. This force, shown with the red arrows in [Figure 4.13](#), comes from the forced elongation of the bolt. Due to tightening of the nut, the distance between the nuts becomes smaller, while the square hollow section wants to keep its length. The SHS section is slightly taller than the thickness of the hollow core slab to ensure that all pretensioning force are transferred to this section. As a result, a compressive force is exerted on the SHS profile. Thick cover plates ensure that the load is spread over the entire cross sectional area of the SHS section. Shear forces located at the lower flange are transferred by friction. The cross-sectional area of the hollow section is in contact with the bottom flange of the integrated beam; this interface has a certain roughness expressed by the parameter μ and gives a friction resistance. For the compressive force on the upper side, the absence of mortar filling inside the section results in the fact that the load should be taken by the section. This, in combination with the pretensioning force, makes the section susceptible to local buckling of the section web.

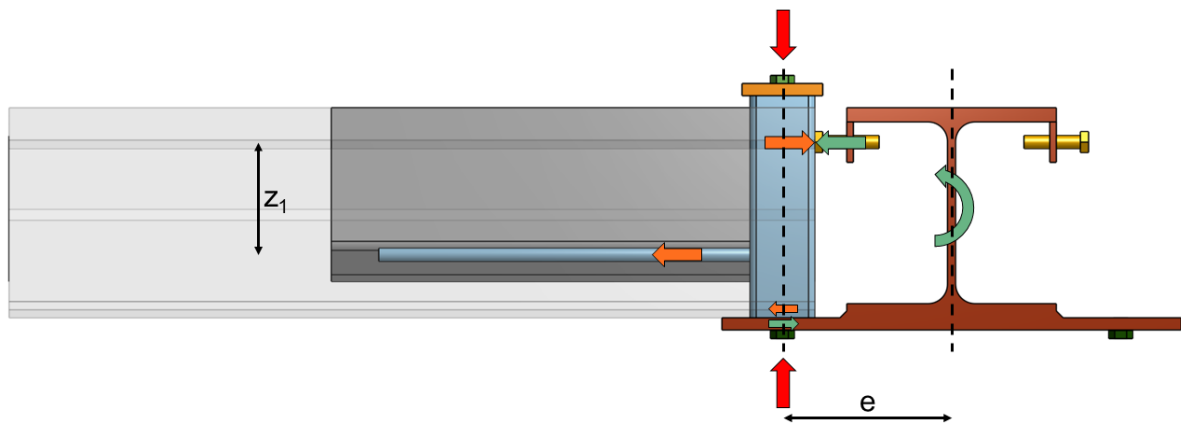


Figure 4.13: Flow of forces for the pretensioned injected connection

Disassembly

During disassembly, the pretensioned rod should be untightened and removed together with the cover plate on the top side. After this, the hollow core slab can be removed and is ready for a reuse cycle. No additional steps are needed to prepare the slab for reuse since the connection has no bonded components. To install the element in its second life, phase (b) is repeated.

5

Qualitative trade-off analysis

In the following chapter, a comprehensive qualitative trade-off analysis is presented in which the alternatives mentioned in [subsection 4.3.1](#), [subsection 4.3.2](#), and [subsection 4.3.3](#) are evaluated based on criteria that include tolerances, ease of installation, demountability, and costs. In [section 4.1](#) various design requirements were presented. Not all are weighted in this section since functional and production requirements are met for all variants. Therefore, these points will not generate a basis for decision making. Since the four criteria are not all equally important, a weighting factor with a scale from one to three is added. The costs, for example, are one of the main drivers of decision making. Reducing the additional costs to the bare minimum can convince decision makers to implement the reusable connection, resulting in more reusable structures. This results in the fact that this criteria gets the highest weighting factor of three.

All criteria addressed in the trade-off analysis are analysed, reviewed, and eventually weighted in a trade-off matrix. This evaluation is based on quantitative and qualitative approaches. As a result of this analysis, one alternative receives the highest score and is selected for a more detailed verification.

5.1. Tolerances

In [chapter 3](#) the minimum required tolerances to create a reusable connection was reviewed. All alternatives are designed so that they can incorporate the minimum requirements. However, accounting for more tolerances than the bare minimum can result in an increased speed of erection, and therefore creates a beneficial effect. In the following paragraphs, the different tolerances for the three alternatives are considered.

Injected connection

The tolerances for the injected connection are based on the oversize of the bolt hole in the bottom flange of the beam. Several limiting factors set the maximum oversize. First, the minimal edge distances according to Table 3.3 of Eurocode 1993-1-8 [20] should be incorporated. For larger hole sizes, the edge distances increase as well, which is related to the width of the beam flange. Increased flange width also results in a greater eccentricity of the bearing point and subsequently an increased load. Another limiting factor is the stiffness of the resin, with a Young's modulus of 11.6 GPa under confined conditions for a standard resin and 29.8 GPa for steel-reinforced resin [76]. Slip should be limited since hollow core slabs are generally designed with the maximum serviceability limit state deflections taken into account. Increased connection slip could result in excessive deformations.

Bolted shear connector connection

For the bolted shear connector connection, tolerances are expressed as the gap between the inner dimensions ($h-2t$) of the square hollow section and the bolt head. Since the mortar casted around the bolt is under confined conditions, it is expected to slip minimally. Compared to the standard resin material, the stiffness is higher with a Young's modulus of 29 GPa [81] based on unconfined conditions as prescribed in the NEN-EN 12390-3 [32]. For confined conditions as present in the actual situation the stiffness of the mortar increases. Theoretically, the dimensions of the SHS section can be increased until the full width of the hollow core slab's sleeve is reached; however, this also implies that the bottom flange of the beam should be wider. This increased width of the bottom flange can result in a larger eccentricity of the bearing point and sequentially increases the loads. In conclusion, a detailed analysis of the most optimal dimensions of the SHS sections should be performed.

Prestressed connection

The prestressed connection uses the same SHS section as the shear connector connection. The prestressed connection can, in theory, account for more tolerance compared to the bolted shear connector connection; the dimension of the anchor rod is smaller than the dimension of the bolt head. This results in an additional tolerance capacity or the possibility to reduce the dimensions of the SHS section. However, for the most critical situation, this implies that the pretensioned anchor rod is placed eccentrically in the section. Resulting in an uneven compressive stress in the section and reduced slip resistance. Further investigation into the maximum eccentricity and the load spreading of the compressive stresses should be performed in case the prestressed alternative scores best in the trade-off matrix.

5.2. Installation

The ease and speed of installation is an important factor to consider. Conventional installations between steel beams and hollow core slabs occur from the upper side of the slab. During this process, the beam must be propped until the concrete hardens. Reinforcement bars are placed in the hollow core sleeves and welded to the integrated beams; after this operation, the sleeves and the void between the beam and the hollow core slab are filled with Spramex concrete. A special type of concrete with a small aggregate size.

For the three alternatives, the installation method varies. The various installation steps are already prescribed in [chapter 4](#). In this section, the installation procedures are reviewed qualitatively; for completeness, a quantitative overview is presented in [Appendix E](#). Quantitative results were discussed with an expert from the Rotterdam-based engineering firm Multicall¹. Based on the acquired knowledge, it was decided that the quantitative results are not presented in the main report for various reasons. First, the differences obtained in installation costs are minimal, and precise time estimations are susceptible to several influences. For example, the contractor may have preferences or more experience with a certain construction method. The preferred method of execution is chosen based on costs, but also based on availability of certain resources (equipment/ construction workers). Lastly, the price of labour is subject to high variability, and the relation between labour prices and material prices at a certain moment in time can have a strong influence on the most favourable alternative in terms of total costs.

The installation consists of two phases; first, the installation of the connectors inside the sleeves of the hollow core slab and subsequently the installation of the hollow core slab with the integrated steel beam. For the first phase, the procedures are more or less similar. A minor difference is found in the fact that the positioning of the DEMU for the injected connection is slightly more challenging than that of the square hollow section with welded reinforcement bar for the bolted shear connector and prestressed connection. The installation part that takes place on-site is reviewed below for the three alternatives.

Injected connection

The installation of the injected connection on site comprises four steps. First, the slab should be placed on the beam flange. To ensure easier alignment, a centering pin can be used. The threaded part is screwed into the bottom DEMU and the slabs are placed at the correct location. Afterwards, the centering pins are removed, and the cover plates with injection bolts are tightened. After this step, the

¹An engineering firm specialised in building costs.

resin is injected with a special caulking gun. Multiple slabs are installed with one batch of Expoy resin, but the limited pot time results in the fabrication of multiple batches to install all the hollow core slabs in the complete structure. Since the placement of the bolts and injection of the resin is done from below, additional equipment is required. To perform these steps, the minimum necessity is a mobile scaffold, but preferably a scissor lift or even a cherry picker. The latter is mandatory in case the floor slabs have openings for stairs, elevators, or architectural purposes. Adjusting the compression bolt located on the upper side is similar for all alternatives and therefore does not make any impact difference. The curing time of the resin is 14 hours [52], and after this the props are removed, resulting in a fast execution time.

Bolted shear connector connection

The installation of the bolted shear connector alternative comprises four steps, similar to the injected connection. The first step is to place the shear connectors on the beam flange. This is done before the beams are installed, and therefore no additional equipment is needed. After this, the slabs should be lifted into place and carefully placed over the shear connectors; the procedure should be performed with great precision, otherwise damage to the bolted shear studs may occur. The main advantage of this alternative is that all the installation steps are performed from the upper side of the slab. After placing the slabs, the SHS sections should be treated with a release agent and the mortar is poured into the section. Treatment of the SHS section can be done in advance to minimise the installation time on-site. The mortar mixture has a slump of 700 mm [38], which implies that it is very fluid and can easily be poured into the section. Mortar can be mixed on site with the help of a handheld cement mixer and a mortar tub. The strength of the mortar develops rapidly and therefore the props are removed after 24 hours [38]. Installation of this connection could be even faster than the traditional alternative, since there is no need to weld and pour concrete on site.

Prestressed connection

Installation of the prestressed connection consists of six steps, and this means two more with respect to the other alternatives. The procedure starts with the placement of the slabs on the beam flange. After this step, the thick cover plate and the anchor rod are placed from above. However, a bottom nut is still needed, which requires a procedure similar to that used for the injection bolt. This means that this connection requires operations from above and below and, therefore, is the most complicated. After all components are installed, the connector is pretensioned; due to initial pretension losses such as embedment relaxation (Table 2.4.2), another pretension cycle is performed after 24 hours. In addition to the additional installation steps, the use of pretension bolts in the building construction industry is not a common practice. Therefore, it is highly likely that a specialist firm is needed, resulting in higher installation costs.

5.3. Demountability

The demountability of the connection is the key part of a reusable structure. For demountability, a qualitative reasoning is presented below. For the quantitative approach, there are the same uncertainties as for the installation and, therefore, the results are only presented in Appendix E. Demountability is assessed based on the number of steps required to demount and prepare the slab for a new installation. Measures permanently installed in the slabs, indicated by phase (a), in chapter 4, should not be damaged during the demounting process. From experience with the demolition of hollow core slabs for reuse, it was found that the removal of the first slab can be difficult. This point was addressed by an expert from Lagemaat Circulair BV² who dismantled the temporary courthouse. Therefore, it is recommended to use lifting eyes for the slabs located along the edges of the structure. Once the edge slab is removed, a crowbar is used to move the slabs laterally and remove the filling from the longitudinal joints. As a next step, the slabs are removed with the help of a lifting clamp. For all alternatives, props are necessary to prevent unwanted torsion of steel frames during deconstruction. Specific demounting operations for the alternatives are presented below.

Injected connection

The demountability of the injected connection depends on the bonding between the resin and the steel.

²An demolition and deconstruction company who focus on circularity.

Proper application of a release agent around the perimeter of the bolt hole and the bolt threads ensure easy disassembly [69]. After the bottom bolt is unscrewed and the compressive force in the top bolt is released, the slab is lifted and ready for reuse. The bolt has to be scrapped, and other components should be cleaned of excess resin.

Bolted shear connector connection

The bolted shear connector connection is removed by unscrewing the bottom nut and in the following step the slab is lifted. After the slabs have been removed from the steel frame, the square hollow sections are cleaned of the mortar and the bolts. The demountability depends on the bonding between the mortar and the square hollow section. The bonding between the SHS section and the mortar originates from a chemical bond and friction resistance. The chemical bond is broken by the application of a release agent. Friction resistance is influenced by imperfections in the SHS profile; to reduce friction, a lubricant should be applied. Because the effect of these measures is highly uncertain and little to no research is available on the magnitude of the chemical bond, further investigation should be performed in case the alternative scores best in the matrix and is further investigated. In a worst-case scenario, the mortar can also be drilled out of the section. This is a more time-consuming process and, therefore, an unfavourable option due to the associated costs.

Prestressed connection

The prestressed connection is a so-called "dry" connection which implies that there is no physical bonding between the elements. After unscrewing the bottom nut, all connector elements are removed and the slab is lifted.

5.4. Costs

In addition to tolerances, installation, and demountability, costs play an important role. The cost of the connections is based on the general modifications needed for all of the alternatives and the additional materials needed for the specific connections. Labour costs are not taken into account in the cost breakdown, as they were qualitatively described in the installation and demountability sections.

This cost breakdown will not take into account the non-reusable alternative, as there are multiple other factors influenced by the design choice of reusable and non-reusable. The costs presented in [Table 5.1](#), [Table 5.2](#) and [Table 5.3](#) are the costs for the elements that differ by connection type. Elements such as sleeve concrete, compressive plates, and drilling of the bolt holes are excluded from this connection price to make the price differences clearer. However, the price of these elements is calculated separately to show the total connection costs.

The costs for most steel components are provided by Vic Obdam Staalbouw BV³, if this is not the case, it is specified. All prices shown are excluding VAT and are based on the price point of 7 November 2023 and on a purchase volume of 400 pieces. Since most of the parts in the connection require 4 units per slab element, the 400 pieces correspond to 100 reusable hollow core slabs. Some alternatives require special-made parts, and therefore, the prices of these components are subject to high variability. Standardising the details for future work could drastically reduce costs.

Injected connection

In [Table 5.1](#) the cost breakdown for the injected alternative is shown. The injection bolt is a modified and more complex item that includes an injection hole through the head of the bolt and a modified washer. The price for this element was provided by the specialist firm Peco Douwes and was set at € 6.80 per set. A set includes a bolt, two washers, and a nut. For the intended application, the nut and one of the washers in the set are deducted from the price, as these are not needed. This results in a reduced price of € 5.72 for the injection bolt and washer. Research carried out by Gîrbacea [48] gives a unit price of € 3.75 for an M20 8.8 injection bolt and washer. The price found by Gîrbacea is a significantly lower, a possible cause is found in the change in price point over time. The price point for 2018 and 2023 can differ significantly due to external influences such as the 2019 Covid pandemic, environmental measures, or geopolitical unrest.

³A steel construction firm.

The air escape groove in the washer is important to ensure full injection of the bolt hole. The injection material and the release agent price were adopted from Viba [91]. The volume of resin was calculated for an M16 bolt with a 20 mm oversize and a flange thickness of 15 mm. For the air escape groove and spilling, a loss of 20 % was taken into account. Prices of the release agent were estimated based on the research carried out by Nijgh [70]. The cost data for the injection and release agent are in line with the research of Gîrbacea [48], where a price of € 2.50 per unit was found for an injection including labour costs. For the second lifetime of the element, the costs are expected to be lower, since most of the elements are fully reused. This is accomplished when the release agent is applied to the bolt thread and around the perimeter of the bolt hole. This release agent ensures that the bonding between the resin and the steel is minimised, and the research by Nijgh [69] shows promising results. Unlike the good demountability potential of the structure, bolts cannot be reused due to the regulations prescribed in NTA 8713 [60]. Additionally, the injection bolts cannot be reused due to the hardened resin inside the injection channel; if reuse was allowed, the bolts could be downcycled and used as standard bolts instead.

Table 5.1: Cost overview for the resin injected design in euros per slab element

		[n]	PPU €	Price €
Production stage	DEMU Ø12 M16, l = 615 mm	4	5.43	21.72
	DEMU Ø12 M16, 90° l = 615 mm	4	10.87	43.48
	Bolt M16 8.8, l = 50 mm	4	0.70	2.80
	Bolt M16 10.9, l = 50 mm injection set (bolt + washer + nut)	4	5.72	22.88
	Steel plate S355, 100 x 100 x 15 mm	4	3.58	14.32
	Epoxy resin, RenGel SW404 + Ren HY5159	4	1.06	4.22
	Release agent, AC MOS 82-2405	4	0.25	1.00
	Total:			110.42
Reuse stage	Bolt M16 8.8, l = 50 mm	4	0.70	2.80
	Bolt M16 10.9, l = 50 mm injection set (bolt + washer + nut)	4	5.72	22.88
	Epoxy resin, RenGel SW404 + Ren HY5159	4	1.06	4.22
	Release agent, AC MOS 82-2405	4	0.25	1.00
	Total:			30.90

Bolted shear connector connection

Table 5.2 shows the cost overview for the demountable bolted shear connector. The cost estimation for the bolted shear connector was made using a normal M16 bolt with a nut on both sides of the flanges, two in total. As an alternative, a costum-made shear connector could be made that outperforms the option with the M16 bolt in terms of tolerances due to the absence of the bolt head and embedded nut. However, this alternative is an expensive option. The M16 bolt, with a price of €1.03, is approximately 15 times cheaper than the costum-made shear connector, which would cost €15.60 per piece. For the reuse situation, new bolts, nuts, and mortar are used. As a result, this connection has the lowest initial costs and the lowest reuse costs, and therefore receives the highest score.

Table 5.2: Cost overview for the demountable bolted shear connector design in euros per slab element

		[n]	PPU €	Price €
Production stage	SHS 80/80/5 S355, h = 260 mm	4	8.99	35.96
	Stirrup B500, 500 x 180 mm	4	1.40	5.60
	Bolt M16 8.8, l = 50 mm	4	0.70	2.80
	Nut M16 C8	8	0.25	2.00
	Bolt M16 8.8, l = 100 mm	4	1.03	4.12
	Washer M16 C8	4	0.21	0.84
	CUGLATON gietmortel 5 mm	4	4.28	17.12
	Release agent wax U	4	0.06	0.25
	Total:			68.69
Reuse stage	Bolt M16 8.8, l = 50 mm	4	0.70	2.80
	Nut M16 C8	8	0.25	2.00
	Bolt M16 8.8, l = 100 mm	4	1.03	4.12
	CUGLATON gietmortel 5 mm	4	4.28	17.12
	Release agent wax U	4	0.06	0.25
	Total:			26.29

Prestressed connection

In [Table 5.3](#) the cost overview for the prestressed connection is shown. This variant used the same SHS profile as the one with the demountable bolted shear connector. The prestressed connection used a class 10.9 threaded rod, as bolts with a length of 300 mm are not available. In terms of costs, threaded rods are fairly expensive, and this is a determining factor for the total price of the connection. With a total price of just over €110.- this connection is equally expensive as the injected alternative. Since bolt reuse is not allowed according to the current standards mentioned above, the reuse phase is calculated as the most expensive. In theory, dry connections have a major advantage, as all components are separated without demolition. However, reusing pretensioned bolts can result in lower capacities in the second lifetime due to the yielding of the bolt, and currently no regulations prescribe how to proceed. For future applications, regulations might change, and optical assessment or testing could verify the reuse potential of pretensioned bolts. Subsequently, the friction surface between the beam flange and the SHS section needs a thorough investigation before reusing to assess the coating and the associated friction resistance. Applied coatings are prone to wear with time.

Table 5.3: Cost overview for the prestressed connection design in euros per slab element

		[n]	PPU €	Price €
Production stage	SHS 80/80/5 S355, h = 260 mm	4	8.99	35.96
	Stirrup B500, 500 x 180 mm	4	1.40	5.60
	Bolt M16 8.8, l = 50 mm	4	0.70	2.80
	Steel plate S355, 100 x 100 x 15 mm	4	3.58	14.32
	Thread M24 10.9, l = 300 mm	4	10.63	42.52
	Nut M24 C10	8	0.99	7.92
	Washer M24 C10	8	0.20	1.60
	Total:			110.72
Reuse stage	Bolt M16 8.8, l = 50 mm	4	0.70	2.80
	Thread M24 10.9, l = 300 mm	4	10.63	42.52
	Nut M24 C10	8	0.99	7.92
	Washer M24 C10	8	0.20	1.60
	Total:			91.67

5.5. Results

The results section scores the alternatives according to the set criteria. Alternatives are scored on a scale of --, -, o, +, and ++. These scores represent a value from one to five and therefore the maximum score is equal to 5.0. In addition to scores, the four categories are weighted based on the level of importance. The most important categories are scored with a multiplication factor of 3, the medium important categories with a score of 2, and the less important categories with 1.

5.5.1. Tolerances

For the tolerance category, a multiplicity factor of 2 is used. The reason behind this score is that the inclusion of tolerances is one of the main drivers of the improved reusable connection design.

Based on the reasoning provided in [section 5.1](#) the injected connection is scored with an "o", the demountable bolted shear connector is scored with a "+", and the prestressed connection with a "-". The injection connection is a good alternative to incorporate the required tolerances, but accommodating more results in an unfavourable flow of forces and reduced stiffness of the connection. The demountable bolted shear connector alternative can incorporate more tolerances than needed without having to adjust the geometry and is therefore scored with a "+". The prestressed variant can accommodate the tolerances, but the eccentric pretensioned anchor rod results in uneven compressive stress in the SHS section. This effect is highly unfavourable, and therefore, this alternative is graded with a "-".

5.5.2. Installation

The installation category is weighted with a score of 1. The installation and speed of installation are important, but compared to traditional installation, all alternatives score relatively well. This is due to the absence of concrete pouring and welding.

The installation of the injection alternative is scored with an "o", the demountable bolted shear connector with a "+" and the prestressed connection with a "--". Installation of the injection alternative is fairly easy and, compared to the demountable bolted shear connector alternative, the number of steps required is the same. However, the injection has to be done from an awkward position and additional equipment is needed. It is assumed that the mixing and injection of the resin cost an equal amount of time compared to the mixing and pouring of the grout. The prestressed connection requires specialist equipment, access from below, and two additional steps compared to the alternatives; this results in a "--" score. In conclusion, the demountable bolted shear connector is considered the easiest in the field of installation.

5.5.3. Demountability

The demountability of a structure plays an important role when decision makers decide to scrap or reuse a building. However, the number of demounting cycles is similar to the highly uncertain and, in theory, it can also occur that a building is only demounted at the end of its technical life. Demountability is an important category, but subject to great uncertainty. The number of steps associated with the demountability is equal to the installation, and therefore the category is weighted with a score of 1.

The demountability scores are the opposite of the installation scores. Alternatives with a more difficult installation procedure score better in terms of demountability. The prestressed connection is seen as the easiest to demount since this is a "dry" connection, and therefore it is scored with "++". The injected connection in combination with a release agent is easy to demount and behaves similar to a bolted connection. Because of the residual resin, it is scored slightly worse than the pretensioned alternative with a "+". The demountability potential of the demountable bolted shear connector depends on the bond between the steel and the mortar. More detailed research can improve the score, but since the resistance between the steel and mortar is expected to be significant, it is scored with a "-".

5.5.4. Costs

Costs are the key driver in the decision to implement reusable connections. Often the decision making upfront is solely based on the actual costs, and the additional potential that the construction has in its second life is overlooked because the builder will not benefit from the residual value of the structure. Different investment constructions can change this principle, but for now it is most likely that the

lowest price is decisive. Therefore, this category is weighted as the most important category and gets the corresponding weighting factor of 3.

The connection design cost overview gives a clear indication of the material costs associated with the designs. The design consisting of a demountable bolted shear connector and a mortar-filled SHS profile has the lowest initial costs, which are around half of the alternatives. In addition to this, the design also has the lowest reuse costs. In [Figure 5.1](#) the costs of the connection are compared to the number of times the structure is reused. The graph displays cumulative values divided into initial investment costs and costs for reinstatement. For every reuse cycle, the reinstatement costs are added to the previous sum. In this figure, the dashed lines indicate the situation where the reuse of (pretension)bolts is allowed. This strongly influences the pretensioned connection, as there are no additional costs. However, this is not allowed with current standards and assessment methodology. In addition to this fact, the demountable bolted shear stud alternative is still more economical if only one reuse cycle is taken into account.

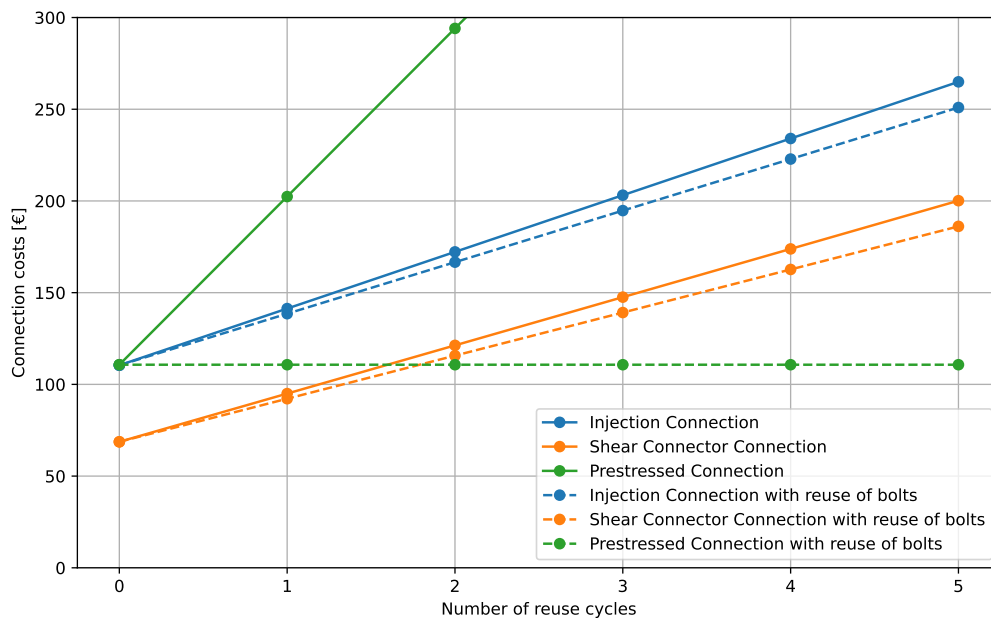


Figure 5.1: Connection costs vs. number of reuse cycles, initial investment costs are presented at reuse cycle 0 and for every reuse cycle the reinstatement costs are added cumulative

This results in a neutral (o) score for the injected one, a positive score (++) for the shear connector alternative, and a negative score (--) for the pretensioned alternative.

5.5.5. Matrix

A summarization of the scores above leads to one alternative outperforming the other two. In [Table 5.4](#) the final results are presented in tabular form. From this it is clear that the demountable bolted shear connector alternative scores best, followed by the injected alternative, and finally the pretensioned connection.

Table 5.4: Trade-off matrix for the design alternatives, scoring scale from 1-5, where 1 represents the lowest possible score and 5 the highest

	Tolerances		Installation		Demountability		Costs		
	Weight	Score	Weight	Score	Weight	Score	Weight	Score	
Injected		o		o		+		o	3.14
Shear connector	2	+	1	+	1	-	3	++	4.14
Pretensioned		-		--		++		--	1.86

Part III

Connection verification

6

Strength verification

The result of the qualitative trade-off analysis, presented in [chapter 5](#), shows that the demountable bolted shear connector alternative came out on top. This chapter aims to verify the structural behaviour in terms of strength for the alternative chosen. If all the components are verified, the design could be approved and declared feasible. The connection consists of three parts that should be verified: the hollow core slab sleeve, the integrated beam, and the connection elements. For these parts, the following checks are performed:

- Compressive resistance of the sleeve concrete,
- Reinforcement bar diameter and anchorage length,
- Shear resistance of the bolted shear connector,
- Shear and bending resistance of the square hollow section,
- Compressive and buckling resistance of the upper compression bolt,
- Compressive resistance of the mortar,
- Transverse bending of the integrated beam,
- Longitudinal bending of the integrated beam,
- Bearing resistance of the bottom flange of the integrated beam.

To verify the elements in terms of strength, the loads on the demountable bolted shear stud connection are determined. The loads calculated in [section 4.2](#) are geometry-specific. The variables e and z are determined based on the geometry of the connection and the dimensions of the case study building. In [Figure 4.10](#) the geometry of the connection is shown, the parameter e is dependent on the dimension of the SHS profile and the location of the bolt. For the first assumption, it is assumed that the bolted shear stud is an M16 8.8 according to the design of the case study ([Appendix B](#)). The maximum dimension of the bolt head is taken and equals 27.7 mm (M16) across the corners. This dimension in combination with the minimum tolerances of 32.8 mm as prescribed in [chapter 3](#) would result in an inner diameter of 60.5 mm. To have some margin in the design, the initial design is made with an SHS 80/80/5, which gives 70 mm of inside clearance.

To determine the maximum eccentricity, two scenarios are examined: one in which the SHS section is positioned as close to the edge of the bottom flange of the integrated beam and the other in which it is positioned as close to the top flange of the beam as possible. The first situation is critical, as the bottom flange of the integrated beam should still have sufficient width to enclose the entire bottom side of the SHS section. If this is not the case, the mortar filling pours out of the section. The latter situation is critical, as the bolt should be located in such a way that there is sufficient space between the compressive plate of the beam and the face of the slab to accommodate the tolerances. In [Figure 6.1](#) graphical representations of the two situations are shown.

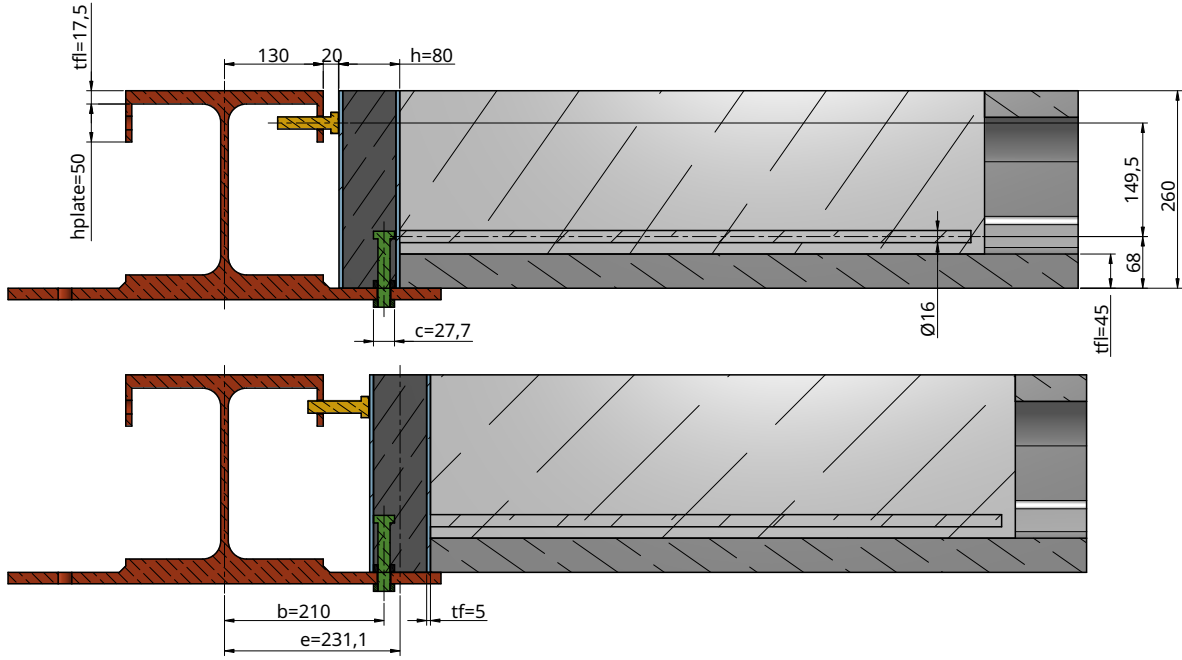


Figure 6.1: Slab eccentricity for the most inward and outward position on the beam flange, all dimensions in millimetres

From the geometry shown in the figure and the dimensions of the case study, the eccentricity is calculated in Equation 6.1. All parameters are shown in Figure 6.1, the c dimension for the bolt head is the M16 bolt head dimension measured over the corners (24 mm over the flats).

$$e_{\max} = b + (h - 2 \cdot t_f) - \frac{c}{2} = 210 + \frac{80 - 2 \cdot 5}{2} - \frac{27.7}{2} = 231.1 \text{ mm} \quad (6.1)$$

The internal lever arm, z , is based on the location of the reinforcement bar and the compressive upper bolt. An increased lever arm results in lower bending moments, and therefore the reinforcement bar should be placed as low as possible but with taking into account sufficient concrete cover for the sleeve concrete. The bottom thickness of the cores is equal to 45 mm for the hollow core slabs specified in the case study. The upper bolt that provides the compressive point is positioned at the midpoint of the compressive plate, initial dimensions of 50x50 mm were assumed. The initial diameter of the reinforcement bar is equal to 16 mm, which will be reviewed at a later stage. As a result, the lever arm z is calculated in Equation 6.2 and the dimensions are shown in Figure 6.1.

$$z = 260 - t_{fl,hcs260} - \frac{\varnothing}{2} - t_{fl,HE260B} - \frac{h_{plate}}{2} = 260 - 45 - \frac{16}{2} - 17.5 - \frac{50}{2} = 164.5 \text{ mm} \quad (6.2)$$

Now that the final connection-specific parameters are known, the loads are calculated. As stated in Equation 4.15 the horizontal load consists of an part caused by eccentricity, wind, and column imperfections. The top bolt can only transfer compression, and as a result the bottom bolt has to transfer the wind and imperfection loads. In Equation 6.3 and Equation 6.4 the design horizontal loads in kN/m^1 are given for the upper bolt $F_{h,d,u}$ and the shear stud $F_{h,d,s}$, respectively.

$$F_{h,d,u} = F_{h,fl,d} = 11.6 \cdot \left(\frac{11 - 0.2311}{2} \right) \cdot \frac{231.1}{164.5} = 86.6 \text{ kN/m}^1 \quad (6.3)$$

$$\begin{aligned} F_{h,d,s} &= F_{h,fl,d} + \psi_2 \cdot Q_{w,fl,d} + \psi_3 \cdot Q_{e,fl,d} \\ &= 86.6 + 0.5 \cdot 5.14 + 0.3 \cdot 0.50 = 89.3 \text{ kN/m}^1 \end{aligned} \quad (6.4)$$

For the slab width of 1.2 metres and two connectors per slab, the loads are equal to:

Table 6.1: Connector loads

Component	$F_{h,Ed}$ [kN/m ¹]	Width [m]	n	$F_{h,Ed}$ [kN]
Top bolt in compression t	86.6	1.2	2	52.0
Bottom bolt in shear b	89.3	1.2	2	53.6

The loads exerted by the upper compressive and the bottom shear stud are transferred to the slab. To calculate the magnitude of the compressive load on the slab and the tensile stress on the reinforcement bar the moment and shear force equilibrium should be satisfied. First the moment equilibrium ($\sum M = 0$) around the reinforcement bar is taken, this point is assumed as the "hinge" in the system, the dimensions are obtained from Figure 6.1. As a result, a compressive load on the upper side of the slab $F_{h,Ed,c}$ of 76.4 kN is calculated. In practice, this load is uniformly distributed and is assumed to have its compressive centre opposite of the compressive load from the top bolt as indicated with the big yellow arrow. After the magnitude of the compressive load is known, the force equilibrium $\sum V = 0$ determines the tensile force on the reinforcement bar. The tensile load $F_{h,Ed,r}$ is equal to 78.0 kN. The result in terms of shear forces and bending moments in the SHS section is shown in Figure 6.2.

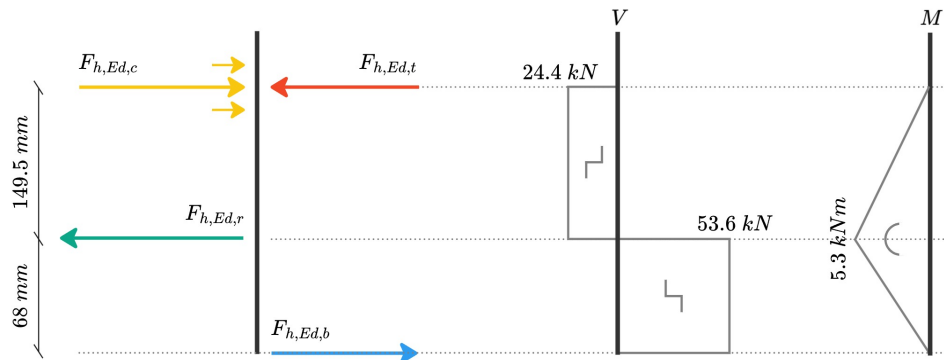


Figure 6.2: Mechanical scheme for shear and bending of the SHS section; orange line is at the location of the compressive bolt, green line is located in the heart of the reinforcement bar, and the blue line at the heart of the beams bottom flange

6.1. Hollow core slab sleeve

The purpose of the hollow core slab sleeve concrete is to introduce loads into the slab. For verification, the compressive resistance of the concrete on the upper side and the anchorage length and diameter of the reinforcement bar are checked. The verified parts are shown in [Figure 6.3](#).

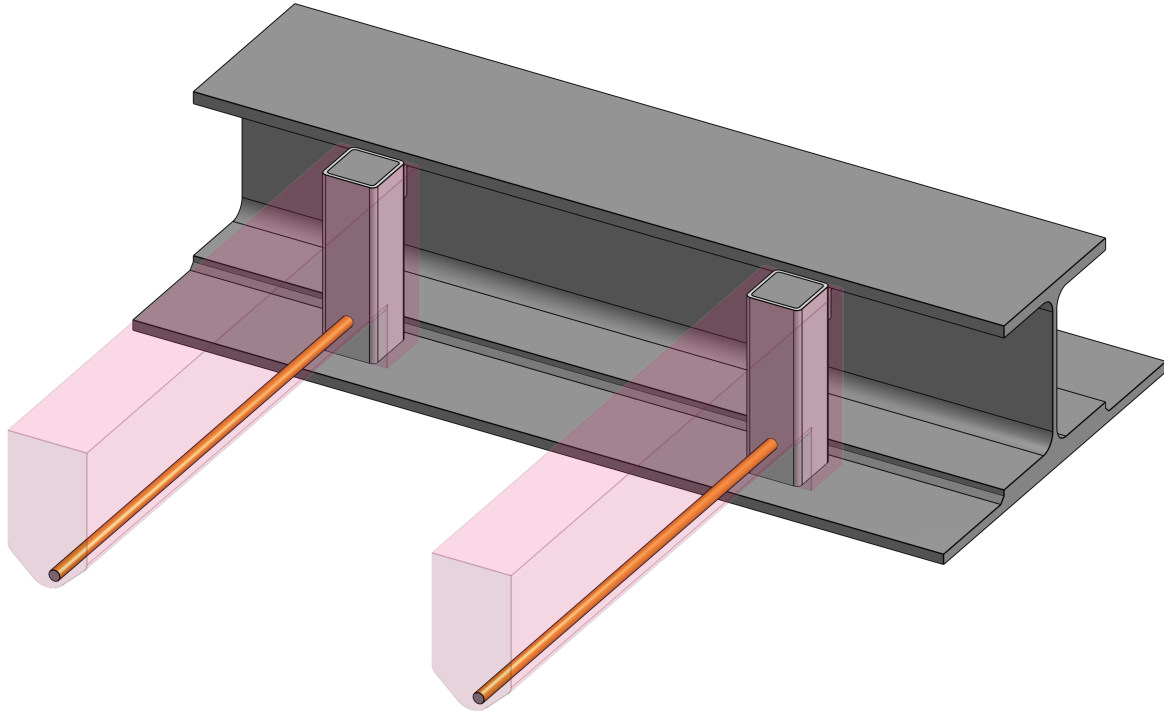


Figure 6.3: Components of the hollow core slab sleeve; reinforcement is shown in orange and the sleeve concrete in pink

6.1.1. Sleeve concrete

The compressive load of the upper bolt results in compressive stresses on the sleeve concrete. For the concrete mixture, Spramex C20/25 is used; this concrete has a smaller aggregate size and a higher slump compared to standard concrete. These modifications make the concrete more suitable for the application on site. Additionally, a bonding agent should be applied to the sleeve to ensure bonding between the precast concrete hollow core slab and the concrete sleeve that is poured at a later stage. For the upper bolt, the load spreading angle is set to 45 degrees or a 1:1 ratio. In [Figure 6.4](#) the spread of the load is represented schematically. The SHS section is filled with mortar and as a result the load is spread from the front face loaded by the bolt to the rear face. Part of the compressive force is spread to the sides; however, for a safe approximation, it is assumed that the load spread takes place only over the width of the section. For the load spreading over the height, the mortar is a limiting factor.

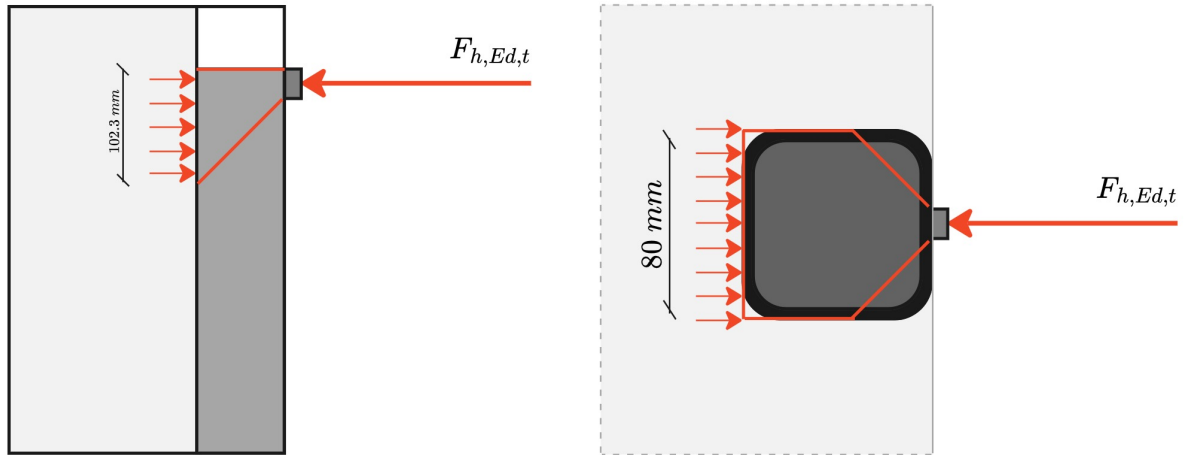


Figure 6.4: Load spreading of the compressive force, vertically (left) and horizontally (right)

The loading area is equal to the area of the bolt head. A standard metric bolt is shaped hexagonally and, depending on its position, the width can vary slightly. To simplify the calculation, the total area of the bolt head of 498 mm^2 is represented in terms of a square. This square has sides with a length of 22.3 mm ($\sqrt{498}$). Resulting in a load spreading height of 102.3 mm and the width was already determined to be equal to the width of the section. As a result, the total compressive area is equal to 8184 mm^2 . The design value of the compressive stress on the concrete is shown in [Equation 6.5](#).

$$\sigma_{c,Ed} = \frac{F_{h,Ed,c}}{A} = \frac{76.4.0 \cdot 10^3}{8184} = 9.34 \text{ MPa} \quad (6.5)$$

6.1.2. Reinforcement

The maximum allowable stress determines the diameter of the reinforcement bar. For a standard B500 ribbed reinforcement bar, the design yield strength f_{yd} is 435 MPa . With a maximum load of 78.0 kN , the required diameter is 179.3 mm^2 . This results in a $\varnothing 16$ bar with a sectional area of 201 mm^2 . The required diameter is in line with the assumption made for the approximation of the lever arm. For the anchorage length, l_{bd} , the rule of thumb prescribes that the bar should be $47\varnothing$ for C20/25 concrete with good bond conditions as prescribed in Section 8.4.4 of NEN-EN 1992-1-1 [23]. This reinforcement length may be reduced by the actual stress on the reinforcement bar that equals 267 MPa and is indicated by σ_{sd} . The minimum anchorage length is calculated by [Equation 6.6](#) and results in a length of 671 mm .

$$l_{bd} = 47\varnothing \cdot \frac{\sigma_{sd}}{f_{yd}} = 47 \cdot 16 \cdot \frac{388}{435} = 671 \text{ mm} \quad (6.6)$$

6.1.3. Unity check

In [Table 6.2](#) an overview is shown with unity checks of the components. The unity checks show that the utilisation of both components is within an acceptable range.

Table 6.2: Unity check for the hollow core slab sleeve components

Component		Value	Unit
Sleeve concrete	$\sigma_{c,Ed}$	9.34	MPa
	f_{cd}	13.33	MPa
	UC	0.70	[-]
Reinforcement	σ_{sd}	388.06	MPa
	f_{yd}	435.00	MPa
	UC	0.89	[-]

6.2. Connection

The connection consists of an SHS section, a bolted shear connector, an adjustment bolt, and mortar. For these components, various strength checks are performed. The parts subjected to verification are shown in [Figure 6.5](#).

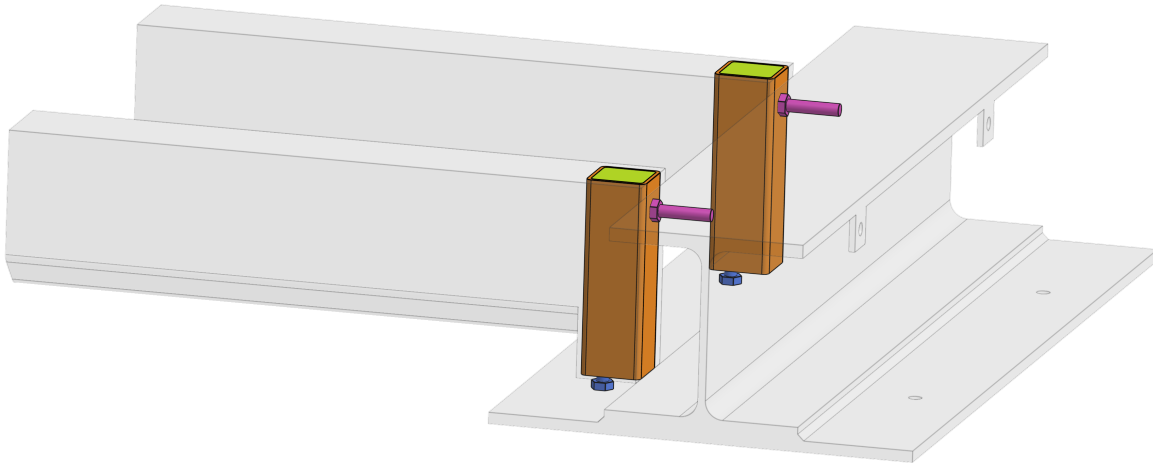


Figure 6.5: Components of the connection; shear stud is shown in blue, SHS section in orange, adjustment bolt in pink, and the mortar in yellow

6.2.1. Bolted shear connector

The resistance of the shear connector is verified using the verification requirements of a bolted connection specified in the NEN-EN 1993-1-8 [20]. For the initial calculation, an M16 8.8 bolt is used. In [Equation 6.7](#) the formula for the shear resistance per shear plane is shown. Where α_v is equal to 0.6 for bolts of class 8.8, $f_{ub} = 800$ MPa, $A = 157$ mm², and $\gamma_{M2} = 1.25$. A shear resistance per bolt of 60.3 kN is found.

$$F_{v,Rd} = \frac{\alpha_v f_{ub} A_s}{\gamma_{M2}} = \frac{0.6 \cdot 800 \cdot 157}{1.25} = 60.29 \text{ kN} \quad (6.7)$$

6.2.2. Square Hollow Section

The SHS section must transfer a shear load and a bending moment as indicated in [Figure 6.2](#). The diagram shows that the critical shear load is $V_{Ed} = 53.6$ kN and a bending moment $M_{Ed} 5.3$ kNm. For the dimensions of the SHS profile, an SHS 80/80/5 was assumed initially, in this section, the wall thickness is optimised. A reduction in wall thickness results in an additional inclusion of tolerance and reduced material consumption. All SHS 80/80 sections are Class 1 profiles, and therefore plastic resistance may be used for the bending moment resistance calculation.

The bending moment resistance is given by NEN-EN 1993-1-1 [21]. In [Equation 6.8](#) the equation is shown with W_{pl} as the plastic section modulus, f_y the steel yield strength of the S235 construction

steel, and γ_{M0} the partial safety factor. Since the SHS 80/80/5 has overcapacity, the dimensions of the section are reduced to an SHS 80/80/4. The moment capacity of the SHS 80/80/4 is 8.0 kNm and the calculation is shown in [Equation 6.8](#).

$$M_{c,Rd} = M_{pl,Rd} = \frac{W_{pl}f_y}{\gamma_{M0}} = \frac{33980 \cdot 235}{1.00} = 7.98 \text{ kNm} \quad (6.8)$$

The shear resistance of the same SHS 80/80/4 depends on the shear area A_v and the aforementioned parameters f_y and γ_{M0} . The shear resistance obtained is shown in [Equation 6.9](#) and equals 81.3 kN.

$$V_{c,Rd} = V_{pl,Rd} = \frac{A_v (f_y / \sqrt{3})}{\gamma_{M0}} = \frac{599}{1.00} = 81.33 \text{ kN} \quad (6.9)$$

The last check for the SHS section is the interaction of the bending moment and the shear force. To verify whether the interaction is sufficient, a reduction ρ on the maximum stress is applied to calculate the bending moment resistance. In [Equation 6.10](#) the reduced bending moment resistance due to the presence of shear is calculated. The reduced yield stress is denoted with subscript _{red}.

$$\begin{aligned} \rho &= \left(\frac{2V_{Ed}}{V_{pl,Rd}} - 1 \right)^2 = \left(\frac{2 \cdot 53.60}{81.33} - 1 \right)^2 = 0.10 \\ f_{y,red} &= (1 - \rho) \cdot f_y = (1 - 0.10) \cdot 235 = 211.2 \text{ MPa} \\ M_{pl,Rd,red} &= \frac{W_{pl}f_{y,red}}{\gamma_{M0}} = \frac{33980 \cdot 211.2}{1.00} = 7.18 \text{ kNm} \end{aligned} \quad (6.10)$$

6.2.3. Adjustment bolt

The adjustment bolt transfers the compressive force on the upper side of the connection. NEN-EN 1993-1-8 does not provide any regulations regarding bolts in compression. The tensile resistance of the bolt can indicate whether the load can be transferred by the bolt. However, besides the actual capacity of the bolt, the buckling resistance of the bolt in the most unscrewed position should be checked.

First the capacity is calculated in terms of the tensile resistance. According to the NEN-EN 1993-1-8 [20] the tensile resistance is given by [Equation 6.11](#). Parameters are equal to those used in [Equation 6.7](#) except the factor k_2 which is equal to 0.9.

$$F_{t,Rd} = \frac{k_2 f_{ub} A_s}{\gamma_{M2}} = \frac{0.9 \cdot 800 \cdot 157}{1.25} = 90.43 \text{ kN} \quad (6.11)$$

For flexural buckling, the bolt is analysed as a solid rod. Only the stress area of the threaded part is considered, resulting in an area of 157 mm². The buckling resistance of members is specified by the NEN-EN 1993-1-1 [21]. For the application of high-strength steels, the buckling curve of the current version of NEN-EN 1993-1-1 is incomplete. The updated draft version [34] specifies buckling curves for steel grades up to S700, since the yield stress of the bolts is given at 640 MPa, these curves are adopted for design verification. This results in a buckling curve c with the corresponding imperfection factor of $\alpha = 0.49$. In [Equation 6.12](#) the resistance to buckling is shown, where χ expresses the buckling reduction factor, A the area of the threaded part bolt, f_{yb} the yield strength of the bolt and γ_{M1} the partial safety factor. The complete derivation of the buckling reduction factor is provided in [Appendix F](#). The buckling length factor k equals 1.0. The bolt thread connected to the steel plate is assumed to be clamped and the compressive contact point as fixed in terms of rotations, but with the possibility to accommodate translations. A modification to the buckling formula was made. The partial safety factor γ_{M1} from EN 1993-1-1 was replaced by the factor γ_{M2} since this is the corresponding partial safety factor for bolts according to Table 2.1 of NEN-EN 1993-1-8 [20].

$$N_{b,Rd} = \frac{\chi A f_{yb}}{\gamma_{M1}} = \frac{0.942 \cdot 157 \cdot 640}{1.25} = 75.72 \text{ kN} \quad (6.12)$$

6.2.4. Mortar

The shear force in the bottom bolted shear connector exerts pressure on the mortar, necessitating the selection of a mortar with adequate compressive strength. Additionally, the maximum aggregate size and layer thickness should be taken into account as important factors. The mortar should easily flow around the shear stud even in the most critical situation of full contact between the SHS section and the stud. The required layer thickness is slightly smaller than the height of the SHS section, since some clearance is present on the upper side. As a result, the maximum aggregate size is equal to 5 mm and preferably even smaller, for the layer thickness, a minimum of 230 mm is required. In general, mortars with smaller aggregate sizes are stated to be capable of accommodating smaller layer thicknesses and therefore are key considerations when choosing the most suitable mortar.

An expert from Cugla Concrete Solutions was consulted to find the most suitable mortar. This resulted in CUGLATON gietmortel 5 mm due to its maximum layer thickness of 300 mm and an aggregate size of 5 mm. Mortars with smaller aggregate sizes were not possible due to insufficient layer thickness. The mortar is class K70, which implies a compressive strength of more than 70 MPa after 7 days of curing. Rapid strength development is seen as an advantage, as this improves the speed of erection. For the mortar, a characteristic cubic compressive strength of 75 MPa was documented, which is equal to a cylindrical compressive strength of 60 MPa. In [Equation 6.14](#) the compressive resistance of the mortar is calculated for a curing time of 7 days. h_{sc} is the height of the bolted shear connector inside the connection, d the nominal diameter, and f_{cd} the design value of the compressive resistance of the mortar as calculated in [Equation 6.13](#).

$$f_{cd} = \frac{f_{ck,cil}}{\gamma_c} = \frac{60}{1.5} = 40 \text{ MPa} \quad (6.13)$$

$$N_{c,Rd} = \frac{h_{sc} \cdot d \cdot f_{cd}}{\gamma_{M1}} = \frac{100 \cdot 16 \cdot 40}{1.00} = 64.00 \text{ kN} \quad (6.14)$$

6.2.5. Unity check

What is observed from the unity checks in [Table 6.3](#) is that the components have an optimised design with utilisation between 69 and 89 %. The least utilised component is the compressive top bolt; however, the verification for this component was performed based on non-conventional verification methods. Therefore, the additional reserves account for some safety with regard to the verification method.

Table 6.3: Unity checks for the connection components

Component		Value	Unit
Shear stud	$F_{h,Ed,b}$	53.60	kN
	$F_{v,Rd}$	60.29	kN
	UC	0.89	[-]
SHS section	M_{Ed}	5.30	kNm
	$M_{c,Rd}$	7.98	kNm
	UC	0.66	[-]
	$F_{h,Ed,b}$	53.60	kN
	$V_{c,Rd}$	81.33	kN
	UC	0.66	[-]
	UC	0.74	[-]
Adjustment bolt	$F_{h,Ed,t}$	52.00	kN
	$F_{t,Rd}$	90.43	kN
	UC	0.58	[-]
	$F_{h,Ed,t}$	52.00	kN
	$N_{b,Rd}$	75.72	kN
	UC	0.69	[-]
Mortar	$F_{h,Ed,b}$	53.60	kN
	$N_{c,Rd}$	64.00	kN
	UC	0.84	[-]

6.3. Beam

The dimensions of the beam itself will not change depending on the connector type, and therefore the dimensions of the case study are used. However, the width and thickness of the bottom flange must be determined and verified. The bottom plate of the beam is subjected to double bending, the longitudinal bending due to the global loading on the beam and the transverse bending due to the local loads of the hollow core slab. First of all, the resistance of the bottom plate is calculated and subsequently the influence on the longitudinal bending is checked. The capacity of the bottom plate is checked in the transverse bending and shear capacity. This utilisation of the bottom plate and flange in the transverse direction results in a reduced plastic section modulus. The beam is constructed of S355 structural steel with a yield strength of 355 MPa and an ultimate strength of 490 MPa.

Beam dimensioning

The width of the bottom plate was determined by the dimensions of the SHS section as described in [Figure 6.1](#). As a result, a width of 570 mm is needed which, compared to the 450 mm designed for the case study building, is an increase of 60 mm on each side of the beam. This increased cross-sectional area results in the fact that the thickness of the bottom flange is reduced. As a first assumption, the bottom plate was reduced by one standard plate thickness from 15 to 12 millimetres. This resulted in the same area moment of inertia around the y-axis.

- HE260B + 450x15, $I_y = 2.31 \cdot 10^8 \text{ mm}^4$
- HE260B + 570x12, $I_y = 2.30 \cdot 10^8 \text{ mm}^4$

Beam classification

The beam classification determines the calculation methodology for the section. Ideally, a class 1 cross section is used, since class 1 cross sections possess sufficient rotation capacity to form plastic hinges. This implies global plastic analysis, and plastic materials properties are used for verification.

The classification of the beam depends on the relative slenderness ratios β_{rel} and ζ_{rel} [42]. β_{rel} expresses the factor for the upper flange and ζ_{rel} for the web. In [Equation 6.15](#) and [Equation 6.16](#)

the slenderness parameters are shown, the geometry parameters, and the table with the classification demands are shown in [Appendix F](#).

$$\beta_{\text{rel}} = \frac{\frac{1}{2}b_o}{t_o} \sqrt{\frac{355}{235}} = \frac{\frac{1}{2} \cdot 260}{17.5} \cdot \frac{355}{235} = 9.13 \leq 10 \quad (6.15)$$

$$\zeta_{\text{rel}} = 2.46 \frac{h_0}{t_w} \left(\frac{12 - \frac{h_w}{h_o}}{11} \right) = 2.46 \cdot \frac{138.5}{10} \cdot \left(\frac{12 - \frac{38.5}{138.5}}{11} \right) = 36.3 \leq 72 \quad (6.16)$$

Both slenderness ratios satisfy the requirements for a class 1 cross section.

6.3.1. Transverse bending resistance of the bottom flange and plate

Besides the global bending stiffness of the beam, the bearing resistance of the bottom plate is checked. To verify this, the requirements of ECSS83 [42] must be met. The principle of these verifications is shown in [Figure 6.6a](#). As a result, the bottom flange is divided into 4 zones, each of these zones takes another part of the load. In [Figure 6.6b](#) the division of the bottom flange is shown where (1) takes the shear load, (2) and (4) the transverse bending, and (3) the longitudinal bending.

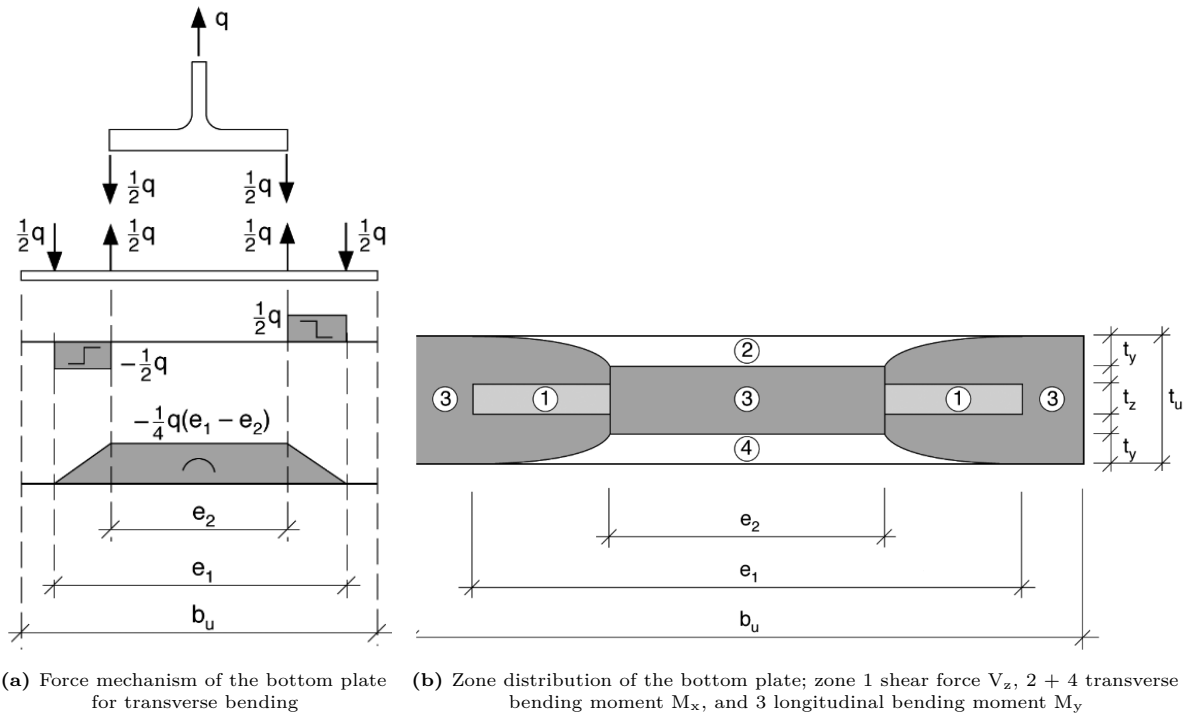


Figure 6.6: Bottom plate principle

The principle of these plastic calculations is translated into the formula shown in [Equation 6.17](#). In this equation γ_M represents the partial safety factor of steel, q the total factored beam load ([section 4.2](#)), ξ the out-of-balance parameter, f_y the characteristic yield strength of steel, e_1 the width of the bottom flange, e_2 the width of the beam flange and t_u the thickness of the bottom flange. The full derivation and the geometry parameters are shown in [Appendix F](#).

$$\frac{3}{4} \cdot \left(\frac{\gamma_M \cdot q \cdot (1 + \xi)}{f_y \cdot t_u} \right)^2 + \left(\frac{e_1 - e_2}{t_u} \right) \cdot \left(\frac{\gamma_M \cdot q \cdot (1 + \xi)}{f_y \cdot t_u} \right) \leq 1 \quad (6.17)$$

$$\frac{3}{4} \cdot \left(\frac{1.15 \cdot 107.4 \cdot (1 + 0.60)}{355 \cdot 12} \right)^2 + \left(\frac{443 - 260}{12} \right) \cdot \left(\frac{1.15 \cdot 107.4 \cdot (1 + 0.60)}{355 \cdot 12} \right) = 0.71 \leq 1$$

6.3.2. Longitudinal bending resistance of the beam

The bending resistance of the beam in the longitudinal direction has a reduced capacity due to the affect of transverse bending. The effective area of the bottom flange of the beam and the bottom plate must be determined. This is calculated with the help of the reduction factor ψ_n , where n represents the subscripts _u and _o for the bottom plate and the bottom flange, respectively. In [Appendix F](#) the full calculation and the calculation of the input parameters are shown. These calculations result in the input reduction factor for the bottom plate equal to 0.92 and 0.95 for the bottom flange.

$$\psi_n = 1 - \frac{3\mu^2\sqrt{3} \cdot t_u + \lambda \cdot \mu (2e_1 + e_2) - \lambda^2 (e_1 - e_2)}{6\mu \cdot b_u} = 0.92 (\psi_u), 0.95 (\psi_o) \quad (6.18)$$

The bending moment of the section, $M_{pl,y,Rd}$ is prescribed according to [Equation 6.19](#). The plastic section modulus $W_{pl,y}$ can be calculated by dividing the cross section into different parts. These different areas are then multiplied by their lever arm to obtain the plastic section modulus. The division of the four parts and their lever arms is shown in [Figure F.1](#).

$$M_{pl,y,Rd} = W_{pl,y}f_y = \cdot 355 = 1.835 \cdot 10^6 \cdot 355 = 651.3\text{kNm} \quad (6.19)$$

6.3.3. Bearing resistance

The bolted shear stud is mounted in a normal bolt hole. The bearing resistance of the bottom flange of the beam should be checked according to EN 1993-1-8 [20]. In [Equation 6.20](#) the calculation of the bearing resistance is shown. The derivation of the geometry and bolt parameters (k_1 and α_b) is performed in [Appendix F](#). Parameter f_u is the ultimate strength of the steel beam, d the diameter of the bolt and t the thickness of the bottom flange, which were both dimensioned above.

$$F_{b,Rd} = \frac{k_1\alpha_b f_u dt}{\gamma_{M2}} = \frac{2.5 \cdot 1.0 \cdot 490 \cdot 16 \cdot 12}{1.25} = 188.16 \text{ kN} \quad (6.20)$$

6.3.4. Unity check

The unity checks for the beam components are shown in [Table 6.4](#). The bending of the bottom flange is checked in two situations. The result of the transverse bending shows a unity check of 0.71. For longitudinal bending, the plastic section modulus was slightly reduced, but it has sufficient capacity to transfer the total beam load. The total beam load was calculated based on the simply supported conditions and the vertical load calculated in [Equation 4.9](#) multiplied by the effective width of the beam. The bearing resistance of the bolt is not crucial due to the significant edge distances prescribed by the design.

Table 6.4: Unity check for the beam components

Component		Value	Unit
Transverse bending	UC	0.71	[-]
	$M_{Ed,y}$	426.8	kNm
Longitudinal bending	$M_{pl,y,Rd}$	651.3	kNm
	UC	0.66	[-]
Bearing resistance	$F_{h,Ed,b}$	53.6	kN
	$F_{b,Rd}$	188.16	kN
	UC	0.28	[-]

7

Stiffness analysis

The stiffness chapter verifies the connection in terms of stiffness. Two major stiffness verifications are made. First, the torsional rigidity of the beam is discussed. All of the design presented in [chapter 4](#) are based on the principle that the integrated beam is not capable of transferring torsional moments. In [section 7.1](#) the assumption is verified. In addition to the stiffness comparison that verifies the relative stiffness between the hollow core slab and the integrated beams, the stiffness of the connection components is verified. This stiffness depends on the stiffness of two individual components, namely the shear stud stiffness and the stiffness of the compressive top plate. In [subsection 7.2.1](#) and [subsection 7.2.2](#) the verification for the shear stud and top plate are presented. There are no specific demands set for this connection stiffness; however, an indication can be found in the effect of connection stiffness on the global deformation behaviour of the hollow core slab.

7.1. Torsional stiffness of the integrated beam

The loads that the connection between the beam and the slab should be able to transfer depend on the torsional stiffness of the integrated beam. This torsional rigidity depends on the resistance of the member against the torsional moments and the torsional resistance of the beam-to-column connection. This stiffness phenomenon can be compared with the classification of joints for bending moments; for these joints, the following classifications exist: rigid, semi-rigid, or pinned. For the rigidity of rotation, a similar classification can be given.

- Torsional rigid,
- Torsional semi-rigid,
- Torsional pinned.

If the connection between the beam and the column is fully rigid, the beam will not rotate when loaded by a torsional moment. In this case, the beam flange remains horizontal, and the bearing point of the hollow core slab acts as a pinned support. For the semi-rigid case, the beam would rotate around its longitudinal axis, but this rotation is partially prevented by the stiffness of the beam-to-column connection and the stiffness of the beam. For a fully pinned connection, the beam-to-column connection acts as a hinge in the longitudinal direction of the beam and will not be able to prevent any rotation initiated by the torsional moment. For the type of connection used in standard construction, the first option is fairly expensive to produce, and the latter one needs some complex rotational bearings. Therefore, in practice, the construction consists of semi-rigid torsional connections.

All the connections presented in [chapter 4](#) are designed with the perspective of having the upper side of the connection in compression and the lower side in tension (shear). To prove that this design assumption is correct, the stiffnesses of the slab elements and the beam elements is verified. Compression on the upper side can only be achieved in the situation where the stiffness of the hollow core slab is greater than the torsional rigidity of the beam. The most critical section to check is directly at the beam-to-column connection, since the rotations of the beam are most restrained in this section. Further along the beam length, the beam rotation increases due to the deformations of the beam and not only the

beam-to-column connection. To validate whether compression at the upper side of the connection is present, the following three rotations are reviewed:

- (a) Rotation of the beam (Figure 7.1a),
- (b) Hollow core slab bending (Figure 7.1b),
- (c) Beam flange bending (Figure 7.1c).

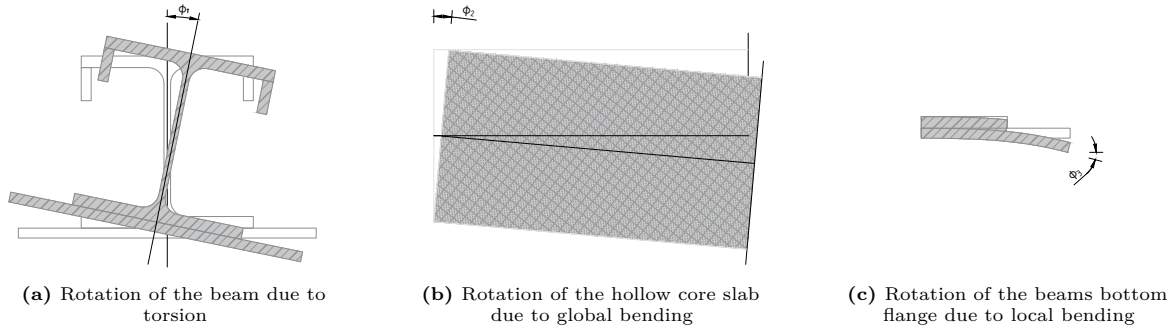


Figure 7.1: Rotations in the connection

The largest rotations occur once the edge beam is fully loaded by the floor load. In this situation, the forces that must be transferred are of the largest magnitude. However, it is also interesting to calculate whether there is compression if the floor is loaded solely by self-weight. Therefore, the two above-mentioned situations are considered.

The results of the connection stiffness analysis determine whether the assumption of compression on the upper side and tension on the lower side is correct. This assumption is correct if the following equation is satisfied. Where ϕ_1 relates to the rotation of the beam due to torsion, ϕ_2 to the rotation of the hollow core slab due to global bending, and ϕ_3 to the rotation of the beams bottom flange due to local bending.

$$\delta_1 \geq \delta_2 + \delta_3 = \phi_1 \cdot z_1 \geq (\phi_2 + \phi_3) \cdot z_{2,3} \quad (7.1)$$

To prove that the reasoning of the stiffness analysis is correct, the parameters of the case study building in combination with the connection geometry are used for verification. Lever arm z_1 is the distance from the centre of gravity of the beam to the compressive point on the top side. The compressive point on the top side is located 37.5 mm from the top of the slab based on the geometry determined in chapter 6. For $z_{2,3}$ the distance is from the bottom of the slab to the compressive point. As a result, the lever arms z_1 and $z_{2,3}$ are equal to 142.5 and 222.5 mm, respectively.

7.1.1. Beam rotation

Firstly, the torsional moment that is exerted on the beam is calculated, this load determines the rotation of the beam. The origin of this moment is the eccentricity of the bearing point relative to the centre of gravity of the beam. The zero bending moment point of the slab is assumed to be at the centre line of the beam. In Figure 7.2b the bending moment line for the hollow core slab is shown; the red dots mark the bearing location of the hollow core slab.

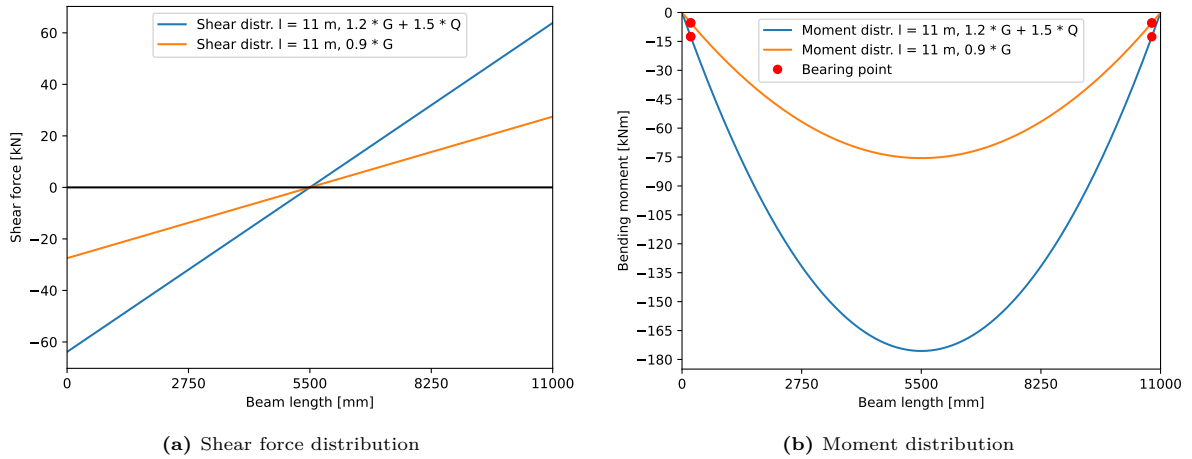


Figure 7.2: Shear force and bending moment distribution along the hollow core slab length

The bending moment at the bearing location is calculated by integrating the area below the shear force line; the shear force line for the simply supported slab with a uniform distributed load is a linear decreasing line as shown in [Figure 7.2a](#). Therefore, the integration can be simplified by taking the average shear force at $e/2$ multiplied by the total eccentricity. The result is shown in [Equation 7.2](#) where q denotes the line load, $L1$ the length of the hollow core slab and e the eccentricity.

$$M_e = \sum_{n=0}^e V(x) = \left[q \cdot \left(\frac{L1 - e}{2} \right) \right] \cdot e \quad (7.2)$$

Vertical slab loads were calculated in [section 4.2](#). The design value for q , in the fully loaded situation is equal to 11.6 kN/m^1 and for the self-weight only situation, where the weight is assumed to be unfavourable equal to 5.0 kN/m^1 . With an 11 m slab length ($L1$) and an most extreme eccentricity of 221.5 mm ([Figure F.1](#)) a bending moment of 13.9 kNm/m^1 and 6.0 kNm/m^1 for fully loaded and self-weight only situations is calculated.

IDEA StaTiCa

The loads calculated above are implemented in an IDEA StaTiCa model. In this model, the connection of the case study building, shown in [section B.4](#) is reconstructed. The connection is first modelled such that it is sufficiently strong, after the strength is approved, the connection stiffness is evaluated. As an output, the unhindered rotation of the beam is given. In [Figure 7.3](#) the model is shown. What can be observed from the model is that the widened bottom flange was not modelled. The effect on the torsional stiffness of this flange is negligible, and for a modified non standard cross section it was not possible to model the web stiffeners. The loads on the connection are shown in [Table 7.1](#).

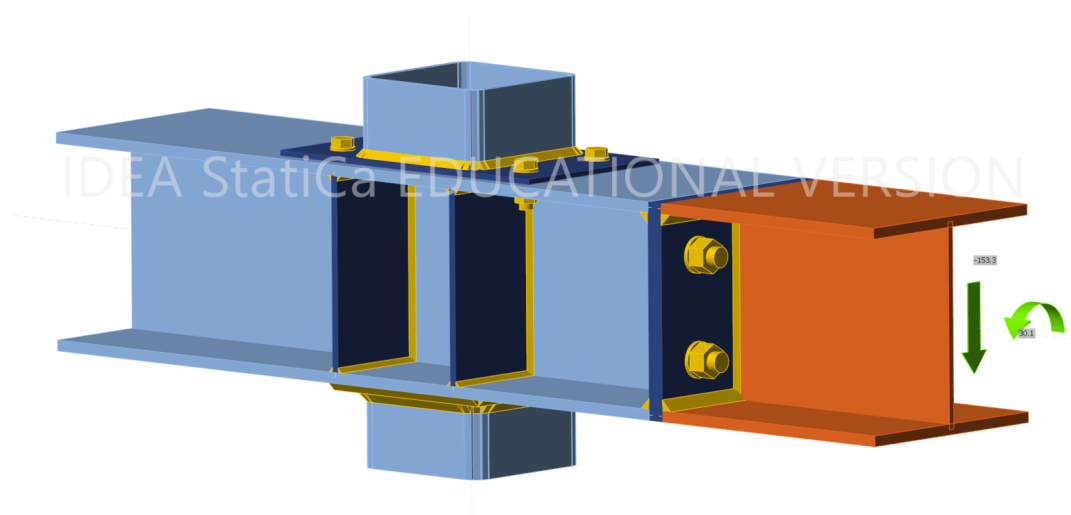


Figure 7.3: Isometric view of connection modelled in IDEA StaTiCa

Table 7.1: Connection loads IDEA StaTiCa

	$V_z [kN]$	$M_x [kNm]$
1.2G + 1.5Q	-153.3	30.1
1.2G	-65.9	13.0

The connection is only modelled on one side due to limitations in the software package. However, the stiffness of the connection is not affected by the connection on the opposite side, since the rotations are hindered by the columns and the fact that the other beam is assumed to be clamped. The properties of the connection elements are shown in [section D.1](#).

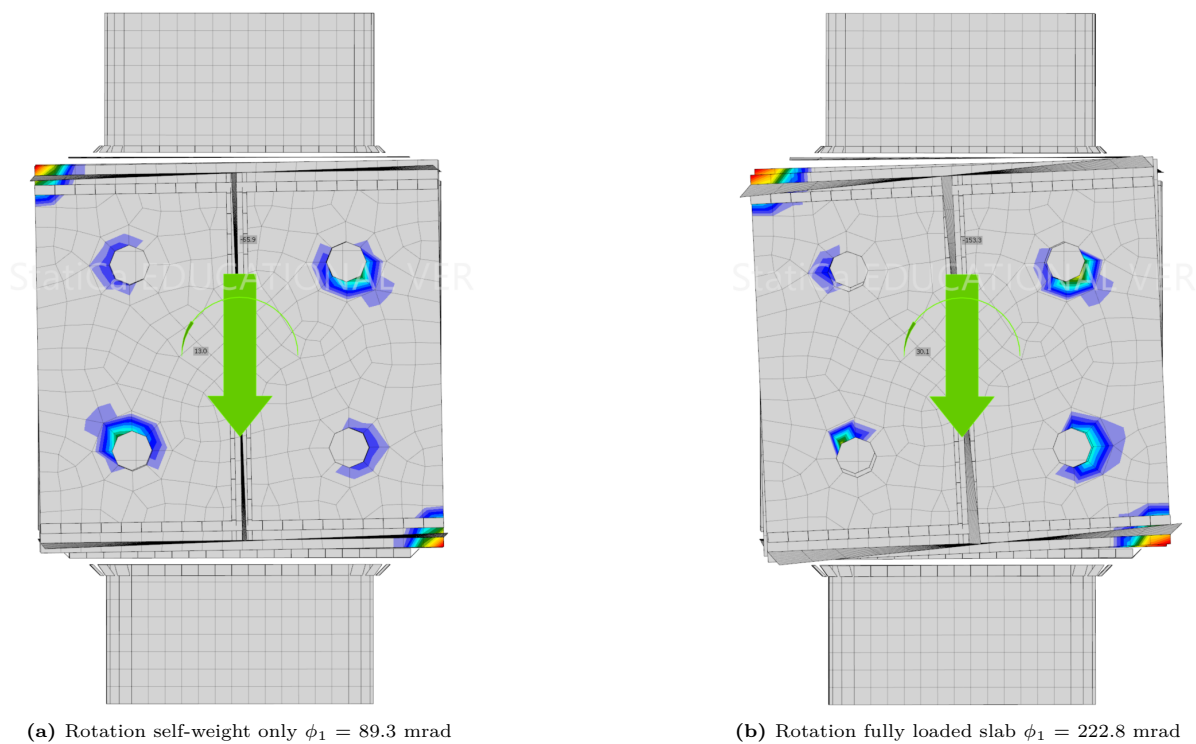


Figure 7.4: Rotation of an unhindered integrated edge beam with contact stresses shown

As a result, the IDEA StaTiCa stiffness analysis calculates the rotation around the x-axis. In [Figure 7.4a](#) and [Figure 7.4b](#) the rotations for the self-weight-only variant and the fully loaded variant are shown. For the first situation the rotation is equal to **89.3 mrad** and for the latter equal to **222.8 mrad**.

The software output in [section D.1](#) does not show an initial stiffness or rotation. This limitation is attributed to the software. According to NEN-EN 1993-1-8 [20], the stiffness of the connection is determined based on the design moment resistance $M_{j,Rd}$ of the connection. However, the calculation of the design moment resistance is based on the effective design tension resistance of a bolt row $F_{tr,Rd}$. The software is unable to calculate the design torsional moment resistance of the connection due to the fact that the bolts are loaded in shear instead of tension. Nevertheless, the connection's behaviour was verified for bending around the y- and z-axis, and based on this it is concluded that the calculated rotations around the x-axis are accurate.

7.1.2. Hollow core slab bending

Global bending of the hollow core slab causes a rotation of the slab at the support. This rotation creates a horizontal displacement that increases along the thickness of the slab. To determine the rotation, a simply supported slab is modelled with the properties of the slabs used in the case study building. For the moment of inertia and the modulus of elasticity, a value of $I_y = 1434.9 \cdot 10^6 \text{ mm}^4$ [90] and $E = 36283 \text{ MPa}$ [23] are used, respectively. The moment of inertia is per slab element and this implies that the load should be multiplied by the width of the slab, in this specific case 1.2 m. For the load, the same loading conditions are used as for beam rotation. As a result, rotations of **12.4 mrad** and **5.3 mrad** are found, the calculations of these values were determined with the help of Maple and are found in [section D.2](#).

7.1.3. Beam flange bending

The bottom beam flange of the edge beam consists of the HEA 260 flange and an additional steel plate of 365 x 12 mm that was welded below the beam flange. Due to bending of the section flange, a rotation of the hollow core slab occurs. This additional rotation should be added to the rotation found for the rotation related to the global bending of the hollow core slab. To calculate the rotation, a simplified model is made where the flange consists of two sections with different moment of inertia. In [Figure 7.1c](#) a schematic representation of the situation is shown. With the help of Maple the rotation at the bearing point is calculated. The calculations are shown in [section D.3](#). As a result, rotations of **9.5 mrad** and **4.1 mrad** are found for the fully loaded and self-weight-only position, respectively.

7.1.4. Result

In [Table 7.2](#) the displacement per rotation type is shown. Since the demands from [Equation 7.1](#) are fulfilled, $27.3 \geq 4.9$ and $10.9 \geq 2.1$, for both the fully loaded and self-weight only situation, it is concluded that *compression is present* on the upper side. Therefore, the flow of forces presented in [Figure 4.10](#) is correct.

Table 7.2: Rotation results and displacements

	$\phi_1[mrad]$	$z_1[mm]$	$\delta_1[mm]$	$\phi_2[mrad]$	$\phi_3[mrad]$	$z_{2,3}[mm]$	$\delta_2[mm]$	$\delta_3[mm]$
1.2G + 1.5Q	222.8	122.5	27.3	12.4	9.5	222.5	2.8	2.1
1.2G	89.3	122.5	10.9	5.3	4.1	222.5	1.2	0.9

7.2. Connection stiffness

The stiffness of the connection depends on all the components present within the connection. However, for a simplified assessment, only two parts are taken into account: the stiffness of the bolted shear stud and the stiffness of the compressive top plate. Additionally, the total stiffness is affected by both the axial stiffness of the reinforcement bar and the stiffness of the SHS section. However, it is assumed that the impact of these components is minimal, and thus disregarded. The stiffness of the top plate and bolted shear stud determine the rotation of the hollow core slab and, subsequently, the deformations.

7.2.1. Bolted shear connector

The stiffness of the bolted shear connector was evaluated based on data from the literature. To measure the actual slippage of the connection and the bending of the bolt for the specific geometry and materials, a push-out test should be performed. Due to the scope of the thesis and limitations in time and financial resources, these tests were not conducted. However, extensive literature is available on the stiffness of these types of connections. The paper by Jakovljević [55] provides a state-of-the-art review of demountable composite steel-concrete floors. The principle used for demountable steel-concrete composite floors is similar to the application used in the demountable bolted shear connector connection.

The connection consists of a bolted shear connector with a diameter of 16 mm (M16) and a contact length of 100 mm. This length of embedding is necessary to ensure that the maximum compressive resistance of the mortar is not exceeded. The total length of the bolted shear connector consists of the embedment length, the thickness of the bottom plate, and the thickness of the closing nut; resulting in the application of an M16 x 130 mm. The bolted connection can be established in three different configurations, as shown in Figure 7.5. The first configuration is a bolt with only a nut on the outside; the other two configurations have an embedded nut, one and two, respectively. The application of the embedded nut has two major advantages. First, bolted shear connectors with embedded nuts show increased stiffness [55]. Second, the embedded nuts make the placement and alignment of the bolts on the bottom flange of the beam significantly easier. A design without an embedded nut requires a threaded hole. Using two nuts instead of one increases the stiffness of the connection.

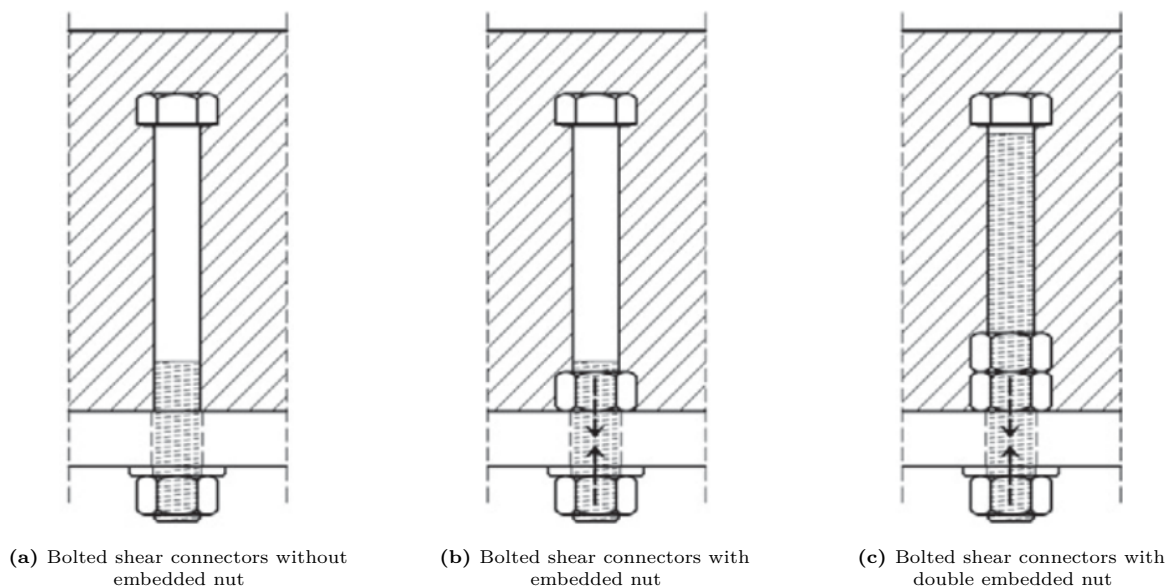


Figure 7.5: Bolted shear connectors in various configurations [75]

Push-out tests on bolted shear connectors with a similar geometry were performed by Pavlovic et al. [75], Kwon et al. [62], and Yang et al. [92]. These tests provide insight into the behaviour of the connection and are standardised for steel concrete composite structures according to EN 1994-1-1 [24]. A load-displacement curve is obtained based on the push-out test. The standard setup comprises 8 bolts, and based on the total resistance, the resistance per individual bolt is calculated. To determine the stiffness of the proposed connection, the main findings of the aforementioned research papers are analysed. In Table 7.3 the results of the three papers are shown. Based on the data, Pavlovic's push-out test aligns most closely with the connection's geometry. An almost identical bolt is used with a single embedded nut. The compressive strength of the concrete in the setup was lower compared to the mortar in the connection. However, more important is the stiffness, which is more or less equal to 32.8 GPa [75] for concrete versus 29 GPa [81] for the mortar. In all push-out test specimens, failure occurred in the bolt and the concrete strength was sufficient. An interesting observation is found in the fact that the total applied load of the M18 bolt by Yang results in almost a double ($1.90 \times$) maximum load compared to the test by Pavlovic [75]. This is interesting, since the difference in the shear area is only a factor

of 1.22. Similarly, the test performed by Kwon shows only slightly higher resistance ($1.07 \times$) compared to Yang, while the bolt shear area is 1.57 times larger and the American Standard A325 steel has more or less similar properties to the European Standard class 8.8. A possible explanation could be found in the configuration difference between a single embedded nut, a double embedded nut, and a coupler. Another important possible explanation is the bolt hole clearance; the tighter clearance results in less total slip, but may also have a positive influence on the maximum applied load.

Table 7.3: Bolted connector stiffness comparison

	Bolt characteristics	Concrete strength [MPa]	n	Config.	Failure	$P_{u,\mu}$ [kN]	Bolt hole clearance [mm]	δ_u
Pavlovic [75]	M16 8.8, $h_{sc} = 105$ mm, $l = 140$ mm	$f_{ck} = 40$	4	Single	Bolt	89.6	1	4.51
Kwon [62]	d=22 A325, $h_{sc} = 127$ mm	$f_{ck} = 43.8$ (7 days)	3	Double	Bolt	183.0	2	9.9
Yang [92]	M18 8.8, $l = 70$ mm, M18 x 54 coupler, M18 8.8, $l = 200$ mm	$f_{ck} = 48.9$ (28 days)	2	Coupler	Bolt	170.0	0.1-0.5	2.27

Pavlovic's test results are adopted to determine the slip in the connection. The main reason is the similar dimensions of the components. In Figure 7.6a the load displacement curve for the tests performed by Pavlovic is presented. The slip at $0.7 P_{rk}$ is taken to determine the slip of the connection. A stiffness of 68.0 kN/mm is obtained for the bolted shear stud. With a maximum load in the bottom flange of 53.6 kN, the design slip is equal to $s = 0.79$ mm.

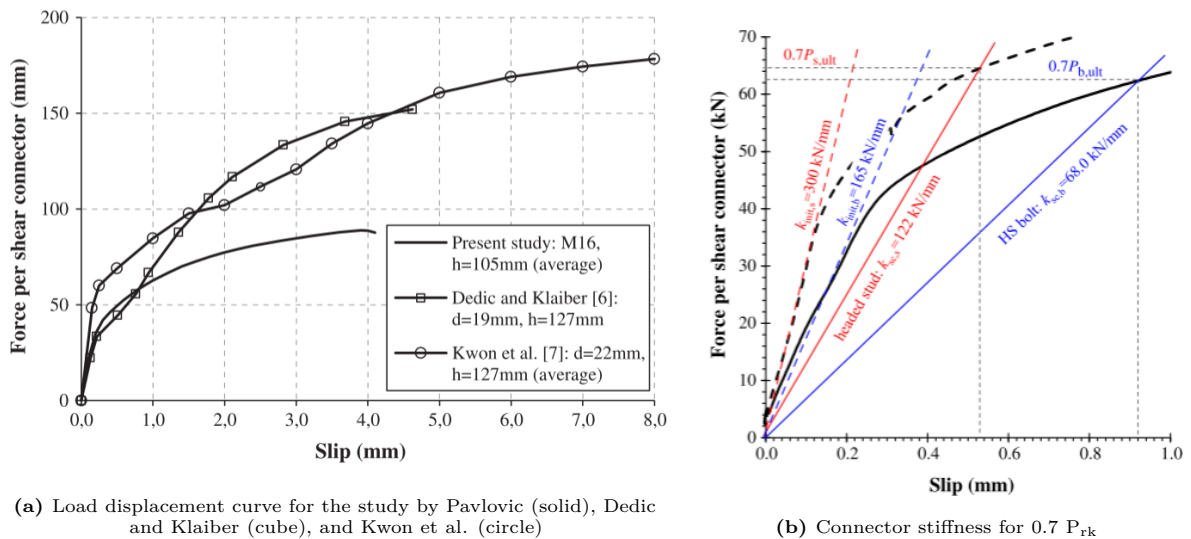


Figure 7.6: Results of the push-out test performed by Pavlovic et al. [75]

7.2.2. Top plate

The top plate must transfer the compressive load to the upper beam flange and subsequently to the beam web. The welded plate should be checked to ensure it is sufficiently rigid to transfer the load without excessive deformations. The plate should have a minimum end distance of $1.2 d_0$ as prescribed in Table 3.3 of EN 1993-1-8 [20]. Resulting in a minimal plate dimension of $2.4 d_0$ in width and height.

For this instance, d_0 is equal to d because the bolt is placed in a threaded hole. The plates are 50 x 50 mm in width, and an initial thickness of 8 mm is assumed. In Figure 7.7 the situation is schematised including dimensions. The beam web is assumed to act as a rigid body and the weld between the top flange and the compressive plate is dimensioned such that the connection between the elements is rigid. The deflection of the top plate consists of two parts: the deformation of the compressive plate due to rotation of the top flange of the integrated beam and the deformation due to bending of the compressive plate.

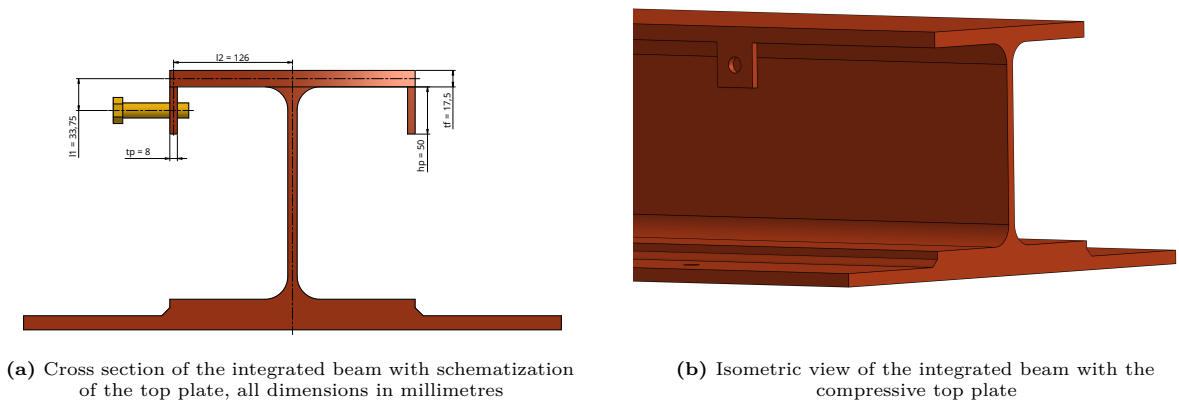


Figure 7.7: Compressive top plate in cross sectional and isometric view

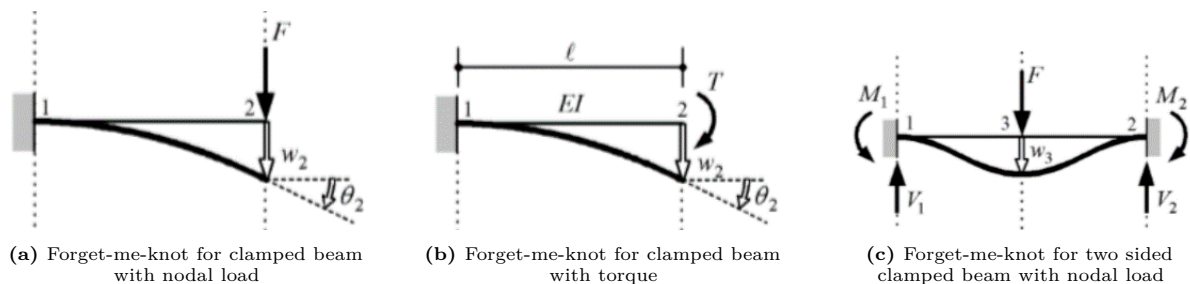


Figure 7.8: Forget me knots for connection stiffness

The total horizontal deformation is obtained by adding the deformations w_1 and w_2 . The deformation caused by the bending of the compressive plate is determined using Figure 7.8a and is represented by w_1 . To calculate the rotation of the top flange of the integrated beam, the compressive load is converted into a torque by multiplying the force by the lever arm l_1 . The compressive plate deformation due to this rotation is denoted by w_2 and is equal to $\theta_2 \cdot l_1$. Equation 7.3 evaluates the total deformation of the top plate. The variables in the equation are shown in Figure 7.7a and Figure 7.9. The rotation of the beam flange depends on the effective width. The 50x50 plate on which the load is applied mobilises an additional area of the top flange of the beam. In Figure 7.9, the area A represents the load spread area. Dividing this area by the distance between the centre line of the compressive plate and the centre line of the integrated beam (l_2) gives the average width of the load spread, which is used to calculate the moment of inertia.

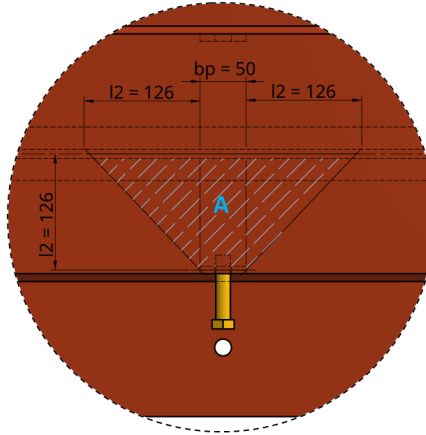


Figure 7.9: Cropped top view of the integrated beam with mobilised area for flange bending (A), all dimensions in millimetres

$$\begin{aligned}
 w &= w_1 + w_2 = w_1 + \theta_2 \cdot l_1 = 1.94 \text{ mm} \\
 w_1 &= \frac{F_{h,Ed,t} l_1^3}{3E(1/12)b_p t_p^3} = \frac{52 \cdot 10^3 \cdot 33.75^3}{3 \cdot 2.1 \cdot 10^5 \cdot (1/12) \cdot 50 \cdot 8^3} = 1.48 \text{ mm} \\
 w_2 &= \frac{(F_{h,Ed,t} l_1) l_2}{E(1/12)b_{eff} t_f^3} \cdot l_1 = \frac{52 \cdot 10^3 \cdot 33.75 \cdot 126}{2.1 \cdot 10^5 \cdot (1/12) \cdot \frac{126 \cdot (126+50)}{126} \cdot 17.5^3} \cdot 33.75 = 0.45 \text{ mm}
 \end{aligned} \tag{7.3}$$

7.2.3. Combined stiffness

The stiffness of the connection is based on the slip of the connection and the stiffness of the top plate. The slip of the connection works opposite to the deformation of the top plate. Therefore, the two deformations are summarised.

$$\delta = s + w = 0.79 + 1.94 = 2.73 \text{ mm} \tag{7.4}$$

This combined deformation allows the slab to rotate as a consequence of the torsional moment. Due to the torsional moment, the slab has full contact with the compressive point, resulting in an angular rotation of θ as shown in [Figure 7.10](#). The angular rotation θ is expressed by deviating the displacement δ over the internal lever arm $z_{2,3}$ which represents the distance between the bottom of the hollow core slab to the compressive points as described in [section 7.1](#).

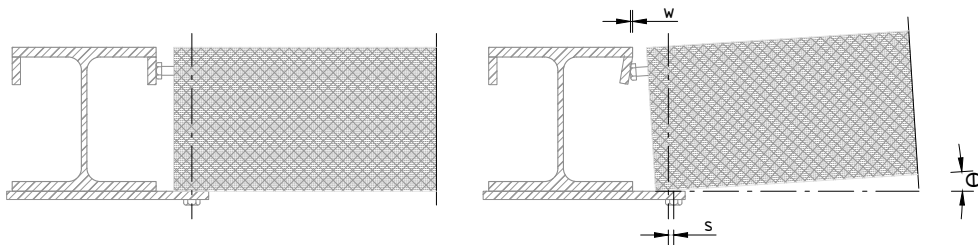


Figure 7.10: Connection behaviour due to slip of the bolted shear connector (s), and deformation of the compressive plate (w)

$$\theta = \frac{\delta}{z_{2,3}} = \frac{2.73}{222.5} = 12.3 \text{ mrad} \tag{7.5}$$

The angular rotation of the slab at the bearing point results in an upward deformation of the hollow core slab at midspan. The maximum span of the case study building equals 11 m (L1). The angular rotation of 12.3 mrad results in a maximum upward displacement of 67.5 mm. The deflection limit for hollow core slabs is equal to $L / 250$ [23] and will be adopted as the upward deformation limit. For the hollow core slab length of 11 metres a deformation limit of 44.0 mm is found. Since the deformation limits are exceeded additional measures to increase the stiffness are implemented. The largest improvement is obtained by increasing the stiffness of the top compressive plate. It is recommended to reinforce the plate with a steel plate behind. This plate connects directly to the beam web, the result is shown in [Figure 7.11](#). A possible solution to create the stiffened plate is an angle steel L-profile welded to the upper flange and web of the beam. The new stiffened situation is calculated with the forget-me-knot shown in [Figure 7.8c](#). The reduced deformation of the plate w_3 is 0.08 mm and with the bolt slip s of 0.79 mm added, the angular rotation is 3.9 mrad. Resulting in a maximum slab deformation of 21.5 mm which is well within the set limit of 44.0 mm.

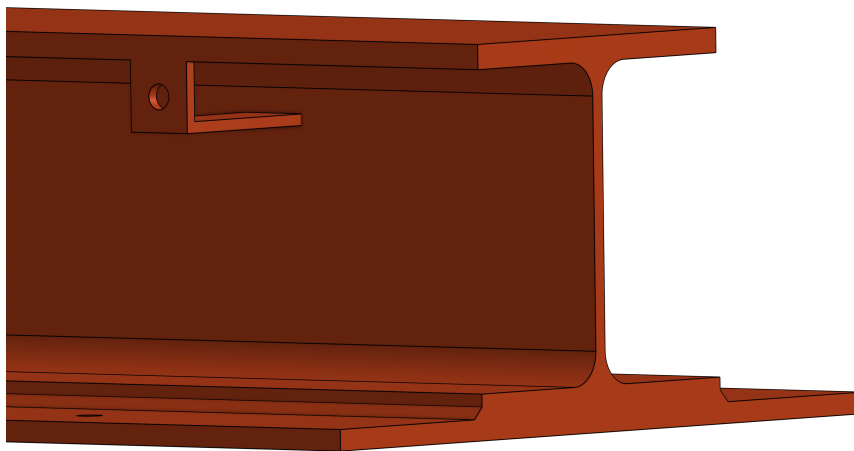
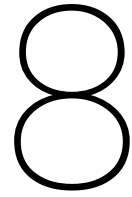


Figure 7.11: Isometric view of the integrated beam with the top plate and stiffener plate



Experimental research on the demountability

From the trade-off analysis presented in [chapter 5](#) the demountable bolted shear connector design was presented as the best alternative. The main drivers were better performance in tolerance accountability, ease of installation, and mainly connection costs. The weakest point of the connection is seen in the demountability. In this third chapter of [Part III](#), the demountability is assessed on the basis of experimental research. The chapter is divided into three sections. The first section addresses the methodology, followed by the data collection, and finally the data interpretation. The objective of the experiments is to establish the feasibility of dismantling the connection. This is done by an experiment which recreates the situation as designed in [subsection 4.3.2](#).

8.1. Method

As mentioned above, the situation presented in [subsection 4.3.2](#) is recreated. Since the demountability is based only on two of the connection's components, a small-scale experiment is performed instead of a full-scale connection. The experiment consists of the SHS section and mortar. The goal of the experiment is to address the separation potential of the two components. Two different methods are used to determine the separation, namely, with the help of a Universal Testing Machine (UTM) or load cell and by using hand tools. The reason behind this is that the load cell of the UTM can provide numerical values, while the hand tools can show the actual demountability potential in practice. The methodology section starts with an explanation of the expected resistance, followed by the testing procedure. Resistance to the separation of mortar and steel originates from two different components. In short, the following components generate resistance:

- Chemical bond,
- Friction resistance.

Chemical bond

The chemical bond, or more specifically, the ionic bond, is based on the principle of atomic exchange between the metal and the non-metal. The steel section "donates" its electrons to create a bond between steel and mortar. The magnitude of the strength of the bond is unknown and the current literature does not give clear values. Generally speaking, the chemical bond is an additional reserve in the bond strength. For example, the bond strength of reinforcement bars and concrete is based on the mechanical interlocking strength. The chemical bond is addressed as an additional safety in strength and is therefore not considered critical. However, in this particular case of the demountable connection, the chemical bond is undesirable and considered critical.

A thorough investigation of the literature resulted in a paper that evaluated the resistance between steel and concrete using a push-out test [11]. In this paper, three different surface treatments were investigated. The direct steel-to-concrete interface is the best representation of the experimental setup.

For the concrete, a standard type of concrete was used with a compressive strength of 60 MPa and modulus of elasticity of 36.600 MPa. In the research two different geometries were evaluated. Geometry (a) consists of two steel plates with a concrete block in between, while geometry (b) consists of two concrete blocks with a steel plate in the middle. The first mentioned geometry is more in line with the demountable shear connector detail, and therefore this value is used as a reference. The average push-out test load was equal to 70.6 kN, which translates into a shear stress of $\tau = 0.8$ MPa.

8.1.1. Expected resistance (hypothesis)

The estimation of the expected resistance determines the required capacity of the load cell and gives an indication of the separation potential with the use of hand tools. For the chemical bond part, a shear strength of 0.8 MPa was found from Berthet's [11] paper. The friction resistance between the steel section and the mortar is difficult to determine. The friction resistance has a static and dynamic part and is dependent on the load level perpendicular to the friction surface. An increase in compressive force results in increased friction. According to NEN-EN 1993-1-8 [20] the friction coefficient is equal to 0.20 for sand-cement mortar and steel. For 1 N vertical pressure, 0.2 N friction resistance is generated. In the specimen, no load is applied in the direction perpendicular to the friction surface. In addition to this, the mortar is expected to shrink and therefore the theoretical perpendicular load can be assumed to be zero. However, imperfections in the steel section generate a friction force between the steel and the mortar. Since 3D laser scanning is not possible on the inside of the section, it is impossible to determine the actual imperfections. Furthermore, regardless of the loading method (whether using a load cell or hand demolition), the loading block experiences an eccentricity related to the specimen while being loaded. This eccentricity causes a horizontal component of the applied vertical load. This contradicts the assumption that there is no force perpendicular to the loading direction.

Since chemical bonding and friction are undesirable, some of the specimens are treated with a release agent. To break the bond, traditional formwork oil is used. Alternatively, a Vaseline is applied, as this product is commonly used in the concrete mould industry and has a higher lubrication potential compared to the oil. As a result, the following specimens are produced:

- Untreated 4x,
- Treated with formwork oil 4x,
- Treated with Vaseline 4x.

From the specimens, the untreated ones are expected to generate the highest resistance. The maximum load is calculated based on the value of the chemical bond that occurs in the untreated specimens. The maximum resistance is given in Equation 8.1. The length and height of the bond are based on the geometry of the SHS section and are indicated with l_b and h_b respectively. For the sections, SHS 80/80/5 are used and with a height of 260 mm. These dimensions are based on the initial geometry used in chapter 6. The sections are casted with 30 mm of clearance from the top edge, and this results in a bond length of 230 mm.

$$\begin{aligned} F_{v,Rd} &= \tau \cdot l_b \cdot h_b = \tau \cdot (4 \cdot (h - 2 \cdot (t_f + r)) + 2 \cdot \pi \cdot r) \cdot h_b \\ &= 0.8 \cdot (4 \cdot (80 - 2 \cdot (5 + 5)) + 2 \cdot \pi \cdot 5) \cdot 230 = 49.9 \text{ kN} \end{aligned} \quad (8.1)$$

The resistance is expected to be significantly lower for the other specimens. In theory, the bond should be broken and the oil and Vaseline lubricate the mortar inside the sections. For these specimens, the only source of resistance is shear friction that arises from imperfections and the loading condition. Since Vaseline creates a thicker layer compared to the formwork oil, it is expected that the friction resistance is the lowest for specimens treated with Vaseline.

8.1.2. Experimental setup

For the experimental setup, the proposed design of subsection 4.3.2 is recreated. For the experiment, the dimensions from chapter 6 are used. Two deviations are made from the dimensions shown in the verification. The first change is the difference in the thickness of the flange. The sections in the experiment have 5 mm thick flanges compared to the 4 mm thick flanges in the final design. The other difference is that S355 steel was used in the experiments, while for strength verification S235 is

sufficient. The decision to apply S355 was made because the compressive resistance of the SHS section should outperform the compressive resistance of the mortar so that a failure of the steel could not occur. The influence of these changes is expected to be minimal. The minor change is that the bond area for SHS 80/80/4 is approximately 1% larger due to the increased interior perimeter. The exact setup of the experiment with detailed drawings of the components, a bill of materials, and the necessary equipment is shown in [Appendix G](#).

The experimental setup comprises the specimens loaded by the load cell. In [Figure 8.1](#) the setup is shown schematically. In the figure, the SHS section is shown in blue and the mortar is indicated with a dashed line. At the bottom of the section, a void is made to allow the mortar to move in the vertical direction. The loading block on the top is pressed inside the section by moving the bottom plate of the Universal Testing Machine (UTM). The UTM's upper plate is fixed in position by the loading frame, and the bottom plate is moved upward by the hydraulic cylinder of the UTM. The displacement and load are calculated using a measuring device attached to the hydraulic cylinder. In theory, the measured values of the displacement can differ slightly, since the load cell's frame is not fully rigid and experiences deformations. This problem could be solved using an LVDT. However, frame deformations due to load are expected to be minimal, since the machine is likely to operate at less than 10 % of its capacity (49.9 kN / 600 kN).

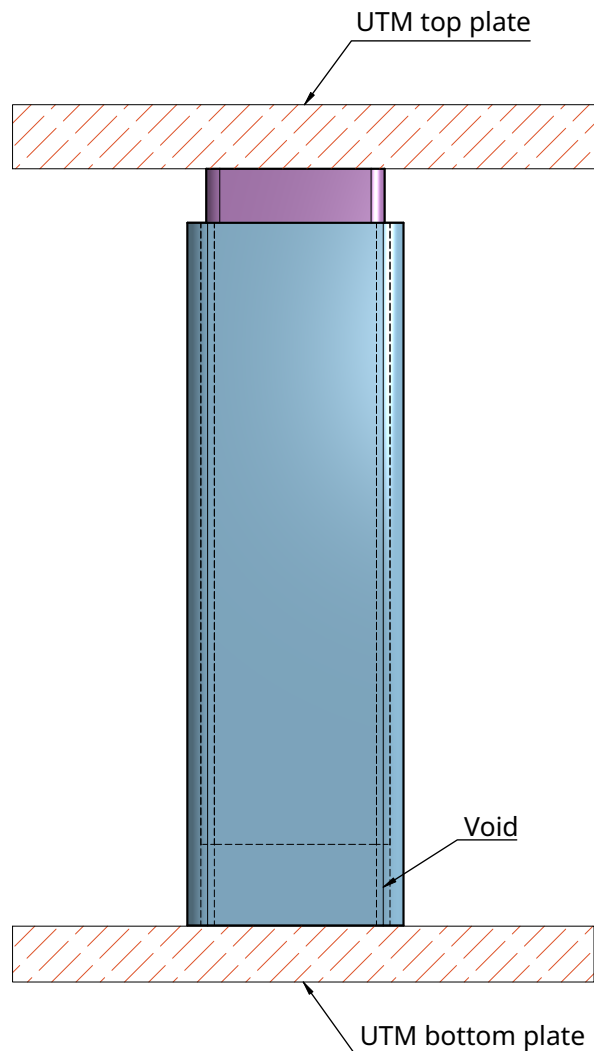


Figure 8.1: Schematization of the experimental setup

8.1.3. Testing procedure

The following bullet points describe the procedure for the execution of the experiments. The first phase comprises the preparation of specimens.

Phase I - preparation

1. Deburring of the edges of the steel section with a metal file.
2. Remove metal shavings/ dust from the inside with a rag and compressed air.
3. Prepare the formwork by screwing the slats to create a grid for the SHS sections; see [Appendix G](#).

After preparation, the samples are divided into three groups and marked accordingly. The first group of specimens are untreated. For the second group, an oil-based formwork release agent is used. The third and last group are treated with a Vaseline-based release agent. In [Figure 8.2](#) the various treatments are shown after application to the section. In the next phase, after the application of the treatments, the sections are casted with the mortar. In [Figure 8.3a](#) the mixing procedure is shown and in [Figure 8.3b](#) the process of casting. To validate the quality of the mortar, a concrete cube is casted. During casting, the maximum processing time of the mortar (30 min) should be satisfied.

Phase II - casting

1. Apply formwork oil to the formwork set-up.
2. Place the SHS sections on the formwork plate.
3. Apply the treatments to the SHS sections.
4. Add CUGLATON gietmortel 5 mm to the mortar tub (20 kg of mortar + 2.0-2.2 L of water) and mix with the cement mixer until a slump of 700 mm is reached (approximately 3 min).
5. Cast the SHS sections with the mortar and keep 30mm from the top edge.
6. Cast the concrete cube.
7. Cover everything with cling film.
8. Wait for at least 7 days (curing time).

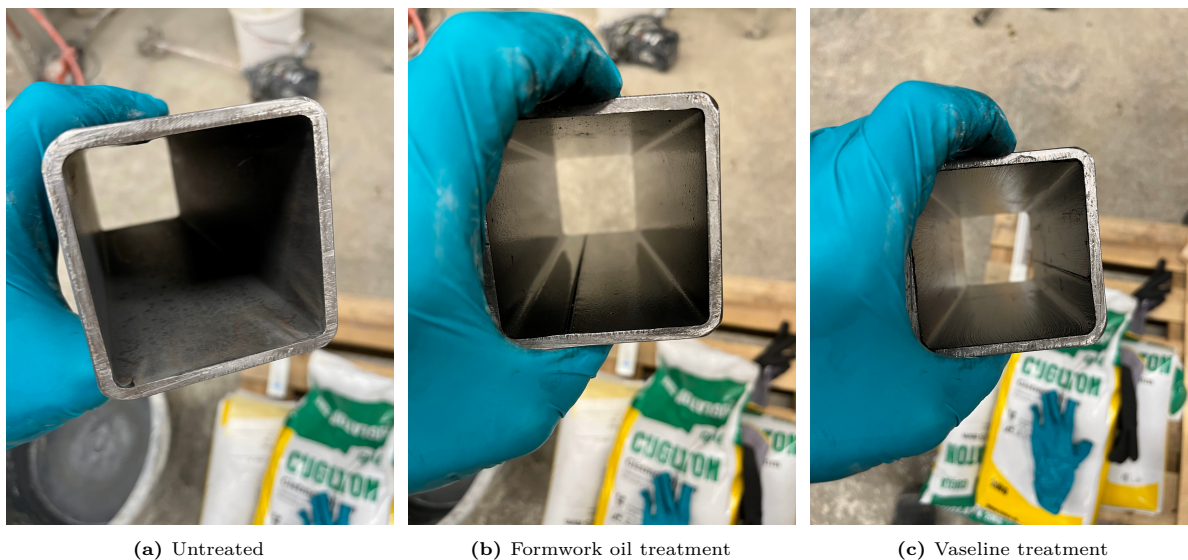


Figure 8.2: Application of different treatments to the specimens

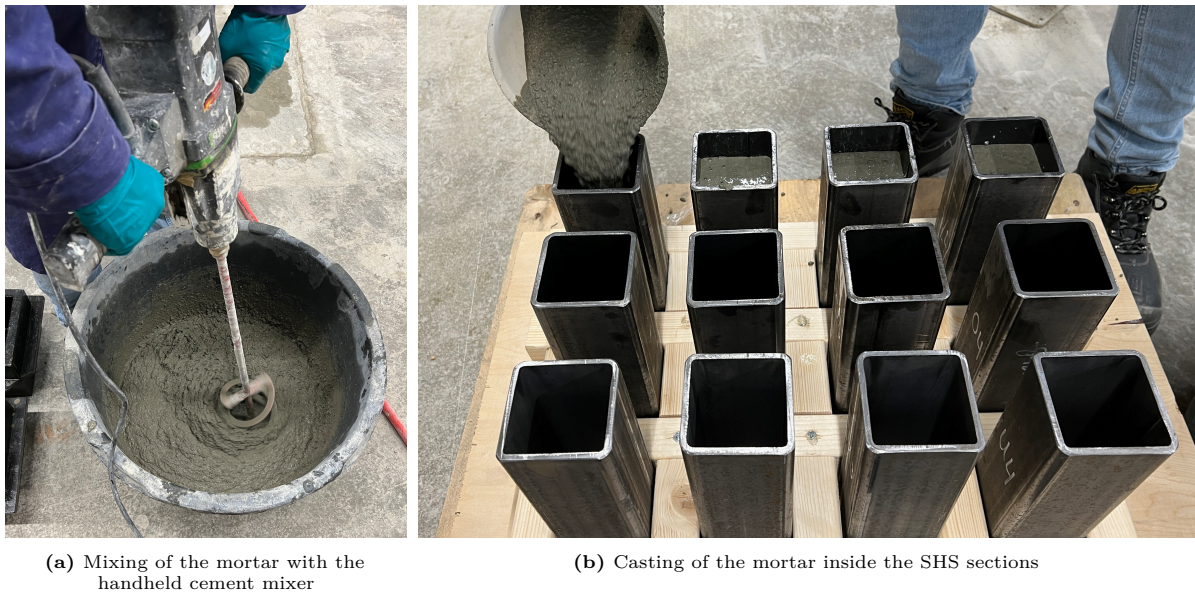


Figure 8.3: Mixing and pouring procedures of phase II

After the curing time has been exceeded, the specimens are tested. For all treatment types, 4 specimens are available. Three of the specimens per group undergo a compressive test on the Universal Testing Machine, and the other undergo manual demolition of the mortar. For manual demolition, the steps are described in *Phase III-B* and for specimens that undergo UTM testing in *Phase III-A*. If the specimens were unbonded and the experiment shows only friction behaviour, they can still undergo manual demolition as a reference.

Phase III-A - testing load cell

1. Measure the length of the steel section and the concrete in the specimens to determine the bond area.
2. Place the buffer block and the specimen in the UTM, make sure that the void is located on the bottom side of the specimen and that the alignment between the top plate and the section is correct (2 mm clearance on all sides).
3. Align the machine to obtain full contact between the machine and the loading block.
4. Start the compressive test; the test should be displacement controlled and with an initial speed of 0.002 m/s.
5. Increase the displacement rate of the cylinder if the obtained measurements are with a large scatter.
6. Stop the test once 20mm displacement (thickness of the loading block) is reached.
7. Read the log data for the applied load, P , and displacement δ .

In [Figure 8.4a](#) the alignment of the loading block is shown, and in [Figure 8.4b](#) the specimens during the testing.

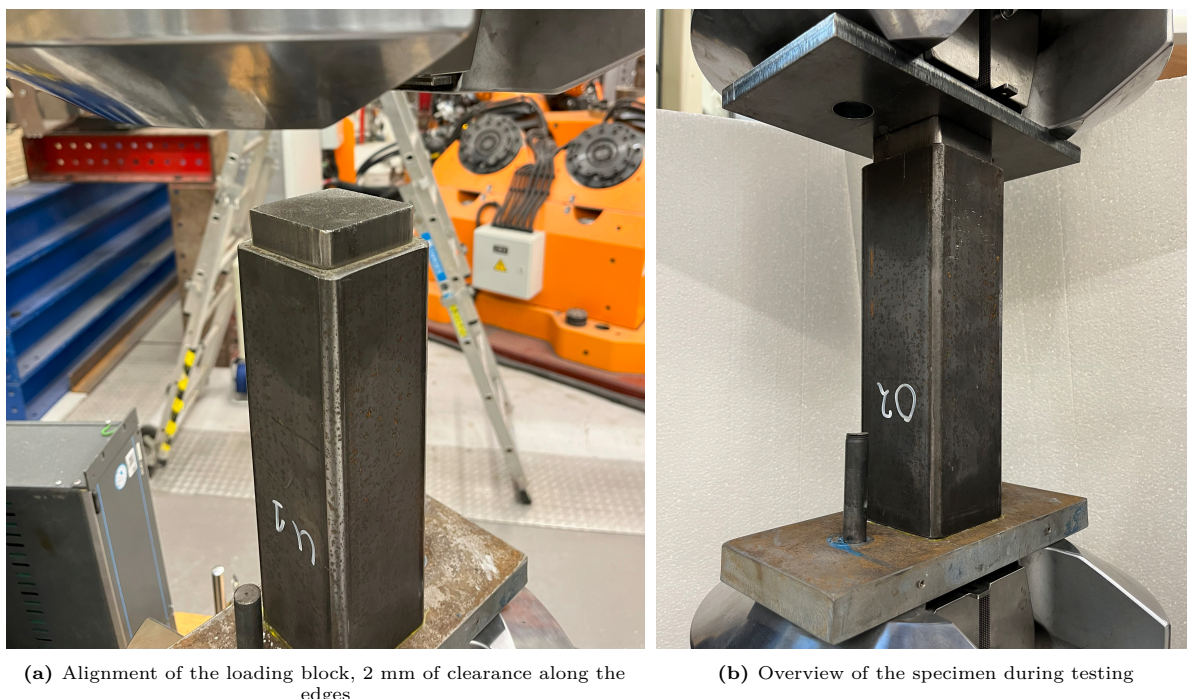


Figure 8.4: Specimens during preparation and testing

Phase III-B - testing manual demolition

1. Place the specimens in a vice or on the ground with a wooding buffer block.
2. Start with the smaller demolition hammer with the Bouchard chisel ¹.
3. In case the small hammer has insufficient power, increase the size of the demolition hammer.
4. If the Bouchard chisel is unable to get the complete mortar block moving; use a normal stone chisel.

For manual demolition, the procedure is shown in [Figure 8.5](#). Two possible demolition positions are shown with both setbacks. For the demolition on the floor shown in [Figure 8.5a](#) the drawback is that only the first 3 cm are moved. After this, the mortar is in contact and further movement of the mortar is impossible. The placement in the vice, shown in [Figure 8.5b](#), has the disadvantage that this generates clamping pressure on the steel section. This pressure is needed because otherwise the specimen will drop under the vibrations of the demolition hammer. However, the clamping pressure generates additional friction resistance. For application in practice, these problems will not occur since the section is positioned in the sleeve of the hollow core slab.

¹Special chisel with large contact area, normally used for flattening of (natural) stone.



Figure 8.5: Specimens during manual demolition

8.2. Data collection

In the data collection the data from the load cell and manual demolition is presented.

8.2.1. Load cell

From the 12 specimens 9 undergo load cell testing. For each set of treatments, a graph is made to show the behaviour of the treatments during loading. In addition to the individual graphs, a combined graph gives insight in the overall behaviour between the treatment types.

For all tests, the raw data sets were modified to account for the different starting positions of the UTM. Differences in starting position result from the fact that force and displacement data were measured directly by the load cell. The lengths of the SHS sections deviate, and the concrete surface is not completely horizontal and smooth. As a result, the UTM starts at a different position at the beginning of each test. The loading block has to "settle" on top of the mortar. The data were modified so that all test data start at the first instance when 1 kN compression was shown in the data set.

The datasets obtained from the load cell have a significant scatter. This effect is caused by three different causes:

- Sampling rate,
- Loading speed,
- Measurement procedure.

The first point of the sampling rate specifies the number of data points measured per second. During the start of the first test, the sampling rate was set at 2 measurements per second. It was noticed that a scatter between the points was obtained. To minimise noise in the data, a reduced sampling rate of 1 measurement per second was set for all upcoming tests. The second cause is found in the loading speed. Initially, the loading speed was equal to 0.001 mm/s. After the drop in stiffness, the relatively

slow loading speed caused a scatter in the data. To minimise scatter, the loading speed was gradually increased. First, the speed was doubled to 0.002 mm/s and eventually even faster to a maximum of 0.05 mm/s. After an increase in speed, the measured resistance tends to increase slightly over a short period of time. Once the new speed is adopted, the mortar block moves again as a whole, and the actual measured resistance is shown. However, all measurements were performed under static loading conditions and the above mentioned influences are expected to be minimal. The last cause of scatter is the measurement technique. Noise in the data is generated because the load and displacement are measured by the load cell and not directly below or inside the loading block by an LVDT. This is expected to have the largest influence since for all obtained results there is an initial linear elastic part which is not as expected. The influence of the measurement procedure comprises the deformation of the load cell, straining of the SHS section, settling of the loading block, and shortening of the mortar block. The straining of the SHS section is small due to the low stresses in the section. The shortening of the mortar is also expected to have a minor influence since the mortar is under confined conditions and the Poisson effect is prevented.

Untreated specimens

In [Figure 8.6](#) the results of the untreated specimens are shown. All of the samples start with a more or less equal stiffness, which is represented by the slope of the curve. For the three specimens U1, U2, and U3 the stiffnesses are equal to 14.7, 16.9, and 17.9 kN/mm. After a linear elastic phase and a displacement between 2.4 and 3.1 mm, a sudden drop in applied force is observed. The magnitude of the maximum load is significantly different with a compressive force of 34.3, 52.5, and 39.4 kN for U1, U2, and U3, respectively. With an average maximum applied force of 42.1 kN, the untreated samples obtain the highest resistance. Following the instant drop in load, the load gradually decreases to a lower level until a new equilibrium is reached. In this equilibrium, the constant applied displacement results in a more or less constant applied force. Subsequently, the resistance starts to increase, similar to that in a hardening phase. During this phase, the stiffness increases again.

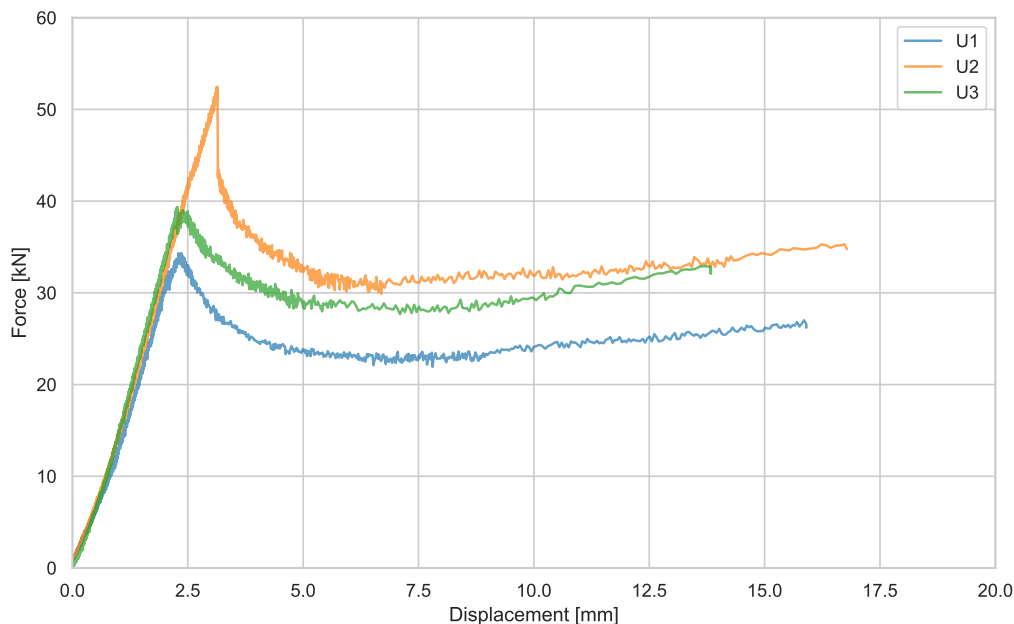


Figure 8.6: Plot of displacement vs. force for untreated specimens (U), lines are adjusted to start at same point (1 kN of compression)

Oil-treated specimens

[Figure 8.7](#) shows the test results of the oil-treated specimens. The oil-treated specimens show an initial behaviour similar to that of the untreated specimens. They both start with a more or less linear elastic

phase but where the average stiffness of the untreated specimens is equal to 16.5 kN/mm the average stiffness of the oil-treated specimens is significantly lower with 12.2 kN/mm. This equals a reduction of just over 25 %. The stiffnesses of the individual specimens are equal to 11.8, 11.1, and 13.7 kN/mm for the specimens O1, O2, and O3, respectively. Following the linear phase, a hardening phase occurs. During the hardening phase, the slopes of the first and second specimens are quite similar, while the slope of the third specimen stays more or less horizontal. What is observed is that after the shorter and less stiff linear elastic initial phase, the hardening phase has significantly higher stiffnesses compared to the third specimen. The maximum resistance of the second specimen approaches the maximum resistance of the third.

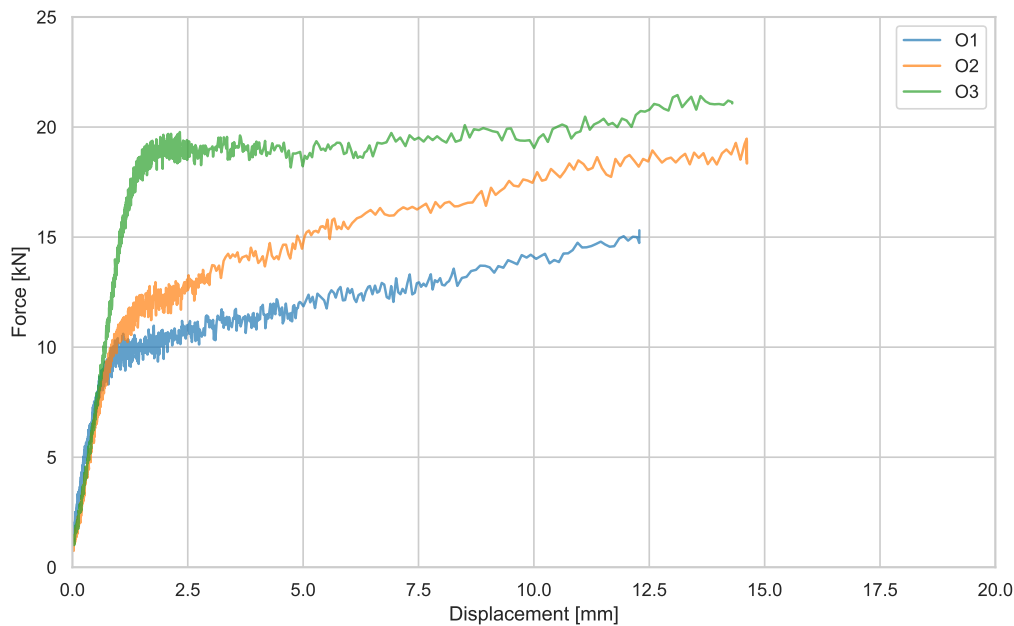


Figure 8.7: Plot of displacement vs. force for oil-treated (O) specimens, lines are adjusted to start at same point (1 kN of compression)

Vaseline treated specimens

The results of the specimens treated with Vaseline are displayed in [Figure 8.8](#). The specimens treated with Vaseline show a linear elastic initial phase similar to that of the oil and the untreated specimens. The specimens have a considerably lower initial stiffness with 4.0, 8.5, and 8.0 kN/mm for specimens V1, V2, and V3, respectively. However, specimen V1 has approximately half the initial stiffness compared to V2 and V3. After the linear elastic phase that ends at approximately 1.0 mm, which is similar to the oil-treated specimens, a plateau phase is reached. This plateau is best visible for specimens V1 and V3. In the plateau phase, the constant displacement of the load cell results in a more or less constant load. The Vaseline specimens show similar to all the other specimens a hardening phase.

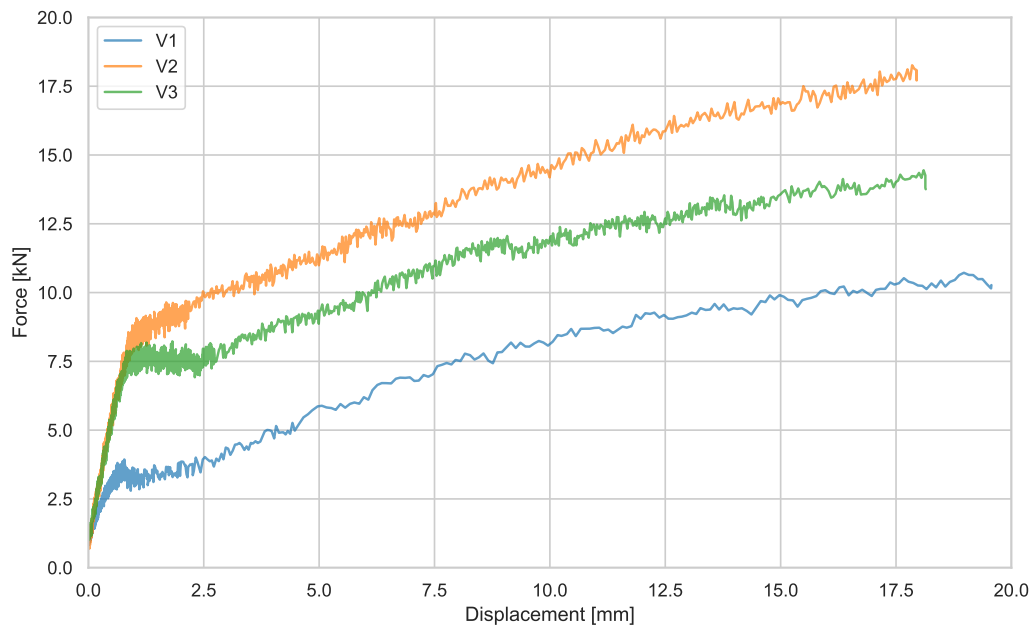


Figure 8.8: Plot of displacement vs. force for Vaseline-treated (V) specimens, lines are adjusted to start at same point (1 kN of compression)

Combined plot

In [Figure 8.9](#) all individual plots are combined into one graph. The general trend shows that the highest resistances are obtained for the untreated specimens, followed by the oil-treated specimens and finally the Vaseline-treated specimens. An interesting observation is the fact that the maximum resistance of V2 is greater than the maximum resistance of O1. In fact, lines V2 and O1 show very similar behaviour, which can also be seen in [Figure 8.9](#). In [Figure 8.10](#) the first 2.5 mm displacement is shown with the linear elastic phase. In this figure, the scatter in the measurements as mentioned before is clearly visible.

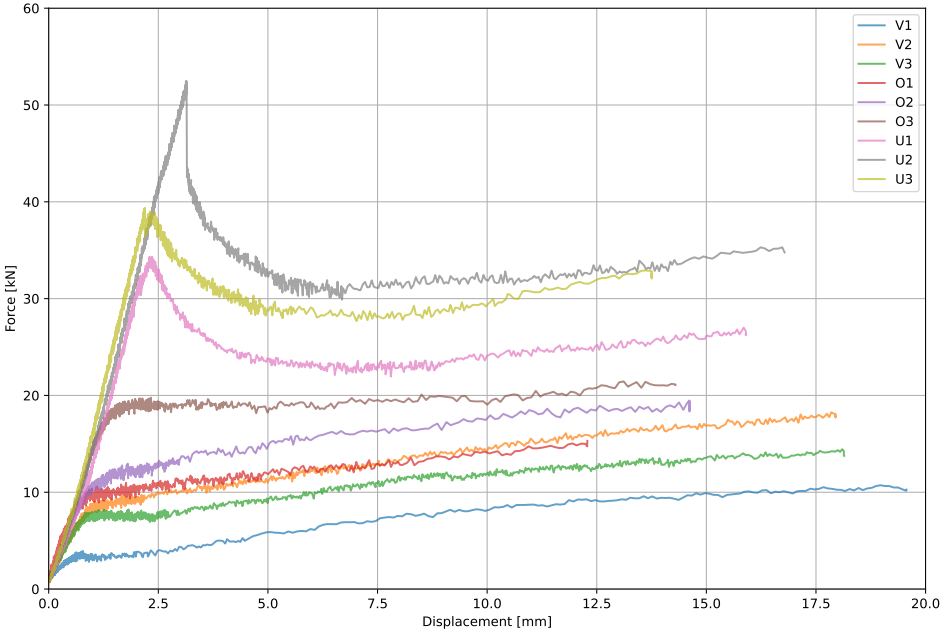


Figure 8.9: Plot of displacement vs. force for untreated (U), oil-treated (O), and Vaseline-treated (V) specimens. Lines are adjusted to start at same point (1 kN of compression)

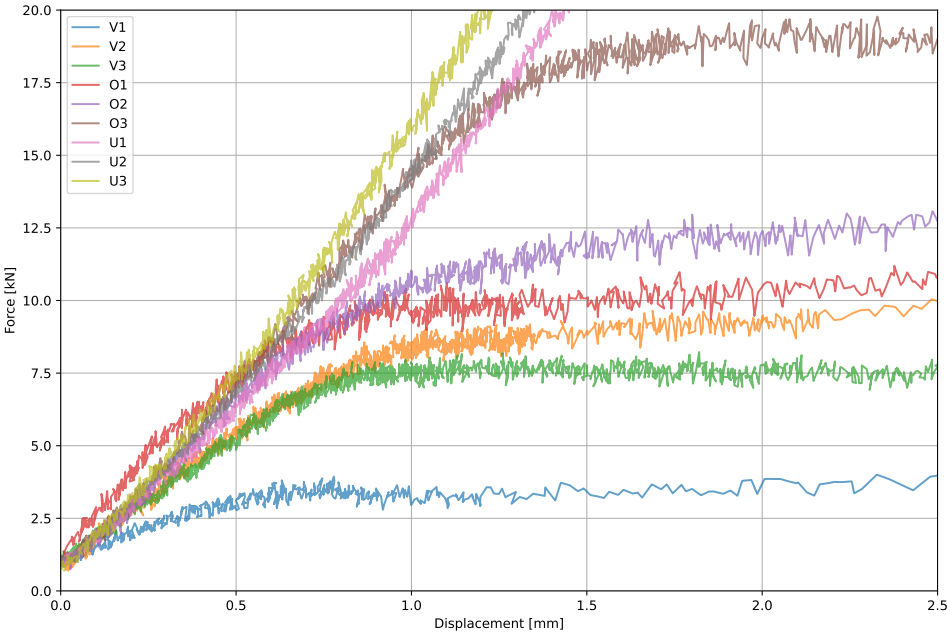


Figure 8.10: Plot of the initial part of displacement vs. force for untreated (U), oil-treated (O), and Vaseline-treated (V) specimens. Lines are adjusted to start at same point (1 kN of compression)

8.2.2. Manual demolition

After the execution of the load cell test, there was one virgin specimen per treatment remaining. From the specimens tested with the load cell, the ones treated with oil and Vaseline are still subjected to a manual demolition cycle. All specimens show a hardening phase that results in resistances that are more severe than initially expected. Due to the magnitude of the loads, the potential for manual demolition was under discussion. Therefore, it was decided to start with the Vaseline-treated specimens, followed by the oil-treated and virgin untreated specimens. The latter was done for reference purposes, since the demolition potential was assessed as "very low".

For the manual demolition the procedure was to start with the Bouchard chisel. This block with an area of 60x60 mm² fits perfectly in the section. The goal was to move the section as a whole and not break the concrete into pieces. As described in [subsection 8.1.3](#), the manual testing procedure gives the option to place the specimens on a wooden block or in a vice. The disadvantage of the vice is found in terms of the additional clamping package, and therefore, the wooden block was initially used. The vibrations of the hammer made it impossible to keep the specimen in its position, which resulted in the use of the vice.

Table 8.1: Method of hand demolition

	V1	V2	V3	V4	O1	O2	O3	O4	U1	U2	U3	U4
Bouchard chisel	×	×	×	×		×		×				
Stone chisel					×		×		×	N/A	N/A	×

In [Table 8.1](#) the results of manual demolition are shown. If the removal of the mortar with the Bouchard chisel this implies the mortar came out as one piece. For the specimens removed with the stone chisel, the Bouchard chisel gave an inadequate result and only crushed the top layer of mortar without moving the mortar block. The stone chisel was used to crush the mortar and resulted in broken confined conditions. Without confinement, the mortar was removed in smaller pieces. The results of the manual demolition show that the Vaseline-treated specimens outperform the oil-treated and untreated specimens.



Figure 8.11: Bonded piece of mortar (U4)

In [Figure 8.11](#) the result of specimen U4 is shown. This shows that even after the hammer vibrations, the chemical bond remains intact. Removal of the mortar in the untreated specimens was possible, but it cost substantially more effort, manpower, and time. To verify the results, an unprocessed sample that had previously been tested with the load cell was selected for manual demolition. In this particular example, the load cell has already caused the chemical bond to break, yet it is still not possible to

remove it using the Bouchard chisel. This resulted in the decision to not submit the other untreated specimens to the manual test.



(a) Friction of the mortar in the section

(b) Mortar after demolition (V4)

Figure 8.12: Mortar specimens after hand demolition

In [Figure 8.12](#) two mortar specimens are shown after removal from the section. In [Figure 8.12a](#) the specimens show clear traces of friction. The virgin specimen with Vaseline-treatment is shown in [Figure 8.12b](#). This section was removed in one piece and shows fewer indications of friction. In addition to this, the sample was the easiest to demolish and the removal was performed in 26 seconds.

8.3. Data analysis

The data analysis involves the review and interpretation of the data collected during the data collection process.

From the load cell data, clear differences are visible between treated and untreated specimens. Specimens that have not been treated show a kind of bond that breaks when the load is sufficiently increased. This moment of breakage was also audible as a small snapping sound during the test. In the hypotheses, a bond strength of 0.8 MPa was assumed, resulting in a maximum resistance of 49.9 kN. The experiment showed an average maximum load of 42.1 kN or an equivalent bond strength of 0.67 MPa, which is slightly less than expected. The oil and Vaseline treated specimens show a different behaviour compared to the untreated specimens. In the graphs, there is no clear point of breakage. For both the oil and Vaseline specimens, their behaviour is dominated by an initial linear phase and a hardening phase. The linear phase stiffnesses are equal to 16.5, 12.2 and 6.8 kN/mm, respectively. From these values, it is observed that the Vaseline-treated specimens have the best potential for easy demolition.

An interesting result of the test is that the treated specimens measure loads larger than expected. The friction between steel and mortar was expected to be caused by imperfections and loading conditions. The linear elastic phase of the untreated specimens showed large displacements before the bond broke. This is an interesting observation, as it is expected that the displacement is minimal before the bond breaks. Most likely, the displacements measured by the load cell are deformations in the load cell, straining of the SHS section, settling of the loading block, and shortening of the mortar. Due to this observation, the linear elastic behaviour of the treated specimens could also be discussed. Another interesting observation is that the applied load increases over time. After the initial linear elastic part, the hardening phase starts. The friction coefficient is divided into static and kinematic parts. Where the static friction coefficient increases linearly until a certain threshold. After the threshold is reached, the friction coefficient normally drops. This effect would result in a drop in the maximum load once the mortar leaves the static phase and starts the kinematic phase. However, the opposite is observed.

A possible reason is the fact that, during the movement of the mortar, it may crumble at the interface. These mortar "crumbles" fill the voids at the interface and an additional friction is created. This statement is substantiated by the hand demolition since the virgin Vaseline treated specimen showed the best demolition potential.

Environmental impact assessment

This chapter aims to measure the impact of the developed reusable connection. To do so, an environmental impact assessment is performed and subsequently, the environmental costs are calculated for the reusable and conventional connection. The chapter is divided into three sections. The first section provides a description of the method. This is followed by a section where the assessment is performed. Finally, a section is dedicated to the interpretation of the results. The steps mentioned above are performed for the following alternatives:

- Reusable connection - circular building process,
- Conventional construction technique - linear building process.

9.1. Method

To make an environmental impact assessment, various steps are taken. In [Figure 9.1](#) a schematic representation of the procedure is shown.

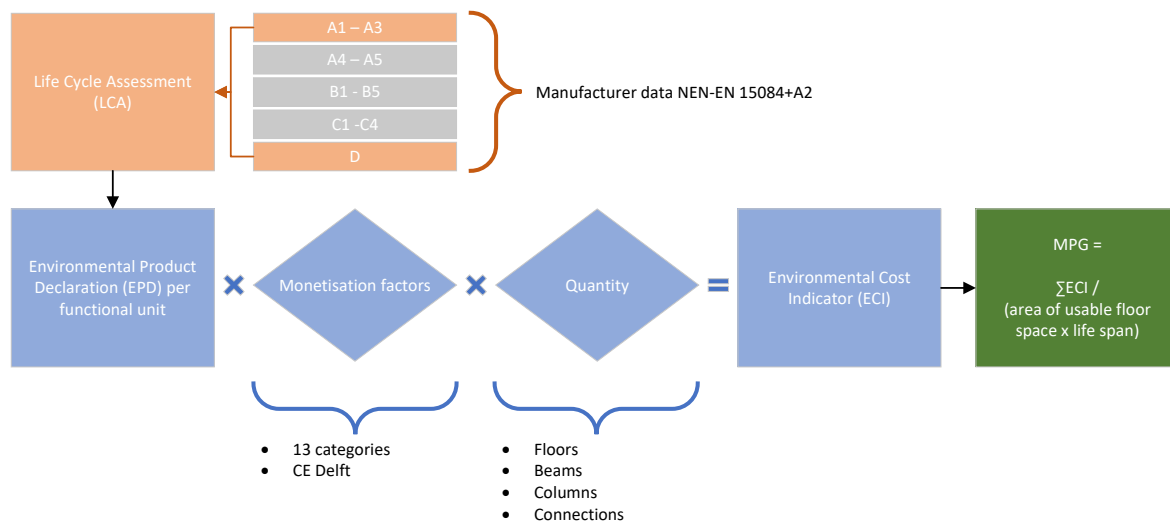


Figure 9.1: Environmental impact assessment, step by step

The structure of the environmental impact assessment starts with the Life Cycle Assessments (LCA). These LCA's are conducted for all components of the connection and load bearing structure. These assessments are material-specific and are performed by the manufacturers of the components. The result of the LCA is summarised in an Environmental Product Declaration (EPD). The EPD provides information on environmental performance in different categories for all stages of the life cycle, as

indicated in [Figure 9.2](#). In addition to the raw data, all assumptions made in the LCA are presented in the EPD. These descriptions clarify the background of the data and are important to consider during the assessment. The EPD's can vary based on the assumptions made within the LCA calculations. For example, the EPD of construction steel is highly dependent on the amount of reclaimed steel used in the process. High percentages of reclaimed steel reduce the EPD score and result in better environmental performance. This results in the fact that EPD's from certain manufacturers score significantly better. Therefore, the EPD's are selected with great care, and good consideration to choose one or another should be made. After representative EPD's are found the values are weighted by 13 monetisation factors and multiplied by the total quantity. For all the EPD's a functional unit is provided and the quantities of the connection and structure are expressed in the same unit. The result of these multiplications is an Environmental Cost Indicator (ECI). This value represents the total environmental costs of the building. These costs are seen as the "shadow" costs of the building and monetises the environmental burden on society. Since the main goal of the reusable connection design is the increased lifespan, an MPG is made. An MPG, Dutch for MilieuPrestatie Gebouwen, is a scoring mechanism for the environmental performance of buildings in the Netherlands. This MPG divides the environmental cost indicator (ECI) by the usable floor space multiplied by the constructions life expectancy. The major advantage of this methodology is that the life span of the building is taken into account. For the conventional construction technique, the average design life of buildings in the Netherlands is adopted, while for reusable construction, the element life span of 100 years is used.

$$\text{MPG} = \frac{\text{ECI}}{\text{usable floor area [m}^2\text{]} \times \text{life span [yrs]}} \quad (9.1)$$

9.2. Goal and scope

The goal and scope describe the purpose of the environmental impact assessment and provide the boundaries and limitations of the assessment.

9.2.1. Goal

The objective of the environmental impact assessment is to provide a deeper understanding of the effect of different construction techniques in terms of environmental costs. By underpinning the potential of the reusable connection and showing the added value of the connection, decision makers could be convinced to stimulate reusable design. The additional costs of the connection and the increase in engineering work in the initial phase could potentially be compensated for by the longer life span of the elements and the improved residual value. With the help of the environmental assessment, this statement is verified.

9.2.2. Scope

The scope provides the boundaries of the life cycle assessment. Limits are set in terms of the stages analysed, the type of data used, and the level of detail.

Life Cycle Assessment stages

The various life cycle stages are presented in [Figure 9.2](#). The analysis only includes the product stage, indicated by A1 to A3 or by the Cradle-to-gate definition. The product stage includes the extraction of raw materials (A1), transport to the manufacturing site (A2), and the manufacturing process (A3). The construction stage (A4-A5), the use stage (B1-B5), and the end-of-life stage (C1-C4) are excluded from the calculation for several reasons. The construction stage was excluded since transport to the construction site (A4) is a project-specific parameter and since connections are a small share of the total transport. Resulting in the impact difference between the various connections is expected to be low. The installation stage (A5) is expected to be fairly similar for all connections and therefore will not make a significant impact difference between the alternatives. The use stage (B) of the structure is independent of the type of connection and is excluded from the analysis. The end of life stage (C) does create an impact difference, the deconstruction and demolition (C1) process is different due to the reusable design of the connection compared to the conventional connection. In addition to the demolition and deconstruction (C1), the other stages of phase C differ and are expected to be beneficial for the reusable connection. However, due to time limitations, it was decided that the end of life stage

is not included in the analysis. A significant factor that underpins this decision is the fact that, in general, between 70% and 90% of the total carbon emissions occur during the product stage. This reduces the effect of neglecting the end of life stage on the total analysis. Special attention should be paid to the reuse stage. In this stage, the potential for reuse, recovery, and recycling is evaluated. These assessments often show a positive environmental impact due to reclaimed materials that do not need to be manufactured. However, the assumptions made in this phase play a determining and sometimes unrealistic role. Concrete, for example, can be deconstructed in theory at the component level. This would result in the fact that raw materials such as cement, aggregate, and additives are reclaimed. However, in practice, this operation is expensive and most concrete is downcycled into concrete rubble. The positive impact of using concrete as rubble instead of on a material level is significantly smaller. Therefore, this stage should be critically assessed and the result of the analysis is presented with and without stage D taken into account.

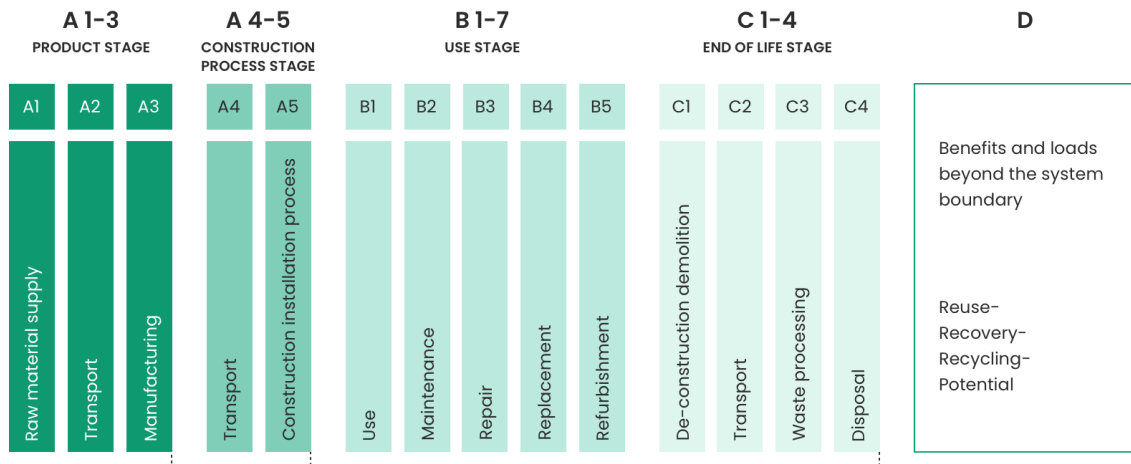


Figure 9.2: LCA stages [64]

EPD data

The ECI values are computed based on data generated using the NEN-EN 15804+A2 standard [33]. This design guide is the updated version of the NEN-EN 15804+A1 [26] and shows significant differences on the Environmental Product Declaration (EPD) level. The number of impact categories has changed, as well as the equivalent units associated with the categories. This results in the fact that the A1 and A2 data is not interchangeable. The A2 standard is mandatory since July 2022 and is used for the analysis. The downside of the A2 data is that the current database with components and materials is small.

Level of detail

The comparison of the connection in terms of environmental impact is interesting; however, direct comparison of the results do not provide any significance in the bigger picture. To overcome this, the main load bearing structure is included in the analysis. The quantities of the case study building (Appendix B) are extracted from the model with the help of Solibri¹. The exclusion of the pile foundation and concrete strips is due to their inability to be reused in both the conventional and reusable designs. As a result, only the following components are used for the analysis:

- Floor slabs,
- Roof slabs,
- Columns,
- Beams,
- Beam-to-column connections,
- Hollow core slab connection.

¹Building Information Modelling (BIM) software for quality assurance and control.

The level of detail in the case study is insufficient to determine the weight of the beam-to-column connections. Therefore, it was assumed that the weight of the connection is equivalent to 7.5% of the total mass of the steel structure.

9.3. Impact assessment

The assessment involved comparing several EPD's and selecting the most suitable one. All EPD's are of type A2 and are selected to match as closely as possible to the actual product/ material of the connection. However, due to the regulations that state that an EPD has a validity of five years, the database with A2 data was limited. Many fabricators made an A1 EPD just before the deadline, since the LCA result for A1 assessments is generally less strict compared to the updated A2 assessment. This resulted in the fact that the EPD data used for the assessment consist of products manufactured throughout Europe.

To start collecting EPD data the materials and products of the main load bearing structure and the connections are inventoried. For the load bearing structure, the materials and quantities are extracted from the 3D model of the case study building. In [Table 9.1](#) the result is shown in tabular form. Besides this result the EPD used for the assessment is shown with the manufacturer and production location included. For verification purposes, the EPDs can be viewed by following the hyperlink in the bibliography.

Table 9.1: Materials and quantities for the main load bearing structure of the case study building as presented in [Appendix B](#), the substructure was excluded

Element	Quantity	Unit	EPD	Manufacturer	Location
Hollow core slab - ground floor	1929	m2			
Hollow core slab - 1st floor	1838	m2	[53]	INHUS Prefab	Lithuania
Hollow core slab - roof floor	1916	m2			
Beam - I and H sections	91.6	tonne	[9]	BE Group	Sweden
Beam - hollow section	3.5	tonne	[85]	Tata steel	Netherlands, United Kingdom
Columns - hollow section	22.4	tonne			
Beam-to-column connections	8.8 ²	tonne	[83]	Stalia AB	Germany, Denmark

9.3.1. Demountable shear connector connection

For the reusable connection the material and quantities of the reusable connection are based on the final verified design made in [chapter 6](#) and [chapter 7](#). Before it was mentioned that all EPD's are based on materials and products produced in Europe. An exception was made for the bolts since there was no EPD available and the closest related product found in the database was used. However, this item is manufactured in Chile. In [Table 9.2](#) the result of the inventarisatation is shown per connector. One hollow core slab is made with the help of four connectors.

²Connection weight assumed to be 7.5 % of the total steel structure mass

Table 9.2: Materials and quantities for a reusable hollow core slab to beam connection, values per connector

Element	Quantity	Unit	EPD	Manufacturer	Location
SHS section	1.98	kg	[85]	Tata steel	Netherlands, United Kingdom
Mortar	2.89	kg	[80]	Sika	-
Reinforcement bar	0.85	kg	[17]	Celsa Steel Service ES	Spain
Bolt assembly	0.48	kg	[37]	Compañía Siderúrgica Huachipato	Chile
Top plate	0.40	kg	[83]	Stalia AB	Germany, Denmark
Sleeve concrete	30.81	kg	[45]	Fedbeton	Belgium

The environmental costs per individual connector are calculated on the basis of the quantities and materials presented above. To do so, several weighting factors monetise the impact categories. These weighting factors are currently still considered as a draft but the prices proposed by CE Delft are presented in [Appendix H](#). The previous prices used for the A1 calculations cannot be adopted since new impact categories are introduced for the A2 calculations as well as the measured units. The result of the multiplication of impact categories by weighting factor is a total ECI price per declared functional unit. For the analysis, the combined price of LCA stages A1 to A3 is presented and separately for stage D the ECI price is given. In [Table 9.3](#) the result of the final ECI price for the demountable connection is shown. The prices in brackets indicate an ECI profit instead of an ECI burden.

Table 9.3: Environmental Cost Indicator calculation for the demountable shear connector connection per individual connector

Element	Quantity [kg]	Quantity [eq. unit]	Eq. unit	A1-A3		D	
				ECI [€/unit]	ECI [€]	ECI [€/unit]	ECI [€]
SHS section	1.98	0.0020	tonne	€ 333.96	€ 0.66	€ (220.83)	€ (0.44)
Mortar	2.89	3.27	kg	€ 0.08	€ 0.28	€ (0.00)	€ (0.01)
Reinforcement	0.85	0.00085	tonne	€ 67.91	€ 0.06	€ 0.62	€ 0.00
Bolt assembly	0.48	0.48	kg	€ 0.52	€ 0.25	€ -	€ -
Top plate	0.40	0.00040	tonne	€ 314.31	€ 0.13	€ (142.68)	€ (0.06)
Sleeve filling	30.81	0.013	m3	€ 25.04	€ 0.31	€ (1.27)	€ (0.02)
				€ 1.68		€ (0.53)	

As a result, the product stage has a price of €1.68. During stage D some of this environmental burden is recovered. The reason for this is mainly the steel that is recycled and used for the production of new steel. If stage D is taken into account, the result would be a price of €1.15 per connector. However, this reduction in stage D does not consider the removal work in the slab, as this was not declared in the EPD. In the EPD of the SHS section stage D assumes that 7% is directly reused and 92% is recycled. The reuse stage is unrealistic for the specified application, and therefore stage D will not be taken into account for the reusable connection.

9.3.2. Conventional connection

The conventional connection consists only of a reinforcement bar and sleeve concrete. The EPD's for these components are similar to the ones used in the reusable connection. For the quantities slight differences occur, the amount of concrete is substantially larger due to the fact that also the void between the beam and the hollow core slab is filled. Additionally, the reinforcement bar is slightly longer since it still needs the bond length but also has to cover the area from the beam web until the start of the hollow core slab. The outcome of the inventory is presented in [Table 9.4](#).

Table 9.4: Materials and quantities for a conventional hollow core slab to beam connection, values per connector

Element	Quantity	Unit	EPD	Manufacturer	Location
Reinforcement bar	1.07	kg	[17]	Celsa Steel Service ES	Spain
Sleeve concrete	82.41	kg	[45]	Fedbeton	Belgium

For the cost calculation per connector, a similar procedure is applied as used for the reusable connection.

Table 9.5: Environmental Cost Indicator calculation for conventional connection per individual connector

Element	Quantity [kg]	Quantity [eq. unit]	Eq. unit	A1-A3		D	
				ECI [€/unit]	ECI [€]	ECI [€/unit]	ECI [€]
Reinforcement	1.07	0.00081	tonne	€ 70.07	€ 0.08	€ 0.62	€ 0.00
Sleeve filling	82.41	0.028	m ³	€ 25.04	€ 0.84	€ (1.27)	€ (0.04)
				€ 0.92			€ (0.04)

As expected, the ECI value of the connection is significantly lower. The total connection costs €0.92 per individual connector, which is around 55% of the reusable connector. The price difference becomes smaller when stage D is considered. The environmental "profit" of having these components is smaller. The energy used to recover reinforcement for recycling is equal to the amount of energy saved by not mining new materials and results in a value of approximately zero. Stage D of the concrete assumes that 95% of the concrete is downcycled to rubble and 5% is scrapped. This results in a small profit within stage D. When considering stages A1 to A3 and stage D, the ECI per connector is equal to € 0.88 or around 52% of the reusable connection connector ECI.

9.3.3. Structure

To calculate the total ECI and MPG value for the building, the number of connections is determined. The width of the structure measures 62.4 metres, equivalent to a total of 52 hollow core slabs (1.2 m per slab). Along the transverse direction of the case study building, 3 spans are present resulting in 156 slabs. Each of the hollow core slabs is connected with two connectors per side so in total 624 connection per building layer. These layers only comprise the first floor and the roof, as the connections on the ground floor are unnecessary due to the presence of stiff concrete strip foundations.

Table 9.6: ECI calculation for stage A1 to A3 for the main load bearing structure including connections and excluding substructure

Element	Qty	Unit	Reusable Design		Conventional Design	
			ECI / unit	ECI	ECI / unit	ECI
Hollow core slab ground floor	1929	[m ²]	€ 7.94	€ 15,326.50	€ 7.94	€ 15,326.50
Hollow core slab first floor	1838	[m ²]	€ 7.94	€ 14,601.92	€ 7.94	€ 14,601.92
Connection first floor	624	[piece]	€ 1.68	€ 1,050.58	€ 0.92	€ 572.63
Beams - I and H sections	91.6	[tonne]	€ 188.51	€ 17,259.16	€ 188.51	€ 17,259.16
Beams - hollow sections	3.5	[tonne]	€ 333.96	€ 1,155.93	€ 333.96	€ 1,155.93
Columns - hollow sections	22.4	[tonne]	€ 333.96	€ 7,475.30	€ 333.96	€ 7,475.30
Beam-to-column connections	8.8	[tonne]	€ 314.31	€ 2,767.49	€ 314.31	€ 2,767.49
Hollow core slab roof	1916	[m ²]	€ 7.94	€ 15,222.05	€ 7.94	€ 15,222.05
Connection roof	624	[piece]	€ 1.68	€ 1,050.58	€ 0.92	€ 572.63
				€ 75,909.49	€ 74,953.60	

Table 9.7: ECI calculation for stage **A1 to A3 + stage D** for the main load bearing structure including connections and excluding substructure

Element	Qty	unit	Reusable Design		Conventional Design	
			ECI / unit	ECI	ECI / unit	ECI
Hollow core slab ground floor	1929	[m2]	€ 7.61	€ 14,691.39	€ 7.61	€ 14,691.39
Hollow core slab first floor	1838	[m2]	€ 7.61	€ 13,996.83	€ 7.61	€ 13,996.83
Connection first floor	624	[piece]	€ 1.68	€ 1050.58	€ 0.88	€ 549.12
Beams - I and H sections	91.6	[tonne]	€ 178.43	€ 16,336.16	€ 178.43	€ 16,336.16
Beams - hollow sections	3.5	[tonne]	€ 113.13	€ 391.57	€ 113.13	€ 391.57
Columns - hollow sections	22.4	[tonne]	€ 113.13	€ 2,532.23	€ 113.13	€ 2,532.23
Beam-to-column connections	8.8	[tonne]	€ 171.63	€ 1,511.18	€ 171.63	€ 1,511.18
Hollow core slab roof	1916	[m2]	€ 7.61	€ 14,591.26	€ 7.61	€ 14,591.26
Connection roof	624	[piece]	€ 1.68	€ 1050.58	€ 0.88	€ 549.12
				€ 66,151.78	€ 65,148.87	

From the calculations of the Environmental Cost Indicator in [Table 9.6](#) and [Table 9.7](#) the differences between the reusable and conventional designs in terms of environmental costs are calculated. Two scenarios are considered; the first scenario only takes into account stages A1 to A3, whereas the second scenario also takes into account stage D. For stage D the reusable connection is excluded since the complicated design makes reusing or recycling hardly impossible and therefore the scenarios presented in the EPD are not representative for these components. The result shows that the reusable design has an additional impact on the environment of €955.89. In [Table 9.8](#) the percentage representing the connection between the beam and the hollow core slab is shown in terms of the ECI value on the total.

Table 9.8: Share of the beam to hollow core slab connection ECI in the total superstructure ECI

	Reusable design	Conventional design
Stage A1 - A3	2.77%	1.53%
Stage A1 - A3 + D	3.18%	1.69%

To investigate the effect of the reusable versus the conventional connection, multiple design life scenarios are analysed.

- Building lifespan 20 years,
- Building lifespan 50 years (design life),
- Building lifespan 100 years (structural element lifespan).

The ECI costs for the three scenarios are presented in [Figure 9.3](#) with a horizontal time axis of 100 years. On the vertical axis the ECI costs are presented. The initial ECI value for all conventional alternatives is €74,953.60 euros and for the reusable €75,909.49. For the conventional construction, the ECI value increases when the associated lifespan is reached and creates a step-like line. The increments after the initial step are slightly lower and equal to €65,148.87 since the old building is assumed to be demolished and recycled in stage D. For reusable designs, an almost horizontal line is presented. At the end of every lifespan scenario, a small increase in ECI costs is expected for stage A1 to A3. The mortar and bolts are replaced, resulting in an ECI of €651.92 for all the 1248 connectors in the case study building. In [Figure 9.4](#) a zoomed-in perspective of [Figure 9.3](#) is provided, this more detailed view shows the small ECI cost increments for the reusable construction. The conventional construction ECI costs are also presented, but due to the bounded y-axis range the steps for 20 and 50 years lifespan are not visible since the costs are exceeding the boundaries.

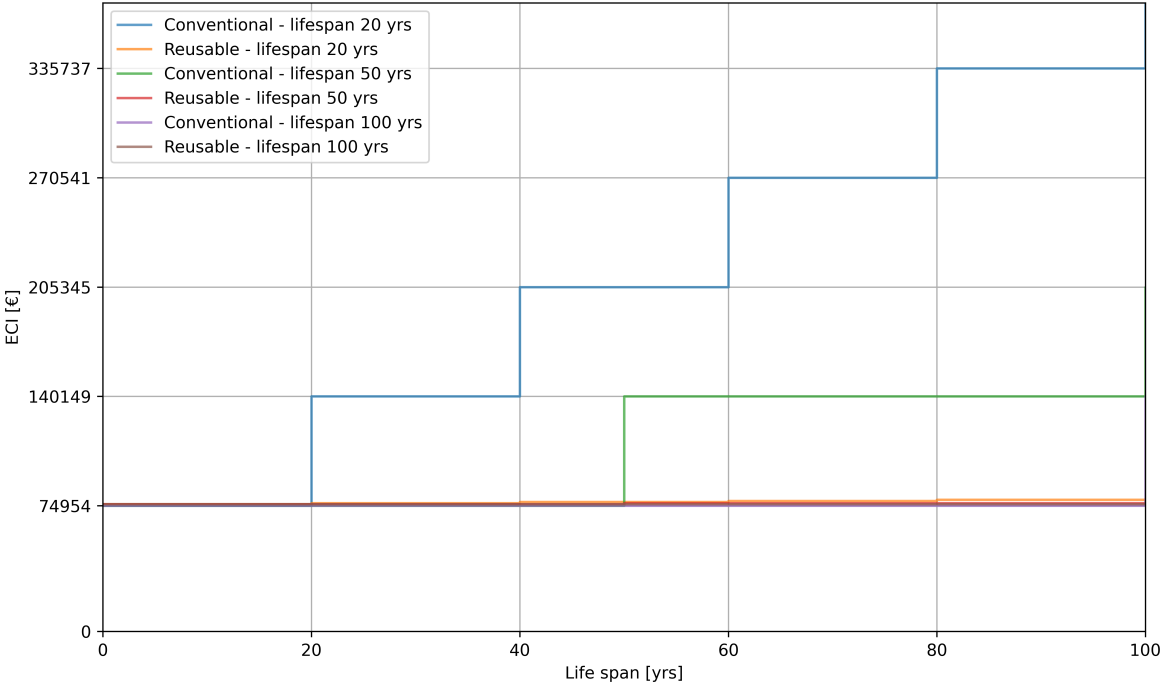


Figure 9.3: Environmental Cost Indicator for three lifespan scenarios, 20, 50, and 100 years for reusable and conventional design with LCA stages A1-A3 + (D)

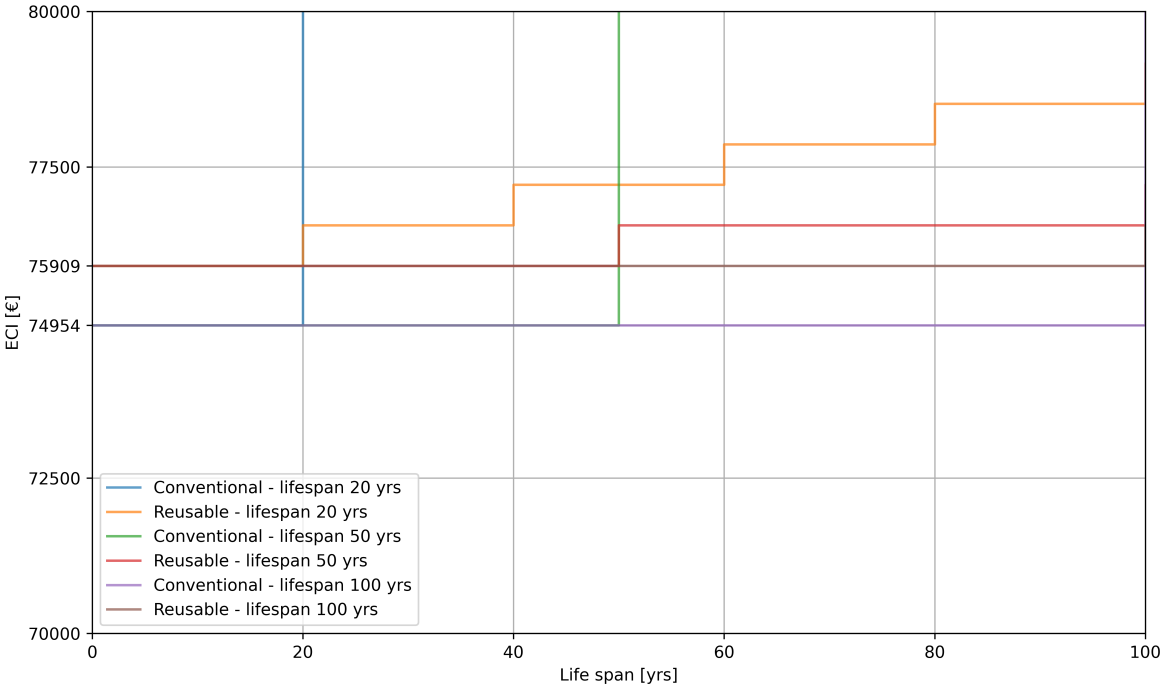


Figure 9.4: Close up of the Environmental Cost Indicator for three lifespan scenarios, 20, 50, and 100 years for reusable and conventional design with LCA stages A1-A3 + (D)

9.3.4. MPG

From the ECI values, the MPG of the building superstructure is calculated. The MPG is, as mentioned above, dependent on the usable floor space and the lifespan of the building and are calculated by [Equation 9.1](#). The first of the two variables is identical for both calculations with a total usable floor space of 3663 m². This area is calculated by the summation of the ground floor area and the first floor area and subtracting all the areas reserved for openings and technical installations as presented in the drawings of [Appendix B](#). The latter point, which addresses the life span, gives different results based on the type of connection. According to NEN-EN 1990 [\[29\]](#) the design life of buildings is equal to 50 years. However, there can be a discrepancy between the design, functional, economical, and technical life span.

Functional life span

The functional life span is the time the building performs as designed. After a certain time, the building can be modernised and the functional lifespan of the building is extended. This can be done multiple times until the economical or technical life span is reached. The economic life span is dependent on many factors and can easily be influenced by political decisions. In the current political climate, the environmental costs become more and more important. This can result in the fact that modernising the current assets is beneficial compared to the demolition of existing assets and creating new real estate. As a simplification, the average building life is adopted for the economical life span. In the Netherlands, the average office building has an economical life of 70 years [\[93\]](#).

Technical life span

The technical life span of a building could be reviewed on component level. The hollow core slabs made of concrete are intended to have a design life of at least 100 years. Concrete only gets stronger over time and environmental influences are the main cause of problems. Since the application of the concrete is in an enclosed environment the technical life span of the slabs might be substantially longer. For the steel parts the recently introduced NTA 8713 [\[60\]](#) shows how to deal with the reuse of steel parts. In the design guide it is stated that if the quality of the steel is tested full capacity of the section may be assumed. Since the steel parts are protected from the environment no significant damage is expected. In addition, the design of the structure can be made such that yielding of the steel is not reached and fatigue is unlikely to play an important role in the building design. If the two above points are combined it could be concluded that the building has an infinite technical life span. On the other hand, the economical life span was just argued to be equal to 70 years. This implies that to reach the technical life span at minimum one reuse cycle is needed. For a reuse cycle the building is demounted and installed after a certain period of time. During the demounting and installation process the elements of the construction could be damaged which might result in an reduced life span of the elements. According to Brand [\[13\]](#) the structural elements have a lifespan between 30 and 300 years.

Calculation

The results of the MPG calculations are shown in [Figure 9.5](#) and [Figure 9.6](#). The first graph indicates the superstructures MPG for a life span of maximum 70 years. Resulting in slightly lower results for the conventional connection compared to the reusable. The differences are small and decreasing for increased life spans. For the analysis considering stage A1 to A3 at 50 years the results are 0.414 and 0.409 for the reusable and conventional alternatives, respectively. At 70 years life span the results are 0.296 and 0.292. Considering stage D in the analysis makes the differences even smaller, with 0.358 and 0.356 for 50 years and 0.255 and 0.254 for 70 years.

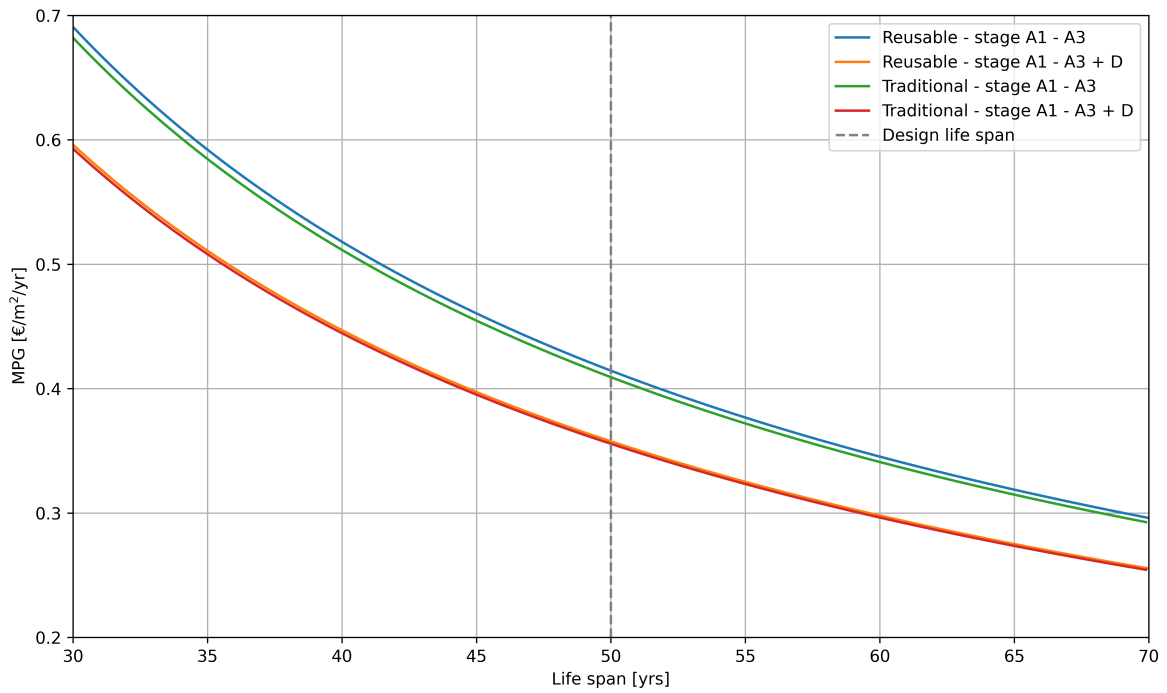


Figure 9.5: MPG calculation for the superstructure for a life span of 30 to 70 years

Looking at the MPG calculation with the time scale for the structural elements provided by Brand in Figure 9.6 you can clearly see that the MPG drops even further. The MPG lines for the conventional connection are discontinued since their economical and technical life span is reached. Due to the small difference between the reusable and conventional design, the lines are almost overlapping, and clear distinction of the lines in the initial phase of the graph is hardly possible.

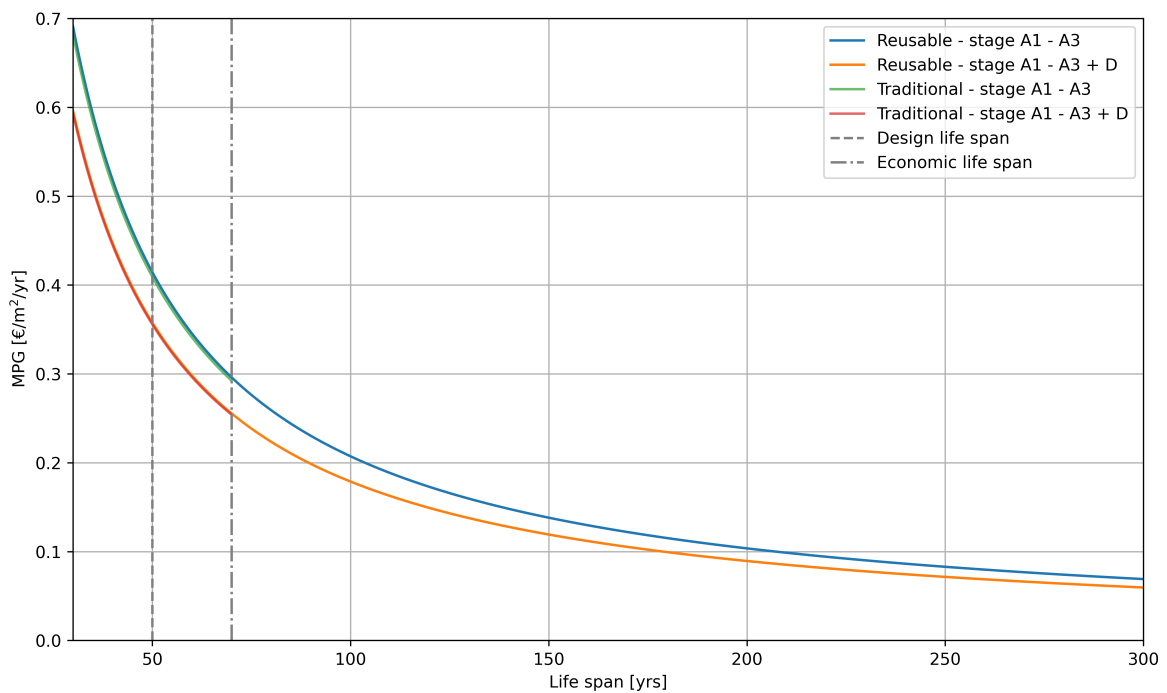


Figure 9.6: MPG calculation for the superstructure for a life span of 30 to 300 years

9.4. Interpretation

The environmental impact assessment shows that the application of reusable connections has hardly an effect on the environmental impact of the structure. For these calculations only the superstructure was reviewed but for the situation where a full building is analysed the share in terms of environmental impact for the hollow core slab to beam connections almost equals zero.

For the comparison of ECI with different building life expectancies, the environmental impact of the reusable connection becomes clear. Although the calculation is a simplification since not all lifecycle stages are considered, it provides a good indication of the positive environmental impact of the reusable connection compared to a conventional connection construction. The number of times a building is reused increases the advantage of using reusable construction, generally speaking. However, the ECI associated with the conventional alternative is seen as conservative. A scenario in which conventional connections are created and the slabs are removed by sawing after the lifespan is reached would result in a significantly lower ECI value. This technique accounts for the partial reuse of the components and an improved score in stage D.

From the MPG data, clear asymptotic behaviour is observed. This results in the fact that increased life spans mainly affect the MPG in the first years. The difference in MPG between 100 and 150 years of life span is significantly smaller than the difference between 50 and 100 years. However, an increased life span can still be considered beneficial, as the MPG value will only drop further. In conclusion, the additional environmental impact created by the reusable design is compensated for by the longer potential life span of the structure.

Part IV

Research outcome

10

Discussion

This chapter focusses on the interpretation, implications, and limitations of the research outcome. Throughout the design and verification process, several assumptions and simplifications were made. The potential impact of these on the research outcome is addressed in different sections of the discussion.

The aim of this research is to develop a new reusable connection between a hollow core slab and a steel frame to increase the lifespan of the structural components and reduce environmental impact. The research comprises the design process and verifications of the structural behaviour. The design process was supported by a Monte Carlo simulation that investigates the tolerances required in the reusable connection. Furthermore, small-scale experiments were performed that demonstrate the separation potential of steel square hollow sections and mortar. Finally, the environmental impact of the reusable connection was assessed and compared to its non-reusable counterpart.

10.1. Interpretation

The result of the research shows that a reusable connection is a viable option compared to the conventional non-reusable connection. In this section, an explanation and interpretation of the key findings are provided.

Tolerances

Statistical analysis on building tolerances showed that to ensure easy installation and consequent service life of the elements, a significant amount of tolerances are required. This statement was confirmed by industry experts from cepezed bouwteam¹, who pointed out that tolerance-related problems often occur even during initial construction. The results of the tolerance study showed that the building method has a strong influence on the level of tolerances that must be accommodated in the design. The installation procedure on-site requires smaller tolerances compared to the fully prefabricated alternative, as only the tolerances in the structural grid are accounted for. The prefabricated method accounts for significantly more types of tolerances, which logically results in a larger overall required tolerance. One of the benefits of this larger tolerance is that it increases the speed of erection. Furthermore, the implementation of additional tolerances makes the structural elements more valuable. With a prefabricated design approach, elements can be reused at the component level rather than being reused on the building level. This makes them more adaptable and creates greater reuse potential since the newly designed building can be adopted to the needs of the new building owner. Generally speaking, a larger tolerance accountability has solely positive effects on the reusability while simultaneously increasing the speed of erection.

¹A project management firm.

Connection design and trade-off analysis

The result of the design part showed that there are various feasible options for the connection between the hollow core slab and the steel frame. From the requirements, it became evident that an integrated beam is considered the preferred option over under-mount floor beams in reusable connections. The main reason for this is the improved adaptability of building systems such as wiring, heating, ventilation, and air conditioning. For the successful implementation of reusable connections, the economic requirements are considered the most critical. Therefore, the initial scope bounded the research to a relatively inexpensive construction method, making the reusable design easier to apply for various situations and not only prestige projects. These prestige projects have an additional dedicated budget and a specific vision to create a reusable structure. All designed connections are feasible in terms of structural behaviour. However, the major design requirement is the economic aspect, and on this basis, it was determined to further investigate the demountability potential of the bolted shear connector alternative. This alternative outperformed the others mainly in cost, while the demountability potential scored the lowest. To assess the demountability potential, small-scale experiments were performed.

Experiments on demountability

The results of small-scale experiments on demountability showed a clear trend. The pre-treatment of the specimens increased the demountability potential compared to that of the untreated ones. However, the results showed resistance ranging from approximately 10 ~ 20 kN for the treated specimens. The magnitude of the data was obtained by the experiments performed using the load cell, but manual demolition showed similar results. On the basis of these results, it was proven that the frictional resistance that originated from imperfections and eccentric loading conditions can be overcome when pre-treatment is applied. This shows the feasibility of the demountable bolted shear connector connection.

Environmental impact assessment

Results from the environmental impact assessment showed that the effect of a reusable connection between hollow core slabs and integrated beams compared to a non-reusable alternative is negligible. The Environmental Cost Indicator showed a marginal difference between the reusable and non-reusable alternative when stages A1 to A3 of the Life Cycle Assessment were considered. These stages, also called cradle-to-gate analysis, only assess the product stage of the materials. When considering a multi-lifespan scenario the reusable connection shows its potential. The ECI value for conventional designs shows a step-like behaviour with an additional ECI almost equal to the initial ECI for every reuse cycle. The reusable connection shows a marginal increase in ECI for every reuse cycle, this marginal increase evolves from the application of new bolts and mortar. To make the comparison more realistic, the environmental costs of the analysed building elements are divided by life expectancy. This comparison shows the full potential of the reusable design, as the technical lifetime of the structural elements can be reached. Then, the reusable design generates a higher residual value for the components when compared to the non-reusable alternative, which offsets the additional investment costs.

10.2. Implications

This study was carried out with the vision of developing a reusable connection between hollow core slabs and steel frames. The objective of the research was to reduce the use of primary resources and the associated CO₂ emissions by implementing reusable connections in a well-known construction technique. This thesis contributes to the vision in several ways. First, the result of the research showed that it is technically feasible to create a reusable connection between hollow core slabs and steel frames. The Monte Carlo simulation analyses various scenarios and provides data on combined tolerances from different sources. The simulation can be adopted to certain geometries and can predict tolerance magnitudes for other constructions. For example, the analysed connection of the Temporary Courthouse which was described in the state-of-the-art currently has insufficient tolerances. At the current stage, the building is deconstructed, but the building will be reassembled in the foreseeable future. Based on the data generated by the Monte Carlo simulation for installation on site, the current connection can be adjusted by oversizing the bolt holes to the injected variant presented in the design part ([subsection 4.3.1](#)) of the report. Second, the research outcome supports the application of reusable structures by underpinning the result that small additional investments upfront can lead to a substantial improvement in the environmental performance of a building. This finding can help convince project developers, building

owners, and (semi-)governmental organisations to implement reusable connections in their real-estate. The results of this study show that the additional components used for the connection marginally affect the environmental performance of the superstructure. When the entire building would be assessed, this impact is negligible, while the reusable connection matches or outperforms the non-reusable connection for all situations conceivable. Lastly, the results of the experiments on the demountability of steel and mortar show the potential for the application of wet connections in demountable or reusable structures. The separation potential of a steel section and mortar in combination with a pre-treatment can have various applications. In conclusion, the outcome of this research can be implemented in future buildings consisting of hollow core slabs and steel frames. Additionally, direct application of the tolerance results is possible in the Temporary Courthouse case.

10.3. Limitations

The limitations of the research touch on different parts of the study. In this section, the various limitations in the tolerance study, case study geometry, qualitative trade-off analysis, demountability experiments, and environmental impact assessment are addressed.

10.3.1. Tolerance study

The tolerance study reviewed several situations based on data from European Standards, data from the literature, and input from experts. Unfortunately, limited data was available for some specific elements, such as tolerances in the location of the shear connector. Therefore, data from the American Concrete Industry standard for anchor bolts were implemented in the design. These data prescribed significant tolerances ranging from 1/4 in (6.4 mm) to 1/2 in (12.7 mm). This is significant compared to the bolt hole location, which requires a tolerance of 2, 1 or 0.1 mm (manufacturer data) and can potentially be smaller in practice. Eventually, the geometry of the connection used in the final design differs from the geometry analysed in the tolerance study. The expected influence of this different connection on the required level of tolerances is minimal. The tolerance in the DEMU placement, which was analysed in the tolerance study, is expected to be similar to the positioning tolerance of the square hollow section. Additionally, during the design process, the decision was made to implement more tolerances than the required norm since this was easy to accommodate in the demountable bolted shear connector alternative.

For the Monte Carlo simulation, it was assumed that the tolerance data provided in the European Standard has a normal distribution and a 95% confidence interval (CI). To see the effect of the assumed confidence interval, two additional simulations have been performed. The first is for the situation where the European Standard tolerance data are based on a confidence interval of 90% and the second on a confidence interval of 99%. In [Figure 10.1](#) the results of the different confidence intervals are shown. In the situation where the input variables have a lower confidence interval ([Figure 10.1a](#)) the required tolerance level increases, while the effect of the larger 99% confidence interval ([Figure 10.1c](#)) is the opposite. For the upper limit of the tolerance confidence interval, denoted by the 95% CI line in the three different graphs, the values differ by +15.5% and -17.7% compared to the results used in the report for the 90% CI and 99% CI, respectively.

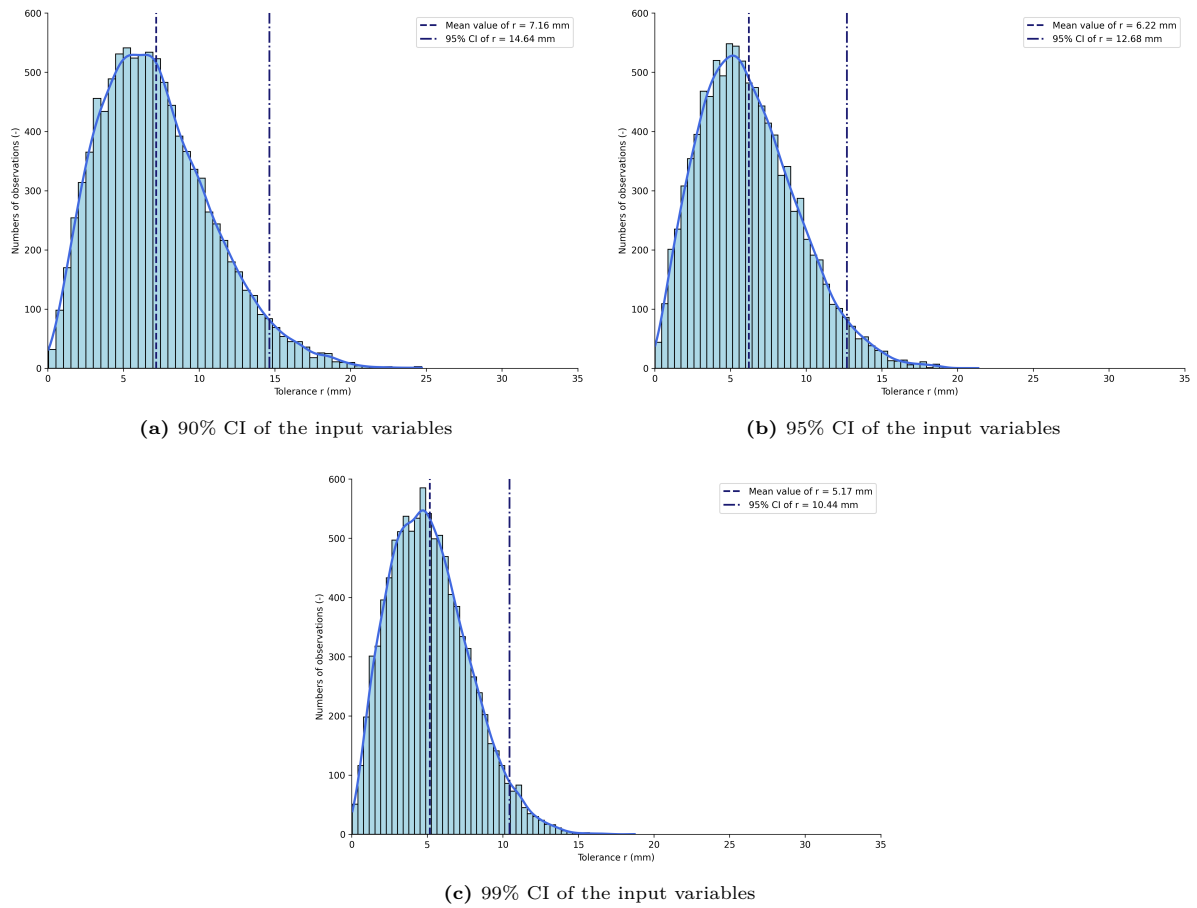


Figure 10.1: Monte Carlo simulation with $N = 10^4$ simulations based on literature and manufacturer data (simulation 3) for a prefabricated situation with different confidence intervals (CI) of 90%, 95%, and 99% for the input variables

Another factor that could affect the outcome of the experiments is the number of simulations. To keep the computational time low, the number of simulations was set at $N = 10^4$. According to the theory, increasing the number of simulations gives more accurate results. Therefore, the effect of increasing the number of simulations was checked for one of the situations. The result of an increasing number of simulations is shown in Figure 10.2. From these two graphs, it is observed that the effect of the increment in number of simulations is minimal. The mean value differs with 0.02 mm and the 95% CI value with 0.04 mm, these differences do not limit the results obtained by the tolerance study.

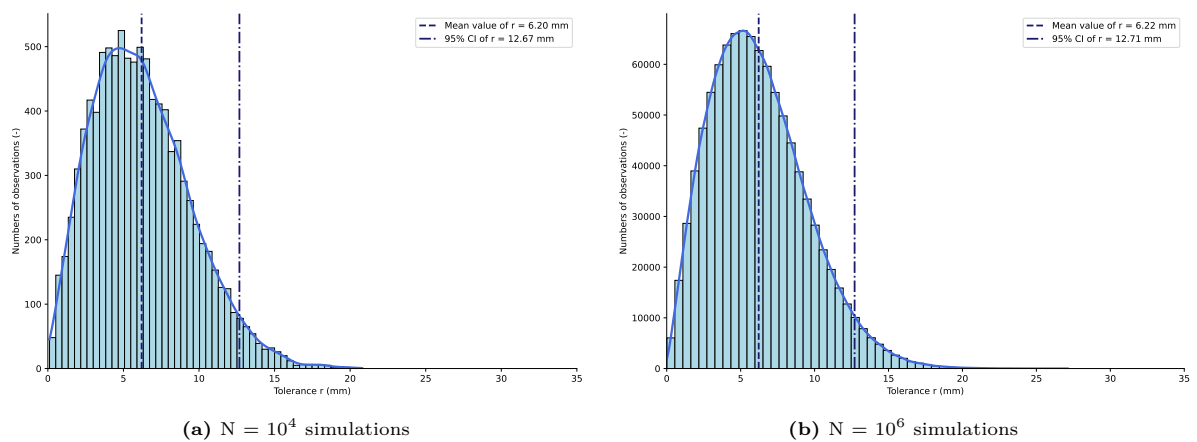


Figure 10.2: Monte Carlo simulation based on literature and manufacturer data (simulation 3) for a prefabricated situation with different number of simulations

10.3.2. Case study

The geometry of the case study presented in [Appendix B](#) plays an important role throughout the research. The effect of changing the geometry could influence several factors, such as tolerances and loading conditions. The effect on the first point, the tolerances, lies in the fact that the tolerances in the structural grid are geometry dependent. The influence of geometry on beam spacing is expected to be minimal, as the European Standards provides a fixed value for the maximum spacing between beams. However, the spacing of the columns is based on the length of the beams in between. For increased beam lengths, the tolerance demand increases linearly. Increased beam lengths also come with an increase in the maximum beam out-of-straightness. For the case study, the out-of-straightness was determined to be non-critical, and the most critical situation was at the columns. For longer beams, this critical section may shift.

The loading conditions and the most critical loaded beams are determined based on the geometry of the case study. An increase in the length of the hollow core slab results in additional load on the beam. On the other hand, the current hollow core slab is designed based on its maximum span, and increasing the length of the slab would require a thicker slab and increased dimensions of the steel beam section. Associated with this increase in dimensions is a larger internal lever arm, and the loads between the beam and the slab are expected to have a similar magnitude. Nevertheless, if the building has a different geometry, it is necessary to verify the connection using the steps outlined in the verification section.

10.3.3. Trade-off analysis

Another limitation of the research is the weighting of the alternatives. Since all reusable connections presented were feasible in terms of structural behaviour, the qualitative trade-off analysis focused mainly on the costs associated with the design. The actual costs of the components could be verified quantitatively as prices were requested from various suppliers. A limitation of cost analysis, in general, is that they are susceptible to high variability and influenced by external influences. The cost assessment of the installation and demountability procedure was carried out mainly on a qualitative basis and was supported by the quantitative data. The data were verified with a cost expert from Multicall². However, the costs associated with certain steps involved in the reusable connection design process can differ between contractors. Different contractors have different qualities, and also the availability of resources in terms of equipment and manpower plays an important role. In conclusion, it can be said that the demountable shear connector design is the best connection in most cases, but under specific conditions or contractor preferences, this might change.

10.3.4. Experiments

The experiments aim to investigate the separation potential of the steel section and mortar used in the demountable bolted shear connector alternative. The demountability performance is one of the main aspects in a reusable structure, and therefore, these experiments were added as an additional investigation within the scope of the research. Different pre-treatments were applied, and untreated specimens function as the base reference. Due to time and financial limitations, only twelve specimens were prepared, which implies four specimens per type. For the specimens subjected to the load cell testing quite a large scatter in results was obtained which is seen in [Figure 10.3](#). The behaviour of all specimens per treatment type was similar; however, the magnitude differs substantially. Due to the limited number of specimens and data, it is hard to determine whether the obtained values are representative. Most likely, the origin of scatter is the difference in imperfections within the steel section. Additional experiments and more research on the imperfections of steel square hollow section profiles could improve the validity of the experiment. Another limitation is found in the measurement procedure of the load and displacement. The load and displacement measurements were obtained by the load cell, resulting in less precise data. The deformations of the structure, the uneven surface of the mortar, straining of the square hollow section, and compression of the mortar influence the measurements. Accuracy can be improved by applying LVDT's³ and load measuring devices located at the bottom or top of the specimen.

²An engineering firm specialised in building costs.

³Device that can measure displacements, Linear Variable Differential Transformer.

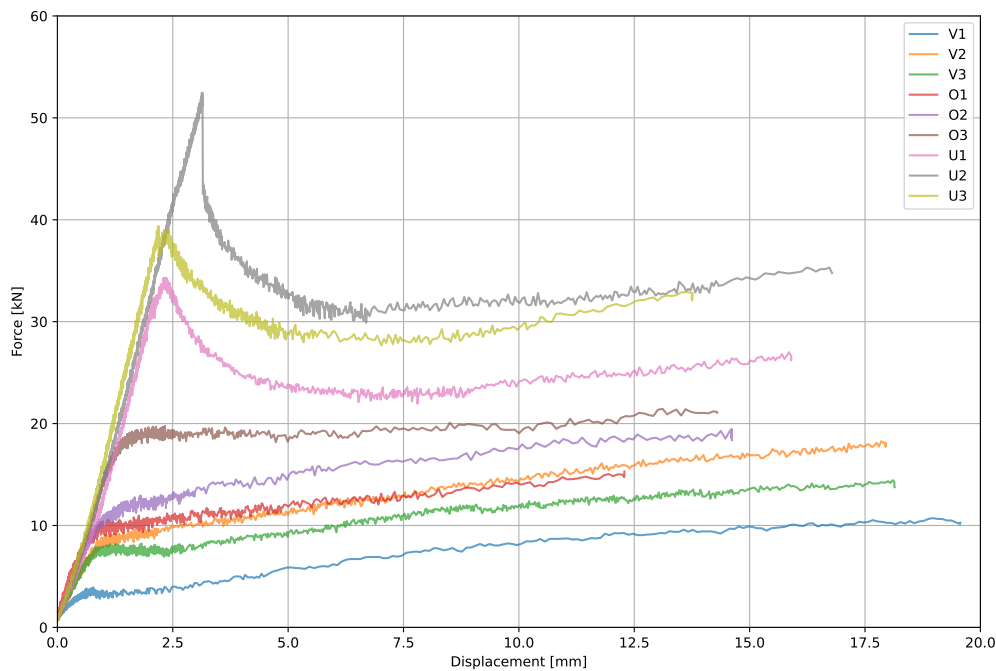


Figure 10.3: Plot of the displacement vs. force for untreated (U), oil-treated (O), and Vaseline-treated (V) specimens. Lines are adjusted to start at same point (1 kN of compression)

10.3.5. Environmental impact assessment

The environmental data used for the impact assessment did not always align with the exact materials used in the design of reusable connections. The effect of this on the outcome of the environmental impact of the connectors is assumed small, since the connections are a minor part of the load bearing structure and even a smaller part on the total environmental costs of the building. The environmental impact assessment did not include stage B and stage C, which correspond to the use stage and end-of-life stage, respectively. The impact of the missing use stage is most likely small; for both the reusable as the non-reusable design the use-stages are similar. Implementing the end-of-life stage however could affect the outcome. The deconstruction, transport and waste processing are different for a reusable design compared to conventional design. The effect of taking into account stage C is likely to be positive for the reusable connection compared to the traditional connection. The demountable design makes the deconstruction easier and saves on transport since the volume of stacked hollow core slabs is lower compared to rubble. On the other hand, the result of the environmental impact shows that the additional initial impact of the reusable connections is marginal, so this effect would even result in a more positive result of the application of reusable connections between hollow core slabs and steel frames. Another limitation can be found in the assessment of the non reusable conventional structure. The research assumes that after the lifespan of the structure the building is scrapped according to the data presented in the manufacturers EPD. However, in practice the structure could be demolished with a circular vision. The steel frame could be reused in another function and the hollow core slabs are removed by sawing and can be reused in another building with a shorter span. This would result in additional environmental burden in the C stage but on the other hand generates more environmental profit in stage D. As a result, the differences in terms of ECI would become smaller, however, the reusable construction will most likely still outperform the conventional construction if more than one reuse cycle is applied.

Conclusion and recommendations

The final chapter presents the research conclusions and answers the main- and subresearch questions. In addition, various recommendations are presented for further research.

11.1. Conclusion

The aim of this research is to develop a new reusable connection between a hollow core slab and a steel frame to increase the lifespan of the structural components and reduce their environmental impact. To achieve this, the design incorporates increased execution tolerances that exceed the values allowed by the standards. The structural behaviour is investigated to verify the compliance of this newly developed connection with the structural requirements. To evaluate whether this goal is achieved, this section presents the final conclusions by answering the main and sub-research questions. The following main research question was formulated:

”Does the structural behaviour of a newly proposed reusable connection between a hollow core slab and a steel frame comply with structural requirements while increasing execution tolerances beyond the allowed values according to the standard?”

In order to provide a conclusive response to the primary research question, it is necessary to address the conclusions to the various sub-questions beforehand.

SQ1. What are the required tolerances to create a reusable connection between a hollow core slab and a steel frame?

- The first point that determines the required level of tolerances is the tolerance class for execution and production of the components. Based on analysis of the literature and manufacturer data, it is concluded that the tolerance data of NEN-EN 1090-2 Class 2 [27], ACI117-10 [2], and NEN-EN 1168 [25] provide the most accurate results to determine the required tolerances for a reusable connection.
- Second, the execution method has a large influence on the amount of required tolerances; completely pre-fabricated elements were chosen instead of on-site installed elements. The increased required tolerances associated with prefabrication of the elements improve the versatility in a second life and the ability to be reused at the component level rather than only at the building level.
- The last point that determines the level of tolerances required is the geometry of the building. An increase in the distance between columns requires larger tolerances. To conclude, there is no exact number that determines the required tolerances in connections between hollow core slabs and steel frames for all situations, as they depend on the geometry of the building.
- For the geometry of the case study, a tolerance of $d + 32.8$ mm is required based on a Monte Carlo simulation with a 95% Confidence Interval and 10^4 simulations, where d is the diameter of the bolt used in the reusable connection.

SQ2. To develop a reusable connection between a hollow core slab and a steel frame, what changes can be made in the manufacturing process?

- From the research it is concluded that modifications to the manufacturing process of the hollow core slabs are highly undesirable due to the automated production process.
- Adjustment of the steel frames in terms of additional stiffeners, plates, and holes can be easily implemented since the production of these parts is similar to standard manufacturing procedures of steel fabricators.

SQ3. What are the requirements for reusable connections with adequate tolerances?

- The trade-off analysis showed that the main requirements for reusable connections are related to tolerances, installation, demountability, and the economic part. The conclusion regarding tolerances is addressed in SQ1.
- The installation requirements prescribe that installation from the top side is preferred compared to installation from below.
- The demountability potential of the bolted shear stud connection was considered critical. Therefore, small-scale experiments investigated the behaviour. From these results, it is concluded that for specimens with Vaseline pre-treatment the lowest resistance is obtained. Furthermore, hand demolition verified this demountability potential.
- The economic requirements address the costs of material, installation, and dismantling. The demountable bolted shear connection has the lowest material investment and reuse cost with €68.69 and €26.29 per connector. This is significantly lower compared to the injected connection with €110.42 and €30.90 and the prestressed connection with €110.72 and €91.67, respectively. The quantitative assessment of installation and demountability costs resulted in small differences.

SQ4. What is the environmental impact of a reusable connection compared to a conventional connection?

- The environmental impact of the connection between the steel frame and the hollow core slab, whether reusable or non-reusable, has a negligible effect on the overall environmental costs. The Environmental Cost Indicator (ECI), comprising life cycle stages A1 to A3, for the superstructure of the case study buildings is equal to € 75,909.49 for the reusable design and €74,953.60 for the conventional one.
- The ECI for the reusable connector is calculated at €1.68 for stages A1 to A3, while the conventional connection is €0.92. With 1248 connectors in the case study building, these values represent 2.8% and 1.5% of the superstructure ECI, respectively. If the assessment includes the entire building, encompassing substructure, facades, and other components related to the building, this percentage would decrease as the total ECI increases.
- A multiple-lifespan scenario highlights the added value of the reusable connection. It is concluded that after a single reuse cycle, the reusable design already outperforms the conventional one. A reuse cycle incurs an ECI of €651.92 for stages A1 to A3 for the reusable connection, which accounts for the application of new bolts and mortar. In contrast, the conventional design incurs an approximately hundred times higher ECI of €65,148.87. This cost is reduced compared to the initial ECI due to the inclusion of reuse stage D. As the number of reuse cycles increases, the differences become more pronounced, revealing the full potential of the reusable connection.

Main research question

To conclude the main research question, there are various possibilities to develop a reusable connection between a hollow core slab and a steel frame that comply with the structural requirements. In addition to structural requirements, there are several other crucial requirements to consider during the development process, including tolerances, installation and disassembling procedures, and associated costs. The analysed alternatives included an injection connection, a demountable bolted shear stud connection, and a prestressed connection. The second connection resulted in the largest inclusion of tolerances, the lowest initial investment costs, and the easiest installation, which were the main decisive points

in the trade-off analysis. Small-scale experiments were conducted to assess the uncertain requirement regarding demountability, which was the final requirement. The results of the experiments showed a great demountability potential. Therefore, it is concluded that the structural behaviour of the newly proposed reusable connection, consisting of a bolted demountable shear stud, complies with structural requirements while implementing increased execution tolerances.

11.2. Recommendations

Based on the research conducted in this thesis, several recommendations for further research can be formulated:

Expand the tolerance analysis to account for different geometries

- The first recommendation points out that the effect of the geometry of the building should be further investigated. For the current study only the geometry of the case study was analysed. However, it could be interesting to further investigate the effect of different geometries. The spacing of the beam and column are the parameters that determine the level of tolerances in the structural grid. Eventually, a design formula could be formulated for the required tolerance level for on-site and prefabricated installation methods.

Investigate the effect of an increased pre-treatment layer thickness in terms of demountability

- The effect of the pre-treatment was clearly visible in the experimental results on the separation potential of the steel section and the mortar. Vaseline-treated specimens showed better performance compared to their oil-treated counterparts. Possible explanations can be found in the thickness of the treatment. Vaseline is a paste-like substance, whereas formwork oil, as the name suggests, is an oil-based solution. The better results of Vaseline could be explained by the fact that the increase in layer thickness evens out some of the imperfections within the steel section. Another theory could be that the lubrication potential of Vaseline outperforms that of the formwork oil. Further investigation of the increased layer thickness could result in better separation potential between the steel section and the mortar and subsequently better demountability of the structure.

Validate the experimental outcome on the demountability to a (semi)full scale connection

- The experiments were carried out on a small scale. Scaling up the experiment and using part of a hollow core slab with the connector could result in a better assessment of the demountability potential. During the manual demolition of the mortar, the specimens were clamped in a vice which negatively affects the separation of the components due to the additional clamping pressure applied by the vice. When a (semi)full-scale connection is modelled, the actual demountability potential can be reviewed. A point of attention could be the effect of the vibrations induced by the demolition hammer on the sleeve concrete.

Long term effect of the mortar inside the steel section

- The mortar casted in the steel section was tested by the load cell after 9 days of curing and manual demolition occurred after 15 days. It would be interesting to assess the effect of longer curing times on the separability of the steel section and the mortar. From one perspective, an increase in the cure time would result in more shrinkage of the material and exposure to vibrations, which could result in an improved demountability potential. However, the mortar becomes stronger with time and in combination with the imperfections of the section, the friction resistance might increase.

Bibliography

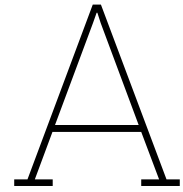
- [1] Muhammad Abid, Muhammad Shahid Khalil, and Hafiz Abdul Wajid. “An experimental study on the relaxation of bolts”. In: *IUM Engineering Journal* 16.1 (May 2015). ISSN: 1511-788X. DOI: [10.31436/IIUMEJ.V16I1.539](https://doi.org/10.31436/IIUMEJ.V16I1.539).
- [2] ACI Committee 117. *Specifications for tolerances for concrete construction and materials (ACI 117-10) and commentary*. Tech. rep. 2010, p. 76.
- [3] AISC. *Specification for Structural Steel Buildings*. Tech. rep. Chicago: American Institute of Steel Construction, July 2016.
- [4] AISC. *Code of Standard Practice for Steel Buildings and Bridges*. Tech. rep. Chicago: American Institute of Steel Construction, May 2022.
- [5] T Aoki and Y Fukumoto. “On the buckling strength distribution of welded H-columns”. In: *Proceedings of the Japan Society of Civil Engineers* 1974.222 (Feb. 1974), pp. 37–48. ISSN: 0385-5392. DOI: [10.2208/JSCEJ1969.1974.222{_}37](https://doi.org/10.2208/JSCEJ1969.1974.222{_}37).
- [6] ASTM International. *Standard Specification for General Requirements for Rolled Structural Steel Bars, Plates, Shapes, and Sheet Piling*. Tech. rep. West Conshohocken: ASTM International, 2021. DOI: [10.1520/A0006{_}A0006M-21](https://doi.org/10.1520/A0006{_}A0006M-21). URL: www.astm.org.
- [7] Reza Mokarram Aydenlou. *Understanding the basic concepts in seismic rehabilitation*. Elsevier, 2020, pp. 1–63. DOI: [10.1016/b978-0-12-819959-6.00001-4](https://doi.org/10.1016/b978-0-12-819959-6.00001-4).
- [8] Eric Barelts. “Assessing the viability of implementing significantly oversized holes in high strength friction grip bolted connections: Towards the increased modularity of bridge decks and ease of their replacement”. PhD thesis. Delft: Delft University of Technology, Dec. 2022. URL: <https://repository.tudelft.nl/islandora/object/uuid%3A708fdb7-f96a-4336-a758-692630721de8>.
- [9] BE Group Sverige AB. *EPD - Merchant bars*. Tech. rep. 2021. URL: <https://www.environdec.com/library/epd4889>.
- [10] H Beer and G Schulz. “The European column curves”. In: *IABSE reports of the working commissions* 23 (1975). DOI: [10.5169/seals-19828](https://doi.org/10.5169/seals-19828). URL: <https://doi.org/10.5169/seals-19828>.
- [11] J. F. Berthet, I. Yurtdas, Y. Delmas, and A. Li. “Evaluation of the adhesion resistance between steel and concrete by push out test”. In: *International Journal of Adhesion and Adhesives* 31.2 (Mar. 2011), pp. 75–83. ISSN: 0143-7496. DOI: [10.1016/J.IJADHADH.2010.11.004](https://doi.org/10.1016/J.IJADHADH.2010.11.004).
- [12] L.P. Bouwman. “De invloed van de dikteverhoudingen van hoofd- en stukplaten op de toelaatbare stukspanning bij verbindingen met injectiebouten”. In: *Stevin rapport 6-74-11* (1974). URL: <https://repository.tudelft.nl/islandora/object/uuid%3A296bfa8d-3600-4998-8f13-6826c5d4e8f0>.
- [13] Stewart Brand. *How Buildings Learn: What Happens After They’re Built*. Penguin Books, 1995. ISBN: 0140139966.
- [14] Edwin Buitelaar, Stefano Moroni, and Anita De Franco. “Building obsolescence in the evolving city. Reframing property vacancy and abandonment in the light of urban dynamics and complexity”. In: *Cities* 108 (Jan. 2021). ISSN: 02642751. DOI: [10.1016/j.cities.2020.102964](https://doi.org/10.1016/j.cities.2020.102964).
- [15] Brian Burns. “Re-evaluating Obsolescence and Planning for It”. In: *Longer Lasting Products: Alternatives to the Throwaway Society* Kosteci 1998 (2010). Ed. by Tim Cooper, pp. 39–60. URL: https://books.google.com/books/about/Longer_Lasting_Products.html?hl=nl&id=1fpbrpTha50C.
- [16] Ruben Buunk and Esmee Heebing. “Scriptie Remontabel ontwerpen met kanaalplaten”. PhD thesis. Arnhem: HAN University of Applied sciences, 2017.
- [17] Celsa Steel Service ES. *EPD - Steel reinforcement product for concrete*. Tech. rep. 2023. URL: <https://www.environdec.com/library/epd11218>.

- [18] CEN. *Structural steel I and H sections - Tolerances on shape and dimensions*. Tech. rep. Brussels: European Committee for Standardization, Sept. 1993.
- [19] CEN. *Eurocode 1: Actions on structures - Part 1-3: General actions-Snow loads*. Tech. rep. Brussels: European Committee for Standardization, July 2003.
- [20] CEN. *Eurocode 3: Design of steel structures - Part 1 - 8: Design of joints*. Tech. rep. Brussels: Eurocode 3: Design of steel structures - Part 1- 8: Design of joints, May 2005.
- [21] CEN. *Eurocode 3: Design of steel structures - Part 1-1: General rules and rules for buildings*. Tech. rep. Brussels: European Committee for Standardization, May 2005.
- [22] CEN. *Eurocode 1: Actions on structures - Part 1-4: General actions - Wind actions*. Tech. rep. Brussels: European Committee for Standardization, Dec. 2011.
- [23] CEN. *Eurocode 2: Design of concrete structures - Part 1-1: General rules and rules for buildings*. Tech. rep. Brussels: European Committee for Standardization, Nov. 2011.
- [24] CEN. *Eurocode 4: Design of composite steel and concrete structures - Part 1-1: General rules and rules for buildings*. Tech. rep. Brussels: European Committee for Standardization, Dec. 2011.
- [25] CEN. *Precast concrete products - Hollow core slabs*. Tech. rep. Brussels: European Committee for Standardization, Oct. 2011.
- [26] CEN. *NEN-EN 15804+A1 Sustainability of construction works - Environmental product declarations - Core rules for the product category of construction products*. Tech. rep. Brussels: European Committee for Standardization, Nov. 2013.
- [27] CEN. *Execution of steel structures and aluminium structures - Part 2: Technical requirements for steel structures*. Tech. rep. Brussels: European Committee for Standardization, June 2018.
- [28] CEN. *Eurocode 1: Actions on structures - Part 1-1: General actions - Densities, self-weight, imposed loads for buildings*. Tech. rep. Brussels: European Committee for Standardization, Nov. 2019.
- [29] CEN. *Eurocode: Basis of structural design*. Tech. rep. Brussels: European Committee for Standardization, Nov. 2019.
- [30] CEN. *National Annex to NEN-EN 1990+A1:2006+A1:2006/C2:2019 Eurocode: Basis of structural design*. Tech. rep. Brussels: European Committee for Standardization, Nov. 2019.
- [31] CEN. *National Annex to NEN-EN 1991-1-1+C1+C11: Eurocode 1 - Actions on structures - Part 1-1: General actions - Densities, self-weight, imposed loads for buildings*. Tech. rep. Brussels: European Committee for Standardization, Nov. 2019.
- [32] CEN. *NEN-EN 12390-3 Testing hardened concrete - Part 3: Compressive strength of test specimens*. Tech. rep. Brussels: European Committee for Standardization, July 2019.
- [33] CEN. *NEN-EN 15804+A2 Sustainability of construction works - Environmental product declarations - Core rules for the product category of construction products*. Tech. rep. Brussels: European Committee for Standardization, Nov. 2019.
- [34] CEN. *National Annex to NEN-EN 1992-1-1+C2 Eurocode 2: Design of concrete structures - Part 1-1: General rules and rules for buildings*. Tech. rep. Brussels: European Committee for Standardization, Feb. 2020.
- [35] CEN. *Eurocode 7: Geotechnical design - Part 1: General rules*. Tech. rep. Brussels: European Committee for Standardization, Sept. 2022.
- [36] CEN. *National Annex to NEN-EN 1991-1-4+A1+C2: Eurocode 1: Actions on structures - Part 1-4: General actions - Wind actions*. Tech. rep. Brussels: European Committee for Standardization, Mar. 2023.
- [37] Compania Siderúrgica Huachipato. *EPD - Helical Bolts*. Tech. rep. 2023. URL: <https://www.environdec.com/library/epd8527>.
- [38] Cugla BV. *Cuglaton Gietmortel 5 mm*. Breda, Oct. 2023.
- [39] M Danschutter de, P.A. Noomen, and B Oostdam. “Tijdelijke rechtbank Amsterdam (2): tenderfase - Warmlopen voor circulariteit”. In: *Bouwen met Staal 257* (2017), pp. 12–21.

- [40] M. Dörre, R. Glienke, M. Schwarz, and K. H. Henkel. “Slip resistance of bolted joints with slotted holes”. In: *Materialwissenschaft und Werkstofftechnik* 53.2 (Feb. 2022), pp. 139–155. ISSN: 15214052. DOI: [10.1002/mawe.202100206](https://doi.org/10.1002/mawe.202100206).
- [41] P F Dux and S Kitipornchait. “Inelastic Beam Buckling Experiments”. In: *Journal of Constructional Steel Research* 3.1 (1983), pp. 3–9.
- [42] ECCS Advisory Committee 1. *ECCS 83 Book Slim floors with built-in beams*. Tech. rep. 1995.
- [43] ECCS Technical Committee 10. *European recommendations for bolted connections with injection bolts*. Tech. rep. Brussel: European convention for constructional steelwork, 1994.
- [44] Hesham S. Essa and D. J. Laurie Kennedy. *Distortional buckling of steel beams*. Tech. rep. 1993. DOI: [10.7939/R3KC19](https://doi.org/10.7939/R3KC19). URL: <https://era.library.ualberta.ca/items/3367a7b4-4002-4aee-b6ee-4909e5955400>.
- [45] FEDBETON vzw. *EPD - Fedbeton typical belgian ready-mixed concrete*. Tech. rep. 2021. URL: <https://www.fedbeton.be/nl/news/een-epd-voor-de-sector>.
- [46] Constanze Fetting. *THE EUROPEAN GREEN DEAL*. Tech. rep. 2020.
- [47] Y Fukumoto and Y Itoh. “Evaluation of Multiple Column Curves using the Experimental Database Approach”. In: *Journal of Constructional Steel Research* 3.3 (1983), pp. 2–19.
- [48] Ioan Andrei Gîrbacea. *Assessment of demountable steel-concrete composite flooring systems*. Tech. rep. Delft: Delft University of Technology, Oct. 2018.
- [49] A.M. Gresnigt and J.W.B. Stark. “Design of bolted connections with injection bolts”. In: *Connections in Steel Structures III* (Jan. 1996), pp. 77–87. DOI: [10.1016/B978-008042821-5/50067-5](https://doi.org/10.1016/B978-008042821-5/50067-5).
- [50] A.F. Hamerlinck and B. Potjes. *Technisch Dossier #2, vloeren van kanaalplaten met geïntegreerde stalen liggers*. Tech. rep. Zoetermeer: Bouwen met Staal, 2007.
- [51] Dorian A.H. Hanaor, Yixiang Gan, and Itai Einav. “Contact mechanics of fractal surfaces by spline assisted discretisation”. In: *International Journal of Solids and Structures* 59 (May 2015), pp. 121–131. ISSN: 0020-7683. DOI: [10.1016/J.IJSOLSTR.2015.01.021](https://doi.org/10.1016/J.IJSOLSTR.2015.01.021).
- [52] Huntsman. *RenGel SW 404 / Ren HY 2404 or HY 5159*. Basel, Mar. 2007.
- [53] INHUS Prefab UAB. *EPD - Precast concrete hollow core slab*. Tech. rep. 2022. URL: <https://www.environdec.com/library/epd3858>.
- [54] IPHA. *IPHA - International Prestressed Hollowcore Association*. URL: <https://hollowcore.org/>.
- [55] Isidora Jakovljević, Milan Spremić, and Zlatko Marković. *Demountable composite steel-concrete floors: A state-of-the-art review*. Mar. 2021. DOI: [10.14256/JCE.2932.2020](https://doi.org/10.14256/JCE.2932.2020).
- [56] Chao Jiang, Wen Xiong, C. S. Cai, Yanjie Zhu, and Zhongxiang Liu. “Experimental study on the shear behavior of friction connections with corrosion damage”. In: *Journal of Constructional Steel Research* 197 (Oct. 2022). ISSN: 0143974X. DOI: [10.1016/j.jcsr.2022.107449](https://doi.org/10.1016/j.jcsr.2022.107449).
- [57] Zdeněk Kala. “Sensitivity analysis of steel plane frames with initial imperfections”. In: *Engineering Structures* 33.8 (Aug. 2011), pp. 2342–2349. ISSN: 01410296. DOI: [10.1016/j.engstruct.2011.04.007](https://doi.org/10.1016/j.engstruct.2011.04.007).
- [58] Dr. Florentia Kavoura and M. Veljkovic. “Technical Practices Of Re-Usable Steel-Concrete Composite Structural Systems”. In: *CESARE’22 Coordinating Engineering for Sustainability and Resilience*. Jordan University of Science and Technology, 2022. URL: <https://repository.tudelft.nl/islandora/object/uuid%3A54965356-6284-4924-8dde-27a1e25df951>.
- [59] Will Kenton. *Monte Carlo Simulation: History, How it Works, and 4 Key Steps*. 2023. URL: <https://www.investopedia.com/terms/m/montecarlosimulation.asp>.
- [60] Koninklijk Nederlands Normalisatie Instituut. *Nederlandse technische afspraak NTA 8713 (nl) Hergebruik van constructiestaal Reuse of structural steelwork*. Tech. rep. 2023. URL: www.nen.nl.
- [61] Gunup Kwon, Aff M Asce, Michael D Engelhardt, M Asce, and Richard E Klingner. “Experimental Behavior of Bridge Beams Retrofitted with Postinstalled Shear Connectors”. In: (2011). DOI: [10.1061/\(ASCE\)BE.1943-5592](https://doi.org/10.1061/(ASCE)BE.1943-5592).

- [62] Gunup Kwon, Michael D. Engelhardt, and Richard E. Klingner. “Behavior of post-installed shear connectors under static and fatigue loading”. In: *Journal of Constructional Steel Research* 66.4 (Apr. 2010), pp. 532–541. ISSN: 0143974X. DOI: [10.1016/j.jcsr.2009.09.012](https://doi.org/10.1016/j.jcsr.2009.09.012).
- [63] Marcantonini Concrete Technology. *Prestressed Hollowcore Slabs - MCT Italy*. URL: <https://www.marcantonini.com/en/prestressed-hollowcore-slabs/>.
- [64] Shaun Masson. *Life Cycle Stages*. Aug. 2023.
- [65] J Melcher. *Structural stability research council: proceedings 1980*. Tech. rep. Structural stability research council, 1980. URL: <https://scholarsmine.mst.edu/ccfss-library>.
- [66] Ministerie van Infrastructuur en Waterstaat. *Nationaal Programma Circulaire Economie | 2023 - 2030*. Tech. rep. 2023.
- [67] Daniel Moroder. “Floor diaphragms in multi-storey timber buildings”. PhD thesis. Canterbury: University of Canterbury, 2016.
- [68] M. P. Nijgh. *Loss of preload in pretensioned bolts*. 2016. URL: <https://repository.tudelft.nl/islandora/object/uuid%3A4776e217-d7b7-4122-8e36-61ab7ed8c672>.
- [69] M. P. Nijgh. “New Materials for Injected Bolted Connections A Feasibility Study for Demountable Connections”. PhD thesis. Delft: Delft University of Technology, 2017.
- [70] M. P. Nijgh. “A multi-scale approach towards reusable steel-concrete composite floor systems”. PhD thesis. Delft: Delft University of Technology, 2021. DOI: [10.4233/uuid:983b06e7-c30b-465c-a032-2439a7e9863f](https://doi.org/10.4233/uuid:983b06e7-c30b-465c-a032-2439a7e9863f). URL: <https://doi.org/10.4233/uuid:983b06e7-c30b-465c-a032-2439a7e9863f>.
- [71] M. P. Nijgh, I.A. Gîrbacea, and M. Veljkovic. “Elastic behaviour of a tapered steel-concrete composite beam optimized for reuse”. In: *Engineering Structures* 183 (Mar. 2019), pp. 366–374. ISSN: 18737323. DOI: [10.1016/j.engstruct.2019.01.022](https://doi.org/10.1016/j.engstruct.2019.01.022).
- [72] M. P. Nijgh and M. Veljkovic. “Design of composite flooring systems for reuse”. In: *IOP Conference Series: Earth and Environmental Science*. Vol. 225. 1. Institute of Physics Publishing, Feb. 2019. DOI: [10.1088/1755-1315/225/1/012026](https://doi.org/10.1088/1755-1315/225/1/012026).
- [73] M. P. Nijgh and M. Veljkovic. “Requirements for oversized holes for reusable steel-concrete composite floor systems”. In: *Structures* 24 (Apr. 2020), pp. 489–498. ISSN: 23520124. DOI: [10.1016/j.istruc.2020.01.021](https://doi.org/10.1016/j.istruc.2020.01.021).
- [74] Sheila F O and Qi Long Yi. “How do I interpret a confidence interval?” In: (). DOI: [10.1111/trf.13635](https://doi.org/10.1111/trf.13635). URL: <https://onlinelibrary.wiley.com/doi/10.1111/trf.13635>.
- [75] Marko Pavlović, Zlatko Marković, Milan Veljković, and Dragan Bucrossed D Signevac. “Bolted shear connectors vs. headed studs behaviour in push-out tests”. In: *Journal of Constructional Steel Research* 88 (Sept. 2013), pp. 134–149. ISSN: 0143-974X. DOI: [10.1016/J.JCSR.2013.05.003](https://doi.org/10.1016/J.JCSR.2013.05.003).
- [76] Bruno Pedrosa, Linda Bücking, and Milan Veljkovic. “Steel-reinforced resin for bolted shear connectors: Confined behaviour under quasi-static cyclic loading”. In: *Engineering Structures* 256 (Apr. 2022). ISSN: 18737323. DOI: [10.1016/j.engstruct.2022.114023](https://doi.org/10.1016/j.engstruct.2022.114023).
- [77] Precast Concrete Institute. *Manuel for quality control for plans and production of structural precast concrete product*. Tech. rep. Chicago: Precast Concrete Institute, 1999.
- [78] Alexandre Rossi, Daniel Hideyuki Saito, Carlos Humberto Martins, and Alex Sander Clemente de Souza. “The influence of structural imperfections on the LTB strength of I-beams”. In: *Structures* 29 (Feb. 2021), pp. 1173–1186. ISSN: 23520124. DOI: [10.1016/j.istruc.2020.11.020](https://doi.org/10.1016/j.istruc.2020.11.020).
- [79] Ihsan A Al-Shaarbaf, Adel A Al-Azzawi, and Radhwan Abdulsattar. “A state of the art review on hollow core slabs”. In: *ARPJ Journal of Engineering and Applied Sciences* 13.9 (May 2018). ISSN: 1819-6608. URL: www.arpnjournals.com.
- [80] Sika. *EPD - SikaGrout®-312*. Tech. rep. 2022. URL: <https://ipmcdataprod.blob.core.windows.net/cdn/105742-EPDIBUSikaGrout312enGB20270925.pdf>.
- [81] Sika. *SikaGrout®-312*. Sept. 2023.

- [82] H.J. Smits and L.P. Bouwman. “Investigation to the apply of separating liquids for injected bolt-connections”. In: *Stevin rapport 6-72-14* (1972). URL: <https://repository.tudelft.nl/islandora/object/uuid%3Aabfd2b2f-ad41-4af7-b96c-b23bed674717>.
- [83] Stalia AB. *EPD - Steel plates, painted and non-painted*. Tech. rep. 2023. URL: <https://www.environdec.com/library/epd9023>.
- [84] J Strating and H Vos. “Computer Simulation of the E.C.C.S. Buckling Curve using a Monte-Carlo Method”. In: *Heron* 19.2 (1973).
- [85] TATA steel. *EPD - Structural hollow sections*. Tech. rep. 2022. URL: <https://www.tatasteeleurope.com/construction/download-centre/environmental-product-declarations>.
- [86] Negussie Tebedge, Wai-Fah Chen, and Lambert Tall. “Experimental studies on column strength of european heavy shapes”. In: *IABSE reports of the working commissions* 23 (1975), pp. 301–320. DOI: [10.5169/seals-19821](https://doi.org/10.5169/seals-19821). URL: <https://doi.org/10.5169/seals-19821>.
- [87] D Thelen, M Acoleyen van, W Huurman, T Thomaes, C Brunshot van, B Edgerton, and B Kubbinga. *Scaling the circular built environment*. Tech. rep. 2018.
- [88] Ad Tissink. “Amsterdams beste gebouw van 2017 staat binnenkort in Enschede”. In: *Cobouw* (Nov. 2021). URL: <https://www.cobouw.nl/300862/amsterdams-beste-gebouw-van-2017-staat-binnenkort-in-enschede>.
- [89] Transitieteam Circulaire Bouweconomie. *Transition agenda circular economy | 2018*. Tech. rep. 2018. URL: <https://hollandcircularhotspot.nl/wp-content/uploads/2019/09/Circular-Construction-Economy.pdf>.
- [90] VBI. *Kanaalplaatvloer 260*. Tech. rep. URL: www.vbi-techniek.nl..
- [91] VIBA verbindingstechniek BV. *Epoxy gelcoat*.
- [92] Fei Yang, Yuqing Liu, Zhibo Jiang, and Haohui Xin. “Shear performance of a novel demountable steel-concrete bolted connector under static push-out tests”. In: *Engineering Structures* 160 (Apr. 2018), pp. 133–146. ISSN: 18737323. DOI: [10.1016/j.engstruct.2018.01.005](https://doi.org/10.1016/j.engstruct.2018.01.005).
- [93] M.V. Zuidema, L.L.M. Elp van, and M.J. Schaaf van der. *Landelijke samenvatting kantorenmonitor*. Tech. rep. 2012.



Hollow core slab manufacturing tolerances

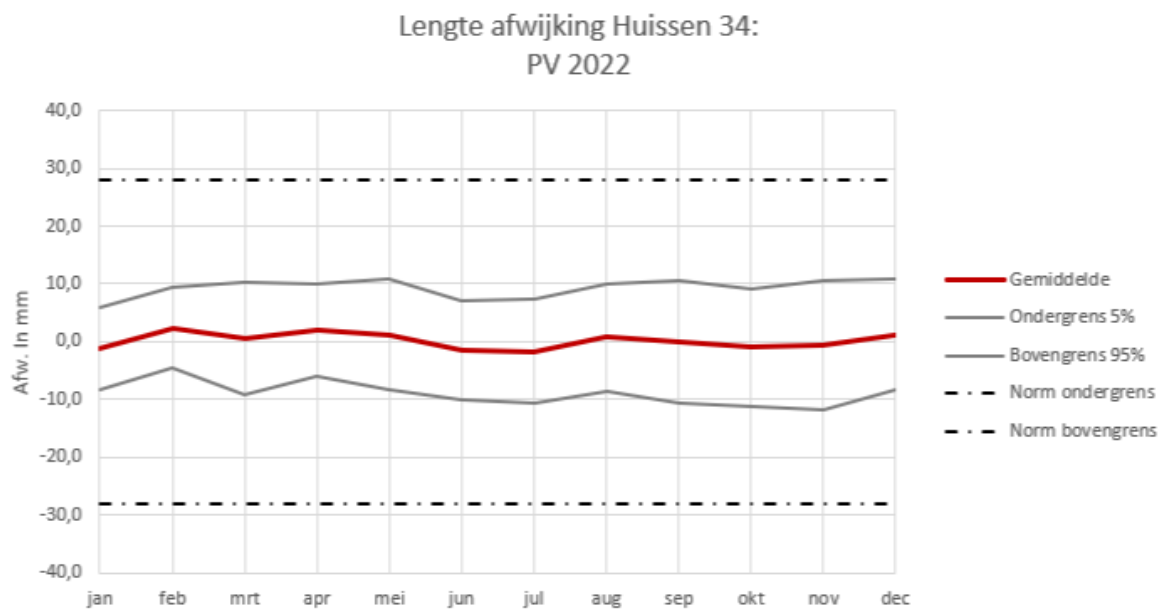


Figure A.1: Measured tolerances of the hollow core slab length, data obtained from VBI for unit 3 and 4 in 2022

B

Case study building

The case study building was designed by IMd Raadgevende Ingenieurs for the municipality of Rotterdam. The design vision for the structure was to create a reusable office building, this vision is in line with the scope of this thesis. Therefore, this building can serve as an ideal case study. The case study building is used for defining the level of tolerances and the loading conditions. The building falls into consequence class 2 (CC2) [29].

B.1. Geometry

The superstructure of the building is constructed of a bolted steel frame and concrete hollow core slab elements for the floors and roof. For the substructure, a concrete strip foundation is used with prefabricated concrete piles below. The ground floor level is constructed of hollow core slabs between the strip foundation to create a larger reuse potential. Unfortunately, the strips and piles cannot be reused. The steel frame of the superstructure consists of the following elements:

- Columns,
- Integrated floor beams,
- Edge beams,
- Bracing elements,
- Strut elements for wind loading.

The building is a two-story rectangular building with the technical installations placed on the roof. In [section B.2](#) isometric projections of the building are shown.

B.1.1. Dimensions

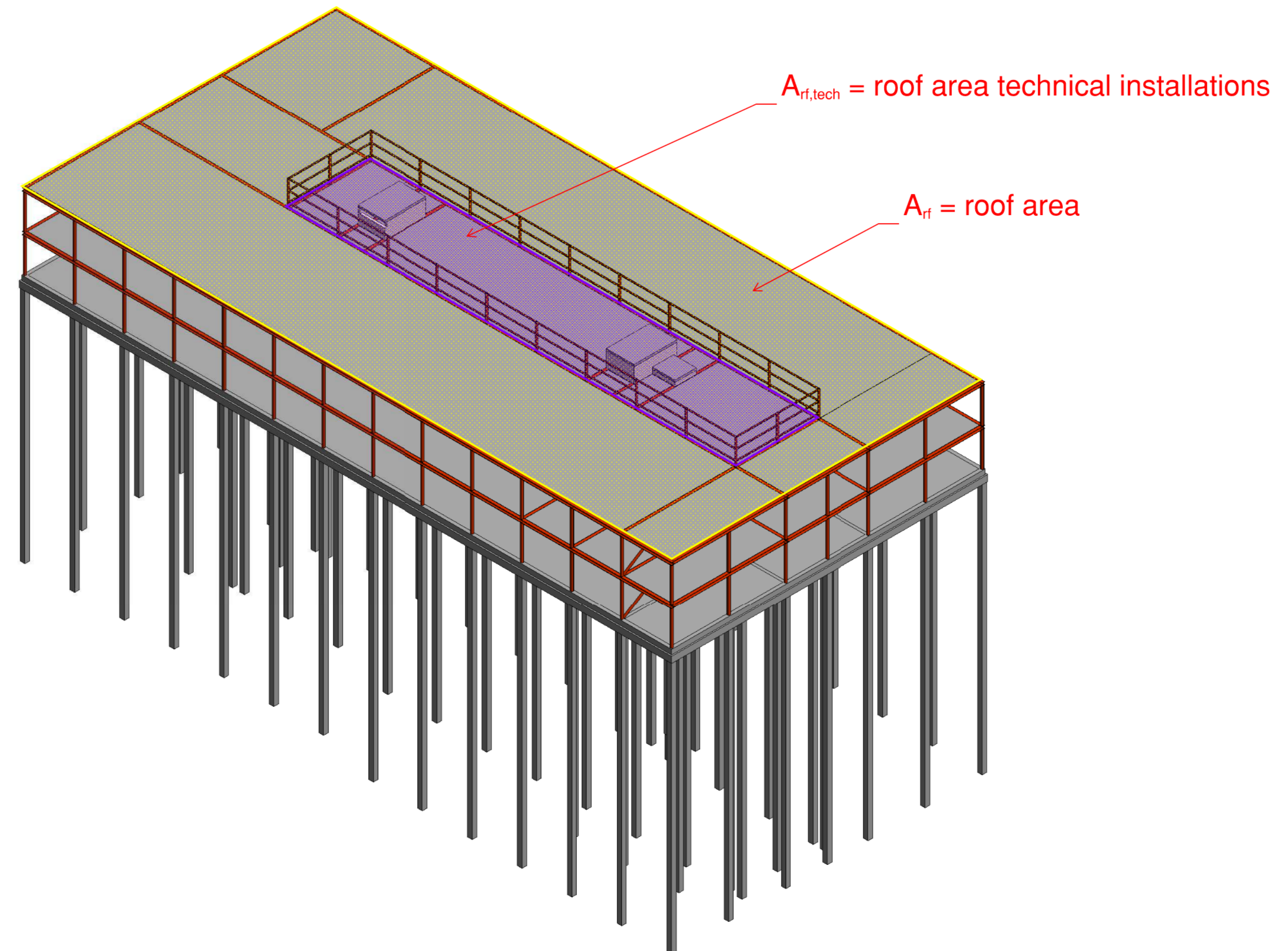
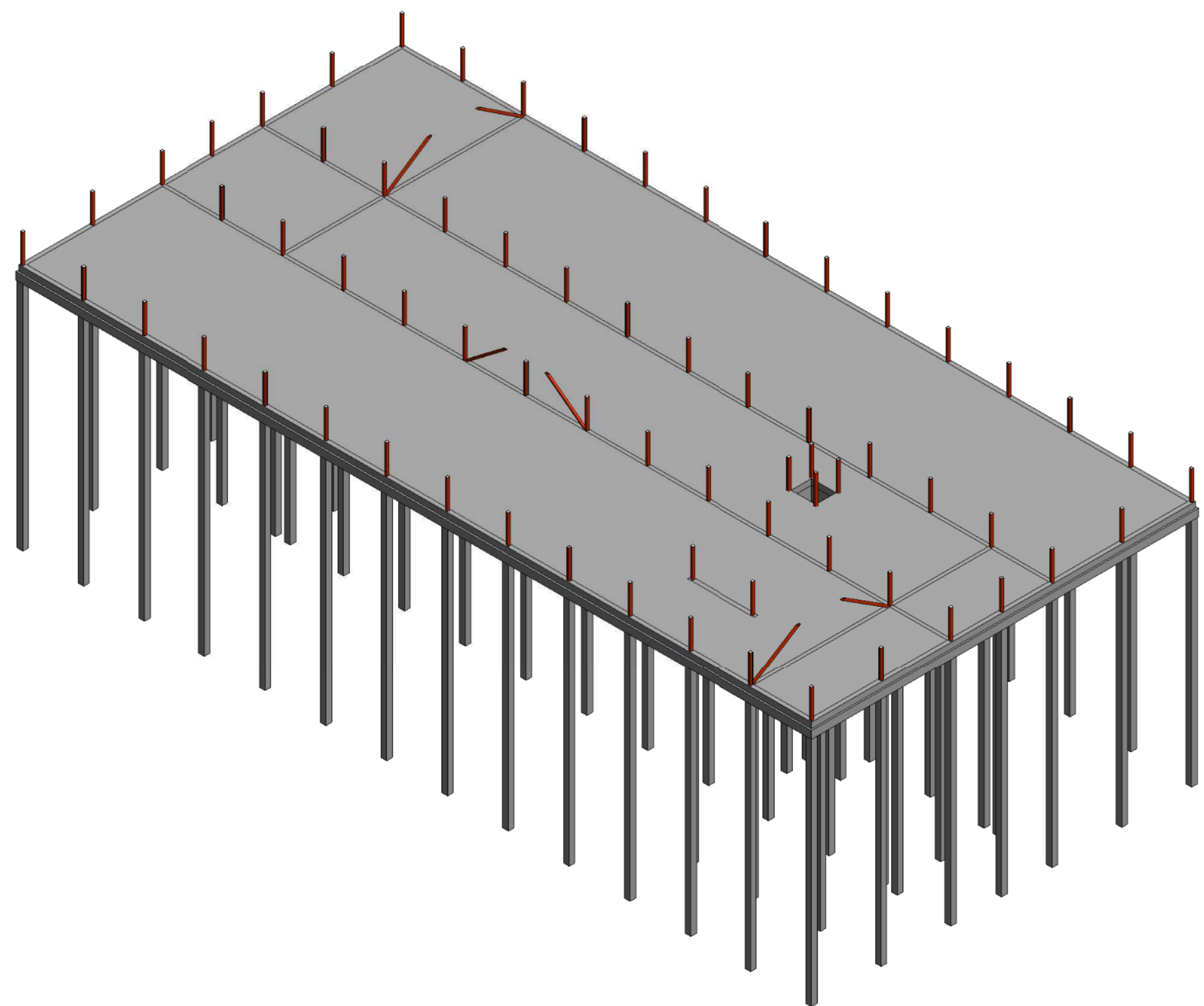
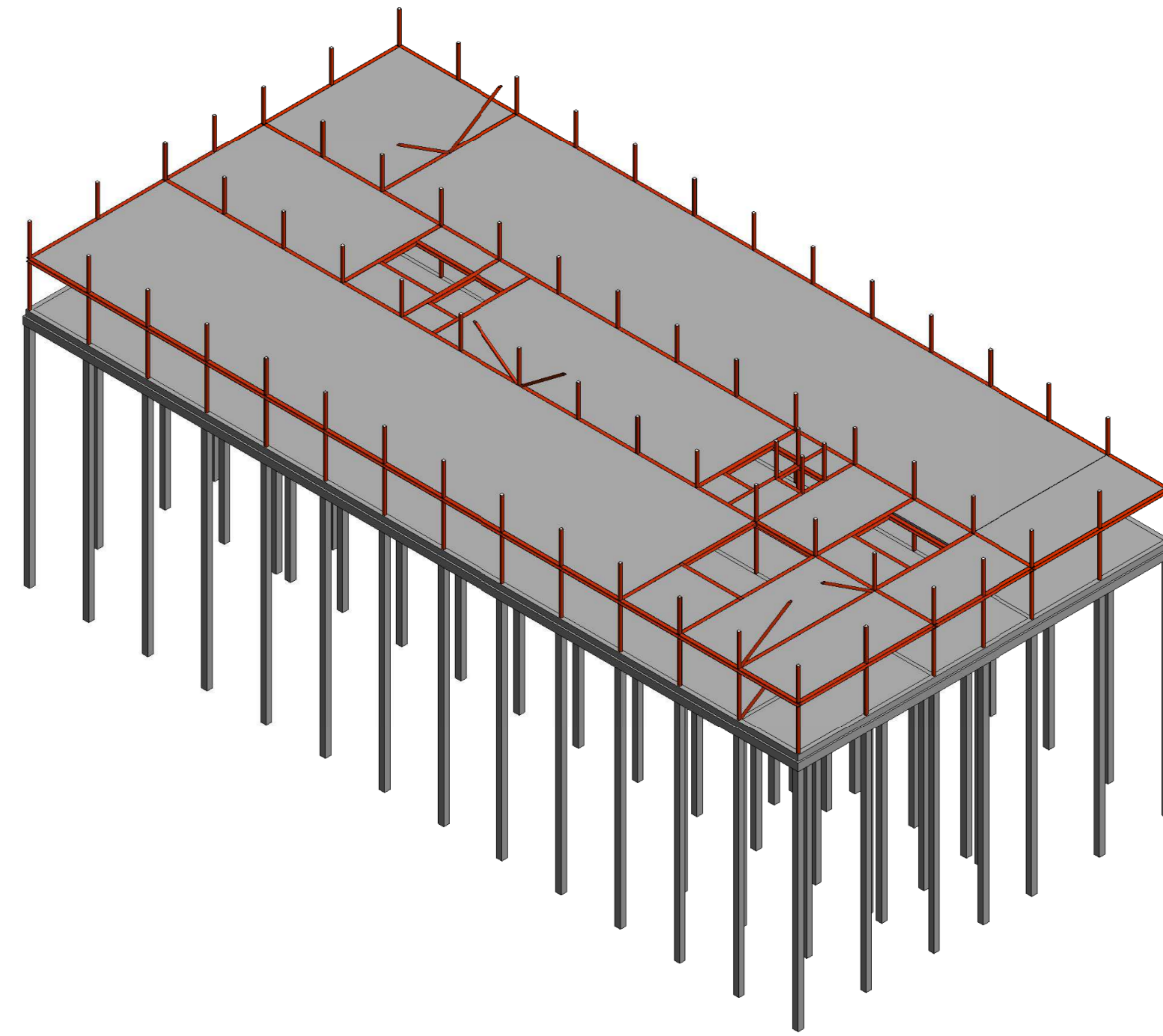
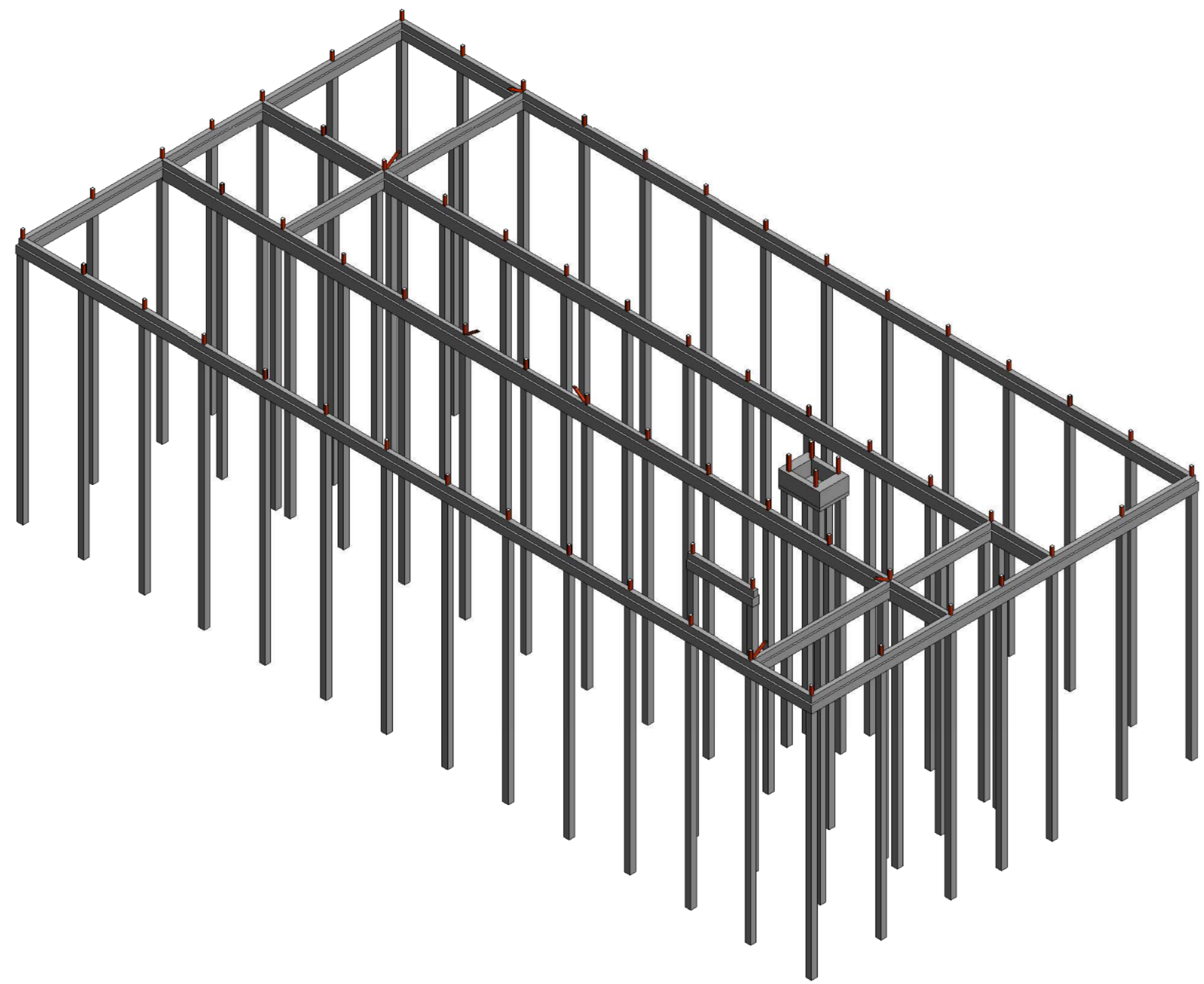
In terms of dimensions, the building is quite straightforward; it has 4 major axes parallel to the longitudinal axis of the building. These axes, labelled A-D, function as the support axes for the hollow core floor elements. On ground floor level this function is provided by the strip foundation and on the first and second floor the integrated floor beams will act as the supporting members. Perpendicular to these longitudinal axes, 14 more grid lines are made. On the two outer axes, 1, and 14, the steel edge beams are located. On the other lines bracing and strut elements will be located.

- $W = 30$ [m],
- $w_1 = 8$ [m],
- $D = 62.4$ [m],
- $d_1 = 43.2$ [m],
- $H = 9.8$ [m],
- $S = 4800$ [mm],
- $L_1 = L_3 = 11000$ [mm],
- $L_2 = 8000$ [mm],

- $H_1 = H_2 = 3650$ [mm],
- $H_3 = 2490$ [mm].

In [section B.2](#), [section B.3](#), [section B.4](#), and [section B.5](#) the drawing of the building is shown.

B.2. Isometric 3D building overview



IMd
Raadgevende
Ingenieurs

Postbus 50521
3007 JA Rotterdam
Pakstraat 77
3071 EL Rotterdam
t 010 201 23 60
e imd@imd.vi.nl
www.imd.vi.nl

: project
: opdrachtgever
: architect

: projectnummer
: projectleider
: projecttekenaar

: omschrijving wijziging
: datum wijziging

3D aanzichten

: onderdeel

: schaal

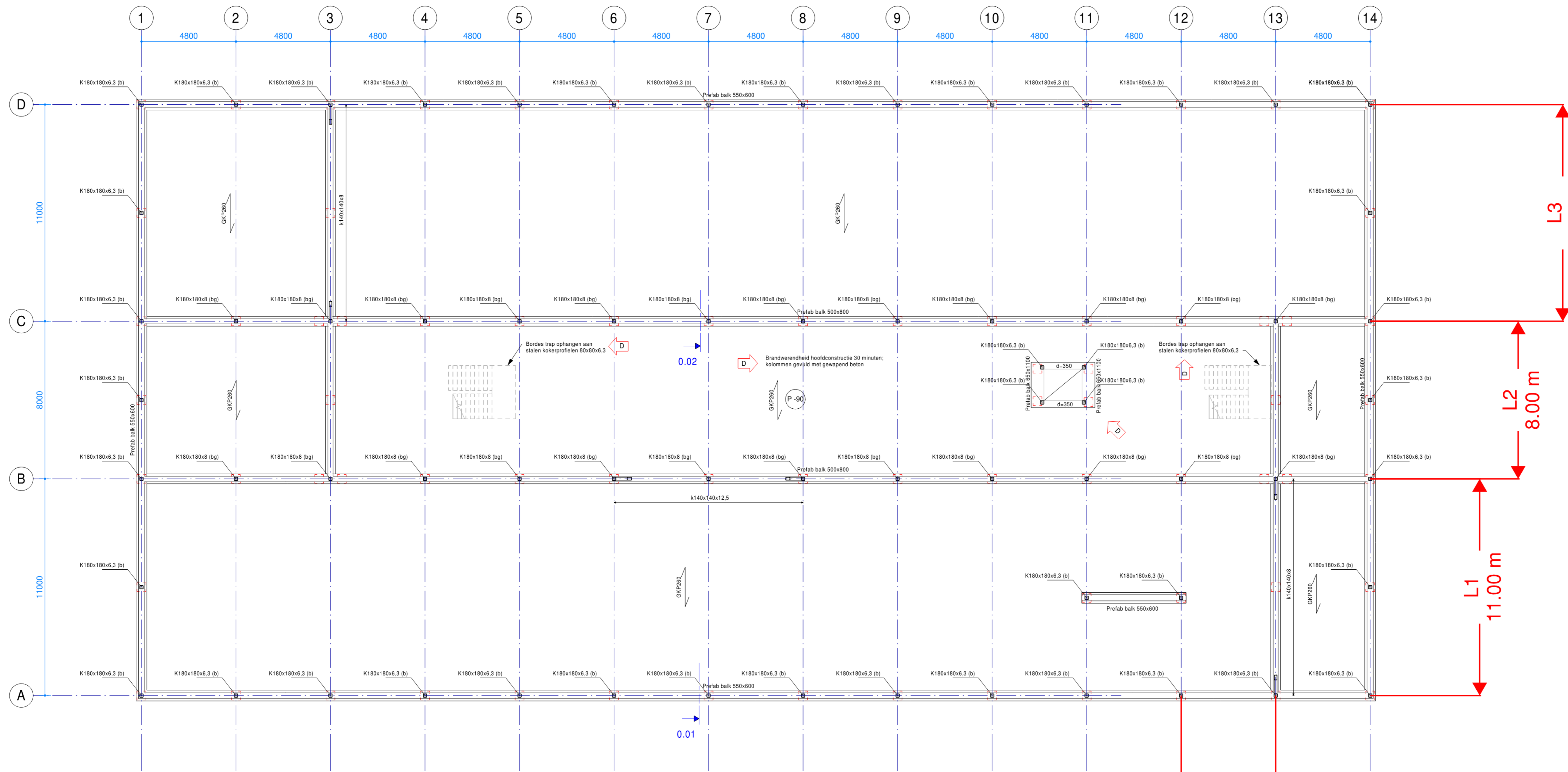
: papierformaat

: datum

DO 3D1V-B

: fase-tekeningnaam-versie

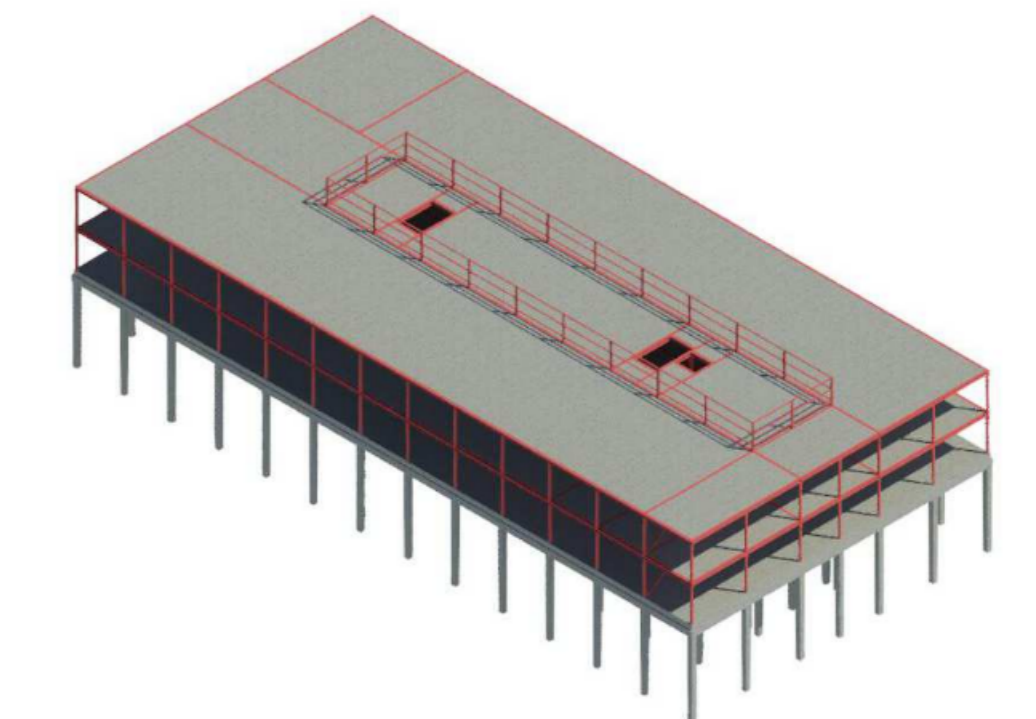
B.3. Ground floor plan



(b) kolommen (180x180x6,3) met beton gevuld (betonkwaliteit C30/37 en wapening 4ø12, c=30mm)
 (bg) kolommen (180x180x8) met beton gevuld (betonkwaliteit C35/45 en wapening 4ø20, c=30mm)

- ← wvb / wvb → Windverband naar bovenliggende verdieping / Windverband naar onderliggende verdieping
- K4 / K3 K4 = kolom boven de vloer / K3 = kolom onder de vloer
- GKP <a> Overspanningsrichting geïsoleerde kanaalplaatvloer d=<a>
- D Vloerluiken en doorvoeren installaties conform bouwkundige tekeningen

Voor constructieve uitgangspunten zie rapport 5015-DO-01



IMd

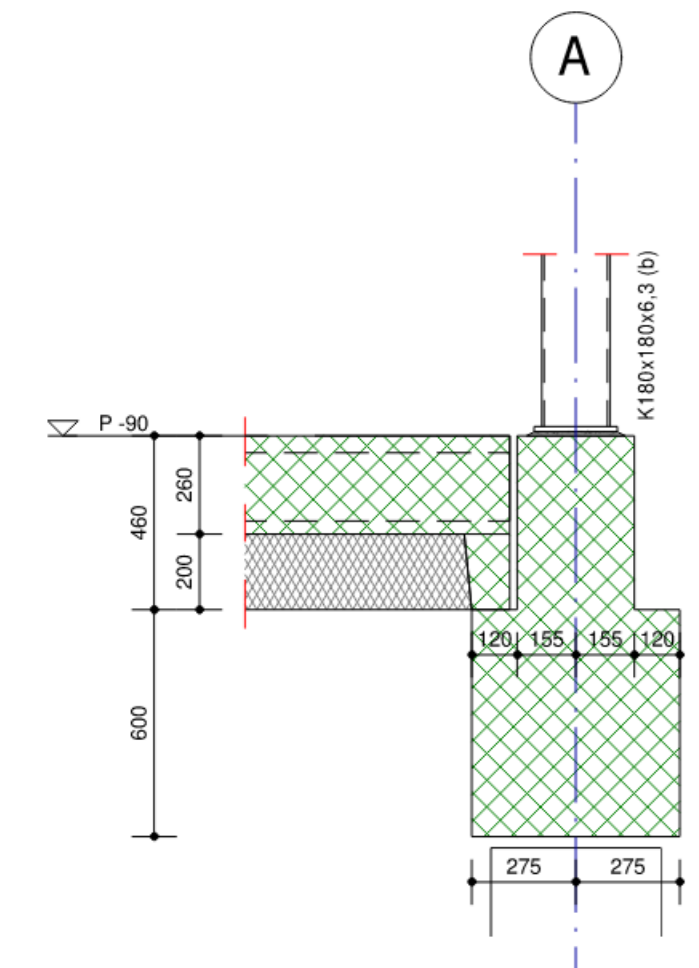
Raadgevende Ingenieurs

Postbus 50521
 3007 JA Rotterdam
 Plekstraat 77
 3071 EL Rotterdam
 t 010 201 23 60
 e imd@imdbv.nl
 www.imdbv.nl

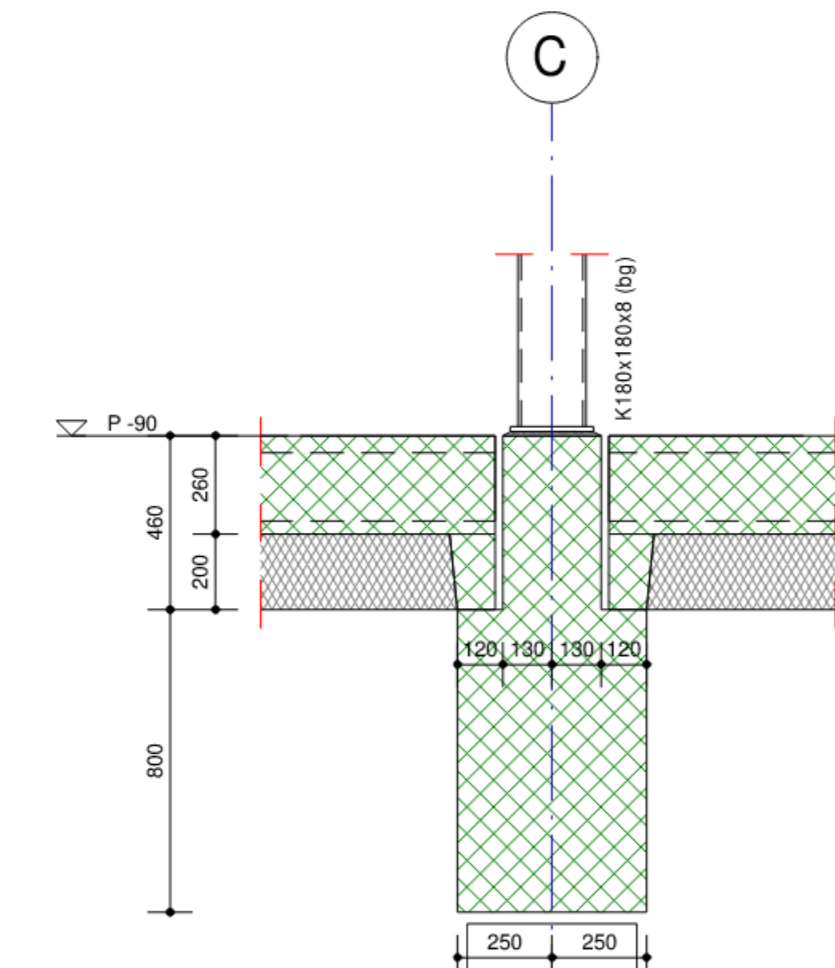
- : project
- : opdrachtgever
- : architect
- : projectnummer
- : projectleider
- : projectkenaar
- : omschrijving wijziging
- : datum wijziging

Plattegrond begane grond : onderdeel
 1:100 : schaal
 A1+ [1051x594] : papierformaat
 : datum

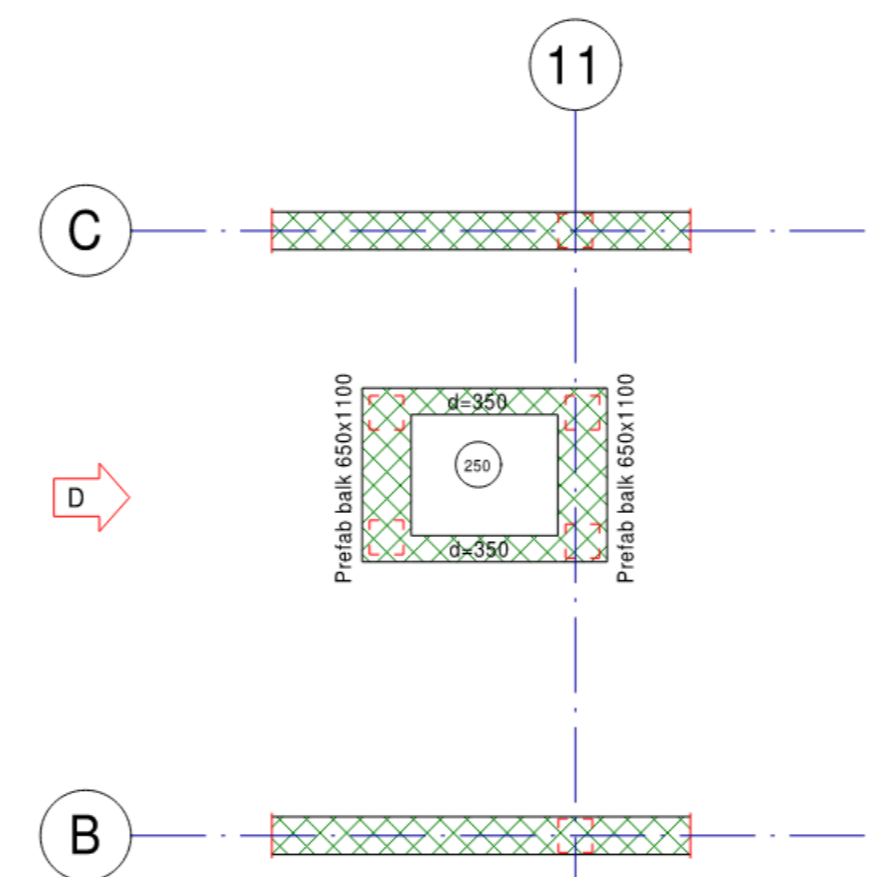
DO 0.01V-D : fase-tekeningnaam-versie



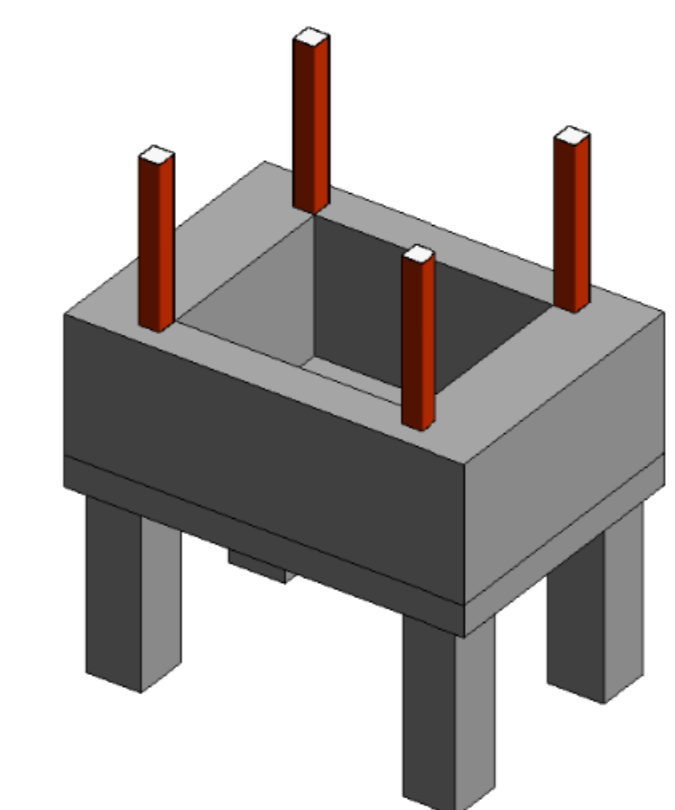
Principle detail 0.01
 Schaal: 1 : 20



Principle detail 0.02
 Schaal: 1 : 20

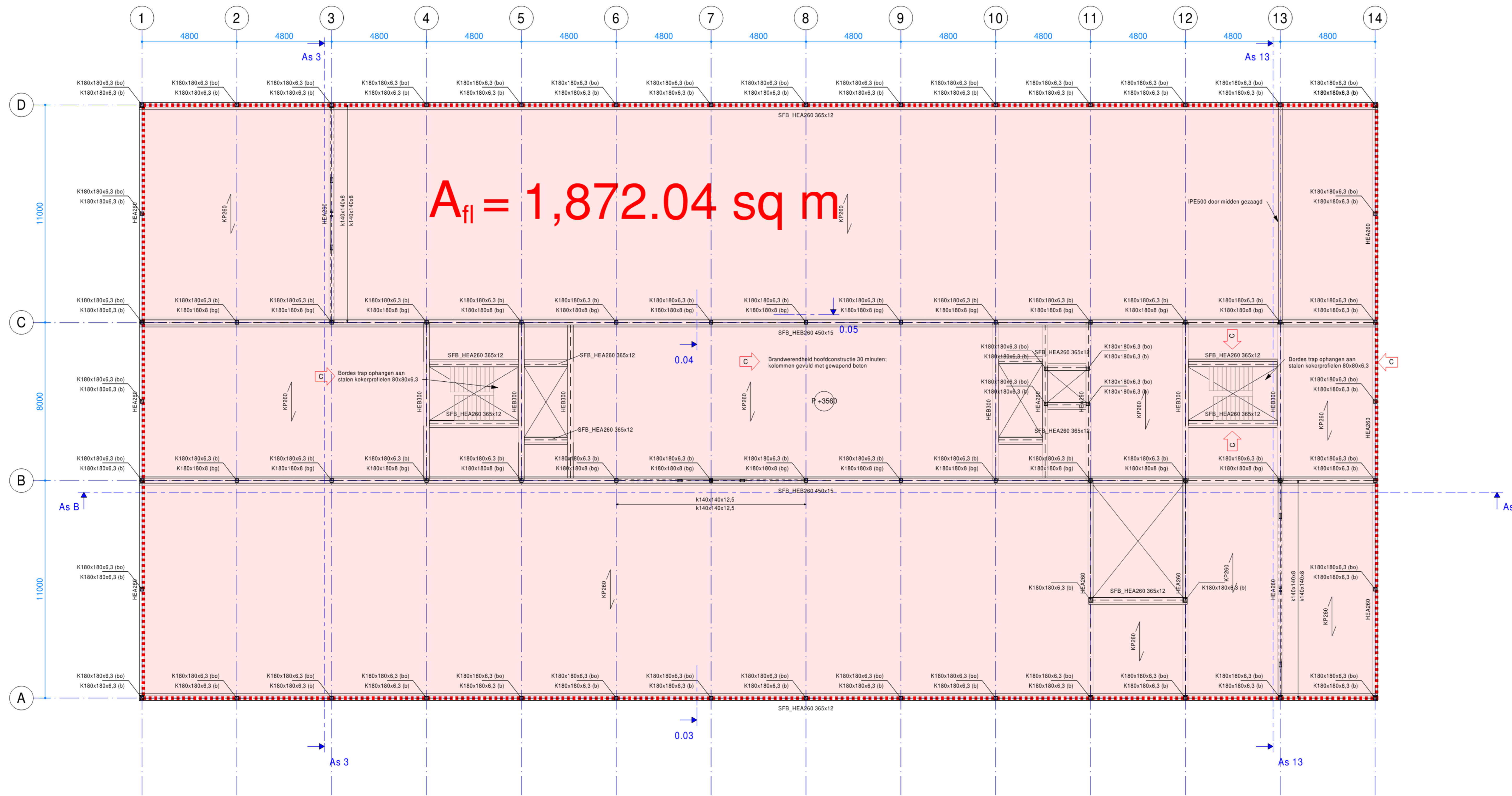


Plattgrond liftput
 Schaal: 1 : 100

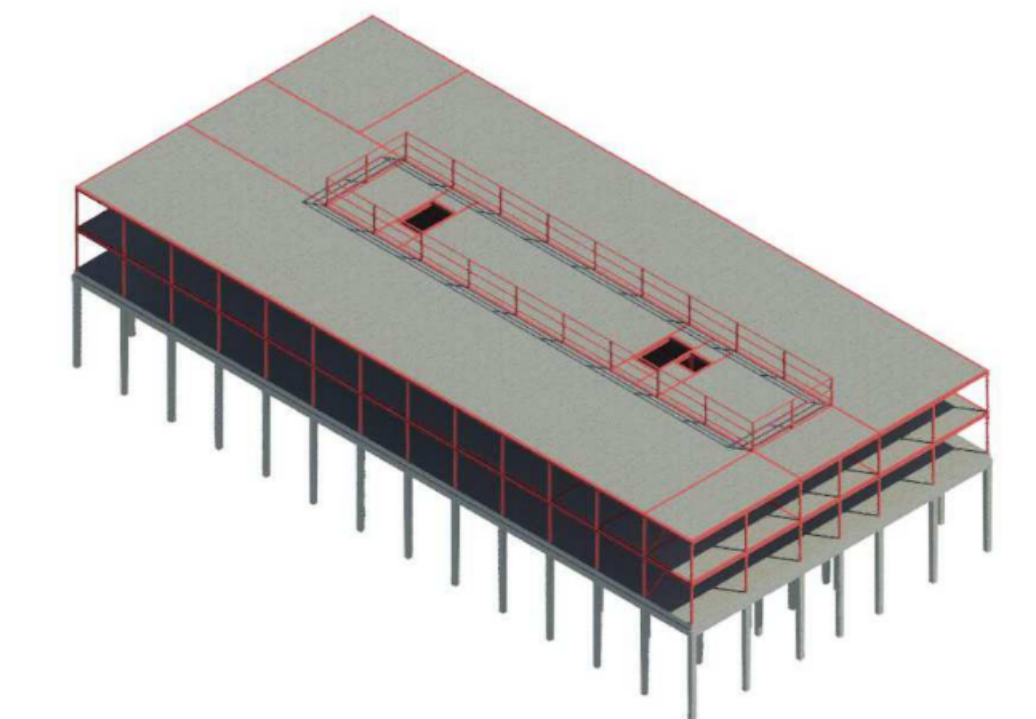


D

B.4. First floor plan



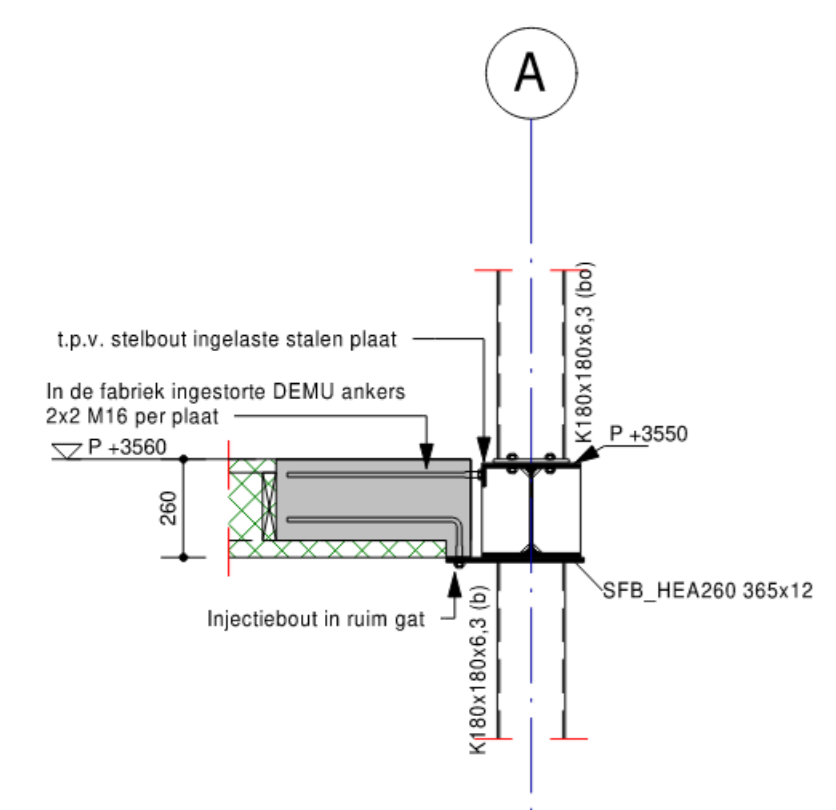
- (bo) kolommen (180x180x6,3) beton gevuld (betonkwaliteit C30/37 en ongewapend)
- (b) kolommen (180x180x6,3) beton gevuld (betonkwaliteit C30/37 en wapening 4ø 12, c=30mm)
- (bg) kolommen (180x180x8) beton gevuld (betonkwaliteit C35/45 en wapening 4ø 20, c=30mm)
- ← wvb → Windverband naar bovenliggende verdieping
- ← wv → Windverband naar onderliggende verdieping
- K4 K3 K4 K3 K4 K3
- K4 = kolom boven de vloer
- K3 = kolom onder de vloer
- GKP <a> Overspanningsrichting geïsoleerde kanaalplaatvloer d=<a>
- KP <a> Overspanningsrichting kanaalplaatvloer d=<a>
- ▨ Dragend kalkzandsteen d=214mm tenzij anders aangegeven
- ▨ Uitwerking kalkzandsteen / metselwerk incl. lateien voor leverancier
- Voor constructieve uitgangspunten zie rapport 5015-DO-01



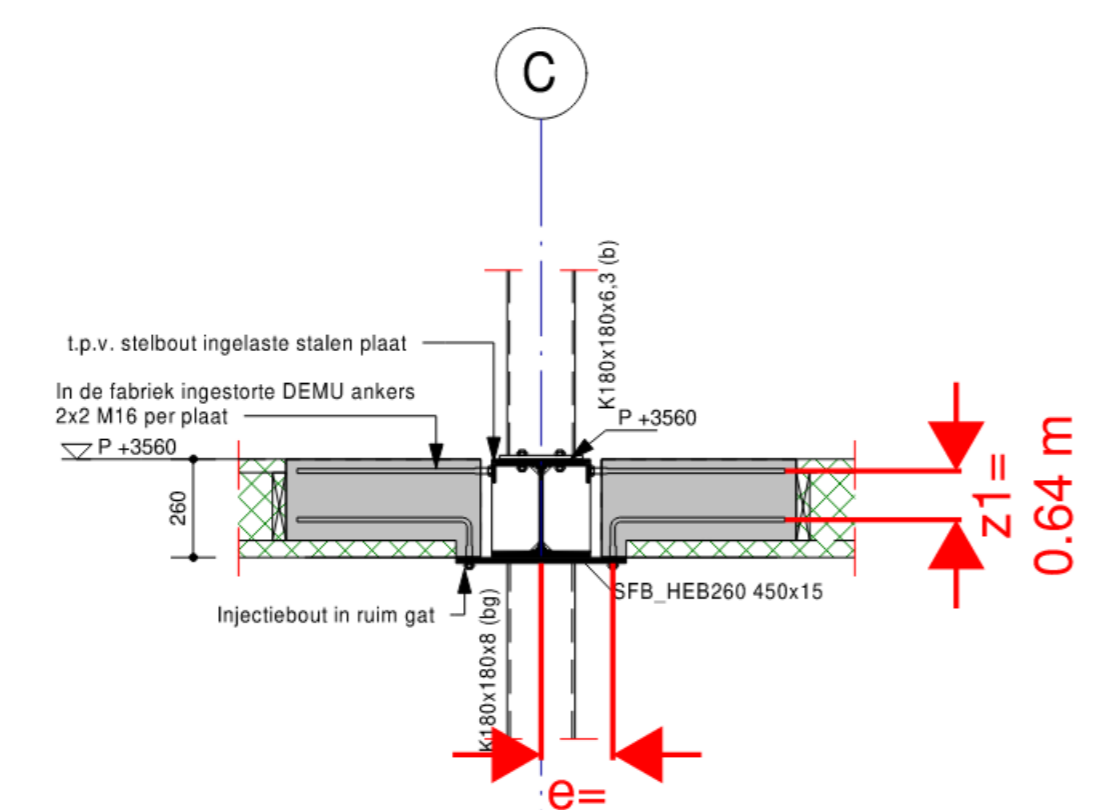
IMd
Raadgevende Ingenieurs

Postbus 50521
3007 JA Rotterdam
Plekstraat 77
3071 EL Rotterdam
t 010 201 23 60
e imd@imdbv.nl
www.imdbv.nl

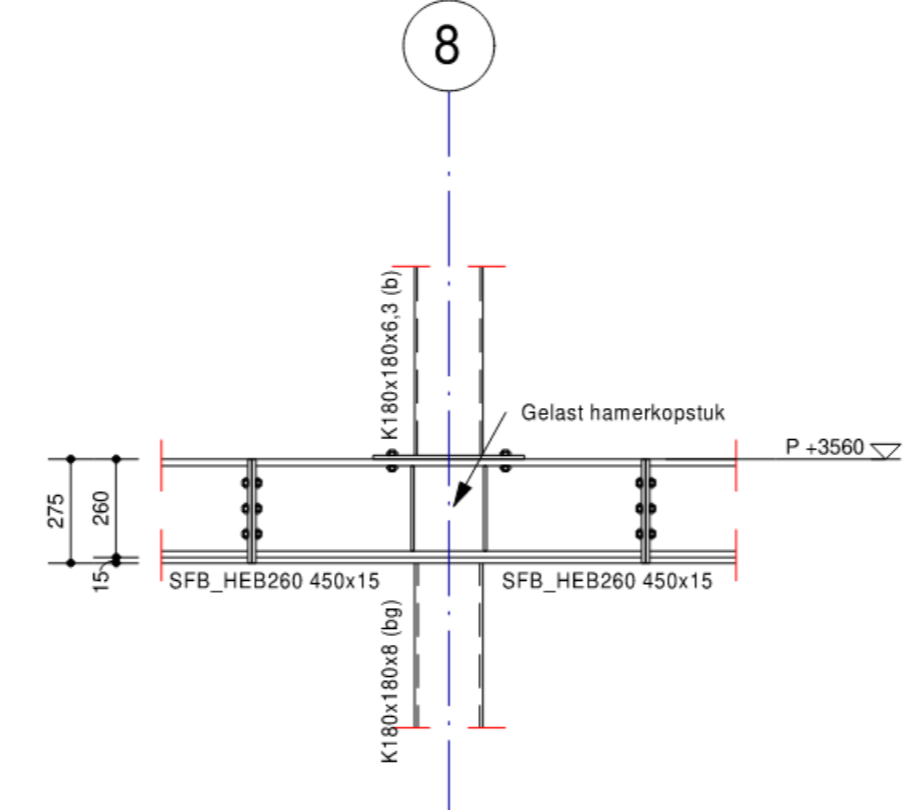
- : project
- : opdrachtgever
- : architect
- : projectnummer
- : projectleider
- : projecttekenaar
- : omschrijving wijziging
- : datum wijziging



Principe detail 0.03
Schaal: 1 : 20



Principe detail 0.04
Schaal: 1 : 20

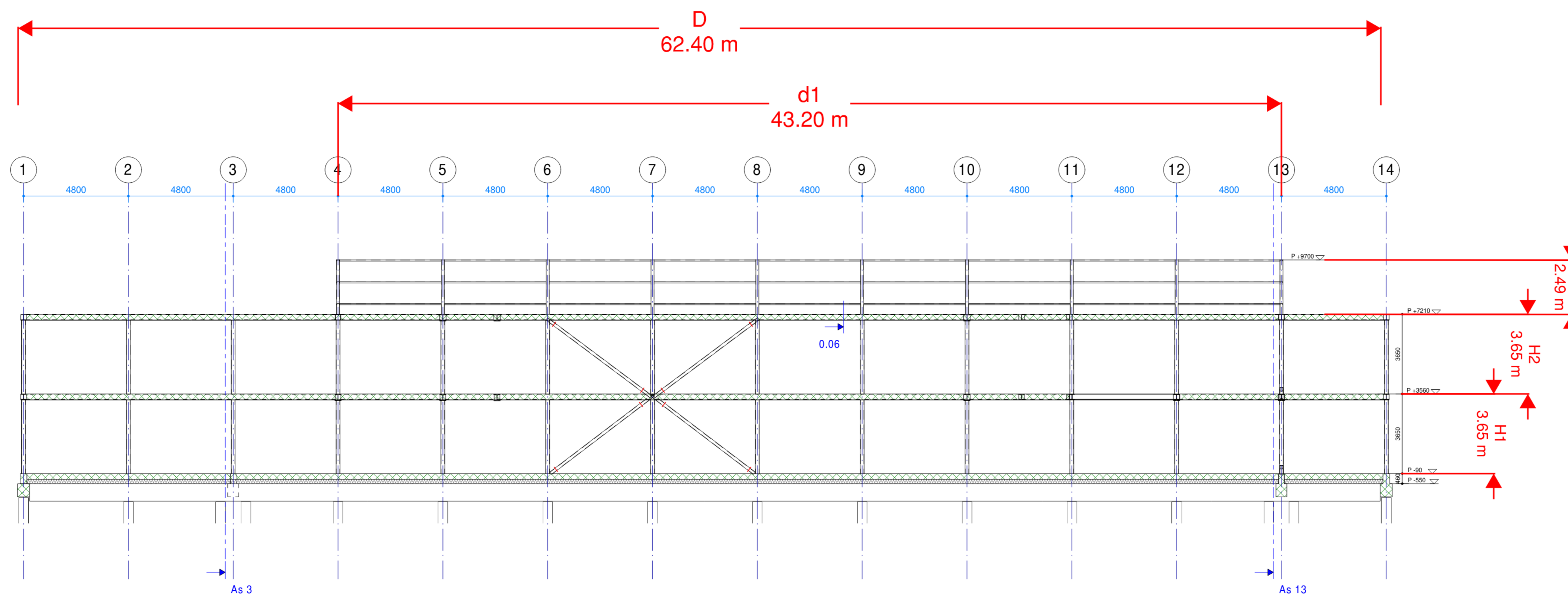


Principe detail 0.05
Schaal: 1 : 20

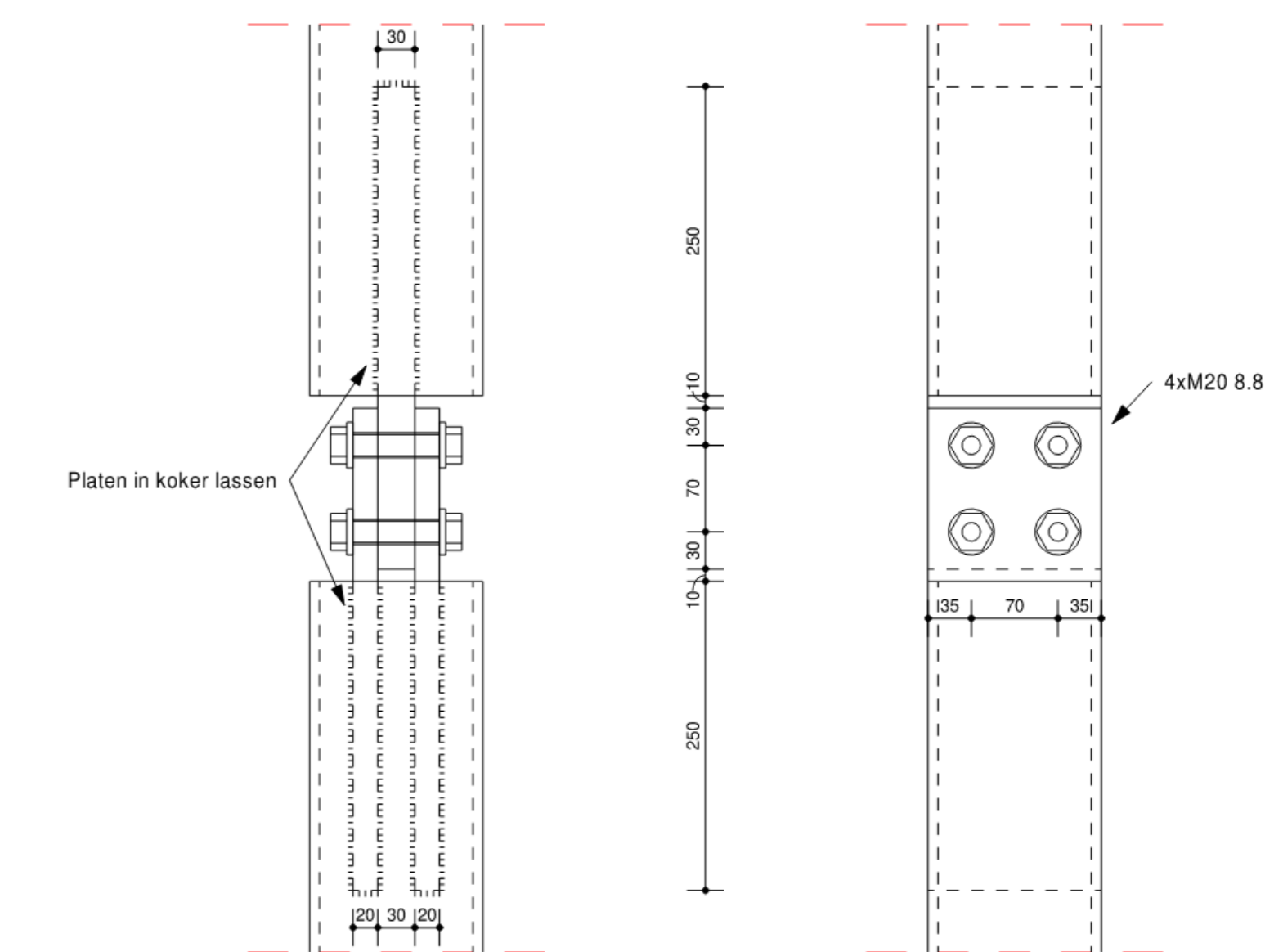
Plattegrond 1e verdieping : onderdeel
1:100 : schaal
A1+ [1051x594] : papierformaat
: datum

DO 1.01V-C : fase-tekeningnaam-versie

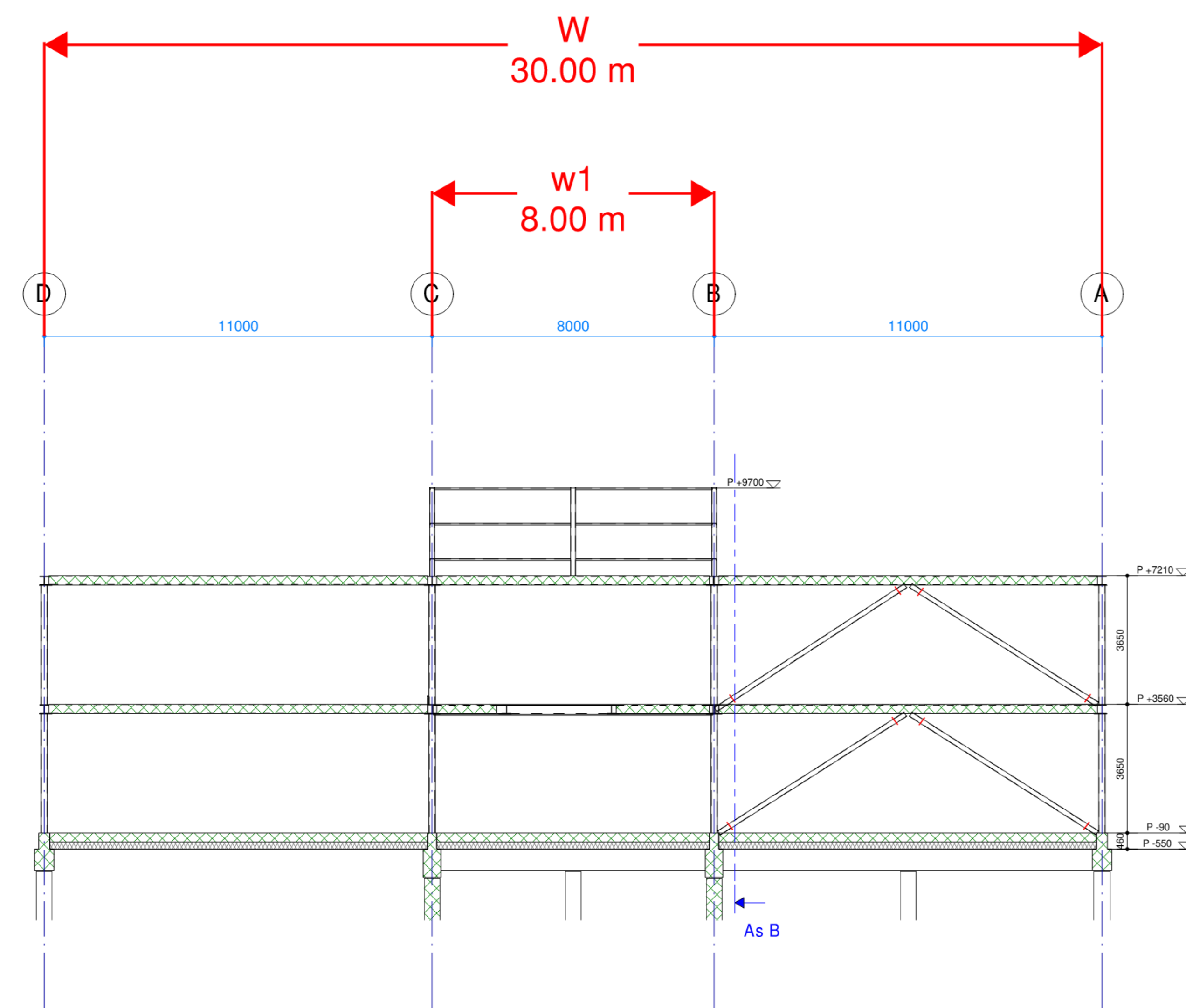
B.5. Cross-sectional views



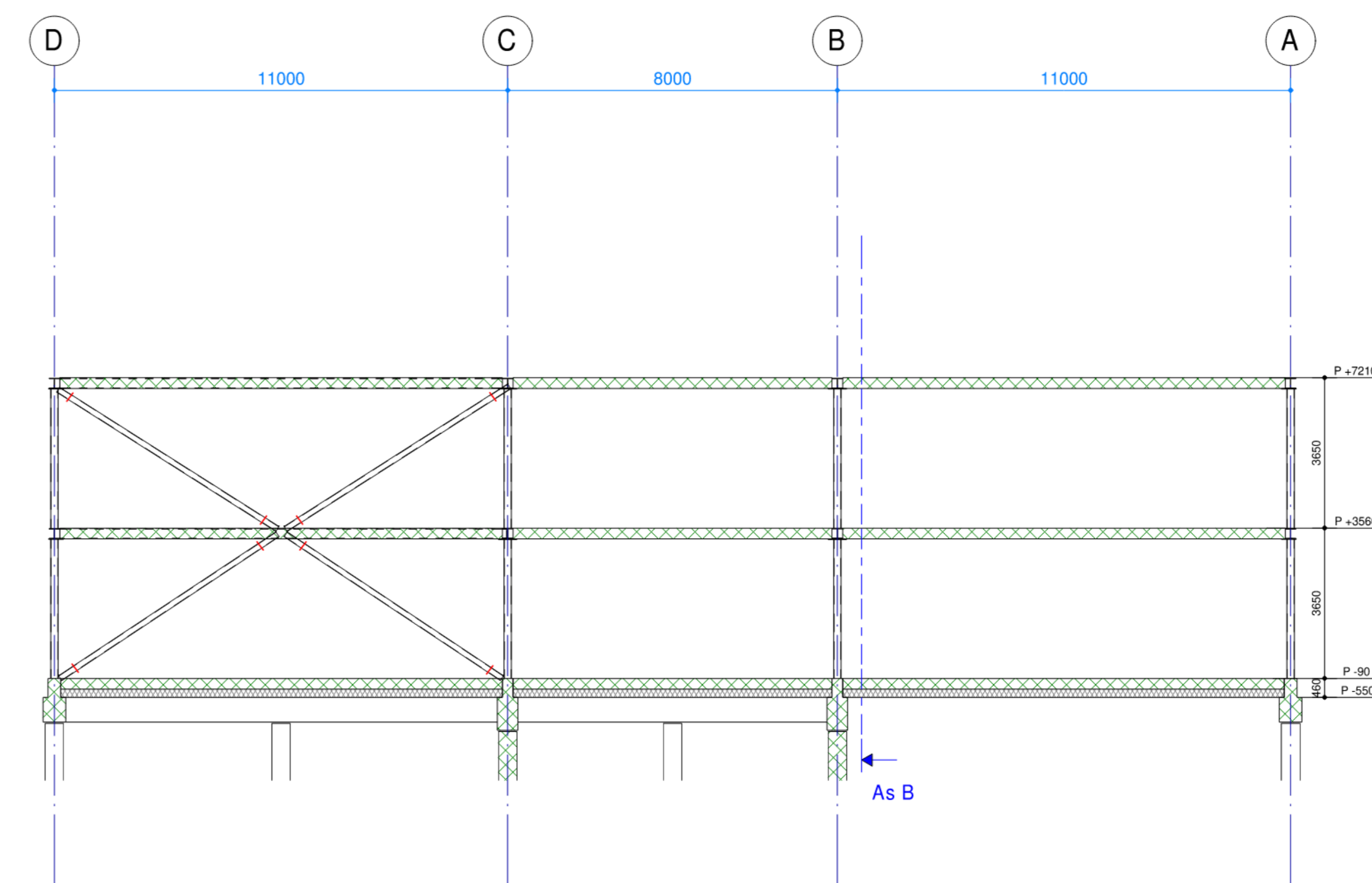
Doorsnede As B
Schaal: 1 : 100



Positie principe aangegeven met rode lijn in doorsnedes
Principe detail aansluiting windverband
Schaal: 1 : 5

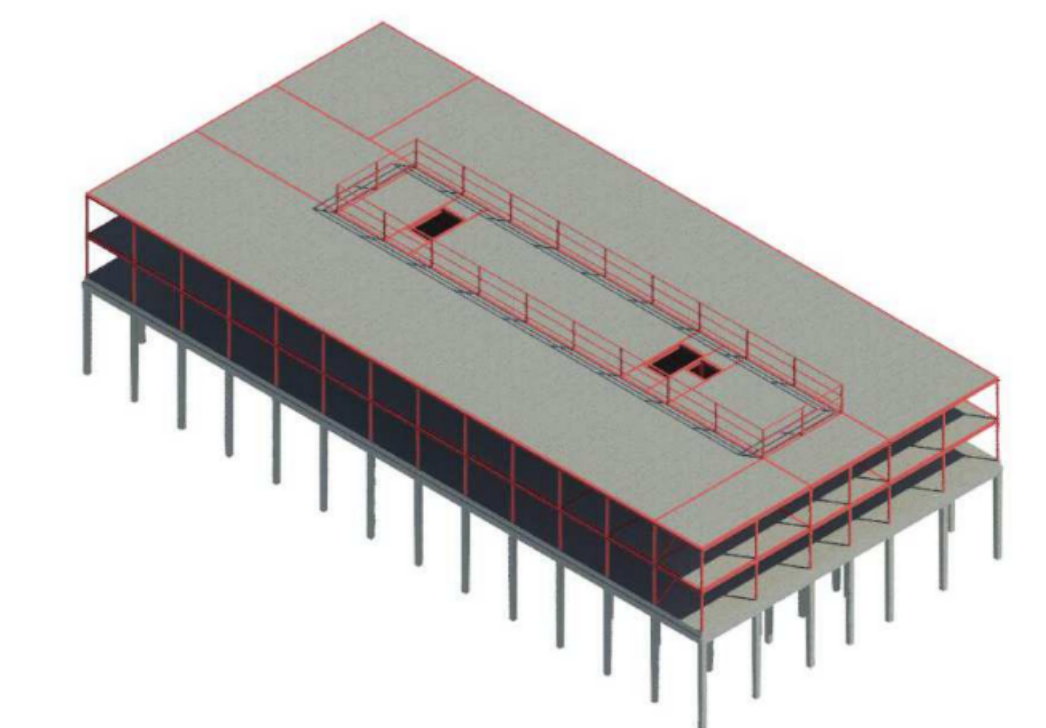


Doorsnede As 13
Schaal: 1 : 100



Doorsnede As 3
Schaal: 1 : 100

Voor constructieve uitgangspunten zie rapport 5015-DO-01



IMd
Raadgevende
Ingenieurs

Postbus 50521
3007 JA Rotterdam
Plekstraat 77
3071 EL Rotterdam
t 010 201 23 60
e imd@imd.nl
www.imd.nl

: project
: opdrachtgever
: architect

: projectnummer
: projectleider
: projectkenaar

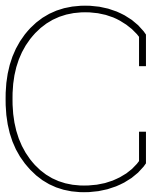
: omschrijving wijziging
: datum wijziging

Doorsnedes windverbanden : onderdeel
1:100 : schaal

A0 [1189x841] : papierformaat

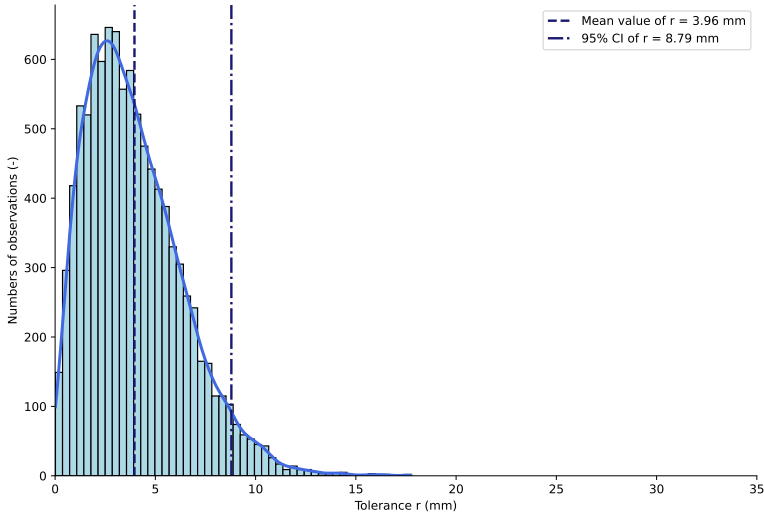
: datum

DO -.01V-B : fase-tekeningnaam-versie

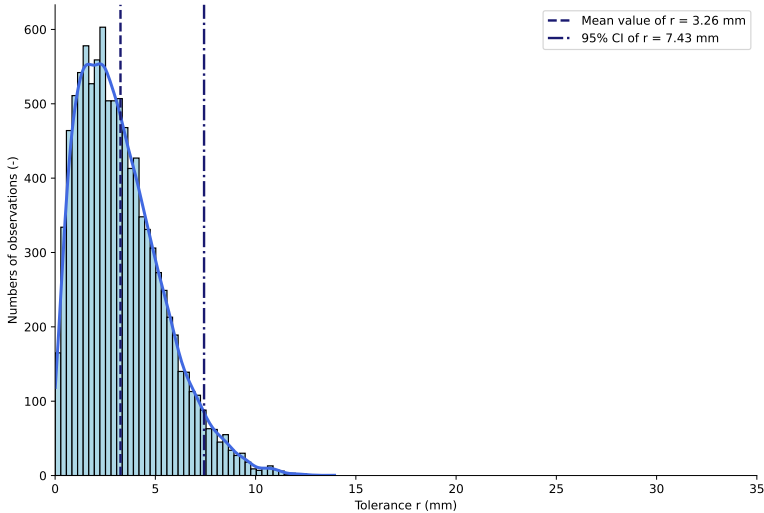


Monte Carlo Simulation

C.1. Simulation results

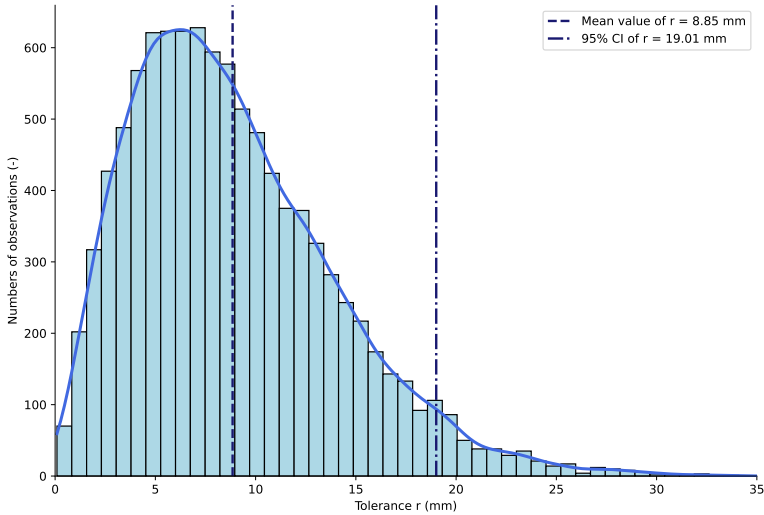


(a) Monte Carlo simulation tolerances EN class 1

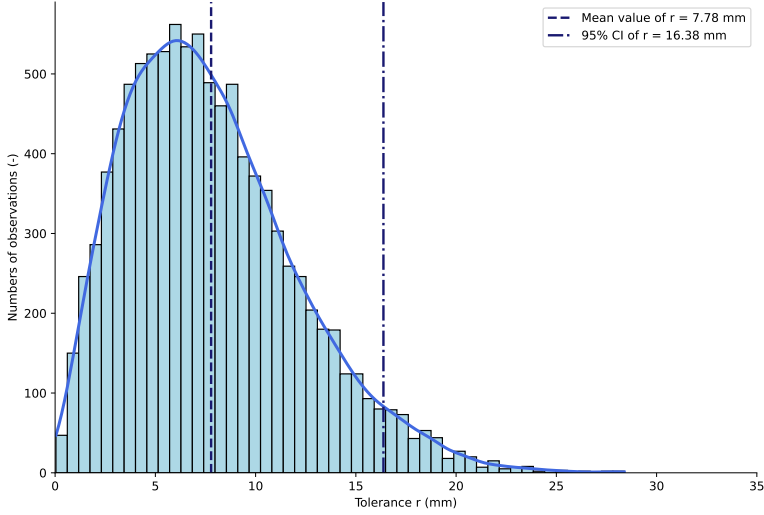


(b) Monte Carlo simulation tolerances EN class 2

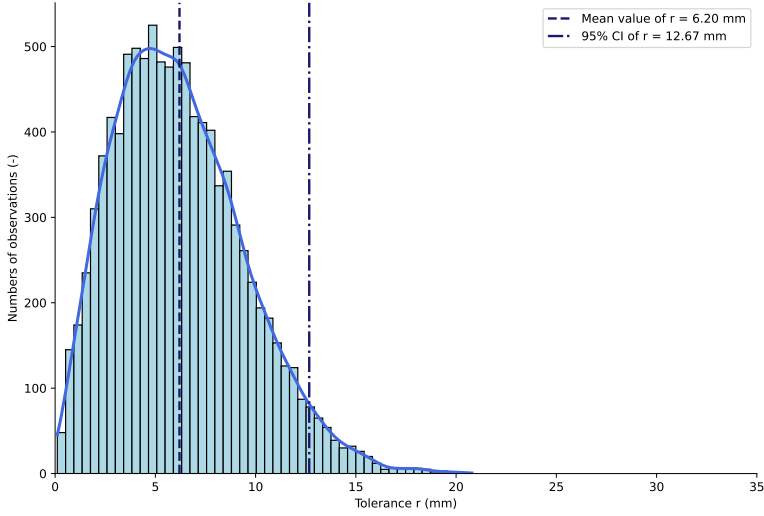
Figure C.1: Monte Carlo simulation with $N = 10^4$ simulations for NEN-EN class 1 and class 2 for a on site installed situation at $y = 0 = L$



(a) Monte Carlo simulation tolerances EN class 1



(b) Monte Carlo simulation tolerances EN class 2



(c) Monte Carlo simulation based on literature and manufacturer data

Figure C.2: Monte Carlo simulation with $N = 10^4$ simulations for NEN-EN class 1, class 2, and literature data for a prefabricated situation at $y = 0 = L$

C.2. Python script

```

1 # Import packages
2 import matplotlib.pyplot as plt
3 import numpy as np
4 import os
5 import seaborn as sns
6
7 # Set the working directory to the "Python graphs" folder
8 os.chdir(r'C:\Users\martel\OneDrive - Delft University of Technology\Documents\TUDelft\Master\
  Thesis\06_Calculations\01_Tolerances\Python_tolerances') # Replace with the actual path
9
10 # Fixed parameters based on Case study geometry
11 N          = 10 ** 4      #Number of simulations
12 B          = 11000       #Slab length
13 L          = 4800        #Beam length
14 n          = 1.96        #Confidence interval: 1.00 (68%), 1.96 (95%) or 2.56 (99%)
15 y          = L           #Most critical location along the beam span
16 d          = 16          #Diameter of the bolt hole for the case study geometry
17
18 # Monte Carlo simulation function, input parameter sets are specified at the bottom of the
  script
19 def generate_plot(delta_bs, delta_hcs_l, delta_hcs_w, delta_oos, R_, D_, filename, on_site,
  delta_oos_literature):
20     if L <= 5000:
21         delta_cs      = 7                #Column spacing L<5000
22     else:
23         delta_cs      = 0.2 * (L / 1000 + 30) #Column spacing L>5000
24
25     #Generating the mean and standard deviation variables based on the input data of the
  function
26
27     #Beam spacing
28     mu_delta_bs      = 0
29     sigma_delta_bs   = delta_bs / n
30
31     #Column spacing
32     mu_delta_cs      = 0
33     sigma_delta_cs   = delta_cs / n
34
35     #Hollow core slab length
36     mu_delta_hcs_l   = 0
37     sigma_delta_hcs_l = delta_hcs_l / n
38
39     #Hollow core slab width
40     mu_delta_hcs_w   = 0
41     sigma_delta_hcs_w = delta_hcs_w / n
42
43     #Beam out-of-straightness
44     if delta_oos_literature:
45         mu_delta_oos   = L / 1774
46         sigma_delta_oos = L / 2558
47     else:
48         mu_delta_oos   = 0
49         sigma_delta_oos = delta_oos / n
50
51     #Bolt hole location
52     mu_R              = 0.00
53     sigma_R           = R_ / n
54
55     #Shear connector location
56     mu_D              = 0.00
57     sigma_D           = D_ / n
58
59     #Array of random variables with length N
60     delta_X_A         = np.random.normal(mu_delta_bs, sigma_delta_bs, N)
61     delta_X_B         = np.random.normal(mu_delta_bs, sigma_delta_bs, N)
62     alpha             = np.random.uniform(0, 1, N)
63     beta              = np.random.uniform(0, 1, N)
64
65     #Column location in x direction

```

```

66 delta_X_C1      = alpha * delta_X_A
67 delta_X_C2      = (1 - alpha) * delta_X_A
68 delta_X_C3      = beta * delta_X_B
69 delta_X_C4      = (1 - beta) * delta_X_B
70
71 #Array of random variables with length N
72 delta_Y_1       = np.random.normal(mu_delta_cs, sigma_delta_cs, N)
73 delta_Y_2       = np.random.normal(mu_delta_cs, sigma_delta_cs, N)
74
75 #Column location in the y direction, the beam is assumed to be axial stiff so identical y
    positioning
76 delta_Y_C1      = delta_Y_1
77 delta_Y_C2      = delta_Y_2
78 delta_Y_C3      = delta_Y_1
79 delta_Y_C4      = delta_Y_2
80
81 #Empty array
82 delta_X_L       = []
83 delta_X_R       = []
84
85 #Tolerances for the left and right beam in y direction
86 delta_Y_L       = delta_Y_1
87 delta_Y_R       = delta_Y_2
88
89 #For loop with conditions that prescribe 3 tolerance scenarios in x direction to fill the
    empty array
90 for i in range(0, N):
91     if delta_X_A[i] > delta_X_B[i]:
92         delta_X_L.append(delta_X_C1[i] + (delta_X_C3[i] - delta_X_C1[i]) * y / L)
93         delta_X_R.append(delta_X_C2[i] - (delta_X_C2[i] - delta_X_C4[i]) * y / L)
94     elif delta_X_A[i] < delta_X_B[i]:
95         delta_X_L.append(delta_X_C1[i] - (delta_X_C1[i] - delta_X_C3[i]) * y / L)
96         delta_X_R.append(delta_X_C2[i] + (delta_X_C4[i] - delta_X_C2[i]) * y / L)
97     else:
98         delta_X_L.append(delta_X_C1[i])
99         delta_X_R.append(delta_X_C2[i])
100
101 #Array of random variables with length N for the hollow core slab length and width
102 delta_X_hcs     = np.random.normal(mu_delta_hcs_l, sigma_delta_hcs_l, N)
103 delta_Y_hcs     = np.random.normal(mu_delta_hcs_w, sigma_delta_hcs_w, N)
104
105 #Array of random variables with length N for the beam out-of-straightness
106 delta_oos       = np.random.normal(mu_delta_oos, sigma_delta_oos, N)
107
108 #Array of random variables with length N for the bolt hole location
109 R               = np.random.normal(mu_R, sigma_R, N)
110 theta           = np.random.uniform(0, 2 * np.pi, N)
111
112 #Array of random variables with length N for the shear connector location
113 D               = np.random.normal(mu_D, sigma_D, N)
114 omega           = np.random.uniform(0, 2 * np.pi, N)
115
116 #On-site or prefabricated installation scenario conditions
117 if on_site:
118     # On_site installation calculation
119     deltaX_beam = delta_X_L
120     deltaY_beam = delta_Y_L
121     deltaX_slab = np.zeros(N)
122     deltaY_slab = np.zeros(N)
123 else:
124     # Prefabricated calculation
125     deltaX_beam = delta_X_L + R * np.cos(theta) + delta_oos * np.cos(np.pi * y / L)
126     deltaY_beam = delta_Y_L + R * np.sin(theta)
127     deltaX_slab = delta_X_hcs / 2 + D * np.cos(omega)
128     deltaY_slab = delta_Y_hcs + D * np.sin(omega)
129
130 #Total required tolerance calculation for N simulations
131 r_x = deltaX_beam - deltaX_slab
132 r_y = deltaY_beam - deltaY_slab
133 r = np.sqrt(r_x ** 2 + r_y ** 2)
134

```

```

135 #Calculation of the mean and standard deviation values for the arrays with length N
136 mean_r = np.mean(r)
137 sd_r   = np.std(r)
138
139 #Plot code
140 sns.displot(r, bins=50, kde=True, color="#4169E1", facecolor="lightblue", edgecolor='k',
141            linewidth=1, line_kws={"linewidth": 2.5}, height=6, aspect=1.5)
142
143 plt.xlabel("Tolerance_r(mm)")
144 plt.ylabel("Numbers_of_observations(-)")
145 plt.axvline(mean_r, color='midnightblue', label=f"Mean_value_of_r={mean_r:.1f}mm",
146            linestyle="--", linewidth=2)
147 plt.axvline(mean_r + 2 * sd_r, color='midnightblue', label=f"95%CI_of_r={mean_r+2*sd_r:.1f}mm",
148            linestyle="-.", linewidth=2)
149
150 plt.xlim(0, 35)
151 plt.legend()
152 plt.savefig(filename, dpi=300, format="pdf", bbox_inches="tight")
153 plt.close()
154
155 # Parameters for specific simulations, here the different input tolerances are specified to
156 # generate different results
157 parameter_sets = [
158     {'delta_bs': 10, 'delta_hcs_l': 25, 'delta_hcs_w': 5, 'R_': 2, 'D_': 1/4 * 25.4, 'delta_oos':
159     L/500, 'filename': 'prefabricated_simulation_1.pdf', 'on_site': False, '
160     delta_oos_literature': False},
161     {'delta_bs': 5, 'delta_hcs_l': 25, 'delta_hcs_w': 5, 'R_': 1, 'D_': 1/4 * 25.4, 'delta_oos': L
162     /1000, 'filename': 'prefabricated_simulation_2.pdf', 'on_site': False, '
163     delta_oos_literature': False},
164     {'delta_bs': 5, 'delta_hcs_l': 10, 'delta_hcs_w': 5, 'R_': 0.1, 'D_': 1/4 * 25.4, 'delta_oos':
165     L/10000, 'filename': 'prefabricated_simulation_3.pdf', 'on_site': False, '
166     delta_oos_literature': True},
167     {'delta_bs': 10, 'delta_hcs_l': 25, 'delta_hcs_w': 5, 'R_': 2, 'D_': 1/4 * 25.4, 'delta_oos':
168     L/500, 'filename': 'on_site_simulation_1.pdf', 'on_site': True, 'delta_oos_literature'
169     : False},
170     {'delta_bs': 5, 'delta_hcs_l': 25, 'delta_hcs_w': 5, 'R_': 1, 'D_': 1/4 * 25.4, 'delta_oos': L
171     /1000, 'filename': 'on_site_simulation_2.pdf', 'on_site': True, 'delta_oos_literature'
172     : False},
173 ]
174
175 # Generate plots for each parameter set
176 for parameters in parameter_sets:
177     generate_plot(**parameters)

```


D

Stiffness comparison

D.1. Output IDEA StaTiCa

Project: Connection
Project no:
Author: M.W. Wintermans

Project data

Project name: Connection
Project number:
Author: M.W. Wintermans
Description: IMd / TU Delft
Date: 10/30/2023
Code: EN

Material

Steel: S 355

Project: Connection
 Project no:
 Author: M.W. Wintermans

Project item CON9

Design

Name CON9
 Description
 Analysis Stiffness

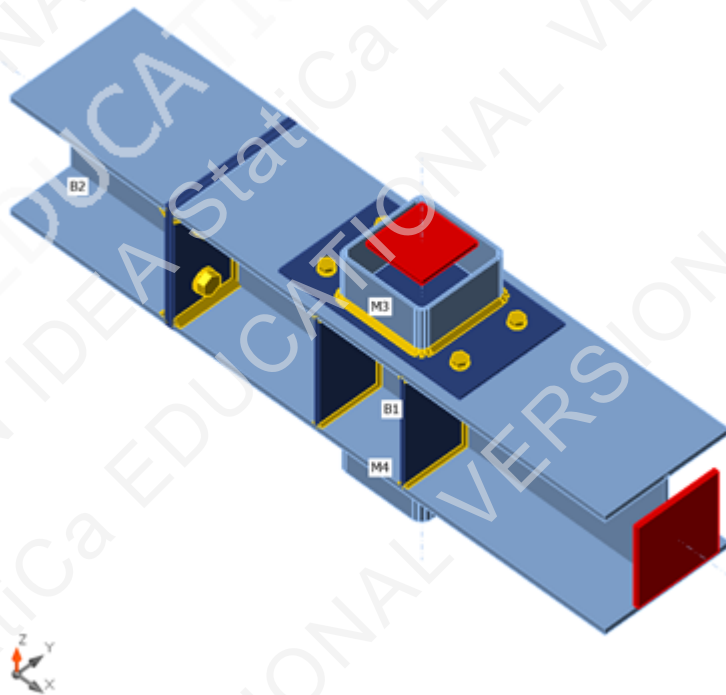
Members

Geometry

Name	Cross-section	β - Direction [°]	γ - Pitch [°]	α - Rotation [°]	Offset ex [mm]	Offset ey [mm]	Offset ez [mm]
B1	8 - HEA260	0.0	0.0	0.0	0	0	0
B2	8 - HEA260	180.0	0.0	0.0	0	0	0
M3	3 - SHS180/180/6.3	0.0	90.0	0.0	0	0	-400
M4	4 - SHS180/180/8.0	0.0	-90.0	0.0	0	0	400

Supports and forces

Name	Support	Forces in	X [mm]
B1 / end	N-Vy-Vz-Mx-My-Mz	Node	0
B2 / end		Bolts	0
M3 / end	N-Vy-Vz-Mx-My-Mz	Node	0
M4 / end	N-Vy-Vz-Mx-My-Mz	Node	0



Cross-sections

Name	Material
8 - HEA260	S 355
3 - SHS180/180/6.3	S 355
4 - SHS180/180/8.0	S 355

Bolts

Name	Bolt assembly	Diameter [mm]	f_u [MPa]	Gross area [mm ²]
M24 8.8	M24 8.8	24	800.0	452
M16 8.8	M16 8.8	16	800.0	201

Load effects

Name	Member	N [kN]	Vy [kN]	Vz [kN]	Mx [kNm]	My [kNm]	Mz [kNm]
LE1	B1 / End	0.0	0.0	0.0	0.0	0.0	0.0
	B2 / End	0.0	0.0	-153.3	30.1	0.0	0.0
	M3 / End	-278.3	0.0	0.0	0.0	0.0	0.0
	M4 / End	-417.4	0.0	0.0	0.0	55.6	27.1
LE2	B1 / End	0.0	0.0	0.0	0.0	0.0	0.0
	B2 / End	0.0	0.0	-65.9	13.0	0.0	0.0
	M3 / End	-278.3	0.0	0.0	0.0	0.0	0.0
	M4 / End	-417.4	0.0	0.0	0.0	55.6	27.1

Check

Rotational stiffness

Name	Comp.	Loads	Mj,Rd [kNm]	Sj,ini [MNm/rad]	Φ_c [mrad]	L [m]	Sj,R [MNm/rad]	Sj,P [MNm/rad]	Class.
B2	Mx	LE1	0.0	0.0	0.0	4.00			
	Mx	LE2	0.0	0.0	0.0	4.00			

Secant rotational stiffness


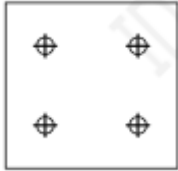




Name	Comp.	Loads	M [kNm]	Sjs [MNm/rad]	Φ [mrad]
B2	Mx	LE1	30.1	0.0	-222.8
	Mx	LE2	13.0	0.0	-89.3

Stiffness diagram Rotational stiffness, LE1

Stiffness diagram Rotational stiffness, LE2

Bill of material

Manufacturing operations

Name	Plates [mm]	Shape	Nr.	Welds [mm]	Length [mm]	Bolts	Nr.
PP1	P10.0x260.0-250.0 (S 355)		1	Fillet: a = 9.0 Fillet: a = 9.0 Double fillet: a = 4.0	520.0 520.0 475.0	M24 8.8	4
	P10.0x260.0-250.0 (S 355)		1				
EP1	P6.0x220.0-380.0 (S 355)		1	Fillet: a = 6.0	672.3	M16 8.8	4
EP2	P10.0x220.0-220.0 (S 355)		1	Fillet: a = 10.0 Fillet: a = 8.0	659.4 880.0		
STIFF1	P8.0x126.3-225.0 (S 355)		2	Double fillet: a = 4.0	955.0		
STIFF2	P8.0x126.3-225.0 (S 355)		2	Double fillet: a = 4.0	955.0		

Project: Connection
 Project no:
 Author: M.W. Wintermans

Welds

Type	Material	Throat thickness [mm]	Leg size [mm]	Length [mm]
Fillet	S 355	9.0	12.7	520.0
Fillet	S 355	9.0	12.7	520.0
Double fillet	S 355	4.0	5.7	2385.0
Fillet	S 355	6.0	8.5	672.3
Fillet	S 355	10.0	14.1	659.4
Fillet	S 355	8.0	11.3	880.0

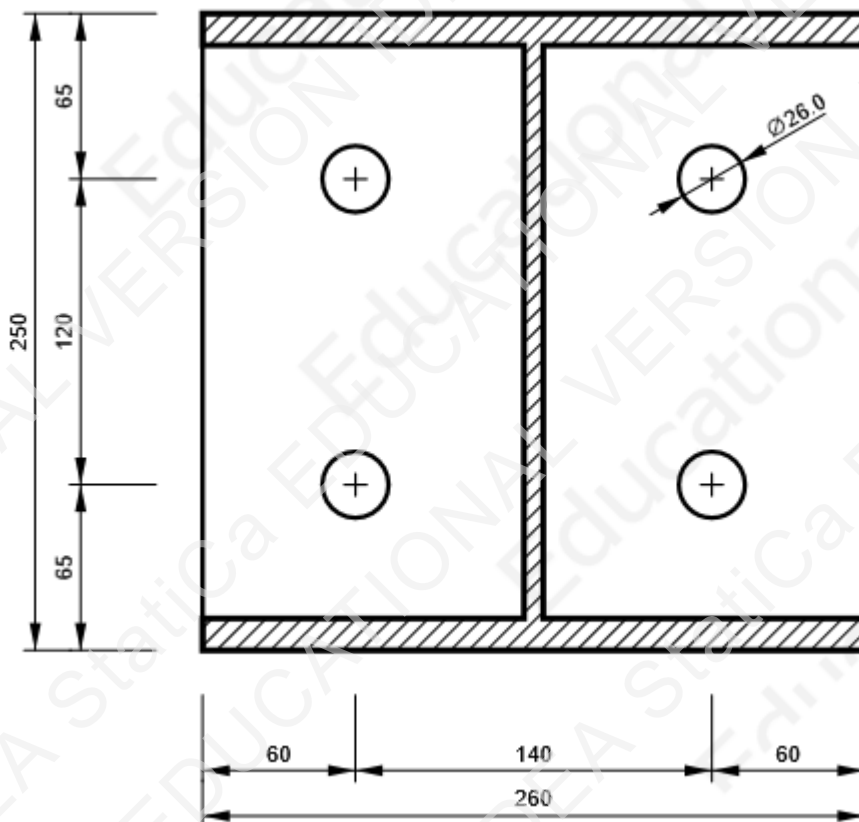
Bolts

Name	Grip length [mm]	Count
M24 8.8	20	4
M16 8.8	19	4

Drawing

PP1 - PP1a

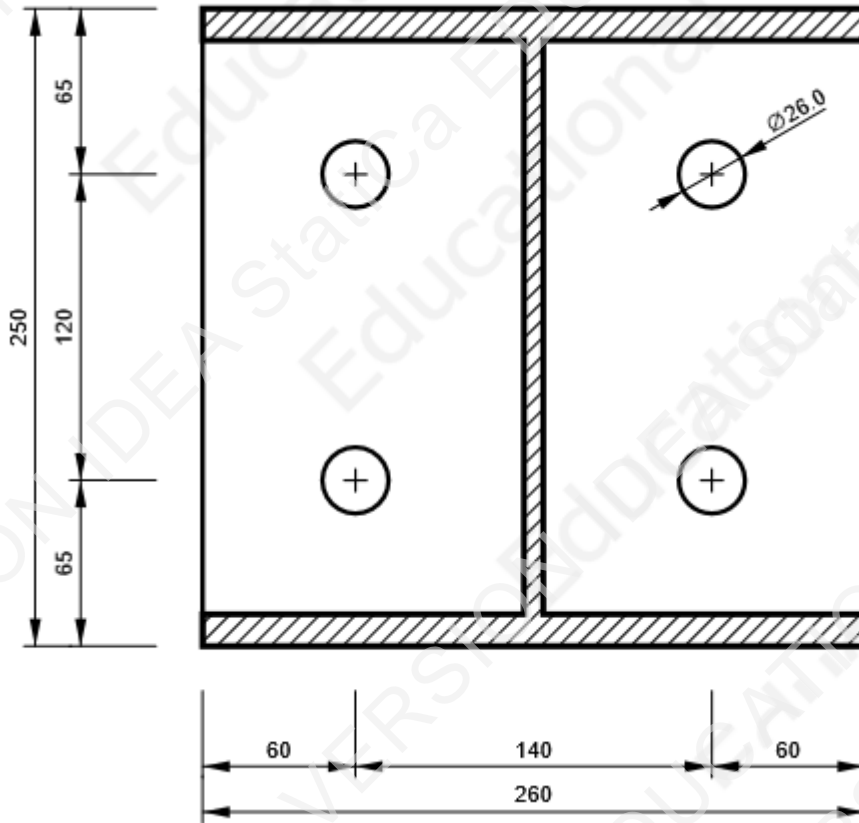
P10.0x250-260 (S 355)



Project: Connection
Project no:
Author: M.W. Wintermans

PP1 - PP1b

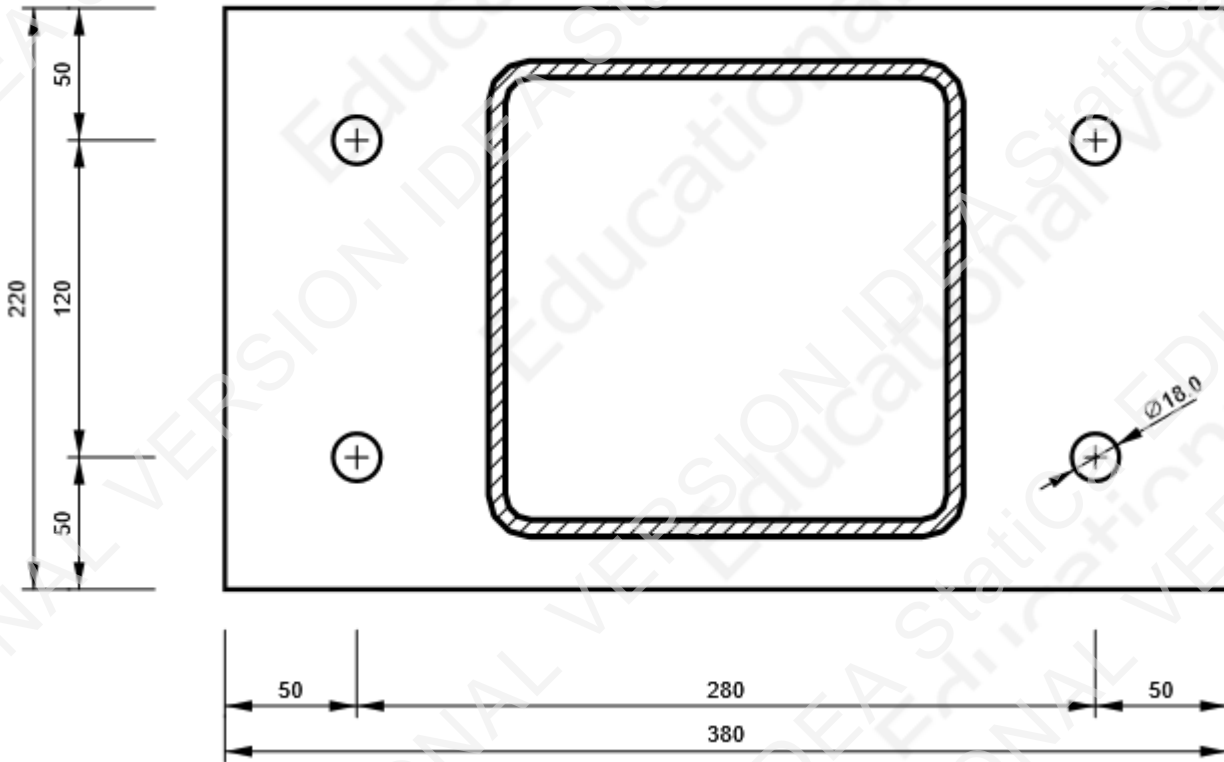
P10.0x250-260 (S 355)



Project: Connection
Project no:
Author: M.W. Wintermans

EP1

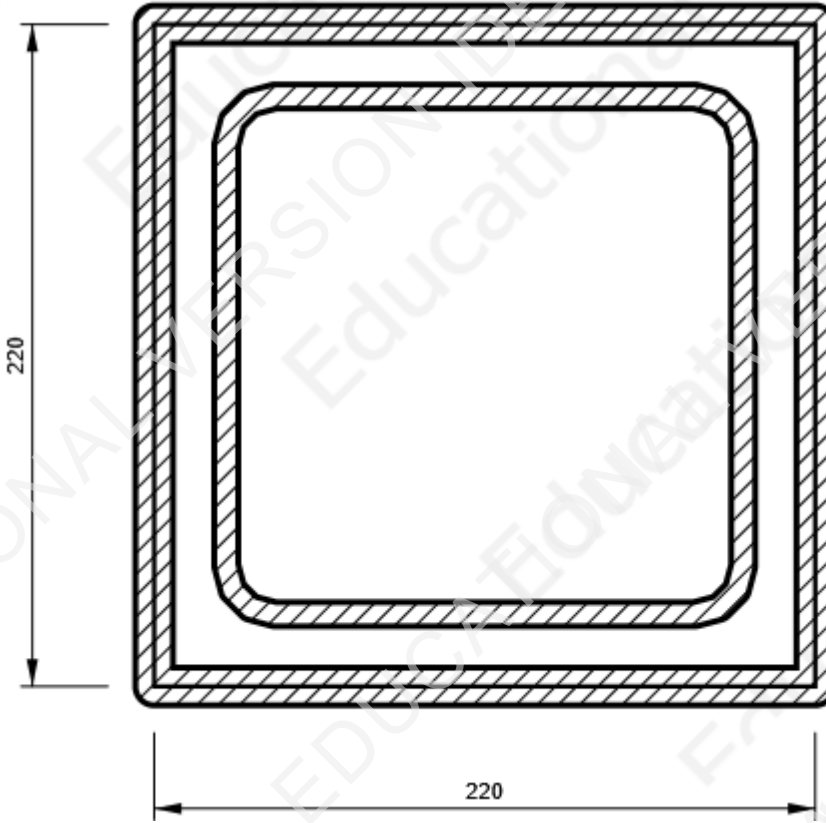
P6.0x380-220 (S 355)



Project: Connection
Project no:
Author: M.W. Wintermans

EP2

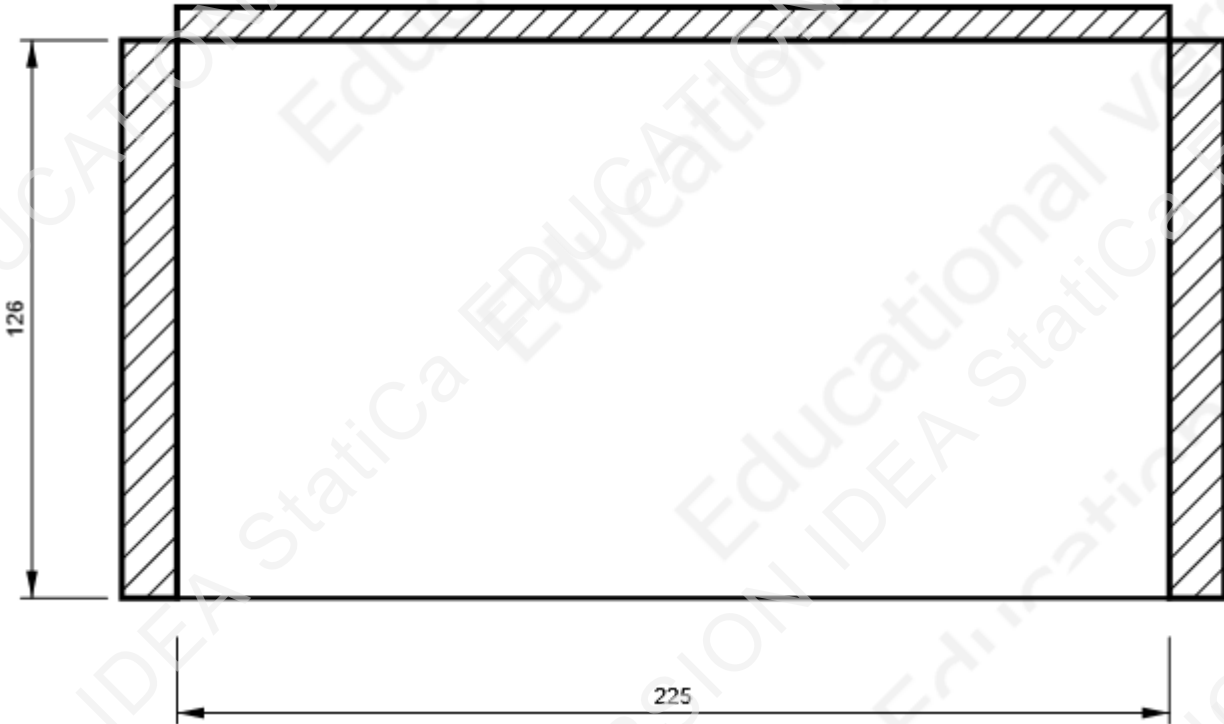
P10.0x220-220 (S 355)



Project: Connection
Project no:
Author: M.W. Wintermans

STIFF1

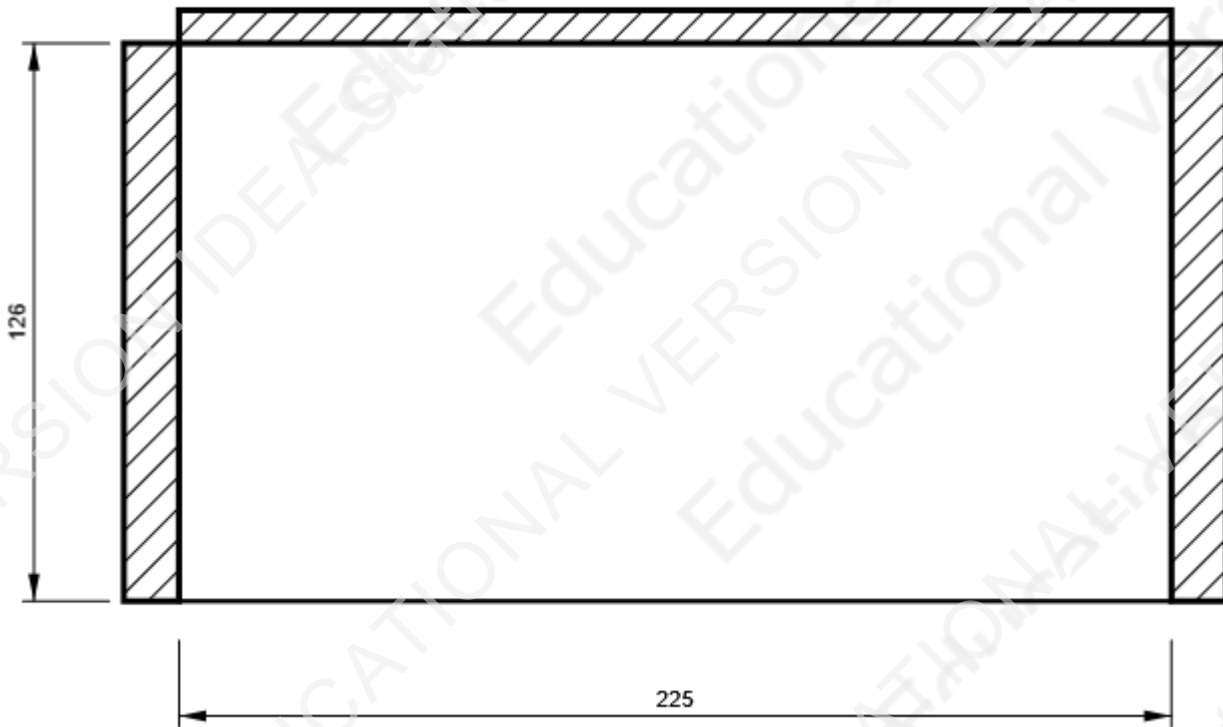
P8.0x225-126 (S 355)



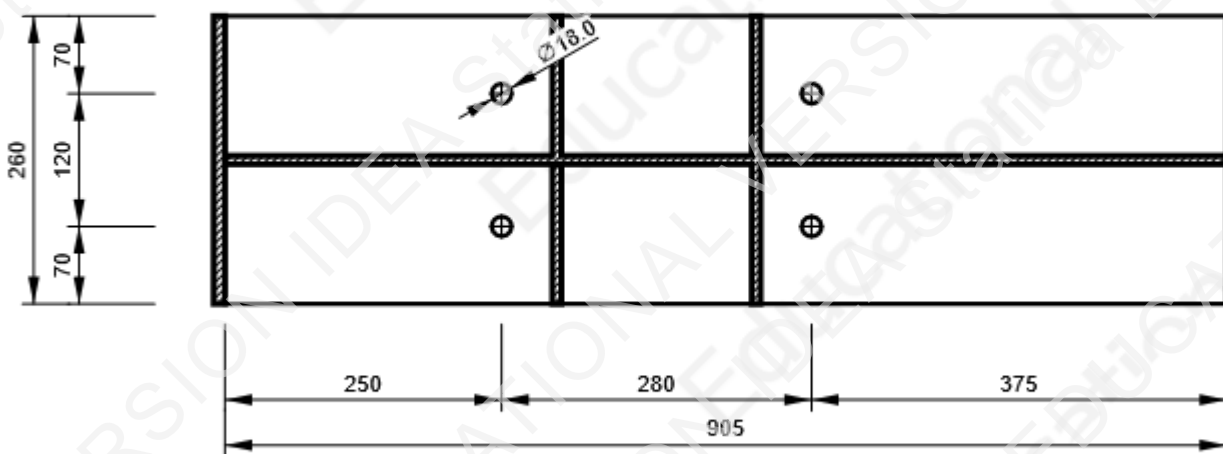
Project: Connection
Project no:
Author: M.W. Wintermans

STIFF2

Ø8.0x225-126 (S 355)



B1, HEA260 - Top flange 1:



Symbol explanation

Symbol	Symbol explanation
$M_{j,Rd}$	Bending resistance
$S_{j,ini}$	Initial rotational stiffness
$S_{j,s}$	Secant rotational stiffness
Φ	Rotational deformation
$S_{j,R}$	Limit value - rigid joint
$S_{j,P}$	Limit value - nominally pinned joint
Φ_C	Rotational capacity

Code settings

Item	Value	Unit	Reference
Safety factor γ_{M0}	1.00	-	EN 1993-1-1: 6.1
Safety factor γ_{M1}	1.00	-	EN 1993-1-1: 6.1
Safety factor γ_{M2}	1.25	-	EN 1993-1-1: 6.1
Safety factor γ_{M3}	1.25	-	EN 1993-1-8: 2.2
Safety factor γ_C	1.50	-	EN 1992-1-1: 2.4.2.4
Safety factor γ_{Inst}	1.20	-	EN 1992-4: Table 4.1
Joint coefficient β_j	0.67	-	EN 1993-1-8: 6.2.5
Effective area - influence of mesh size	0.10	-	
Friction coefficient - concrete	0.25	-	EN 1993-1-8
Friction coefficient in slip-resistance	0.30	-	EN 1993-1-8 tab 3.7
Limit plastic strain	0.05	-	EN 1993-1-5
Detailing	No		
Distance between bolts [d]	2.20	-	EN 1993-1-8: tab 3.3
Distance between bolts and edge [d]	1.20	-	EN 1993-1-8: tab 3.3
Concrete breakout resistance check	Both		EN 1992-4: 7.2.1.4 and 7.2.2.5
Use calculated a_b in bearing check.	Yes		EN 1993-1-8: tab 3.4
Cracked concrete	Yes		EN 1992-4
Local deformation check	No		CIDECT DG 1, 3 - 1.1
Local deformation limit	0.03	-	CIDECT DG 1, 3 - 1.1
Geometrical nonlinearity (GMNA)	Yes		Analysis with large deformations for hollow section joints
Braced system	No		EN 1993-1-8: 5.2.2.5

D.2. Output Maple hollow core slab

```

> restart;
ODE := EI·diff(w(x), x$4) = q :
dsol := dsolve(ODE, w(x)) : assign(dsol) :

```

```

> w := w(x) :
> φ := -diff(w, x) :
κ := diff(φ, x) :
M := EI·κ :
V := diff(M, x) :

```

```

> x := 0 :
eq1 := w = 0 :
eq2 := M = 0 :

x := L :
eq3 := w = 0 :
eq4 := M = 0 :

```

```

> q := 1.2·5.55 + 1.5·3.3 :
L := 11000 :
EI := 36283·1434.9·106 :

```

```

> sol := solve({eq1, eq2, eq3, eq4}, {_C1, _C2, _C3, _C4}) : assign(sol) : x := 'x':

```

```

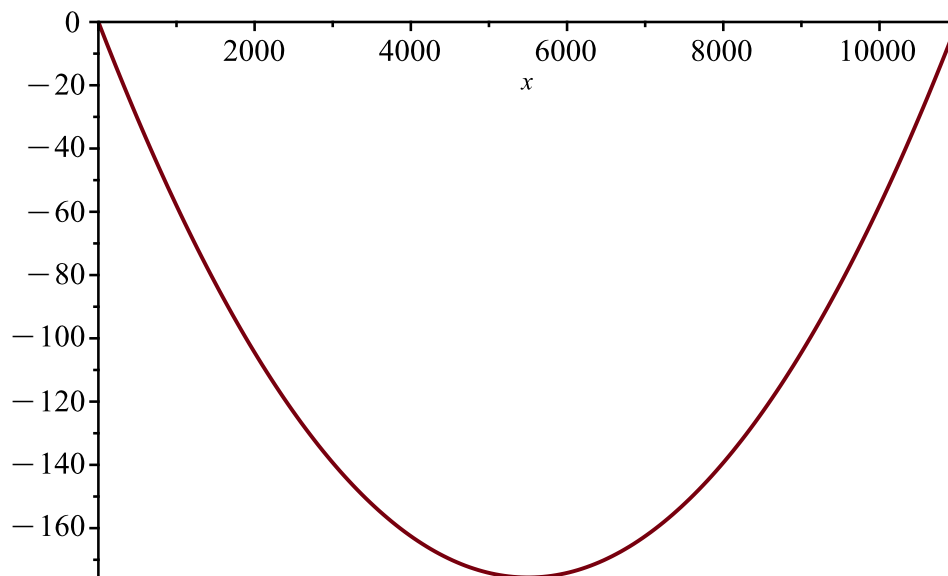
plot(-M·10-6, x = 0..L, size = [500, 300]);
plot(-φ, x = 0..L, size = [500, 300]);

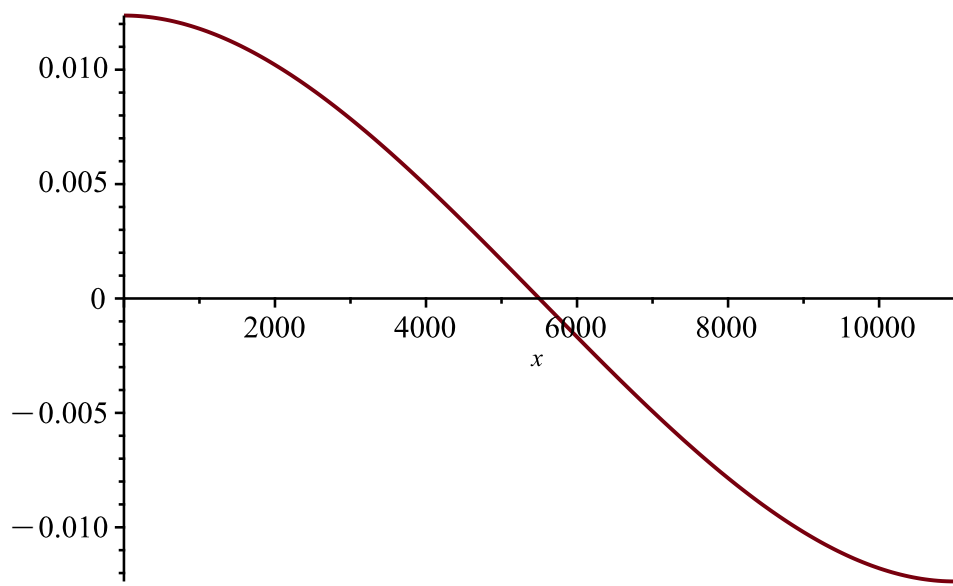
```

```

x := 0 :
-φ·103;

```





12.36728045

(1)


```

> restart;
ODE := EI·diff(w(x), x$4) = q :
dsol := dsolve(ODE, w(x)) : assign(dsol) :

```

```

> w := w(x) :
> φ := -diff(w, x) :
κ := diff(φ, x) :
M := EI·κ :
V := diff(M, x) :

```

```

> x := 0 :
eq1 := w = 0 :
eq2 := M = 0 :

x := L :
eq3 := w = 0 :
eq4 := M = 0 :

```

```

> q := 0.9·5.55 :
L := 11000 :
EI := 36283·1434.9·106 :
> sol := solve({eq1, eq2, eq3, eq4}, {_C1, _C2, _C3, _C4}) : assign(sol) : x := 'x':

```

```

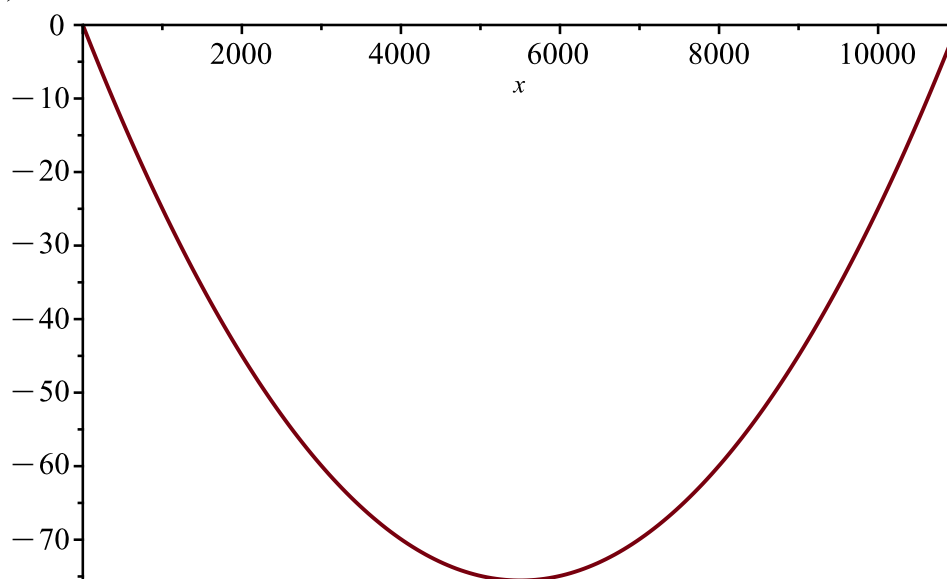
plot(-M·10-6, x = 0..L, size = [500, 300]);
plot(-φ, x = 0..L, size = [500, 300]);

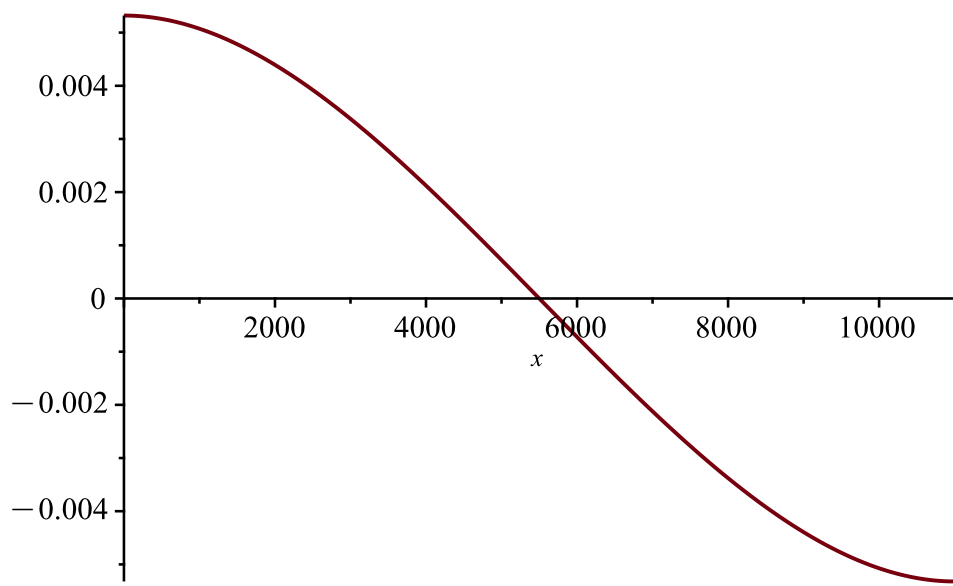
```

```

x := 0 :
-φ·103;

```





5.320806705

(1)

D.3. Output Maple beam flange

```
> restart; with(plots) :
```

```
>
```

```
Differential equation:
```

```
> ODE1 := EI1·diff(w1(x), x$4) = q1 :  
ODE2 := EI2·diff(w2(x), x$4) = q2 :  
dsol := dsolve({ODE1, ODE2}, {w1(x), w2(x)}) : assign(dsol) :
```

```
w1 := w1(x) :
```

```
w2 := w2(x) :
```

```
phi1 := -diff(w1, x) :
```

```
kappa1 := diff(phi1, x) :
```

```
M1 := EI1·kappa1 :
```

```
V1 := diff(M1, x) :
```

```
phi2 := -diff(w2, x) :
```

```
kappa2 := diff(phi2, x) :
```

```
M2 := EI2·kappa2 :
```

```
V2 := diff(M2, x) :
```

```
Boundary conditions:
```

```
> x := 0 :
```

```
eq1 := w1 = 0 :
```

```
eq2 := phi1 = 0 :
```

```
x := L1 :
```

```
eq3 := V1 = V2 :
```

```
eq4 := M1 = M2 :
```

```
eq5 := phi1 = phi2 :
```

```
eq6 := w1 = w2 :
```

```
x := L1 + L2 :
```

```
eq7 := M2 = 0 :
```

```
eq8 := V2 = -F :
```

```
Variables:
```

```
> F := (1.2·5.55 + 1.5·3.3)·5.5·1.0·103 : q1 := 0 : q2 := 0 : L1 := 130 : L2 := 70 : EI1 :=  $\frac{1}{12}$   
·1000·(12.5 + 12)3·210000 : EI2 :=  $\frac{1}{12}$ ·1000·123·210000 :
```

```
Solution:
```

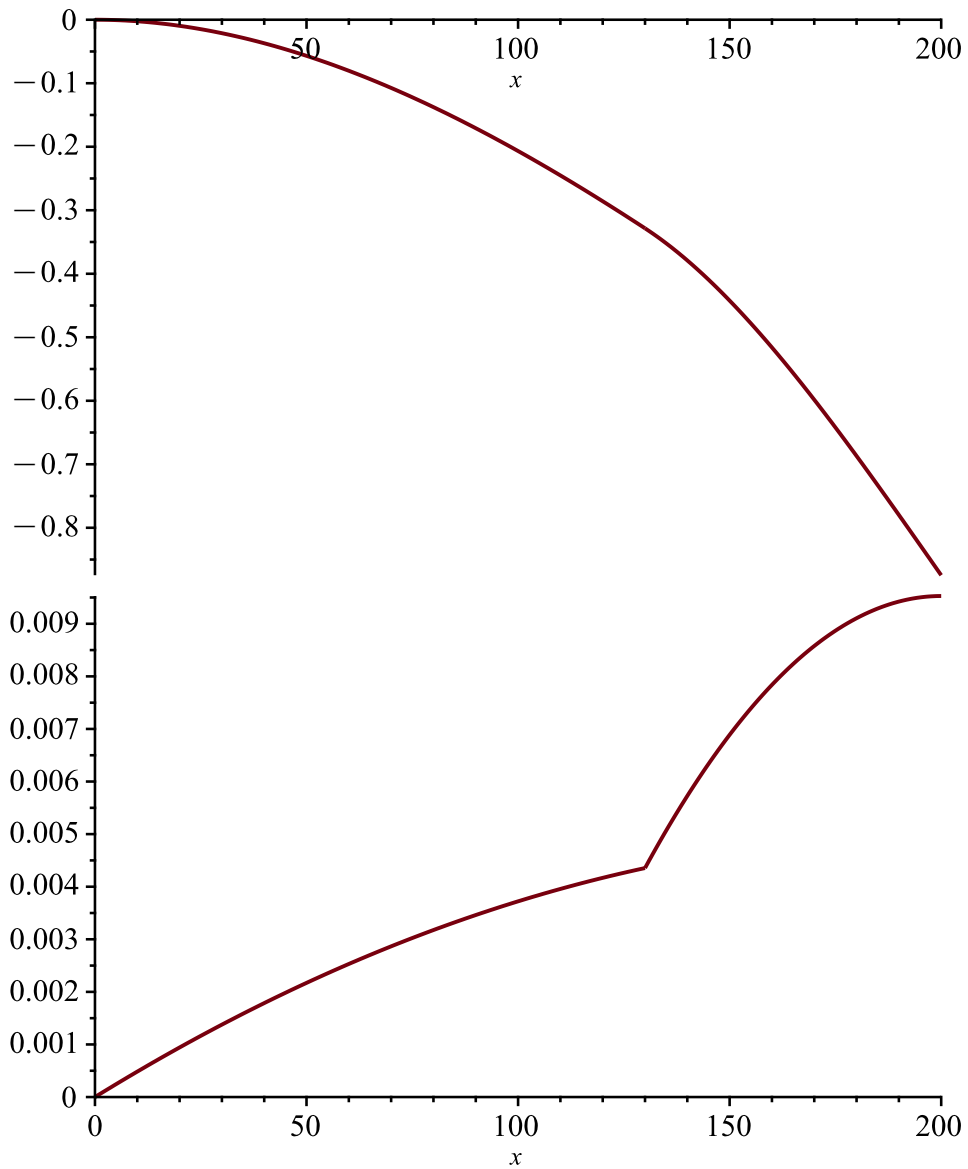
```
> sol := solve({eq1, eq2, eq3, eq4, eq5, eq6, eq7, eq8}, {_C1, _C2, _C3, _C4, _C5, _C6, _C7,  
_C8}) : assign(sol) : x := 'x' :
```

```
Plots:
```

```
> AA := plot(w1, x = 0 .. L1) :
```

```
BB := plot(w2, x=L1..L1+L2) :  
display({AA, BB}, size=[500, 300]);
```

```
CC := plot(phi1, x=0..L1) :  
DD := plot(phi2, x=L1..L1+L2) :  
display({CC, DD}, size=[500, 300])
```



```
> x := L1 + L2;  
phi2·103;
```

```
x := 200  
9.527911770
```

```
>
```

(1)

```
> restart; with(plots) :
```

```
>
```

```
Differential equation:
```

```
> ODE1 := EI1·diff(w1(x), x$4) = q1 :  
ODE2 := EI2·diff(w2(x), x$4) = q2 :  
dsol := dsolve({ODE1, ODE2}, {w1(x), w2(x)}) : assign(dsol) :
```

```
w1 := w1(x) :
```

```
w2 := w2(x) :
```

```
phi1 := -diff(w1, x) :
```

```
kappa1 := diff(phi1, x) :
```

```
M1 := EI1·kappa1 :
```

```
V1 := diff(M1, x) :
```

```
phi2 := -diff(w2, x) :
```

```
kappa2 := diff(phi2, x) :
```

```
M2 := EI2·kappa2 :
```

```
V2 := diff(M2, x) :
```

```
Boundary conditions:
```

```
> x := 0 :
```

```
eq1 := w1 = 0 :
```

```
eq2 := phi1 = 0 :
```

```
x := L1 :
```

```
eq3 := V1 = V2 :
```

```
eq4 := M1 = M2 :
```

```
eq5 := phi1 = phi2 :
```

```
eq6 := w1 = w2 :
```

```
x := L1 + L2 :
```

```
eq7 := M2 = 0 :
```

```
eq8 := V2 = -F :
```

```
Variables:
```

```
> F := (0.9·5.55)·5.5·1.0·103 : q1 := 0 : q2 := 0 : L1 := 130 : L2 := 70 : EI1 :=  $\frac{1}{12}$ ·1000  
·(12.5 + 12)3·210000 : EI2 :=  $\frac{1}{12}$ ·1000·123·210000 :
```

```
Solution:
```

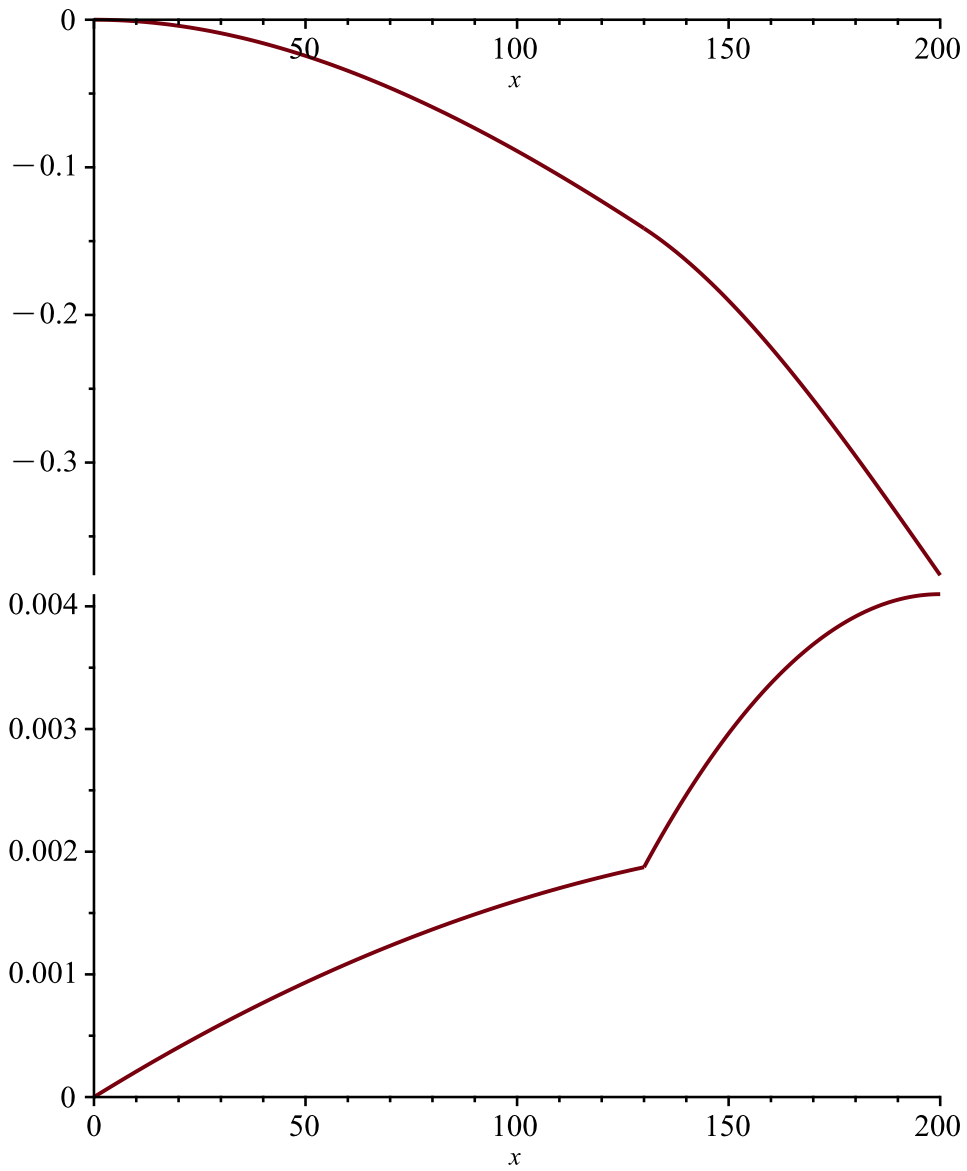
```
> sol := solve({eq1, eq2, eq3, eq4, eq5, eq6, eq7, eq8}, {_C1, _C2, _C3, _C4, _C5, _C6, _C7,  
_C8}) : assign(sol) : x := 'x' :
```

```
Plots:
```

```
> AA := plot(w1, x = 0 .. L1) :
```

```
BB := plot(w2, x=L1..L1+L2):  
display({AA, BB}, size=[500, 300]);
```

```
CC := plot(phi1, x=0..L1):  
DD := plot(phi2, x=L1..L1+L2):  
display({CC, DD}, size=[500, 300])
```

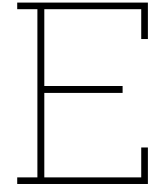


```
> x := L1 + L2;  
phi2 * 103;
```

```
x := 200  
4.099217860
```

```
>
```

(1)



Installation and demountability costs

In Appendix F the quantitative results for the installation and demounting process are reviewed. Time indications are discussed with a cost export from the Rotterdam-based engineering firm Multicall. The results are based on the labour unit prices of December 2023.

- Construction worker €55,-
- Pretensioning expert €70,-

In [Table E.1](#), [Table E.2](#), and [Table E.3](#) installation costs are specified. As a result, the most expensive connection for installation is the prestressed connection with €118.17 (+38.6%), followed by the resin-injected connection €101.75 (+19.4%) and the most economical in terms of installation costs is the demountable shear connector alternative €85.25.

Table E.1: Cost overview for the installation of the resin injection in euros per plate (4 connectors)

Steps	Time [min]	Price [€]
Open up the hollow core slab sleeves	10	€ 9.17
Positioning of DEMU and steel plate	20	€ 18.33
Filling the hollow core sleeve with concrete and compact	25	€ 22.92
	<i>Subtotal</i>	€ 50.42
Prop the beam	8	€ 7.33
Place the slab on the flange of the integrated beam	15	€ 13.75
Tightening of the injection bolts on the bottom flange	20	€ 18.33
Inject the bolt hole with resin	8	€ 7.33
Adjust the compression bolt at the top side	5	€ 4.58
	<i>Subtotal</i>	€ 51.33
	Total	€ 101.75

Table E.2: Cost overview for the installation of the demountable shear connector in euros per plate (4 connectors)

Steps	Time [min]	Price [€]
Open up the hollow core slab sleeves	10	€ 9.17
Positioning of SHS section with anchor	10	€ 9.17
Filling the hollow core sleeve with concrete and compact	25	€ 22.92
	<i>Subtotal</i>	€ 41.25
Prop the beam	8	€ 7.33
Place the demountable shear connectors on the beam flange	10	€ 9.17
Place the slab on the flange over the demountable shear connectors	18	€ 16.50
Add concrete filling to the SHS section	7	€ 6.42
Adjust the compression bolt at the top side	5	€ 4.58
	<i>Subtotal</i>	€ 44.00
	Total	€ 85.25

Table E.3: Cost overview for the installation of the pretensioned connector in euros per plate (4 connectors)

Steps	Time [min]	Price [€]
Open up the hollow core slab sleeves	10	€ 9.17
Positioning of SHS section with anchor	10	€ 9.17
Filling the hollow core sleeve with concrete and compact	25	€ 22.92
	<i>Subtotal</i>	€ 41.25
Prop the beam	8	€ 7.33
Place the slab on the beam flange	15	€ 13.75
Place thick cover plate and anchor rod from the top side	6	€ 5.50
Add nut on the bottom side	9	€ 8.25
Pretension the top nut	15	€ 18.75
Pretension the top nut second time for pretension losses	15	€ 18.75
Adjust the compression bolt at the top side	5	€ 4.58
	<i>Subtotal</i>	€ 76.92
	Total	€ 118.17

For deconstruction costs, the results are shown in [Table E.4](#), [Table E.5](#), and [Table E.6](#). The prestressed variant was the most expensive for installation, but compensates for demounting costs. As a result, the demountable shear connector alternative is the most expensive, with €46.75 (+30.8 %), followed by the resin injected with €41.25 (+15.4 %) and finally the prestressed connector with €35.75.

Table E.4: Cost overview for the demounting process of the resin injection in euros per plate (4 connectors)

Steps	Time [min]	Price [€]
Prop the beam	8	€ 7.33
Unscrew the compression bolt at the top side	5	€ 4.58
Remove the injection bolt on the bottom flange	12	€ 11.00
Lift the slab off the flange of the integrated beam	15	€ 13.75
Clean bolt hole in the flange	5	€ 4.58
	Total	€ 41.25

Table E.5: Cost overview for the demounting process of the demountable shear connector in euros per plate (4 connectors)

Steps	Time [min]	Price [€]
Prop the beam	8	€ 7.33
Unscrew the compression bolt at the top side	5	€ 4.58
Unscrew the nut at the beam flange	8	€ 7.33
Lift the slab off the flange of the integrated beam	15	€ 13.75
Clean SHS profile	15	€ 13.75
	Total	€ 46.75

Table E.6: Cost overview for the demounting process of the pretensioned connector in euros per plate (4 connectors)

Steps	Time [min]	Price [€]
Prop the beam	8	€ 7.33
Unscrew the compression bolt at the top side	5	€ 4.58
Unscrew the nut at the beam flange	8	€ 7.33
Remove the anchor rod and plate	3	€ 2.75
Lift the slab off the flange of the integrated beam	15	€ 13.75
	Total	€ 35.75

E.1. Sensitivity analysis

Based on installation and demounting costs, the labour costs for one reuse cycle can be calculated, the material costs are not included, as they are already provided in [section 5.4](#). For this calculation, initial installation investment costs are not taken into account. To investigate the influence of fluctuating prices, a sensitive parameter s is introduced. This parameter expresses uncertainty in the price of labour. In [Figure E.1](#) the result of the analysis shown. It can be seen that the costs for the injection connection and the shear connector connection are more or less the same, with a price of €92.58 and €90.75, respectively. The price of one reuse cycle for the prestressed connection is substantially higher with €112.67. Since the trends in the graph are linear it is clearly visible that increased labour prices will result in larger differences between the alternatives. For decreased labour prices the opposite will occur, but considering the trends over the past decades this is highly unlikely.

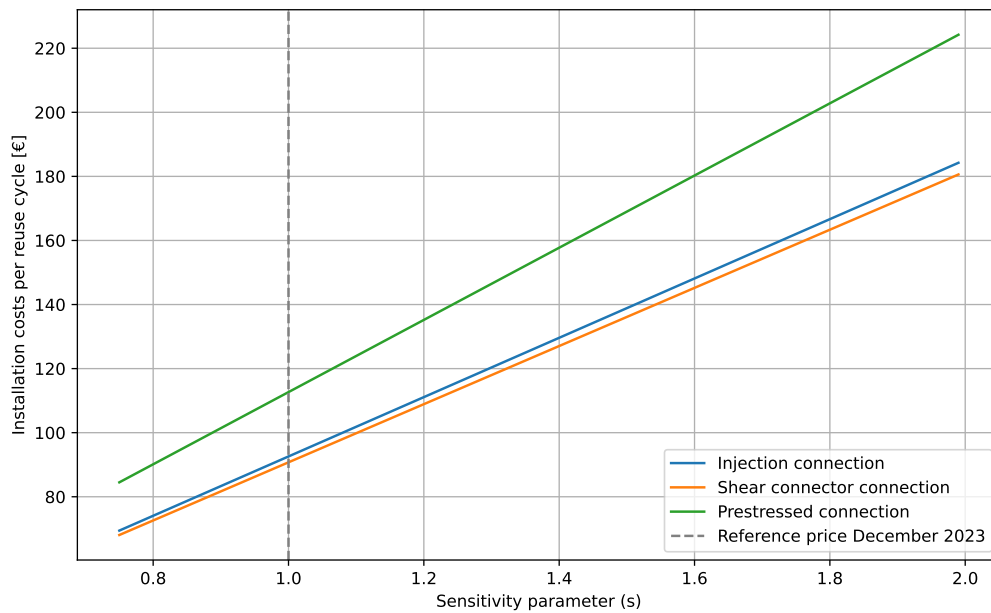
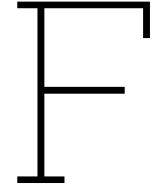


Figure E.1: Sensitivity analysis on the installation costs



Load verifications

F.1. Bolt verification

Euler buckling load with a buckling length of $2L$

$$N_{cr} = \frac{\pi^2 EI}{L_{cr}^2} = \frac{\pi^2 \cdot 2 \cdot 10^5 \cdot \frac{\pi \cdot 14.1^4}{64}}{(1.0 \cdot 61.625)^2} = 1019.5 \text{ kN} \quad (\text{F.1})$$

Relative slenderness of the bolt

$$\bar{\lambda} = \sqrt{\frac{Af_y}{N_{cr}}} = \sqrt{\frac{157 \cdot 640}{1019543}} = 0.314 \quad (\text{F.2})$$

$$\Phi = 0.5 [1 + \alpha(\bar{\lambda} - 0.2) + \bar{\lambda}^2] = 0.5 [1 + 0.49(0.314 - 0.2) + 0.314^2] = 0.577 \quad (\text{F.3})$$

Bolt buckling reduction factor

$$\chi = \frac{1}{\Phi + \sqrt{\Phi^2 - \bar{\lambda}^2}} = \frac{1}{0.577 + \sqrt{0.577^2 - 0.314^2}} = 0.942 \leq 1.0 \quad (\text{F.4})$$

Bearing factor that takes into account the geometry perpendicular to the direction of loading.

$$k_1 = \min \left[1.4 \frac{P_2}{d_0} - 1.7, 2.5 \right] = \min \left[1.4 \cdot \frac{628}{18} - 1.7, 2.5 \right] = 2.5 \quad (\text{F.5})$$

Bearing reduction factor that takes into account the geometry in the direction of loading.

$$\alpha_b = \min \left[\frac{e_1}{3d_0}, \frac{f_{ub}}{f_u}, 1.0 \right] = \min \left[\frac{75}{3 \cdot 18}, \frac{800}{490}, 1.0 \right] = 1.0 \quad (\text{F.6})$$

F.2. Beam verification

Classification table according to Technisch Dossier #2 [50].

Table F.1: Classification demands for integrated Slim Floor Beams [50]

Stress distribution	Relative slenderness ratios	Qualification of cross section
Plastic	$\beta_{rel} \leq 10$ and $\zeta_{rel} \leq 72$	Class 1 (plastic)
Plastic	$\beta_{rel} \leq 11$ and $\zeta_{rel} \leq 83$	Class 2 (compact)
Elastic	$\beta_{rel} \leq 15$ and $\zeta_{rel} \leq 124$	Class 3 (semi-compact)
Elastic	$\beta_{rel} > 15$ or $\zeta_{rel} > 124$	Class 4 (slender)

Plastic section modulus calculation:

$$\begin{aligned} W_{pl,y} &= A_{u,eff} \cdot 86 + A_{o,eff} \cdot 71 + A_1 \cdot 149 + A_2 \cdot 39 = \\ 6326.7 \cdot 86 + 4322.9 \cdot 71 + 6422 \cdot 149 + 872 \cdot 39 &= 1.835 \cdot 10^6 \text{ mm}^3. \end{aligned} \quad (\text{F.15})$$



Experimental set-up

In the following Appendix, the working plan for the lab experiments is described. The plan consists of 3 parts; first the materials that are needed to perform the experiment are described. Subsequently, all equipment is listed and, finally, the testing procedure is explained.

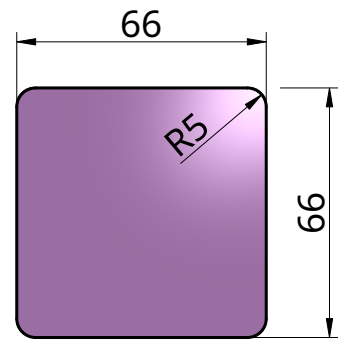
G.1. Materials

- SHS 80/80/5, l = 260 mm 12x
- Loading block
- CUGLATON gietmortel 5 mm 3 x 20 kg
- Formwork plate to cast
- Formwork oil
- Vaseline wax
- Cling film
- Screws

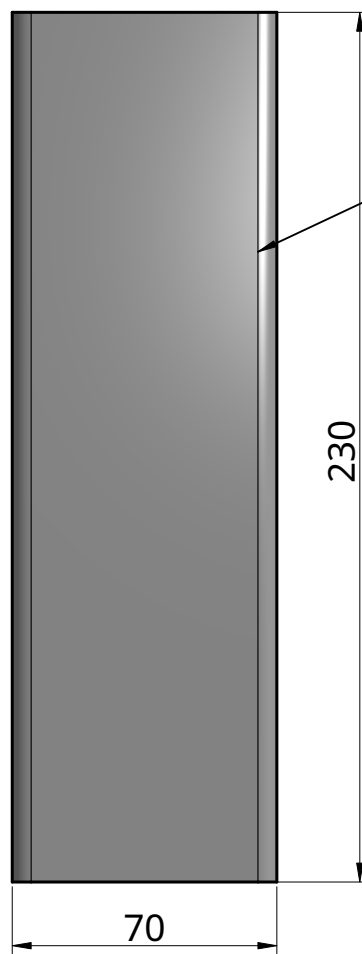
G.2. Equipment

In the list below, all the equipment needed for execution of the experiments is written down. In case an indication is not provided on the amount needed, it is assumed to be equal to one.

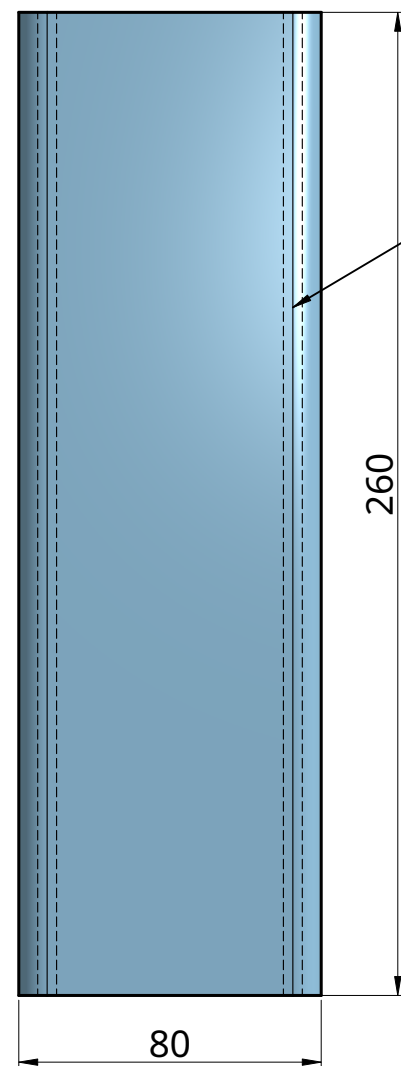
- Metal file
- Cleaning rags
- Mortar tub (50 L)
- Handheld cement mixer
- Concrete cube formwork
- Stone chisel for SDS MAX
- Bouchard chisel 60 x 60 mm for SDS MAX
- Impact driver
- Handheld demolition hammer (1150 W / 8.3J)
- Handheld demolition hammer (1510 W / 18.6J)
- Universal Testing Machine UTM (compressive load cell)
- Vice
- Ruler
- Digital caliper
- Steel chalk
- Pen and paper
- Timer



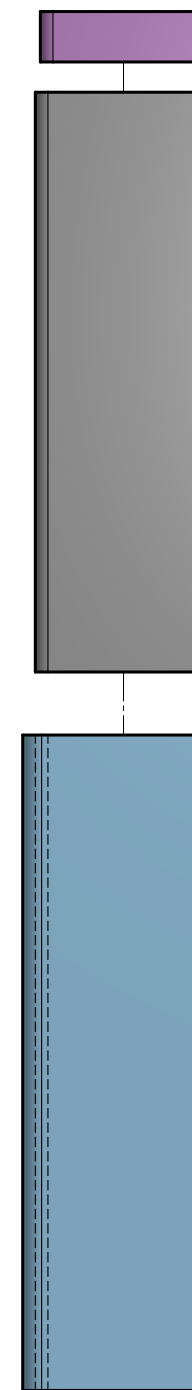
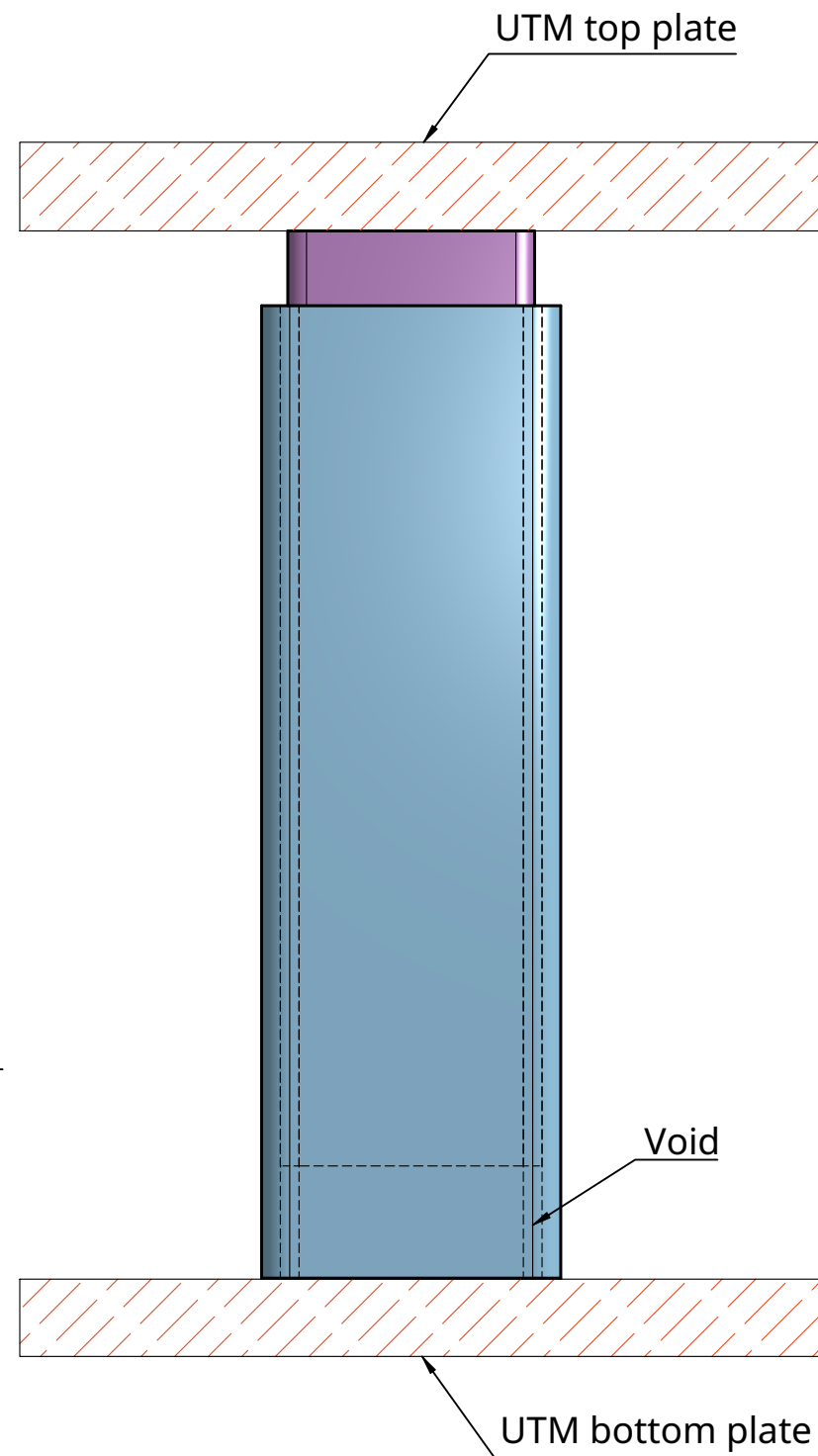
Compressive block, 1x



Mortar;
CUGLATON
gietmortel
5mm, 1.12l



SHS 80/80/5, 12x



UNLESS OTHERWISE SPECIFIED, DIMENSIONS ARE IN MILLIMETERS ANGULAR = ±° SURFACE FINISH DO NOT SCALE DRAWING BREAK ALL SHARP EDGES AND REMOVE BURRS FIRST ANGLE PROJECTION	NAME	SIGNATURE	DATE	TITLE Test set-up chemical bond	
	DRAWN	MW	2023-11-07		
	CHECKED	FK			
	APPROVED				
MATERIAL	FINISH		SIZE A3	DWG NO.	REV.
Steel S355			SCALE 1:2	WEIGHT	SHEET 1 of 1

6

5

4

3

2

1

D

D

C

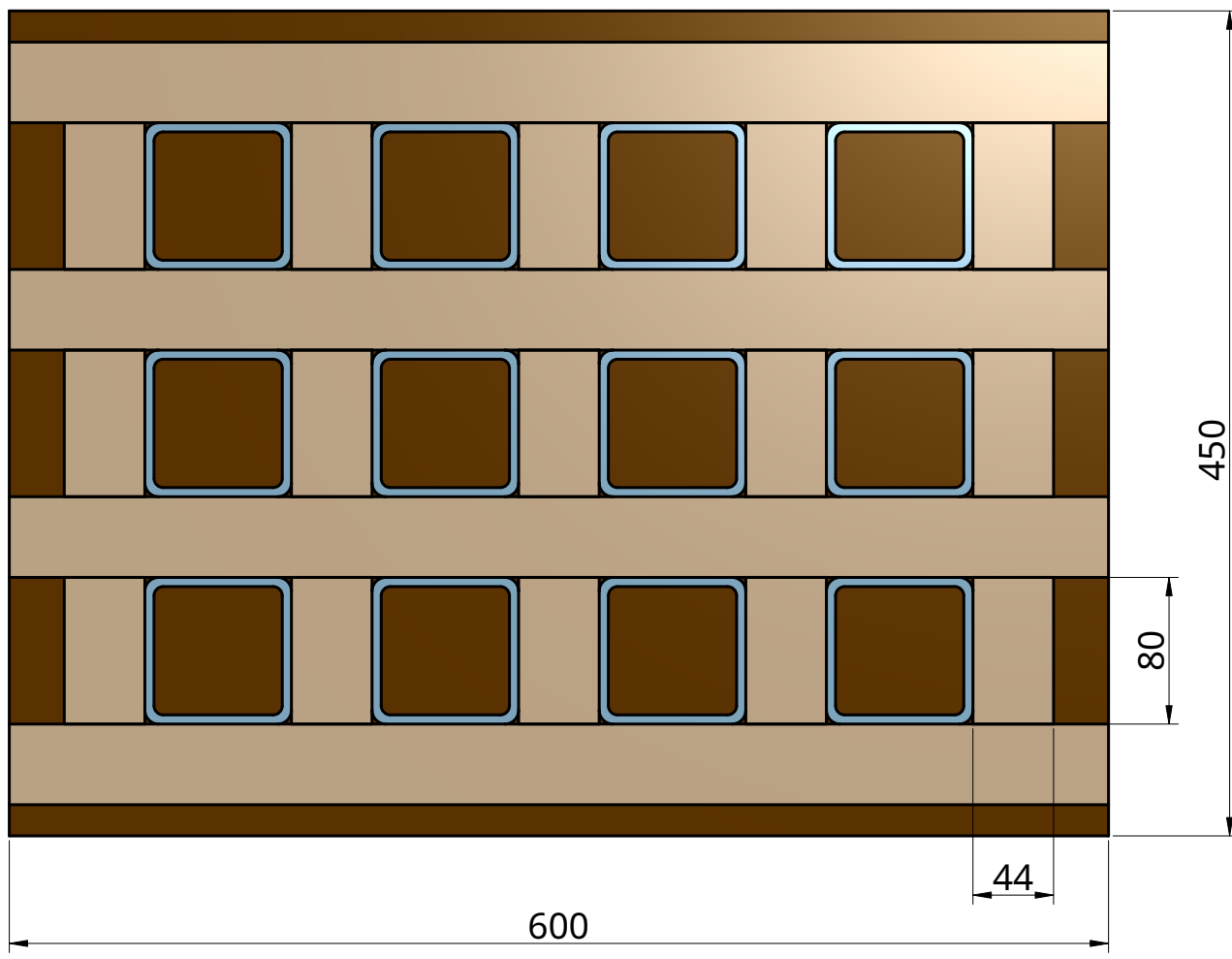
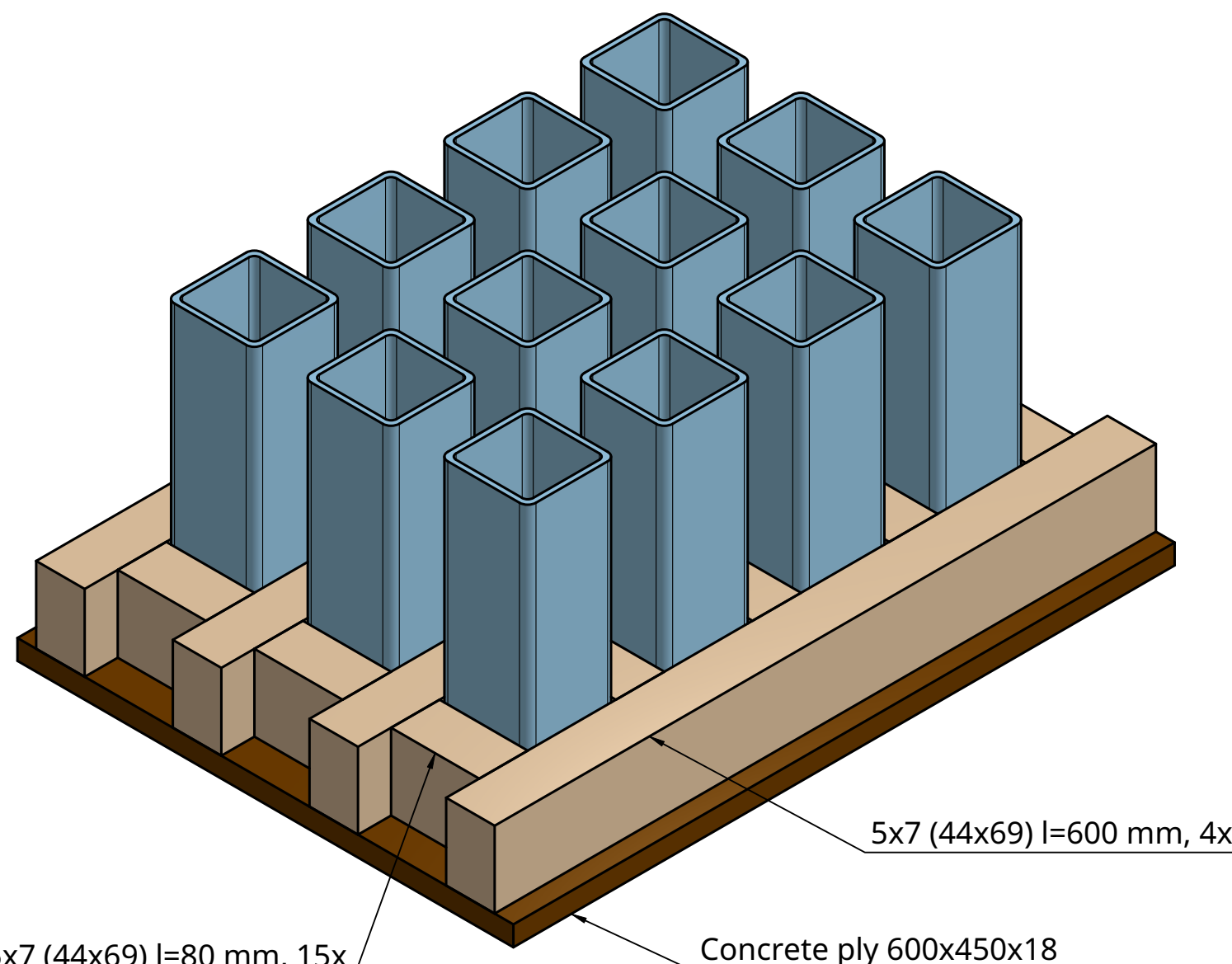
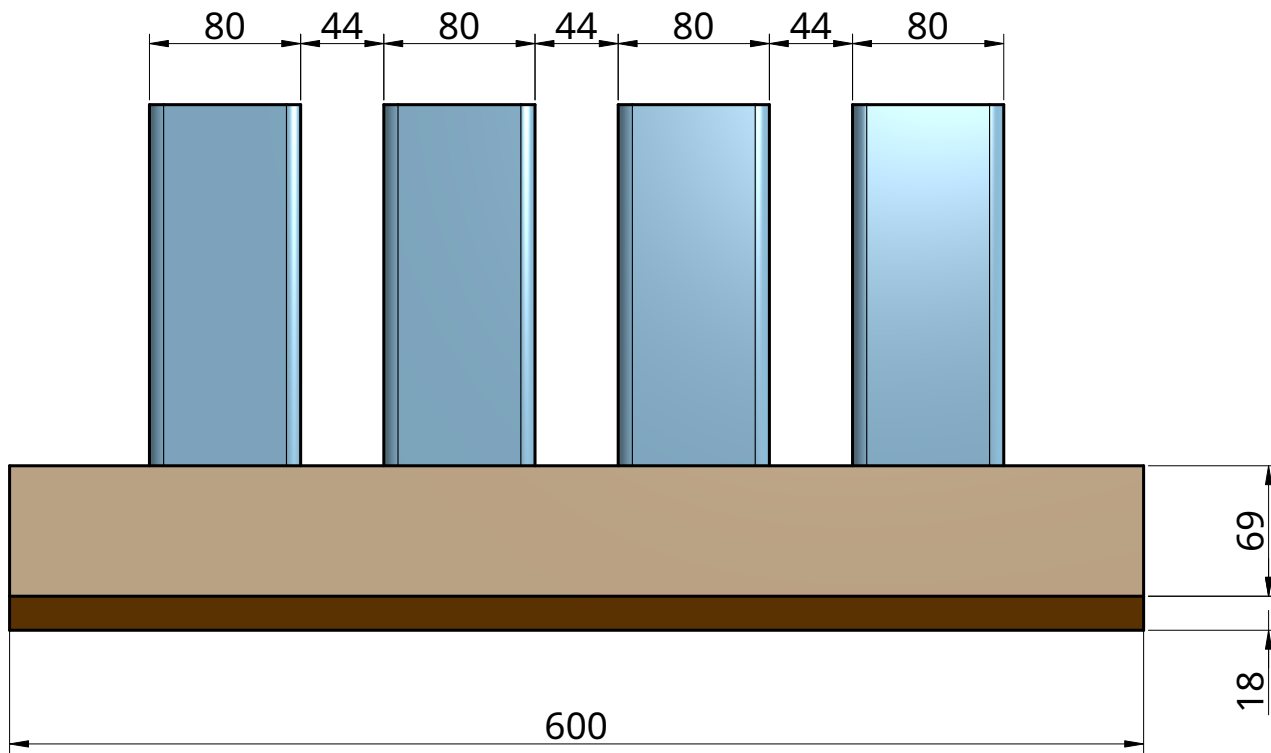
C

B

B

A

A



5x7 (44x69) l=80 mm, 15x

UNLESS OTHERWISE SPECIFIED, DIMENSIONS ARE IN MILLIMETERS

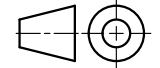
ANGULAR = ±°

SURFACE FINISH

DO NOT SCALE DRAWING

BREAK ALL SHARP EDGES AND REMOVE BURRS

FIRST ANGLE PROJECTION



	NAME	SIGNATURE	DATE
DRAWN	MARTENW		2023-12-04
CHECKED			
APPROVED			

TITLE		SIZE	DWG NO.	REV.
		A3		
SCALE	1:4	WEIGHT	SHEET 1 of 1	

6

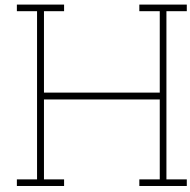
5

4

3

2

1



Environmental impact categories and monetisation factors

Table H.1: Environmental Impact Categories, units, and monetisation factors

Environmental Impact Category	Unit	Impact Category eq.
Climate Change - Total	kg CO ₂ eq	€ 0.116
Climate Change - Fossil	kg CO ₂ eq	€ 0.116
Climate Change - Biogenic Removals and Emissions	kg CO ₂ eq	€ 0.116
Climate Change - Land Use and Land Use Change	kg CO ₂ eq	€ 0.116
Ozone Depletion	kg CFC – 11 eq	€ 32
Acidification	mol H ⁺ eq	€ 0.39
Eutrophication - Aquatic Freshwater	kg P eq	€ 1.96
Eutrophication - Fresh Marine	kg N eq	€ 3.28
Eutrophication - Terrestrial	mol N eq	€ 0.36
Photochemical Ozone Formation	kg NMVOC eq	€ 1.22
Abiotic Depletion - Minerals and Metals	kg Sb eq	€ 0.3
Abiotic Depletion - Fossil Fuels	MJ	€ 0.00033
Water Use	m ³	€ 0.00506